Interplay of *Verticillium* signaling genes favoring beneficial or detrimental outcomes in interactions with plant hosts

Dissertation

For the award of the degree

"Doctor rerum naturalium"

of the University of Goettingen

within the doctoral program

"Plant Responses To Eliminate Critical Threats"

of the Georg-August University School of Science (GAUSS)

submitted by

Jessica Starke

from Celle

May 2019

Thesis Committee and members of the Examination Board

Referee: **Prof. Dr. Gerhard H. Braus**

Department of Molecular Microbiology and Genetics

University of Goettingen

2nd referee: **apl. Prof. Dr. Kai Heimel**

Department of Molecular Microbiology and Genetics

University of Goettingen

3rd referee: **Prof. Ph.D. James W. Kronstad**

Michael Smith Laboratories

University of British Columbia Vancouver

Prof. Dr. Andrea Polle

Department of Forest Botany and Tree Physiology

University of Goettingen

Prof. Dr. Petr Karlovsky

Department of Molecular Phytopathology and Mycotoxin Research

University of Goettingen

Prof. Dr. Volker Lipka

Department of Plant Cell Biology

University of Goettingen

Date of oral examination: July 22nd 2019

I

Declaration of independence

Herewith I declare that the dissertation entitled **"Interplay of *Verticillium* signaling genes favoring beneficial or detrimental outcomes in interactions with plant hosts"** was written on my own and independently without any other aids and sources than indicated.

Jessica Starke

Goettingen, 2019

This work was accomplished in the group of Prof. Dr. Gerhard H. Braus, at the Department of Molecular Microbiology and Genetics at the Institute of Microbiology and Genetics, University of Goettingen.

Table of Contents

Summary

Verticillia and their plant hosts both contribute to pathogenesis as a consequence of their interaction. Evolution-driven genome extension includes hybridization, resulting in amphidiploid species as the rapeseed pathogen *Verticillium longisporum* and the acquirement of Lineage Specific (LS) regions in haploid Verticillia. Whether a fungus-plant interaction results in pathogenicity or reduced susceptibility of the host depends on mutual exchange of secreted signals, their perception and intracellular transduction pathways.

The genome of the haploid tomato pathogen *V. dahliae* JR2 includes an LS region with several genes for putative transcription factors, which is not required for virulence. Hybrid pathogenic *V. longisporum* isolates Vl43 or Vl145c contain the homologous *Vl43LS20kb* region, which is absent in the non-symptomatic hybrid Vl32. Deletion of this region in *V. longisporum* Vl43 led to a hypervirulent phenotype in rapeseed, suggesting a function in reducing virulence as well as susceptibility of the host plant.

The Fus3/Kss1-like *V. dahliae* MAP kinase Vmk1 plays an essential role in regulating virulence in plants. Intracellular transduction pathways can be insulated by scaffold proteins for maintenance of specificity. The *V. dahliae* MAPK scaffold protein Ham5, homologous to *Neurospora crassa* HAM-5, has not yet been analyzed in plant pathogens. Deletion of *V. dahliae HAM5* allowed wild type-like development, whereas deletion of the upstream MAP2K *MEK2* reduced vegetative growth and microsclerotia formation as deletion of *VMK1*. *MEK2* and *VMK1* deletion strains were re-isolated from plant tissue, supporting their potential to invade tomato plants. Both displayed defects in induction of disease symptoms. *HAM5* deletion strains induced wild type-like disease symptoms *in planta*. Therefore, the Vmk1/Mek2 MAPK signaling pathway-mediated regulation of vegetative growth, microsclerotia formation and pathogenicity is independent from the scaffold protein Ham5 and does not require its insulation function in *V. dahliae*.

Plant invasion and immune suppression require secretion of correctly folded proteins monitored by the Hac1-controlled unfolded protein response (UPR) pathway. The bZIP transcription factor Hac1 is essential for virulence of the necrotrophic appressoria-forming ascomycete *Alternaria brassicicola* or of the basidiomycete *Ustilago maydis*. *V. dahliae HAC1* mRNA appears in two splice variants *HAC1^u* (uninduced) and *HAC1^i* (induced), where only *HAC1^i* was translated into a protein. *HAC1* deletion caused significantly decreased vegetative growth, conidiation and impaired microsclerotia formation. *ΔHAC1* could penetrate and initiate colonization of the root cortex of *Arabidopsis thaliana*, but induced only minor disease symptoms in tomato plants. Different to the MAPK deletion strains, *ΔHAC1* could not be re-isolated from plant stems, corroborating deficiency in propagation within the plant. Constitutively active UPR led to increased microsclerotia formation and induced strong disease symptoms *in planta*. In conclusion, *V. dahliae HAC1* is an important regulator of growth and differentiation with strong impact on virulence and susceptibility.

Virulence is connected to fungal hormones. Fungal oxylipins control differentiation processes, secondary metabolite production or manipulation of plant host defense responses. The Ode1 oleate Δ12-fatty acid desaturase is localized to intracellular membranes and catalyzes the oxidation of oleic acid to linoleic acid as major oxylipin precursor. *V. dahliae ODE1* deletion resulted in decreased vegetative growth and microsclerotia formation. However, the defect in *ODE1* had minor impact on fungal virulence.

In summary, the outcome of a fungus-plant interaction as result of a complex interplay of virulence enhancing and reducing mechanisms was analyzed: Lineage Specific insertions can be beneficial for the plant, single enzymes for linoleic acid production as precursor of oxylipins can make a minor contribution, whereas Hac1-regulated UPR or the scaffold-independent pheromone response MAPK pathway are crucial for pathogenicity.

Zusammenfassung

Sowohl Verticillien als auch ihre Wirtspflanzen tragen zur Entwicklung von Krankheitssymptomen als Folge ihrer Interaktion bei. In haploiden Verticillien wurden Hybridisierungen zur Entstehung des amphidiploiden Rapspathogens *Verticillium longisporum*, und der Erwerb von artspezifischen Regionen (LS Regionen) als Mechanismen evolutions-getriebener Genomerweiterung beschrieben. Ob aus einer Pilz-Pflanzeninteraktion Pathogenität oder eine reduzierte Anfälligkeit der Wirtspflanze resultiert, hängt vom gegenseitigen Austausch von sekretierten Signalen und deren Wahrnehmung, sowie von intrazellulären Transduktionswegen ab.

Im haploiden Genom des Tomatenpathogens *V. dahliae* JR2 befindet sich eine *Vl43LS20kb*-Region, die für mögliche Transkriptionsfaktoren kodiert und nicht für die Virulenz benötigt wird. Die Genome der pathogenen, amphidiploiden *V. longisporum* Isolate Vl43 und Vl145c enthalten ebenfalls diese LS Region, die jedoch nicht im Genom des asymptomatischen Hybriden Vl32 zu finden ist. Die Deletion dieser Region führte in *V. longisporum* Vl43 zu verstärkten Krankheitssymptomen in Rapspflanzen, woraus eine Funktion in der Reduzierung der Virulenz oder der Anfälligkeit der Wirtspflanze hervorgeht.

Die Fus3/Kss1-ähnliche MAP Kinase Vmk1 spielt eine essentielle Rolle in der Regulation der Virulenz in Pflanzen in *V. dahliae*. Intrazelluläre Signaltransduktionswege können durch sogenannte Scaffold-Proteine isoliert werden um die Spezifität aufrecht zu erhalten. Das entsprechende Homolog zum *Neurospora crassa* MAP Kinase Scaffold-protein HAM-5 wurde bisher nicht in Pflanzenpathogenen beschrieben und die Rolle der vorgeschalteten Kinase Mek2 ist in Verticillien bisher nicht bekannt. Die Deletion von *V. dahliae HAM5* erlaubte eine Wildtyp-ähnliche Entwicklung, wohingegen die Deletion von *MEK2,* sowie die Deletion von *VMK1*, in reduziertem vegetativen Wachstum und verringerter Mikrosklerotienbildung resultierten. *MEK2* und *VMK1* Deletionsstämme konnten aus Pflanzengewebe re-isoliert werden, was ihr Potenzial in die Wirtspflanze einzudringen bestätigt. Jedoch zeigten beide Stämme Defekte in der Induktion von Krankheitssymptomen in Tomatenpflanzen. *HAM5* Deletionsstämme induzierten Wildtyp-ähnliche Krankheitssymptome in der Pflanze. Somit ist die Regulation von vegetativem Wachstum, Mikrosklerotienbildung und Pathogenität, die durch den Vmk1/Mek2 MAPK-Signalweg vermittelt wird, in *V. dahliae* unabhängig von dem Scaffold-Protein Ham5 und erfordert dessen Isolationsfunktion nicht.

Das Eindringen in die Wirtspflanze und die Immunsuppression erfordert die Sekretion von korrekt gefalteten Proteinen, welche durch den Hac1-kontrollierten Signalweg als Antwort auf ungefaltete Proteine (UPR) überwacht wird. Der bZIP Transkriptionsfaktor Hac1 ist essentiell für die Virulenz des nekrotrophen Appressorien-bildenden Ascomyceten *Alternaria brassicicola,* sowie des Basidiomyceten *Ustilago maydis*. Die *V. dahliae HAC1* mRNA kommt in zwei Spleißvarianten *HAC1^u* (uninduziert) und *HAC1^i* (induziert) vor. Jedoch wird nur *HAC1^i* in ein Protein übersetzt. Die Deletion von *HAC1* führte zu signifikant verringertem vegetativen Wachstum, verringerter Konidienbildung und zur Unfähigkeit Mikrosklerotien als Überdauerungsstrukturen zu bilden. *ΔHAC1* konnte den Wurzelkortex von *Arabidopsis thaliana*-Pflanzen penetrieren und die Kolonisierung initiieren, induzierte jedoch deutlich weniger starke Krankheitssymptome in Tomatenpflanzen. Anders als die MAP Kinase-Deletionsstämme konnte *ΔHAC1* nicht aus dem Pflanzenmaterial re-isoliert werden. Dies spricht für einen Defekt in der Vermehrung des Pilzes in der Pflanze. Ein konstitutiv aktiver UPR Signalweg führte zu verstärkter Mikrosklerotienbildung und einer Induktion von starken Krankheitssymptomen in Tomatenpflanzen. Folglich spielt *HAC1* eine entscheidende Rolle in der Regulation von Wachstum und Differenzierung, und wird für die Virulenz von *V. dahliae* und die Induktion von Krankheitssymptomen in der Pflanze benötigt.

Des Weiteren gibt es Verbindungen zwischen Virulenz und pilzlichen Hormonen. Diese sogenannten Oxylipine können Differenzierungsprozesse, die Produktion von Sekundärmetaboliten und die Manipulation der Immunabwehr der Wirtspflanze beeinflussen. Die Ode1 Oleat-Δ12 Fettsäuredesaturase ist in intrazellulären Membranen lokalisiert und katalysiert die Oxidation von Ölsäure zu Linolsäure als Hauptvorläufer von Oxylipinen. Die Deletion des *V. dahliae* Gens *ODE1* resultierte in verringertem vegetativem Wachstum und einer reduzierten Mikrosklerotienbildung. Allerdings zeigte der Defekt im *ODE1* Gen nur einen geringen Einfluss auf die pilzliche Virulenz.

Zusammenfassend wurde der Erfolg einer Pilz-Pflanzeninteraktion als Ergebnis eines komplexen Zusammenspiels aus Virulenz-verstärkenden und -reduzierenden Mechanismen untersucht: Artspezifische Insertionen im Pilzgenom können vorteilhaft für die Wirtspflanze sein, einzelne Enzyme für die Produktion von Linolsäure als Vorläufer von Oxylipinen haben einen geringen Einfluss, während der Hac1-regulierte UPR Signalweg, sowie der Scaffold-unabhängige Pheromon-MAPK-Signalweg, eine entscheidende Rolle für die Pathogenität spielen.

1 INTRODUCTION

1.1 *Verticillium* spp. – colonizers of the plant´s vascular system

1.1.1 The ascomycete genus *Verticillium*

The plant disease Verticillium wilt is caused by members of the soil-borne ascomycete genus *Verticillium*, which contains ten species: *V. albo-atrum sensu stricto*, *V. alfalfae*, *V. nonalfalfae*, *V. dahliae*, *V. isaacii*, *V. klebahnii*, *V. longisporum*, *V. nubilum*, *V. tricorpus* and *V. zaregamisanum* (Inderbitzin *et al.*, 2011a; Inderbitzin & Subbarao, 2014). Conidiophores carry verticillate arranged phialides as conidia producing cells, giving the genus the name *Verticillium* (Pegg & Brady, 2002). These species are distributed in temperate and subtropical regions world-wide and vary in their host ranges (Pegg, 1984; Fradin & Thomma, 2006). The induced symptoms differ between hosts as well as between isolates from a certain species and may comprise stunting, chlorosis, necrosis, early senescence, defoliation, vein clearing, brownish vascular discoloration, or stem striping (Fradin & Thomma, 2006; Depotter *et al.*, 2016).

Verticillium species produce different dormant structures as resting mycelium, chlamydospores, or microsclerotia, which can persist in the soil (Wilhelm, 1955; Inderbitzin *et al.*, 2011a; Carroll *et al.*, 2018). Increasing temperatures due to climate change are assumed to increase the regional distribution and the economic impact of plant pathogens (Velásquez *et al.*, 2018), like Verticillia, allowing more successful overwintering, extension of the growth season, and potentially earlier infection of younger plants. Furthermore, severity of disease symptoms induced by several *Verticillium* species was observed to be correlated with increasing temperatures (Koike *et al.*, 1994; Jabnoun-Khiareddine *et al.*, 2006; Siebold & von Tiedemann, 2013). Available treatments for disease control include planting of resistant varieties, soil fumigation, and crop rotation with non-susceptible plants, but are costly, have questionable effects on the environment, or are not effective (Subbarao *et al.*, 2007; Klosterman *et al.*, 2009; Enebak *et al.*, 2012; Carroll *et al.*, 2018).

V. dahliae causes vascular wilting disease in almost 200 host species, including a broad range of crop plants and, therefore, has a great economic impact (Pegg & Brady, 2002; Luo *et al.*, 2014). Even if the species *V. dahliae* has a broad host range, single isolates of the species show altered aggressiveness on different plant hosts and can even colonize plants without induction of disease symptoms (Resende *et al.*, 1994; Zeise & von Tiedemann, 2002; Pegg & Brady, 2002; Gibriel *et al.*, 2019). Other members of the genus display narrower host ranges and distributions, however, significant economic losses are caused by *V. albo-atrum*, *V. alfalfae*, *V. nonalfalfae*, *V. tricorpus*, and

V. zaregamsianum (Inderbitzin & Subbarao, 2014). The species *V. isaacii*, *V. klebahnii*, and *V. nubilum* are pathogens with minor economic impact (Inderbitzin & Subbarao, 2014). *V. longisporum* is the only interspecific hybrid of the genus with an amphidiploid genome (Ingram, 1968), mainly virulent on Brassicaceae (Zeise & von Tiedemann, 2002; Eynck *et al.*, 2007). Recently, preliminary data from field trials in the United Kingdom were published, suggesting inconsistent impact on yield reductions caused by rapeseed infections with *V. longisporum* despite the presence of disease symptoms (Depotter *et al.*, 2019). The two species *V. dahliae* and *V. longisporum* are in scope of this study.

1.1.2 Life cycle of *Verticillium*

Species of the genus *Verticillium* induce Verticillium wilt, a monocyclic disease with one infection cycle per growing season (Fradin & Thomma, 2006; Klosterman *et al.*, 2011; Depotter *et al.*, 2016a). *V. dahliae* and *V. longisporum* form thick-walled, black melanized microsclerotia from swollen, septate hyphae as a characteristic dormant structure (Griffiths, 1970; Pegg & Brady, 2002; Figure 1, bottom). These resting structures persist in the soil through the winter or, if necessary, for up to 14 years (Wilhelm, 1955). Recognition of root exudates or plant surface molecules of an appropriate host is the first step in pathogen-plant communication, inducing germination of the fungus (Berlanger & Powelson, 2000). The fungus initially colonizes the root surface and invades the plant via natural root wounds, or by development of swollen hyphal tips, which were described as penetration structures, named hyphopodia (Pegg & Brady, 2002; Reusche *et al.*, 2014; Zhao *et al.*, 2014, 2016; Su *et al.*, 2018; Figure 1, left). Root tips, wounds, and lateral root hairs are favored entry points (Fitzell *et al.*, 1980; Eynck *et al.*, 2007; Vallad & Subbarao, 2008; Su *et al.*, 2018).

From cortical cells hyphae migrate towards the vascular parenchyma and xylem vessels by intercellular growth and some of them successfully reach the xylem (Klosterman *et al.*, 2009). Asexual spores are formed and spread within the vascular system via the transpiration stream (Klosterman *et al.*, 2009). The size and shape of these conidia are the major morphological characteristic to distinguish between *V. dahliae* and *V. longisporum*. *V. dahliae* forms conidia of ovoid shape and a length between 3.5 to 5.5 µm, whereas the name *V. longisporum* hints to the formation of elongated conidia of 7.1 to 8.8 µm (Karapapa *et al.*, 1997; Collins *et al.*, 2003; Tran *et al.*, 2013; Figure 1, top).

A switch from the biotrophic to the necrotrophic life style corresponds with the colonization of tissues neighboring the xylem (Fradin & Thomma, 2006). Disease symptoms induced by *V. dahliae* vary between fungal isolates and host plants and

include stunting, chlorosis, necrosis, early senescence, defoliation, vein clearing, and brownish vascular discoloration (Fradin & Thomma, 2006; Figure 1, right).
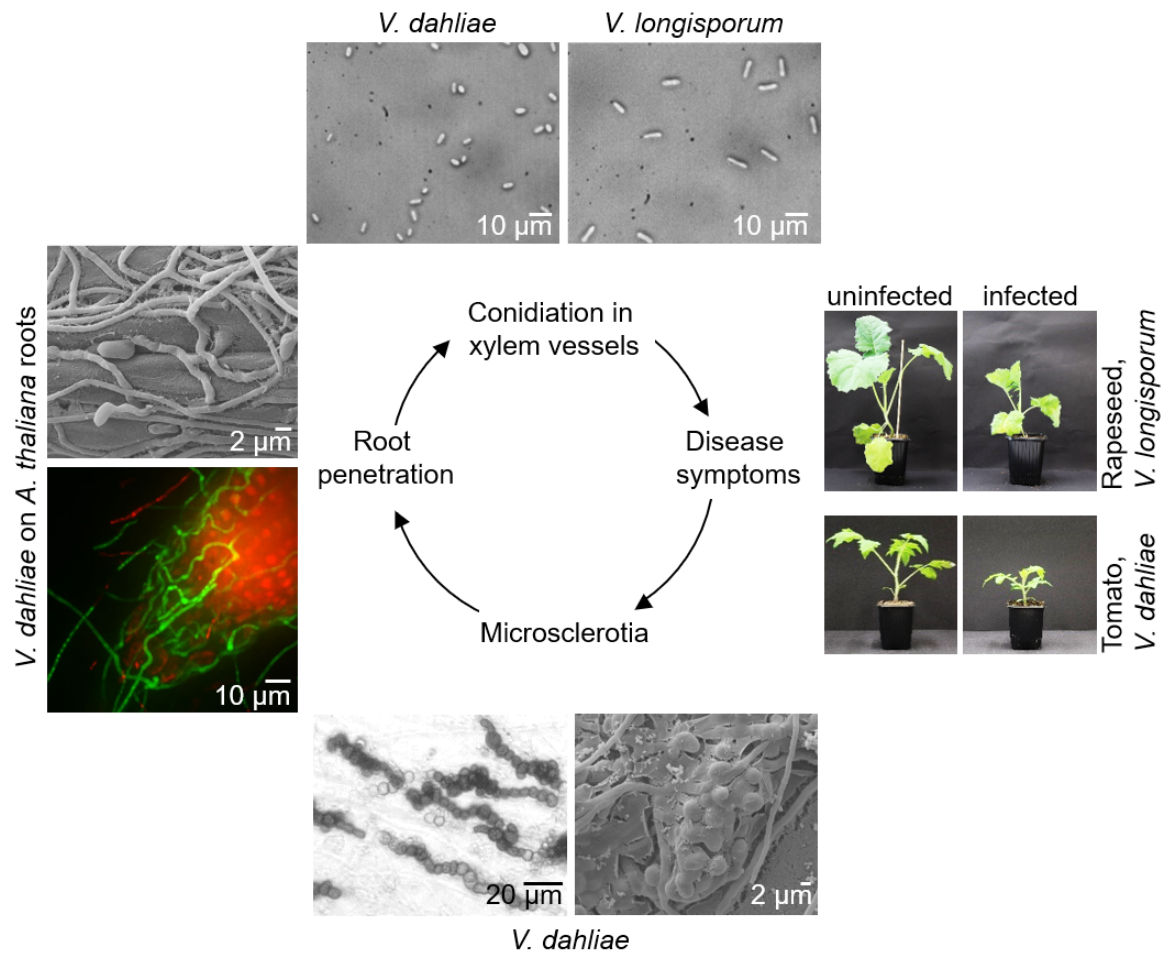
Figure 1: *Verticillium* life cycle. *V. dahliae* and *V. longisporum* form black melanized microsclerotia as dormant structures. In the presence of a suitable host the fungus germinates and grows into direction of the plant (Berlanger & Powelson, 2000). It colonizes the root surface and invades root tips, lateral root hairs, or natural root wounds by intercellular growth or formation of hyphopodia (Fitzell *et al.*, 1980; Eynck *et al.*, 2007; Vallad & Subbarao, 2008; Reusche *et al.*, 2014; Zhao *et al.*, 2014, 2016). Hyphae migrate from the cortex to the xylem vessels (Klosterman *et al.*, 2009). Conidia are formed and spread within the vascular system with the transpiration stream (Klosterman *et al.*, 2009). The fungus starts to colonize tissues neighboring the xylem with or without induction of disease symptoms. Under laboratory conditions the most obvious disease symptoms induced by *V. longisporum* in rapeseed plants or *V. dahliae* in tomato plants is stunting. In the dying host or under nutrient-limited conditions the fungus starts microsclerotia formation. Left: electron microscopy picture of *V. dahliae* growing on *Arabidopsis thaliana* roots (upper, Rabea Schlüter, Greifswald) and confocal fluorescence microscopy pictures from *V. dahliae* expressing ectopic *GFP* colonizing *A. thaliana* root tips stained in red with propidium iodide/silwet solution (lower). Top: *V. dahliae* forms smaller conidia (3.5 to 5.5 µm) with ovoid shape, whereas *V. longisporum* forms elongated conidia (7.1 to 8.8 µm). Right: Rapeseed plants 35 days after root dipping into distilled water or *V. longisporum* Vl43 spore solution (top). Tomato plants 21 days after root dipping into distilled water or *V. dahliae* JR2 spore solution (lower). Bottom: Microscopy picture of microsclerotia formed by *V. dahliae* nine days after spot inoculation of 50 000 spores onto cellulose containing medium (left) and electron microscopy picture of microsclerotia formed by *V. dahliae* after four days on solid simulated xylem medium (Rabea Schlüter, Greifswald).

V. longisporum-induced symptoms in rapeseed plants in the field are stem striping due to necrosis of the cortical tissue, whereas no wilting can be observed (Heale & Karapapa, 1999; Depotter *et al.*, 2016a). In contrast, artificial infection of rapeseed plants with pathogenic *V. longisporum* isolates by root dipping of seedlings results in stunting, chlorosis, necrosis, and increased branching (Zeise & von Tiedemann, 2002; Eynck *et al.*, 2007, 2009; Floerl *et al.*, 2008; Depotter *et al.*, 2016a; Figure 1, right). Verticillia are able to colonize plants without induction of disease symptoms. This can be observed either because the host is not susceptible, these plants are commonly considered as "non-host" or better as "asymptomatic host" plants (Malcolm *et al.*, 2013), or because the *Verticillium* isolate is "non-pathogenic".

The fungus recognizes limited nutrient availability in the dying host plant or in plant debris, which induces the formation of resting structures (Fradin & Thomma, 2006). These resting structures remain in the soil until perception of a new host. A sexual reproduction stage has not been described for any species of the genus (Short *et al.*, 2014).

During all steps of the plant colonization cycle fungi perceive signals from the host environment, which induce differentiated development. On the other hand, the fungus sends signals like effectors to invade and suppress the plant immune system, which is required for successful colonization.

1.2 Niche adaptation

The fungus-host plant interaction is based on coevolution as a process of ongoing adaptation of both to changing external or internal environmental conditions. Success of the fungus requires to overcome the host´s immune system, which evolves to limit the propagation of the invading fungus. Furthermore, fungi evolve to adapt to new host species with other defense mechanisms than previous hosts. Chromosomal recombination by meiosis has been seen as major evolutionary mechanism (Williams, 1975; de Jonge *et al.*, 2013). However, in about 20% of all fungi, including Verticillia, no sexual stage has been observed (Heitman *et al*, 2007; Seidl & Thomma, 2014). Evolution of clonally reproducing asexual fungi can include mechanisms as random mutations due to replication errors, horizontal gene or chromosome transfer, transposable elements, chromosomal rearrangements leading to deletions, duplications, inversions and translocations, and the hybridization of genomes (Brasier, 2000; Coleman *et al.*, 2009; Klosterman *et al.*, 2011; Ma *et al.*, 2011; Mehrabi *et al.*, 2011; Rouxel *et al.*, 2011; de Jonge *et al.*, 2012; Seidl & Thomma, 2014; Faino *et al.*, 2016). The genomes of some filamentous pathogens were grouped into a slowly evolving core genome, that maintains general physiology and a smaller, more quickly evolving pan genome with

higher plasticity, enriched in genes for niche adaptation (Raffaele & Kamoun, 2012; Faino *et al.*, 2016). Regions representing the more flexible pan genome are also described as Lineage Specific (LS) regions, displaying the genomic regions of a lineage, that differentiates it from its relatives (Klosterman *et al.*, 2011; Faino *et al.*, 2016; Shi-kunne & Faino, 2017). The impact of LS regions and genome hybridization on niche adaptation in Verticillia is one focus of this thesis.

1.2.1 *Verticillium dahliae* Lineage Specific regions

Lineage Specific genomic regions, unique or shared by a subset of strains, represent the pan genome as the part of the genome with higher plasticity (Klosterman *et al.*, 2011; de Jonge *et al.*, 2013). LS regions in *V. dahliae* were described to be acquired through horizontal gene transfer from *Fusarium oxysporum* (Chen *et al.*, 2018) and plants (de Jonge *et al.*, 2012), or transposons (Klosterman *et al.*, 2011; Faino *et al.*, 2016), and were observed to be correlated with synteny breakpoints arising from chromosomal reshuffling (de Jonge *et al.*, 2013; Shi-kunne & Faino, 2017). In Verticillia, generally frequent chromosomal rearrangements were observed in pathogenic and non-pathogenic species (Shi-kunne & Faino, 2017). A correlation of synteny breakpoints with LS regions has not been analyzed in other Verticillia than *V. dahliae* yet (Shi-kunne & Faino, 2017).

Research on LS regions to date focused especially on effector genes encoded in these regions. Effectors are typically small, cysteine-rich proteins with secretion signals, which are assumed to support colonization of the host by suppression of the plant immune response or manipulation of the host´s cell physiology (Stergiopoulos & de Wit, 2009; Selin *et al.*, 2016). Gibriel *et al.* defined the relative proportion of the core and LS regions comparing 19 *V. dahliae* strains with 93-97% core genome to 3-7% LS regions (Gibriel *et al.*, 2019). The analyzed core genomes displayed an average gene number of 9886 genes with 171 genes classified as effector genes by bioinformatical prediction. For the LS regions of these strains a total gene number ranging from 517 to 1318 was predicted, with an average effector gene number of 15. Similar results were previously published for comparison of a smaller group of *V. dahliae* strains (de Jonge *et al.*, 2013), suggesting that the relative number of genes important for niche adaptation is enriched in LS regions in *V. dahliae*. Focusing on bioinformatically predicted effector genes in LS regions, virulence factors have been identified in different *V. dahliae* strains (de Jonge *et al.*, 2013; Faino *et al.*, 2016; Kombrink *et al.*, 2017; Li, 2019, Dissertation, University Wageningen). Examples that contribute to pathogenicity are the *in planta* induced effector Ave1 from a subset of *V. dahliae* strains (de Jonge *et al.*, 2012; Faino *et al.*, 2016; Song *et al.*, 2018), the chitin-binding lysin motif effector LysM unique in VdLs.17

(Kombrink *et al.*, 2017), the defoliating pathotype-specific D effector (Li, 2019, Dissertation, University Wageningen), and the effector Sun1 (sunflower 1) specifically required for full pathogenicity of *V. dahliae* strains in sunflower infection (Li, 2019, Dissertation, University Wageningen). The effector protein Tom1 (tomato 1) was found to be essential for pathogenicity on tomato plants following identification of LS regions present in 11 tomato-infecting *V. dahliae* strains in comparison to six strains, which were avirulent on this host (Li, 2019, Dissertation, University Wageningen).

Even if the effector genes were found to be enriched in *V. dahliae* LS regions in comparison to the less flexible core genome, the number of effector genes relative to the total number of genes encoded in the LS regions is rather small (de Jonge *et al.*, 2013; Gibriel *et al.*, 2019). Different to the studies, comparing *V. dahliae* isolates, Klosterman *et al.* identified LS regions of *V. dahliae* by comparison to *V. alfalfae* genomes (formerly *V. albo-atrum*) and found the same relative numbers of secreted proteins in the core and LS regions (Klosterman *et al.*, 2011). Besides transposable elements, the flexible regions contained gene duplications and genes, which were predicted to be potentially involved in pathotype specificity, signaling processes, transcriptional regulation, degradation of plant material, and iron or lipid metabolism (Klosterman *et al.*, 2011). The role of LS genes in niche adaptation different to effector genes remains to be elucidated.

1.2.2 Interspecific hybridization of *Verticillium longisporum*

Genome evolution and niche adaptation through interspecific hybridization was described in several plant colonizing fungi, including the Brassicaceae colonizer *V. longisporum* (Clewes *et al.*, 2008; Oberhofer & Leuchtmann, 2012; Stukenbrock *et al.*, 2012; Menardo *et al.*, 2016). *V. longisporum* is the only interspecific hybrid of its genus with an amphidiploid genome (Clewes *et al.*, 2008). The species evolved from at least three separate hybridization events from two haploid parental lineages (Inderbitzin *et al.*, 2011b; Figure 2). Hybridization occurred for all known *V. longisporum* lineages between one unknown species named A1, which is a close relative of *V. alfalfae*, and either one of two *V. dahliae* species named D2 and D3, or another unknown species named D1, as a close relative of *V. dahliae* (Inderbitzin *et al.*, 2011b). The lineage A1/D2 has been exclusively detected in the USA, whereas the lineages A1/D1 and A1/D3 have been identified in Europe, Japan and the USA (Zeise & von Tiedemann, 2002; Tran *et al.*, 2013; Depotter *et al.*, 2017). A1/D1 and A1/D3 lineages were found as coexisting species as, for example, the A1/D1 isolate Vl43 and the A1/D3 isolate Vl32 analyzed in this study, which were obtained from fields in the same area in Germany (Zeise & von Tiedemann, 2002; Tran *et al.*, 2013). The three hybrids display differences in pathogenicity towards different host plants, with lineages A1/D1 as the most pathogenic

on rapeseed, A1/D2 as the most pathogenic on cabbage and horseradish, and lineage A1/D3 as the least pathogenic, but also found in rapeseed (Novakazi *et al.*, 2015; Figure 2). Overall, *V. longisporum* lineages are mainly virulent on Brassicaceae (Zeise & von Tiedemann, 2002; Eynck *et al.*, 2007), whereas the haploid species *V. dahliae* and *V. alfalfae* cause disease in different hosts (Pegg & Brady, 2002), but are less successful on Brassicaceae (Zhou *et al.*, 2006). One theory is, that the increased fitness of *V. longisporum* on Brassicaceae in comparison to the parental lineages might have outcompeted the unknown parental lineages A1 and D1 (Depotter *et al.*, 2016b).
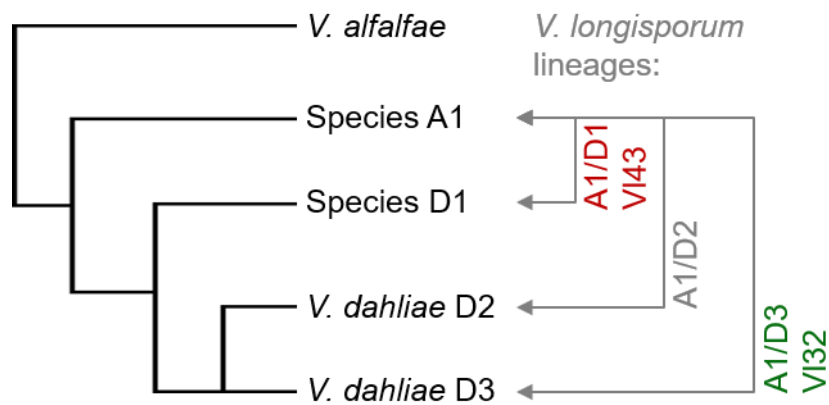
Figure 2: Evolution of *V. longisporum* hybrids. The interspecific hybrids belonging to the species *V. longisporum* evolved at least three times by separate hybridization events, resulting in the lineages A1/D1, A1/D2, and A1/D3. The species A1 is an unknown species, which is phylogenetically closer to *V. alfalfae*. The species D1 is another unknown species closer related to *V. dahliae*. The parental lineages D2 and D3 are *V. dahliae* strains. The lineage A1/D2 has been found exclusively in the USA, whereas the lineages A1/D1 and A1/D3 have been identified in Europe, Japan and the USA (Depotter *et al.*, 2017) and were found as coexisting species. The A1/D1 isolate Vl43 and the A1/D3 isolate Vl32 were obtained from fields in the same area in Germany and are studied in this work (Zeise & von Tiedemann, 2002; Tran *et al.*, 2013). Arrows indicate parental species of *V. longisporum* lineages. The tree is not scaled. (Modified from Inderbitzin & Subbarao, 2014).

Mechanisms leading to hybridization are either sexual mating or the fusion of hyphae. Even if the prerequisites for sexual mating, including mating and meiosis-specific genes, are given in the genomes of Verticillia, a sexual reproduction stage has not been described for any species of the genus (Short *et al.*, 2014; Milgroom *et al.*, 2014). Opposite idiomorphs of the *MAT* locus, the major regulators of sexual recombination in ascomycetes, are required for sexual compatibility (Metzenberg & Glass, 1990; Turgeon & Yoder, 2000; Debuchy & Turgeon, 2006). Most characterized *V. longisporum* isolates harbor copies of the *MAT1-1* idiomorph in their genomes (Inderbitzin *et al.*, 2011b; Depotter *et al.*, 2017). Recently two isolates were described to contain two copies of the *MAT1-1* idiomorph and one *MAT1-2* idiomorph, each (Fogelqvist *et al.*, 2018). In

contrast, in a collection of 1120 *V. dahliae* isolates the distribution of the mating type was skewed towards *MAT1-2* among isolates with 99% (Short *et al.*, 2014). The observation of extensive sequence changes in the *MAT* loci and the absence of intermixing between genetic clusters in population structure analysis suggests that sexual reproduction of *V. longisporum* is unlikely (Depotter *et al.*, 2017).

Another mechanism causing hybridization of genomes is parasexual reproduction by hyphal anastomosis followed by fusion of nuclei, which results in duplication of the parental genomes (Karapapa *et al.*, 1997; Depotter *et al.*, 2016b). Vegetative self-anastomoses of *V. longisporum* hyphae have been observed on specific media (unpublished data Rabea Schlüter, University of Greifswald). However, the observation of interspecific vegetative hyphal fusions of haploid Verticillia relies on auxotrophic mutants and respective selection in the laboratory and does not allow conclusions about the field situation (Hastie, 1973, 1989).

1.3   Mitogen-activated protein kinase signaling

As a result of niche adaptation conserved signaling pathways were shown to be modified in several species. This was also shown for mitogen-activated protein kinase (MAPK) signaling cascades. These cascades are activated by external signals enabling organisms to adapt to certain environmental conditions as ,for example, the germination and activation of infection-related programs following perception of a host plant. The core module of MAPK signaling pathways consists of a MAP kinase kinase kinase (MAP3K), a MAP kinase kinase (MAP2K), and a MAP kinase (MAPK) that sequentially phosphorylate one another and regulate downstream targets by phosphorylation. This module is highly conserved among eukaryotes from yeast to plants and mammals (Widmann *et al.,* 1999). Different MAPK pathways share several components, like the MAP kinases, adaptor proteins or upstream kinases. Certain MAPK cascade scaffold proteins are necessary to bring the components of the MAPK module in proximity and maintain pathway specificity (Schaeffer & Weber, 1999; Patterson *et al.*, 2010). In *Saccharomyces cerevisiae* five MAPK cascades are described, which are defined by the name of the final MAPK: cell wall remodeling is mediated by the MAPK Slt2 (Suppressor of lytic phenotype), response to high osmolarity is achieved by Hog1 (High osmolarity glycerol response), Smk1 (Sporulation-specific mitogen-activated protein kinase) is required for sporulation, Kss1 (Kinase suppressor of Sst2 mutations) induces cell cycle arrest and invasive filamentous growth, and Fus3 (cell fusion 3) regulates mating as a response to pheromones (Herskowitz, 1995; Madhani & Fink, 1998). Within ascomycetes homologs of three MAPK cascades, the Fus3/Kss1, Slt2 and Hog1 signaling pathways, can be found (Turrà *et al.*, 2014). Most filamentous fungi have only

one MAPK homologous to the yeast Fus3 and Kss1 MAPK (Jiang *et al.,* 2018a). During this study the role of a potential scaffold protein for the yeast Fus3/Kss1-like MAPK pathway, known to be essential for pathogenicity of *V. dahliae,* was analyzed. Further, the MAP2K of the corresponding MAPK pathway was characterized. The MAPK signaling cascade is best described in *S. cerevisiae* and the nomenclature often refers to this organism.

1.3.1 Fus3 and Kss1 MAPK signaling in *Saccharomyces cerevisiae*

The yeast pheromone response MAPK pathway is activated upon pheromone binding to the guanine nucleotide-binding (G)-protein coupled membrane receptors Ste2/Ste3 (Sterile2/3), recruiting the scaffold protein Ste5 (Sterile5) to the membrane (Hamel *et al.,* 2012; Figure 3A). The membrane-bound βγ-subunits of the G-protein bind the kinase Ste20 (Sterile20) and the scaffold protein Ste5 to initiate signaling (Sabbagh *et al.,* 2001). Ste20 phosphorylates the first kinase of the MAPK module Ste11 (Sterile11; Van Drogen *et al.,* 2001). Ste11 (MAP3K) assembles with the other pathway components Ste7 (Sterile7; MAP2K), and the MAPK Fus3 at the membrane by binding to the scaffold protein Ste5 (Choi *et al.,* 1994; Marcus *et al.,* 1994; Printen & Sprague, 1994; Kranz *et al.,* 1994; Pryciak & Huntress, 1998), and the adaptor protein Ste50 (Sterile50; Wu *et al.,* 1999; Xu *et al.,* 1996). The MAPK Fus3 as well as the partially redundant MAPK Kss1 are phosphorylated in response to pheromones by Ste7. However, only Fus3 interacts with the scaffold protein Ste5 (Bardwell *et al.,* 1998; Sabbagh *et al.,* 2001; Good *et al.,* 2009). Phosphorylated Fus3 migrates to the nucleus and activates the transcription factor Ste12 (Sterile12), which forms homodimers and regulates mating-specific pheromone responsive genes (Van Drogen *et al.,* 2001). Besides, Fus3 targets the transcription factor Tec1 (Transposon enhancement control) for degradation by phosphorylation (Chou *et al.,* 2006).

The invasive filamentous growth MAPK pathway is activated upon nutrient limitation by the transmembrane receptors Sho1 (Synthetic high osmolarity-sensitive) and Msb2 (Multicopy suppression of a budding defect; Mösch *et al.,* 1999; Hamel *et al.,* 2012; Figure 3A). Heterodimers of Ste12 and Tec1 can be formed and activate filamentation specific genes (Chou *et al.,* 2006).

The invasive filamentous growth and the pheromone response MAPK pathways share several components, including the core MAPK module consisting of Ste11, Ste7, and Kss1, as well as the adaptor protein Ste50, and the kinase Ste20, but activate different responses. The yeast MAPK Kss1 phosphorylates the transcription factors Ste12, which interacts with Tec1 upon nutrient-rich conditions and induces invasive or pseudohyphal growth (Hamel *et al.,* 2012).
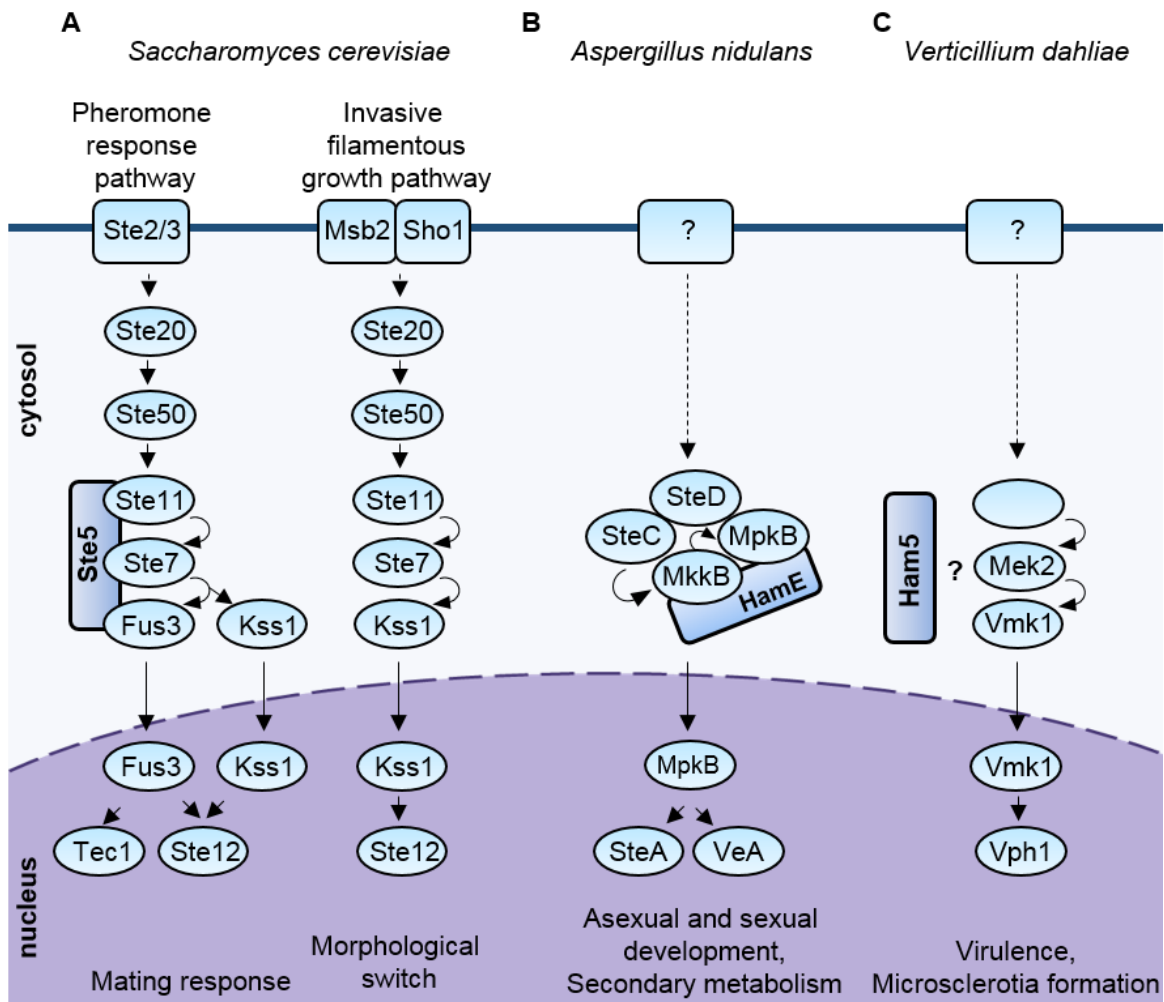
Figure 3: The yeast Fus3 and Kss1 MAPK pathways and homologous cascades in filamentous ascomycetes *A. nidulans* and *V. dahliae*. (**A**) In *S. cerevisiae* the scaffold protein Ste5 is required for assembly and maintenance of pathway specificity in response to pheromones. This leads to phosphorylation of the transcription factors Ste12 and Tec1. Ste12 regulates mating responsive genes. Phosphorylated Tec1 is targeted for degradation. The invasive filamentous growth pathway shares the core MAPK module, but is independent from Ste5. It induces a morphological switch in response to starvation, which is regulated by Tec1-Ste12 heterodimers (modified from Hamel *et al.*, 2012). (**B**) In *A. nidulans* the Ste5 orthologous scaffold protein HamE interacts with the MAP2K MkkB and the MAPK MpkB. The MAP3K SteC interacts with the Ste50-like adaptor protein SteD and the MAP2K MkkB. The cascade results in phosphorylation of the Ste12-like transcription factor SteA and the velvet protein VeA in the nucleus and, thereby, regulates genes involved in asexual and sexual development and secondary metabolism (based on Frawley *et al.*, 2018). (**C**) In plant pathogenic fungi the Fus3/Kss1-like MAPK is essential for pathogenicity, as Vmk1 in *V. dahliae*. Requirement of a scaffold protein in this pathway was not described in any pathogenic filamentous ascomycete, whereas several components of the cascade were described in many organisms. In *V. dahliae* only the MAPK Vmk1 and the Ste12-like transcription factor Vph1 were characterized (Sarmiento-Villamil *et al.*, 2018; Rauyaree *et al.*, 2005). The other components of the MAPK core module in *V. dahliae* are not yet described. During this study the MAP2K Mek2 and the *A. nidulans* HamE/ *N. crassa* HAM-5 homolog in *V. dahliae* were characterized. (More details are given in the text).

1.3.2   Scaffolds in Fus3/Kss1 MAPK signaling in filamentous ascomycetes

Whereas many components of the yeast Fus3/Kss1 MAPK homologs were studied in filamentous ascomycetes for years, orthologs to the scaffold protein Ste5 were identified only recently.

The first ortholog to the yeast scaffold Ste5 encoding gene was identified in the ascomycete *Neurospora crassa* (Dettmann *et al.*, 2014; Jonkers *et al.*, 2014). During chemotropic growth, the *N. crassa* scaffold protein HAM-5 (Hyphal anastomosis mutant 5) assembles a MAPK cascade of NRC-1 (MAP3K), MEK-2 (MAP2K) and MAK-2 (MAPK), anchored to the membrane via the adaptor protein STE-50 (Dettmann *et al.*, 2014; Jonkers *et al.*, 2014). The scaffold protein HAM-5 directly interacts with STE-50 and the MAPK MAK-2, whereas indirect interaction was proposed with the MAP2K MEK-2 and the MAP3K NRC-1 (Dettmann *et al.*, 2014). HAM-5 was described to be essential for oscillation of the MAPK module assembly and disassembly at opposing tips of germlings or hyphae leading to fusion in *N. crassa* (Fleissner *et al.*, 2009; Aldabbous *et al.*, 2010; Fu *et al.*, 2011; Dettmann *et al.*, 2014; Jonkers *et al.*, 2014).

A homolog to *N. crassa* HAM-5, named HamE, was identified in *Aspergillus nidulans* (Frawley *et al.*, 2018). HamE was proposed as a scaffold of the pheromone pathway with roles in regulation of sexual and asexual development as well as in secondary metabolite production (Bayram *et al.*, 2012; Frawley *et al.*, 2018). HamE interacts with the MAP2K MkkB and the MAPK MpkB, but not with the MAP3K SteC (Bayram *et al.*, 2012; Frawley *et al.*, 2018). The MAPK module is anchored to the membrane via the yeast Ste50 homolog SteD (Bayram *et al.*, 2012; Frawley *et al.*, 2018; Figure 3B). In *A. nidulans*, HamE is required for efficient phosphorylation of the MAPK, which regulates the yeast Ste12-like transcription factor SteA as well as the velvet protein VeA, both important for fungal development and secondary metabolite production (Bayram *et al.*, 2012; Frawley *et al.*, 2018).

1.3.3   Fus3/Kss1 MAPK signaling in plant pathogenic fungi

MAPK cascades of both partners are involved in the establishment of the plant-pathogen interaction (Hamel *et al.*, 2012). In response to the recognition of pathogen-associated molecular patterns (PAMPs) the plant activates defense genes via MAPK cascades and calcium signaling, known as PAMP-triggered immunity (Ali & Reddy, 2008). In ascomycetous plant pathogens MAPK pathways corresponding to the *S. cerevisiae* Fus3/Kss1, Slt2, and Hog1 cascades can be found (Turrà *et al.*, 2014). The MAPK pathways display conserved, as well as species-specific roles, as they are involved in chemotropic sensing of plant root exudates, regulation of adhesion, infection-related morphogenesis, cell wall composition, stress response, and formation of dormant

structures (Xu, 2000; Zhao *et al.*, 2007; Ali & Reddy, 2008; Rispail *et al.*, 2009; Rana *et al.*, 2017).

The best described MAPK in phytopathogens with the highest conservation in its impact on virulence is the Fus3/Kss1 MAPK. This pathway controls virulence in diverse fungal pathogenic species with different life styles, developing different infection structures, and colonizing plants from different infection sites, including stomata, roots, and plant surfaces (Hamel *et al.*, 2012). In appressoria-forming plant pathogenic ascomycetes as *Magnaporthe oryzae,* the Fus3/Kss1-like MAPK is essential for appressorium formation (Xu & Hamer, 1996; Lev *et al.*, 1999; Takano *et al.*, 2000; Ruiz-Roldán *et al.*, 2001; Hamel *et al.*, 2012; Jiang *et al.*, 2018a). MAPK-deficient mutants of the non-appressorium forming multi-host pathogen *F. oxysporum* displayed defects in plant penetration as well, correlated with decreased gene expression of pectate lyases (Di Pietro *et al.*, 2001). In contrast, the MAPK is dispensable for pathogenicity in mice (Ortoneda *et al.*, 2004). A role of the Fus3/Kss1-like MAPK in regulation of cell wall degrading enzymes (CWDEs) was observed as well in other phytopathogens (Lev & Horwitz, 2003; Jiang *et al.*, 2018a). The pathway displays positive regulatory effects on secondary metabolite and sclerotia production in some species (Chen *et al.*, 2004; Jiang *et al.*, 2018a). Upstream components of the cascade, like the MAP2K Ste7 and the MAP3K Ste11, as well as the adaptor protein Ste50, and homologs of the downstream transcription factor Ste12 display similar roles in virulence of different plant pathogenic fungi (Park *et al.*, 2002, 2006; Zhao *et al.*, 2005; Zhao & Xu, 2007; Rispail & Di Pietro, 2009; Li *et al.*, 2012).

In *V. dahliae* only the MAPK homolog Vmk1 and the downstream Ste12-like transcription factor Vph1 were characterized (Figure 3C). A conserved essential role in pathogenicity was described for Vmk1 and MAPK-deficient mutants displayed reduced conidiation and microsclerotia formation (Rauyaree *et al.*, 2005). No alterations in their *ex planta* phenotype or in conidiation, but impaired hyphopodia formation and penetration of the root cortex were observed for Vph1-deficient mutants (Sarmiento-Villamil *et al.*, 2018).

A scaffold protein of the Fus3/Kss1-like MAPK signaling pathway was not yet analyzed in any filamentous phytopathogen. However, homologs to *N. crassa* HAM-5 were described to be highly conserved among Pezizomycotina, the biggest subdivision of the Ascomycota, before its scaffold-function was described in any species (Jamet-Vierny *et al.*, 2007). In this work, the role of the HAM-5 homolog was studied in *V. dahliae* combined with the characterization of the MAP2K homolog Mek2, and the MAPK Vmk1 as control.

1.4   The unfolded protein response

Perception of the plant host is transduced by intracellular fungal transduction pathways leading to the upregulation of several genes encoding for proteins involved in plant host colonization. Many of these proteins have to be secreted to facilitate their role in host-fungus interactions. In hemibiotrophic fungi, secretion occurs in waves to induce an initial biotrophic interaction followed by a necrotrophic phase. During initial invasion of the host barriers, extracellular degradation enzymes like CWDEs, or hydrolytic enzymes are required. Subsequent systemic colonization relies on successful adaptation to a new environment by establishment of the nutrient uptake and suppression of the host immune system by effectors or toxic proteins. In later stages, lytic enzymes and defense response activating effectors are secreted (O'Connell *et al.*, 2012; Lo Presti *et al.*, 2015). These processes require increased protein processing and preparation for secretion via the Golgi apparatus, which is accomplished by the endoplasmic reticulum (ER).

The ER is a branched membrane system fused with the outer membrane of the nucleus, which is able to adapt to developmental or environmental conditions (Schwarz & Blower, 2016). In situations requiring increased protein folding and secretion capabilities, the ER senses the imbalance of incoming proteins and protein folding capacity of the cell organelle and triggers expression of genes involved in ER stress relief, referred to as unfolded protein response (UPR) (Kozutsumi *et al.*, 1988; Kohno *et al.*, 1993; Hetz, 2012; Heimel, 2015). These genes encode chaperones, foldases, glycosylation enzymes, as well as proteins required for vesicle transport, ER-associated degradation (ERAD), lipid biosynthesis, and regulators for adaptation of the ER size (Cox *et al.*, 1993; Kaufman, 1999; Travers *et al.*, 2000; Conn, 2011; Hetz, 2012). Whereas in mammals three ER transmembrane receptors, IRE1, PERK, and ATF6 are involved in UPR signaling to the nucleus (Ron & Walter, 2007; Hetz, 2012), in fungi, only the signal transduction pathway initiated by the sensor Ire1 (Inositol requiring 1) was described (Mori *et al.*, 1993; Okamura *et al.*, 2000; Kohno, 2010). This pathway is conserved in eukaryotes, however, species-specific adaptations can be observed. Especially the function of the basic leucine zipper (bZIP) transcription factor Hac1 (Homologous to Atf/Creb1) varies between different organisms and will be focused during this work in respect to its role in fungal differentiation and virulence of *V. dahliae*. In the following, the UPR pathway of *S. cerevisiae* will be summarized as paradigm and UPR functions in pathogenic fungi will be introduced.

1.4.1   The unfolded protein response pathway in *Saccharomyces cerevisiae*

ER stress causes a developmental block in the transition from the yeast form to pseudohyphal growth and sporulation in *S. cerevisiae* (Schröder *et al.,* 2000). The yeast

unfolded protein response is based on perception of un- or misfolded proteins in the ER lumen by the transmembrane sensor Ire1 (Mori *et al.*, 1993; Cox *et al.*, 1993; Figure 4). Ire1 possesses a three domain structure: an ER luminal N-terminal domain, as well as the cytoplasmic kinase, and the endoribonuclease domains. In presence of un- or misfolded proteins, Ire1 oligomerizes and proteins auto-phosphorylate each other via the cytoplasmic kinase domains and the cytoplasmic endoribonuclease domain is activated (Shamu & Walter, 1996; Welihinda & Kaufman, 1996; Sidrauski & Walter, 1997; Okamura *et al.*, 2000; Figure 4).
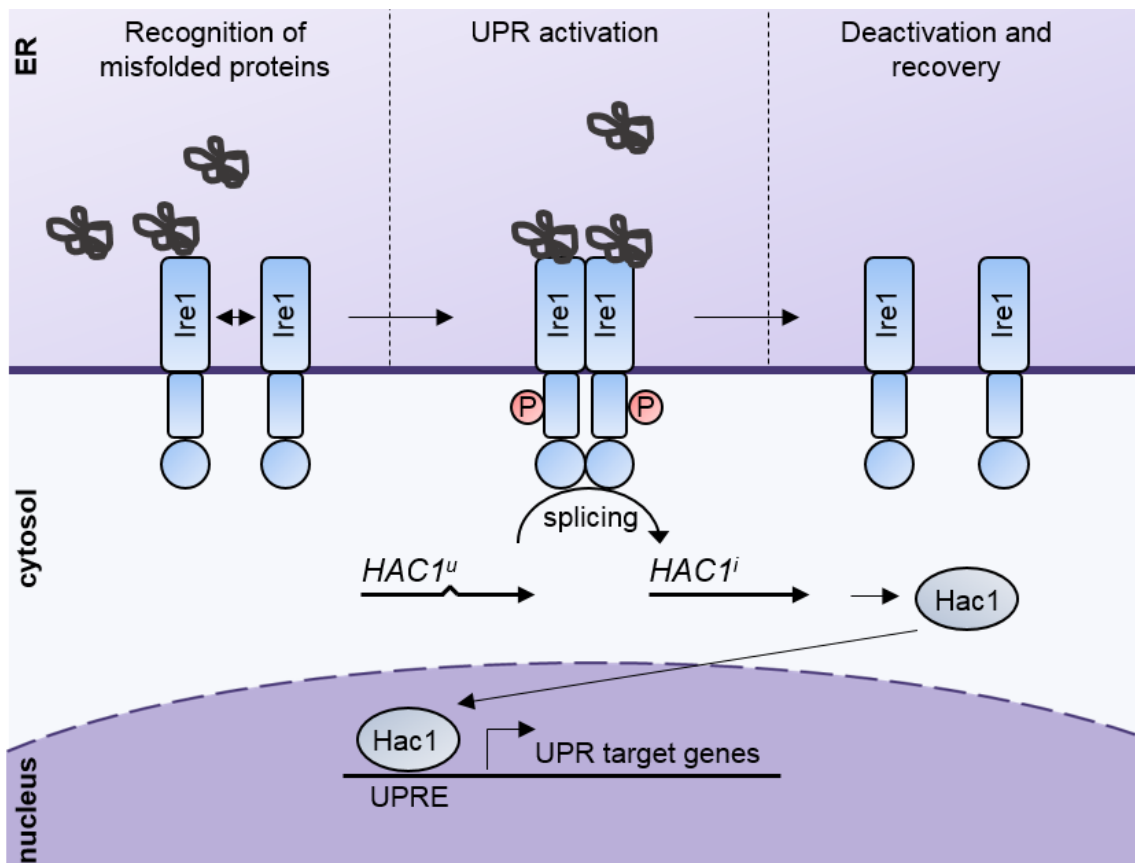
Figure 4: Hac1 is the central unfolded protein response regulator in *S. cerevisiae*. ER stress is perceived by the transmembrane sensor Ire1 in the presence of un- or misfolded proteins in the ER lumen. Ire1 proteins oligomerize and activate autophosphorylation by its cytosolic kinase domain. Thereby, the endoribonuclease domain of Ire1 is activated, resulting in unconventional splicing of the *HAC1^u* mRNA. The spliced *HAC1* mRNA (*HAC1^i*) is translated into the bZIP transcription factor Hac1. Hac1 migrates to the nucleus and regulates UPR target genes with unfolded protein response elements (UPRE) in their promotor regions, like genes encoding for chaperones, foldases, or genes involved in ER-associated degradation (ERAD) or ER expansion, resulting in ER stress relief (based on Heimel, 2015).

The endoribonuclease activity is required for unconventional splicing of the bZIP transcription factor Hac1 encoding mRNA (Sidrauski & Walter, 1997; Gonzalez *et al.*, 1999; Figure 4). Subsequent ligation of the exons is processed by the tRNA ligase Trl1 (Sidrauski *et al.*, 1996; Sidrauski & Walter, 1997). Translation of the unspliced mRNA variant into Hac1[u] is suppressed by base-pairing interaction between the unconventional intron and the 5´UTR (Chapman & Walter, 1997; Rüegsegger *et al.*, 2001).

Furthermore, translation of the unspliced mRNA correlated with accelerated degradation of very unstable Hac1[u] proteins was suggested (Di Santo *et al.*, 2016). Splicing of the *HAC1[u]* mRNA results in the mRNA variant *HAC1[i]*, which is translated into the stable Hac1 protein. Hac1 migrates into the nucleus where it regulates UPR target genes (Mori *et al.*, 1996, 1998; Figure 4). Several of these genes possess a specific palindromic sequence, named UPR element (UPRE), in their promotor regions (Mori *et al.*, 1996, 1998). Expression of UPR target genes mediates ER stress relief by increasing the folding capacity, ER expansion and degradation of misfolded proteins via the ERAD pathway (Cox *et al.*, 1993; Kaufman, 1999; Travers *et al.*, 2000; Jonikas *et al.*, 2009; Heimel, 2015).

1.4.2   The unfolded protein response pathway in pathogenic fungi

Ire1-dependent UPR signaling for regulation of genes involved in ER stress relief was observed as a conserved mechanism for ER stress relief and virulence of several pathogenic fungal species colonizing animal or plant hosts (Cheon *et al.*, 2011; Joubert *et al.*, 2011; Richie *et al.*, 2011; Krishnan & Askew, 2014; Heimel, 2015). The role of homologs and orthologs of the UPR regulatory transcription factor Hac1 varies in human or plant pathogenic fungal species (Krishnan & Askew, 2014).

The ER stress response mechanism of the opportunistic human pathogenic yeast *Candida glabrata* is regulated in an Ire1-dependent decay independently of Hac1 (Miyazaki *et al.*, 2013). This results in splicing of various ER-associated mRNAs by Ire1 as primary mechanism to cope with ER stress (Miyazaki *et al.*, 2013; Heimel, 2015).

In yeast and filamentous ascomycetes, translation of the uninduced *HAC1* mRNA variant into an alternative protein Hac1[u] was described to be blocked by different mechanisms (Chapman & Walter, 1997; Rüegsegger *et al.*, 2001; Saloheimo *et al.*, 2003; Mulder *et al.*, 2004; Joubert *et al.*, 2011; Heimel, 2015). In the basidiomycete *U. maydis*, translation of the unspliced *cib1* (Clp1 interacting bZIP1) mRNA into Cib1[u], possessing a UPR repressing function and an additional Cib1-independent function in ER stress response, was assumed similar to the mechanisms observed in higher eukaryotes (Yoshida *et al.*, 2006, 2009; Heimel *et al.*, 2013).

Hac1 homologs and orthologs are required for regulation of vegetative growth under ER stress inducing growth conditions in most tested fungal species (Richie *et al.*, 2009; Cheon *et al.*, 2011; Joubert *et al.*, 2011; Heimel *et al.*, 2013; Montenegro-Montero *et al.*, 2015). However, the impact of the UPR on vegetative growth under non-stress conditions is species-specific and varies from unaltered growth in absence of ER stressors (Cheon *et al.*, 2011; Heimel *et al.*, 2013; Heimel, 2015), over impacts on conidia or cell morphology (Wimalasena *et al.*, 2008; Joubert *et al.*, 2011), to functions specifically important on complex substrates (Richie *et al.*, 2009; Montenegro-Montero *et al.*, 2015).

A crosstalk between the cell wall integrity (CWI) MAPK pathway and the UPR pathway was suggested following the observation that UPR-deficient strains displayed increased sensitivity not only in response to ER stressors, but as well to cell wall perturbing agents, as for example in *C. albicans*, *C. neoformans*, and *A. fumigatus* (Richie *et al.*, 2009, 2011; Cheon *et al.*, 2011; Malavazi *et al.*, 2014). In the necrotrophic plant pathogenic fungus *A. brassicicola*, the loss of virulence of mutants deficient in the UPR pathway was suggested to be caused by increased susceptibility to antimicrobial plant metabolites inducing membrane damage (Joubert *et al.*, 2011; Guillemette *et al.*, 2014). In contrast, sensitivity to cell wall perturbing agents was unaffected in Hac1-deficient strains of the saprophytic fungus *N. crassa* (Montenegro-Montero *et al.*, 2015).

Besides the role in counteracting host antimicrobial compounds in *A. brassicicola*, the UPR pathway was described to be linked to infection-related morphogenesis, adaptation of the secretion capacity during plant invasion and colonization, and recently also to the regulation of ER stress independent virulence factors (Cheon *et al.*, 2011; Joubert *et al.*, 2011; Richie *et al.*, 2011; Heimel *et al.*, 2013; Hampel *et al.*, 2016; Pinter *et al.*, 2019). In the rice blast fungus *M. oryzae*, homologs of the heat shock protein Bip1 and the bZIP transcription factor Hac1 are involved in induction of the ER stress response and are essential for asexual development and penetration of the plant surface (Yi *et al.*, 2009; Tang *et al.*, 2015; Jiang *et al.*, 2018b). Appressorium formation and initial penetration of the plant surface was unaffected in the avirulent *A. brassicicola* mutant defective in the UPR regulator AbHacA (Joubert *et al.*, 2011). In the dimorphic corn smut fungus *U. maydis*, a morphogenic switch from budding to filamentous growth initiates pathogenic development (Boyce *et al.*, 2005). Here, a functional UPR is required for the mitotic growth of the fungus within the cell after formation of appressoria and penetration of the plant surface (Heimel *et al.*, 2010). Regulation of virulence-specific genes, like the effector genes *pit2* and *tin1-1,* were identified to be regulated by the UPR in the basidiomycete (Hampel *et al.*, 2016). Recently, a UPR-regulated virulence factor, the signal peptide peptidase Ssp1 with specific function in interference with plant defense

responses and dispensable for ER stress resistance, was identified in *U. maydis* (Pinter *et al.*, 2019).

Overall, the UPR pathway plays important roles in developmental processes and plant infections in several fungi. None of the UPR components was studied in Verticillia to date. During this study, the homolog of the bZIP transcription factor Hac1 was characterized in *V. dahliae*.

1.5 Oxylipins

The fungal secretome does not only include proteins, but also lipid metabolites, as oxygenated polyunsaturated fatty acids, named oxylipins. These fungal hormones act as trans-kingdom signaling molecules as they show conserved structures in fungi and plants (Brodhun & Feussner, 2011). Fungal oxylipins and their polyunsaturated fatty acid precursors are involved in fungal development and secondary metabolite production as well as in environmental adaptation. The signaling molecules were described to manipulate plant cellular processes in favor of the survival of the invader within the plant and, on the other hand, plant oxylipins can modulate fungal development (Calvo *et al.*, 2001; Brodhagen *et al.*, 2008; Brodhun *et al.*, 2009; Reverberi *et al.*, 2010; Scala *et al.*, 2014). Oxylipins contribute to fungal differentiation and might affect the outcome of the interaction of Verticillia with their hosts, which was analyzed in frame of this study. In the following, the role of fungal oxylipins in development and plant-fungus interactions will be introduced.

1.5.1 Oxylipins in fungal development

In fungi, fatty acid synthases produce long chain fatty acids. Unsaturated and polyunsaturated fatty acids are produced by introduction of double bonds by ER membrane-bound desaturases. These desaturases transfer electrons from the donor cytochrome b_5 and thereby reduce molecular oxygen to two molecules of water (Uttaro, 2006). The polyunsaturated fatty acid linoleic acid (18:2Δ9,12) is synthesized by oleate Δ12-fatty acid desaturases from oleic acid (18:1Δ9) by introduction of a second double bond into the carbon chain at position 12 from the carboxy-terminus (Uttaro, 2006; Figure 5). Linoleic acid is the most abundant fatty acid in mycelia of several fungal species and displays an important membrane component with functions in adaptation of membrane fluidity and the major precursor of fungal oxylipins (Rambo & Bean, 1974; Evans *et al.*, 1986; Castoria *et al.*, 1995; Goodrich-Tanrikulu *et al.*, 1998; Los & Murata, 1998; Gostinčar *et al.*, 2009; Brodhun & Feussner, 2011).
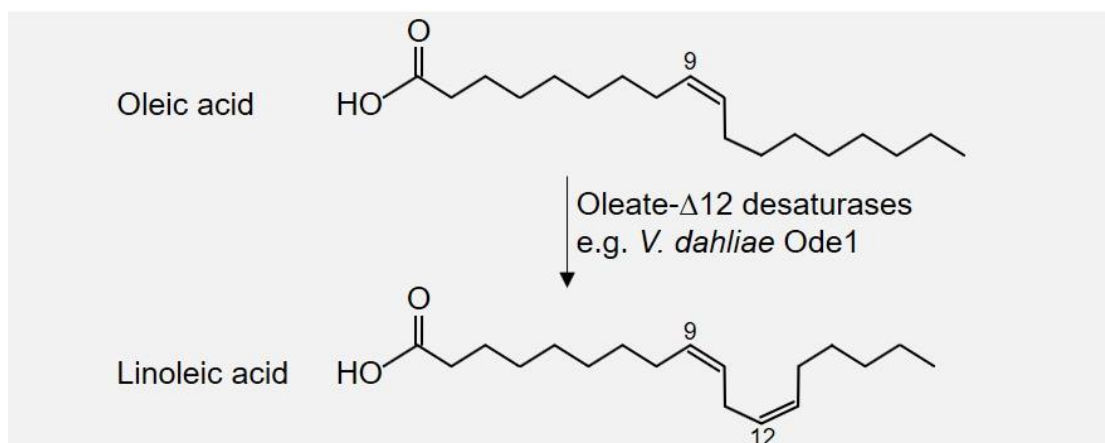
Figure 5: Linoleic acid biosynthesis by oleate Δ12-fatty acid desaturases. Linoleic acid is the most abundant fatty acid in fungal cells as an important component of the cell membrane and the major precursor of oxylipins (Rambo & Bean, 1974; Evans *et al.*, 1986; Castoria *et al.*, 1995; Goodrich-Tanrikulu *et al.*, 1998; Los & Murata, 1998; Gostinčar *et al.*, 2009; Brodhun & Feussner, 2011). Linoleic acid is synthesized by oleate Δ12-fatty acid desaturases, like OdeA in Aspergilli or OdeA corresponding protein Ode1 in *V. dahliae,* from oleic acid by introduction of a second double bond into the carbon chain at position 12 from the carboxy-terminus (Calvo *et al.*, 2001; Chang *et al.*, 2004; Wilson *et al.*, 2004; Uttaro, 2006).

In plants, lipoxygenases (LOXs) catalyze the initial step in oxylipin biosynthesis from polyunsaturated fatty acids whereas different enzymes catalyze oxylipin producing reactions from polyunsaturated fatty acid substrates in fungi (Brodhun & Feussner, 2011). These enzymes group into monooxygenases, LOXs, and cyclooxygenases (Fischer & Keller, 2016). The cyclooxygenases include the linoleate diol synthases (LDSs), also known as precious sexual inducer (Psi) factor-producing oxygenase (Ppo) enzymes (Andreou & Feussner, 2009; Brodhun & Feussner, 2011). Oxylipins were found to play significant roles in the coordination of developmental processes like conidiation, sclerotia formation, production of secondary metabolites, and quorum sensing (Calvo *et al.*, 2001; Brodhun *et al.*, 2009; Reverberi *et al.*, 2010; Brodhun & Feussner, 2011; Scala *et al.*, 2014).

In *A. nidulans* and *Aspergillus parasiticus*, mutants deficient in the conversion of oleic acid into linoleic acid as the major precursor of oxylipins were analyzed by the deletion of the oleate Δ12-fatty acid desaturases OdeA (Calvo *et al.*, 2001; Chang *et al.*, 2004; Wilson *et al.*, 2004). Mutants of both species displayed reduced vegetative growth and conidiation as well as altered ascospore formation. Additionally, a complete loss of sclerotia development was observed in the *A. parasiticus odeA*-deficient mutant (Chang *et al.*, 2004; Wilson *et al.*, 2004).

A. nidulans produces Psi factors, which promote sexual development (Champe & El-Zayat, 1989). Aspergilli possess three to four Ppo enzymes (PpoA, PpoB, PpoC, PpoD)

producing a ratio of these hormones to regulate the balance of asexual to sexual spores (Mazur & El-zayat, 1991; Tsitsigiannis *et al.*, 2004b, 2004a, 2005a, 2005b; Tsitsigiannis & Keller, 2007; Horowitz Brown *et al.*, 2009). Whereas products from PpoA and PpoB induce sexual sporulation, products of PpoC induce asexual sporulation in *A. nidulans* (Champe & El-Zayat, 1989; Tsitsigiannis *et al.*, 2004a, 2004b). Ppo enzymes also affect the balance between asexual and sexual spores in *A. fumigatus*, however, the effect of the different enzymes varies (Dagenais *et al.*, 2008). *Aspergillus flavus* produces a fourth Ppo enzyme, PpoD (Horowitz Brown *et al.*, 2009). In this organism, Ppo enzymes as well as a LOX, were found to regulate the density-dependent morphological transition of conidia to sclerotia as resting structures (Horowitz Brown *et al.*, 2008, 2009). A negative regulatory impact of a LOX on sclerotia production has been observed in *Aspergillus ochraceus* (Reverberi *et al.*, 2010). Besides their roles in regulation of sexual development and quorum sensing, Ppo enzymes are involved in secondary metabolite production in Aspergilli as they promote, for instance, the biosynthesis of the mycotoxins sterigmatocystin as well as aflatoxin and inhibit the production of penicillin (Tsitsigiannis & Keller, 2006; Horowitz Brown *et al.*, 2009). Homologous *ppo* genes were identified in several ascomycete and basidiomycete fungal species (Tsitsigiannis *et al.*, 2005b; Tsitsigiannis & Keller, 2007).

In summary, linoleic acid and oxylipin producing enzymes play crucial roles in fungal growth, development, and secondary metabolite production, which are species-specific and, in some cases, display antagonistic effects.

1.5.2 Oxylipins in plant-fungus interactions

Plant oxylipins were found to modulate fungal development and mycotoxin production and, *vice versa*, fungal oxylipins can manipulate the host lipid metabolism and alter plant defense responses presumably by mimicking endogenous signal molecules. In several cases, the interplay of plant and fungal oxylipins decides on the outcome of the interaction.

The plant stress and defense response to pathogens with different lifestyles is mediated by the hormone jasmonic acid (JA) and JA derivatives synthesized from linoleic acid (Thaler *et al.*, 2004) (Figure 6). Plants deficient in JA biosynthesis display increased susceptibility, for instance to Verticillia and *F. oxysporum* (Thaler *et al.*, 2004; Thatcher *et al.*, 2009; Riemann *et al.*, 2013; Fischer & Keller, 2016; Scholz *et al.*, 2018). Fungal species were described to produce oxylipins similar to the plant hormone JA and active or inactive JA derivatives to manipulate host defense reactions as, for example, *F. oxysporum* and *M. oryzae* (Husain *et al.*, 1993; Miersch *et al.*, 1999; Christensen & Kolomiets, 2011; Brodhun & Feussner, 2011; Andolfi *et al.*, 2014; Cole *et al.*, 2014;

Patkar & Naqvi, 2017; Chini *et al.*, 2018). Due to structural similarities, fungal oxylipins were suggested to be perceived by plant receptors and to mimic plant hormones for manipulation of the immune response (Feys, 1994; Brodhun & Feussner, 2011). The only known JA receptor to date is the F-box protein jasmonate receptor coronatine insensitive 1 (COI1) (Brodhun & Feussner, 2011). COI1 acts as a de-repressor of JA responsive genes by targeting the JAZ (jasmonate ZIM-domain) repressor proteins for degradation (Thines *et al.*, 2007). COI1-deficient *A. thaliana* mutants are insensitive to perception of activated jasmonoyl isoleucine (JA-Ile) derivatives. *F. oxysporum* and *V. longisporum* were found to induce disease symptoms in *Arabidopsis* plants dependent on the presence of COI1 (Thatcher *et al.*, 2009; Ralhan *et al.*, 2012; Cole *et al.*, 2014). However, this is restricted to isolates, which are able to produce JA derivatives in *F. oxysporum* (Cole *et al.*, 2014). Tomato infecting *F. oxysporum* isolates do not produce detectable jasmonates and COI1 is dispensable for virulence on tomato plants (Cole *et al.*, 2014).

Maize plants deficient in LOX3 displayed increased resistance to *Fusarium verticilloides* infection associated with decreased mycotoxin production (Gao *et al.*, 2007). *F. verticillioides* susceptible varieties were found to produce high levels of LOX3 products and the precursor linoleic acid (Dall'Asta *et al.*, 2012, 2015; Battilani *et al.*, 2018). In *F. verticillioides* the Linoleate Diol Synthase 1 (LDS1)-derived oxylipins act as negative regulators of vegetative growth, conidiation, and secondary metabolite production (Scala *et al.*, 2014). The signaling molecules induce LOX3, thereby, suppress the JA-mediated plant defense response and promote fungal virulence (Battilani *et al.*, 2018). Here, oxylipins from both interaction partners are essential for susceptibility (Battilani *et al.*, 2018).

In contrast to fungal oxylipins, which are mimicking plant hormones to suppress the plants defense responses, there are also examples for fungal oxylipins which activate plant defense responses for their benefit. The grapevine pathogen *Lasiodiplodia mediterranea* produces a JA precursor named JA ester lasiojasmonate A (LasA), which activates JA-regulated defense responses in plants presumably after conversion into the active JA-Ile derivative (Chini *et al.*, 2018). Fungal LasA was suggested to be produced in late stages of infection to induce cell death and facilitate fungal infection, but the mode of action of LasA has not been elucidated to date (Chini *et al.*, 2018).

Like pathogenic species, mutualistic fungi found their path to manipulate the host defense responses in order to establish their interaction (Patkar & Naqvi, 2017; Sanders, 2011). Manipulation of the host via oxylipins from mutualistic fungi was not described to date, whereas there are examples of fungal effectors targeting the plant´s jasmonate signaling pathway from *Trichoderma virens* and mycorrhizal fungi as *Laccaria bicolor*

(Djonovic *et al.*, 2007; López-Ráez *et al.*, 2010; Christensen & Kolomiets, 2011; Plett *et al.*, 2014; Patkar & Naqvi, 2017).
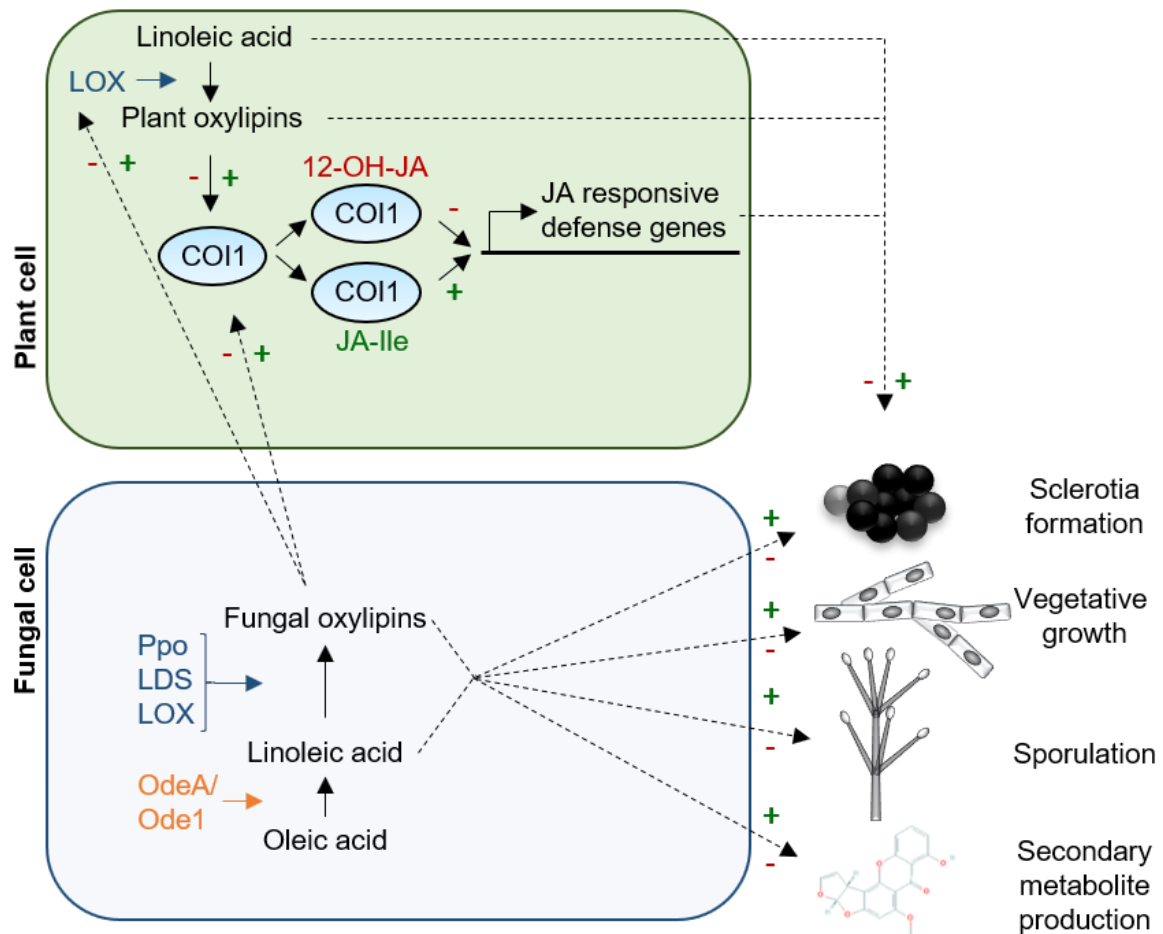
Figure 6: Fungal and plant oxylipins in crosstalk and fungal differentiation. Fungi synthesize oxylipins predominantly from linoleic acid, a polyunsaturated fatty acid which is produced by oleate Δ12-fatty acid desaturases like OdeA in Aspergilli (Calvo *et al.*, 2001; Chang *et al.*, 2004; Wilson *et al.*, 2004) or the corresponding *V. dahliae* desaturase Ode1. The conversion of linoleic acid into fungal oxylipins is catalyzed by different enzymes including precious sexual inducer (Psi) factor-producing oxygenase (Ppo) enzymes, linoleate diol synthases (LDS), and lipoxygenases (LOX) (Andreou & Feussner, 2009; Brodhun & Feussner, 2011; Patkar *et al.*, 2015; Fischer & Keller, 2016). Fungal oxylipins display positive and negative regulatory effects (indicated by arrows with plus and minus) on fungal growth, conidiation, sclerotia formation, and mycotoxin production. Furthermore, fungal oxylipins manipulate the host´s defense responses either by targeting the plant´s biosynthesis of oxylipins or the jasmonate (JA) binding F-box protein coronatine insensitive 1 (COI1) (indicated by arrows with plus and minus). Binding of active JA derivatives like jasmonoyl isoleucine (JA-Ile) to COI1 targets the jasmonate ZIM-domain (JAZ) repressors of JA responsive genes to the degradation machinery and, thereby, activates defense responses. Binding of 12-hydroxy JA (12-OH-JA) inactivates COI1 and negatively regulates JA responsive defense genes. Plant oxylipins regulate their defense responses and can modulate fungal growth, differentiation, and mycotoxin production.

In summary, the communication of fungi and plants via the production of endogenous and perception of exogenous oxylipins determines the susceptibility of the host plant or

the propagation of the fungus (Figure 6). To date, these enzymes were not analyzed in Verticillia and their role in fungal growth, development, and virulence is unknown. In this work *V. dahliae ODE1* coding for the oleate Δ12-fatty acid desaturase was identified for further characterization of its role in differentiation and virulence (Figure 5, Figure 6).

1.6   Aim of the study

Plant colonizing fungi and their hosts coevolve and develop constantly new specialized tools like effectors, oxylipins, mycotoxins, and CWDEs to benefit from or overcome the interaction. To succeed in colonization, these tools have to be prudently orchestrated during the different steps in colonization, which requires perception and adaptation to environmental conditions regulated by endogenous signaling cascades. Conserved signaling pathways were shown to be modified in several species in frame of niche adaptation.

The independently evolved *V. longisporum* lineages adapted to Brassicaceae as a host but display differences in their pathogenicity. In the course of this study, two *V. longisporum* isolates from different lineages and pathotypes but from fields in the same area in Germany (Zeise & von Tiedemann, 2002) were compared to investigate the genomic basis for the establishment of different pathotypes in related species. In the genomes of *V. dahliae*, a relative enrichment of genes with functions in niche adaptation was observed in LS regions (de Jonge *et al.*, 2013; Gibriel *et al.*, 2019). To date, LS regions in the genome of the hybrid *V. longisporum* were not analyzed. In first experiments, the colonization behavior of the two *V. longisporum* isolates in rapeseed plants was compared. Subsequently, LS regions present in the pathogenic and absent in the mutualistic colonizer were searched. In order to narrow down to interesting regions, an LS region originating from the *V. dahliae*-related parental species was focused. Deletion strains of this region were constructed in the pathogenic *V. longisporum* isolate and the haploid relative *V. dahliae* to characterize the role of LS regions in adaptation of the rapeseed colonizer *V. longisporum*.

The pathotype of a fungus depends on both, the defense responses of the host plant and the orchestration of tools enabling plant colonization. Sensing of the fungal environment and signal transduction are important mechanisms for adaptation and colonization of plants. The Fus3/Kss1-like MAPK signaling pathway in *V. dahliae* has a conserved role in fungal pathogenicity and, furthermore, the MAPK Vmk1 was described to positively regulate differentiation processes (Rauyaree *et al.*, 2005). Insulation of homologous pathways by a scaffold protein was recently elucidated in the filamentous ascomycetes *N. crassa* and *A. nidulans* (Dettmann *et al.*, 2014; Jonkers *et al.*, 2014; Frawley *et al.*, 2018). Homologs to these scaffold proteins have been identified bioinformatically in the

biggest subdivision of the Ascomycota, including Verticillia (Jamet-Vierny *et al.*, 2007). However, the role of the homolog has not yet been studied in any pathogenic species. Here, the function of the *V. dahliae* homolog Ham5 on the Fus3/Kss1-like MAPK pathway-mediated regulation of fungal differentiation and virulence was analyzed. Mutants deficient in the pathway components Vmk1 (MAPK) and Mek2 (MAP2K) were compared to a Ham5-deficient strain and double deletion strains defective in either Ham5/Vmk1 or Ham5/Mek2 regarding their vegetative growth, their ability to form microsclerotia, and virulence on tomato plants.

Signaling from the membrane coordinates the expression of tools involved in host colonization. This correlates with increased demands for processing and secretion of proteins in the ER, which requires a functional unfolded protein response (UPR). Variations of the role of the transcription factor Hac1 in development and virulence in different fungal species were observed (Krishnan & Askew, 2014). To date, the UPR is an unstudied field in Verticillia. In frame of this work, the role of the homologous bZIP transcription factor Hac1 in fungal differentiation, ER stress response, and virulence in *V. dahliae* was addressed. The *HAC1* homolog was identified and the occurrence of alternatively spliced mRNA variants was verified. *HAC1* deletion strains were constructed and complemented by ectopic integration of the alternative mRNA splice variants $HAC1^u$ and $HAC1^i$ with 3´-hemagluttinin tags or unspliced *HAC1*. It was tested if translation of $HAC1^u$ into a protein could be detected. The constructed strains were characterized regarding their vegetative growth under physiological and ER stress conditions, conidiation, formation of microsclerotia as resting structures, and virulence in tomato plants.

Besides protein tools, fungi and plants possess lipid metabolites as signaling molecules with significant impact on the outcome of the interaction (Brodhun & Feussner, 2011; Christensen & Kolomiets, 2011; Fischer & Keller, 2016; Patkar & Naqvi, 2017). Here, the so far unknown role of a functional oxylipin biosynthesis in growth, development, and virulence of *V. dahliae* was investigated. Therefore, an oleate Δ12-fatty acid desaturase, catalyzing the oxidation of oleic acid to the major oxylipin precursor linoleic acid, was identified. Localization of the enzyme was tested by fluorescence microscopy of GFP tagged versions. Mutants deficient in this desaturase were constructed and phenotypically analyzed *in planta* and *ex planta*.

2 MATERIALS AND METHODS

Media, buffers, and solutions used in this study were prepared with chemicals provided by AppliChem GmbH (Darmstadt, Germany), BD Biosciences (Heidelberg, Germany), Biozym Scientific GmbH (Hessisch Oldendorf, Germany), Carl Roth GmbH&Co.KG (Karlsruhe, Germany), Fluka (Neu-Ulm, Germany), Invitrogen (Karlsruhe, Germany), Merck KGaA (Darmstadt, Germany), Oxoid Deutschland GmbH (Wesel, Germany), Roche Diagnostics GmbH (Mannheim, Germany), Sigma-Aldrich Chemie GmbH (Munich, Germany), Serva Electrophoresis GmbH (Heidelberg, Germany), and VWR International GmbH (Darmstadt, Germany). The pH was determined with a WTW bench pH/mV Routine meter pH 526 (Sigma-Aldrich, Munich, Germany).

Ampicillin (Carl Roth GmbH&Co.KG), kanamycin (AppliChem), chloramphenicol (AppliChem), clonNAT nourseothricin dihydrogen sulfate (Werner Bioagents GmbH, Jena, Germany), cefotaxime (Wako Chemicals GmbH, Neuss, Germany), and hygromycin B (InvivoGen, San Diego, CA, USA) were used for selection of microorganisms. Small-scale sterile filtration of solutions was performed with Filtropur filters with a pore size of 0.2 µm (Sarstedt AG&Co, Nuembrecht, Germany). Fungal spores were filtered using Miracloth (Calbiochem Merck, Darmstadt, Germany). The Coulter Particle Count and Size Analyzer Z2 and the appropriate Coulter Isoton II Diluent (both Beckman Coulter, Krefeld, Germany) were used for conidiospore counting.

Restriction enzymes were obtained from Thermo Fisher Scientific (Schwerte, Germany) and NEB (Frankfurt am Main, Germany). The GeneArt Seamless Cloning and Assembly Kit and CloneJET PCR Cloning Kit were used from Thermo Fisher Scientific. RNase A was provided by AppliChem. Phusion High-Fidelity DNA polymerase, Taq DNA polymerase, corresponding polymerase buffers, and deoxynucleotides were obtained from Thermo Fisher Scientific (Schwerte, Germany). Q5 High-Fidelity DNA polymerase was purchased from New England Biolabs (Ipswich, MA, USA). Primers were obtained from Eurofins Genomics GmbH (Ebersberg, Germany) and Sigma-Aldrich Chemie GmbH (Munich, Germany). PCRs were performed in T Professional Standard 96, T Professional Trio 48, and T Professional Standard 96 Gradient thermocyclers (Biometra GmbH, Goettingen, Germany), and in Primus 96 Thermal Cyclers (MWG Biotech AG, Ebersberg, Germany). DNA was purified with the NucleoSpin Plasmid Kit or NucleoSpin Gel and PCR clean up Kit from Macherey-Nagel (Dueren, Germany). DNA and RNA concentrations were measured with a NanoDrop ND-1000 spectrophotometer from PeqLab Biotechnology GmbH (Erlangen, Germany). Protein concentrations were measured with an Infinite M200 microplate reader operated with Magellan software (both: Tecan Trading AG, Maennedorf, Switzerland).

RNA was extracted with the Direct-zol RNA MiniPrep Kit (Zymo Research, Freiburg im Breisgau, Germany). The GeneRuler 1 kb DNA ladder and GeneRuler 100 bp DNA ladder (Thermo Fisher Scientific) were used for DNA on-gel band size determination in DNA gel electrophoresis. The PageRuler Prestained Protein Ladder 10-180 kDa (Thermo Fisher Scientific) was used for protein on-gel band size determination. The following named electrophoresis equipment was obtained from BIO-RAD Laboratories (Hercules, CA, USA): DNA agarose gel electrophoresis was performed with Mini-Sub Cell GT chambers and the PowerPac 300 power supply, SDS polyacrylamide gel electrophoresis was conducted with the Mini-Protean Tetra Cell, Mini Trans-Blot Electrophoretic Cell and with the PowerPac 3000 power supply. Amersham Hybond-N nylon membrane for blotting of DNA from agarose gels and Amersham Protran 0.45 μm NC nitrocellulose blotting membrane for blotting of proteins from SDS-polyacrylamide gels were purchased from GE Healthcare life sciences (Munich, Germany). The Amersham AlkPhos Direct Labeling and Detection System was used for Southern hybridization analysis. The Amersham Hyperfilm-ECL (GE Healthcare life sciences, Munich, Germany) and the Optimax X-ray Film Processor from Protec GmbH&Co.KG (Oberstenfeld, Germany) were used for detection of chemiluminescence of Southern and western hybridization. Alternatively, chemiluminescence of western hybridization was visualized with the Fusion SL chemiluminescence detector (PeqLab, Erlangen, Germany). As primary antibodies α-GFP antibody sc-9996 (Santa Cruz Biotechnology, Santa Cruz, CA, USA) and α-HA (clone HA-7; Sigma-Aldrich Chemie GmbH) were used. As secondary antibodies horseradish peroxidase-coupled rabbit G21234 (Invitrogen) and mouse antibody 115-035-003 (Jackson ImmunoResearch, Newmarket, UK) were used.

Pipet tips, reaction tubes, petri dishes, and other plastic consumables were purchased from Sarstedt, StarLab GmbH (Hamburg, Germany), and Nerbe Plus GmbH (Winsen/Luhe, Germany). Centrifugation of 1.5 ml and 2 ml reaction tubes was performed with Heraeus Biofuge Fresco and Heraeus Pico Microcentrifuges from Heraeus Instruments GmbH (Hanau, Germany). For centrifugation of 15 ml and 50 ml tubes, Centrifuge 5804 R from Eppendorf AG (Hamburg, Germany) was used. The GFL (Burgwedel, Germany) shaking water bath 1086, Orbital shaker 3005, Orbital shaker 3020, and the Rotamax 120 (Heidolph, Schwabach, Germany) were used for incubations at constant agitation.

Plates for phenotypical analysis were scanned via Epson Perfection V600 Photo Scanner (Epson, Suwa, Japan). The binocular microscope SZX12-ILLB2-200 (Olympus Deutschland GmbH, Hamburg, Germany) illuminated with the KL1500-LCD light source (Olympus GmbH, Hamburg, Germany) and the Axiolab light microscope (Zeiss, Oberkochen, Germany) equipped with SC30 cameras (Olympus GmbH) and operated

with the cellSens Dimension version 1.4 software (Olympus GmbH) were used for observation of microsclerotia and hypocotyl discolorations of tomato stems.

The confocal Zeiss Observer Z1 microscope (Zeiss) equipped with a CSU-X1 A1 confocal scanner unit (Yokogawa, Ratingen, Germany), QuantEM:512SC digital camera (Photometrics, Tucson, AZ, USA) operated with the SlideBook 6.0 digital microscopy software (Intelligent Imaging Innovations, Goettingen, Germany) was used for fluorescence microscopy. The µ-Slide 8 well (IBIDI, Martinsried, Germany) microscopy chambers were used for localization studies. Vacuoles were visualized in fluorescence microscopy with FM4-64 Dye (Thermo Fisher Scientific).

Planting pots with 70x70x80 mm were purchased from Soparco GmbH (Saarbruecken, Germany). Fruhstorfer Erde Typ T Struktur 1 -fein- (Archut GmbH&Co.KG, Lauterbach, Germany) and 0.4-0.8 mm crystal silica sand (Dorsilit, Hirschau, Germany) were used. Plants were grown in a BrightBoy GroBank (CLF PlantClimatics, Emersacker, Germany). Materials and instrumentations, which were not listed here are indicated in the following chapters.

2.1 Organisms and their cultivation

All media and supplemental substances used in this study were prepared in deionized water and sterilized either by autoclaving at 121 °C for 20 min and 2 bar, or filter-sterilized through a 0.2 µm pore size membrane filter for temperature unstable substances.

2.1.1 Cultivation of bacteria

Escherichia coli and *Agrobacterium tumefaciens* strains were cultivated using liquid lysogeny broth (LB) medium (Bertani, 1951) [1% bacto-tryptone, 0.5% yeast extract, 1% NaCl, pH 7.5, 2% agar for solid medium] on a rotary shaker at 37 °C for *E. coli* and 25 °C for *A. tumefaciens*. Liquid SOC medium (2% bacto tryptone, 0.5% yeast extract, 10 mM NaCl, 2.5 mM KCl, 10 mM $MgCl_2$, 10 mM $MgSO_4$, supplemented with 20 mM glucose after autoclaving) was used for transformation of chemically competent *E. coli* and *A. tumefaciens* cells. Transformants were selected on solid LB medium by supplementation of 100 µg/ml ampicillin or 100 µg/ml kanamycin. For plasmid conservation equal volumes of bacterial overnight cultures and 100% glycerol were mixed and stored at -80 °C.

2.2.2 Cultivation of *Verticillium* strains

Conidia were cultivated in liquid simulated xylem medium (SXM; modified from Neumann & Dobinson, 2003 as described in (Hollensteiner *et al.*, 2017) and in liquid potato dextrose medium (PDM) [2.65% Potato-Dextrose broth (Carl Roth GmbH&Co.KG)] and

incubated at 25 °C under constant agitation at 120 rpm. Mycelium was harvested from PDM liquid cultures for extraction of genomic DNA. Protein extracts were obtained from mycelium harvested from cultures grown in liquid PDM or modified Czapek-Dox Medium (CDM; Smith, 1949) [3% sucrose, 2% 50x AspA (3.5 mM $NaNO_3$, 350 mM KCl, 550 mM KH_2PO_4, pH 5.5), 2 mM $MgSO_4$, 0.001% $FeSO_4$]. Mycelium from liquid SXM or PDM cultures was used for extraction of RNA. Conidia were harvested from SXM cultures by filtration through sterile Miracloth (Calbiochem Merck), washed twice with sterile water, and resuspended in sterile water. The concentrations of spore solutions were determined using the Coulter Particle Count and Size Analyzer Z2 (Beckman Coulter) with the appropriate diluent by counting particles with a size of 1.9-4.5 µm as *V. dahliae* spores or particles with a size of 2.0-5.9 µm for *V. longisporum* spores. For conservation of fungal strains, freshly harvested spores were resuspended in 0.96% NaCl with 0.05% Tween80, adjusted to 2×10^7 spores/ml and preserved as 30% glycerol stock aliquots at -80 °C.

Verticillium transformants were selected on solid potato dextrose medium (PDM, 3.9% potato extract glucose agar (Carl Roth GmbH&Co.KG), 0.5% agar) supplemented with antimycotics clonNAT nourseothricin dihydrogen sulfate (72 µg/ml, Werner Bioagents GmbH) or hygromycin B (50 µg/ml, InvivoGen), and the antibiotic cefotaxime (300 µg/ml; Wako Chemicals GmbH) after autoclaving.

2.2 Strains, plasmids and primers

2.2.1 Bacterial strains

E. coli strain DH5α (Woodcock *et al.*, 1989) was used for cloning, plasmid reproduction, and conservation. *A. tumefaciens* strain AGL-1 (Lazo *et al.*, 1991) was used for *A. tumefaciens*-mediated transformation (ATMT) for generation of different *V. dahliae* and *V. longisporum* strains.

2.2.2 *Verticillium* strains

The *V. longisporum* strain Vl43 isolated from *Brassica napus* (Zeise & von Tiedemann, 2002) was used as parental lineage for the generation of *V. longisporum* strains. The *V. dahliae* strain JR2 (Fradin *et al.*, 2009) isolated from *Solanum lycopersicum* was used for the generation of *V. dahliae* deletion strains in this study. Fungal strains constructed and used in this study are listed in Table 1.

Table 1: *Verticillium* strains constructed and used in this study.

Strain	Description	Reference
V. dahliae strains		
JR2/ WT	*Solanum lycopersicum* isolate	(Fradin *et al.*, 2009)
JR2-*GFP*	*^{p}gpdA:GFP:trpC^t:^{p}gpdA:HYG^R:trpC^t*	(Bui *et al.*, 2019)
VGB392	*^{p}gpdA:GFP:trpC^t:^{p}gpdA:NAT^R:trpC^t*	This study
VGB279/ VGB280	*ΔHAM5::^{p}gpdA:NAT^R:trpC^t*	This study
VGB331/ VGB332	*ΔODE1::^{p}gpdA:NAT^R:trpC^t*	This study
VGB335/ VGB336	*ΔVMK1::^{p}gpdA:HYG^R:trpC^t*	This study
VGB337/ VGB338	*ΔMEK2::^{p}gpdA:HYG^R:trpC^t*	This study
VGB346	*ΔMEK2::^{p}gpdA:HYG^R:trpC^t; ΔHAM5::^{p}gpdA:NAT^R:trpC^t*	This study
VGB358/ VGB359	*ΔODE1::^{p}ODE1:ODE1:GFP:^{p}gpdA:HYG^R:trpC^t:ODE1^t*	This study
VGB360/ VGB361	*ΔODE1::^{p}ODE1:GFP:ODE1:^{p}gpdA:HYG^R:trpC^t:ODE1^t*	This study
VGB371/ VGB372	*ΔHAC1::^{p}gpdA:HYG^R:trpC^t*	This study
VGB380	*ΔHAC1::^{p}gpdA:HYG^R:trpC^t; ^{p}gpdA:GFP:trpC^t:^{p}gpdA:NAT^R:trpC^t*	This study
VGB382	*ΔHAC1::^{p}gpdA:HYG^R:trpC^t; ^{p}HAC1:HAC1:HAC1^t:^{p}gpdA:NAT^R:trpC^t*	This study
VGB383/ VGB393	Vd JR2ΔLS::^{p}gpdA:NAT^R:trpC^t	This study
VGB388/ VGB389	*ΔMEK2::^{p}gpdA:HYG^R:trpC^t; ^{p}MEK2:MEK2:MEK2^t:^{p}gpdA:NAT^R:trpC^t*	This study
VGB413	*ΔVMK1::^{p}gpdA:HYG^R:trpC^t; ^{p}VMK1:VMK1:VMK1^t:^{p}gpdA:NAT^R:trpC^t*	This study
VGB415	*ΔHAM5::^{p}gpdA:NAT^R:trpC^t; ^{p}HAM5:HAM5:HAM5^t:^{p}gpdA:HYG^R:trpC^t*	This study
VGB417	*ΔVMK1::^{p}gpdA:HYG^R:trpC^t; ΔHAM5::^{p}gpdA:NAT^R:trpC^t*	This study
VGB439/ VGB440	*ΔHAC1::^{p}gpdA:HYG^R:trpC^t; ^{p}HAC1:HAC1^u:HAC1^t:^{p}gpdA:NAT^R:trpC^t*	This study
VGB437/ VGB438	*ΔHAC1::^{p}gpdA:HYG^R:trpC^t; ^{p}HAC1:HAC1^i:HAC1^t:^{p}gpdA:NAT^R:trpC^t*	This study
V. longisporum strains		
Vl32	*B. napus* (oilseed rape) isolate	(Zeise & von Tiedemann, 2002)
Vl43	*B. napus* (oilseed rape) isolate	(Zeise & von Tiedemann, 2002)
VGB193/ VGB214	Vl43ΔLSII::^{p}gpdA:NAT^R:trpC^t (*Δvl43ass51scaf493:534161-542607*)	This study
VGB201/ VGB233	Vl43ΔLSI::^{p}gpdA:NAT^R:trpC^t (*Δvl43ass51scaf493:522667-534160*)	This study

Strain	Description	Reference
VGB232	Vl43Δ*LS::^{p}gpdA:HYG^R:trpC^t* (Δ*vl43ass51scaf493:522667-542607*)	This study

^{p}: promoter, ^{t}: terminator, *NAT^R*: nourseothricin resistance marker, *HYG^R*: hygromycin B resistance marker, two VGB numbers for one genotype indicate two independent transformants.

2.2.3 Plants

All plants used in this study were purchased as seeds and are listed in Table 2.

Table 2: Plants used in this study.

Organism	Description	Reference
Brassica napus (falcon)	rapeseed, family: *Brassicaceae*, used as host for *V. longisporum*	Norddeutsche Pflanzenzucht (Holtsee, Germany)
Solanum lycopersicum (moneymaker)	tomato, family: *Solanaceae*, used as host for *V. dahliae*	Bruno Nebelung GmbH&Co. Kiepenkerl-Pflanzenzüchtung (Everswinkel, Germany)
Arabidopsis thaliana (Col-0)	thale cress, family: *Brassicaceae*, used for root colonization analysis by *V. longisporum* and *V. dahliae*	Nottingham Arabidopsis Stock Centre, stock no. N1902

2.2.4 Primers, Plasmid, and strain constructions

All fragments were PCR amplified using the Q5 Hot Start polymerase (New England Biolabs) or Phusion High-Fidelity DNA polymerase (Thermo Fisher Scientific) from given templates. All strains, primers, and plasmids are listed in Table 1, 3, and 4.

2.2.4.1   Primers

Oligonucleotides used in this study are listed in Table 4. Annealing temperatures of primers were calculated using the NEB Tm Calculator v1.9.13 and the Eurofins Genomics Oligo analysis tool for qPCR primers. Primers used in this study are listed in Table 3.

Table 3: Primers used and designed in this study.

Primer name	Primer sequence (5´→ 3´)	Length (bp)	Overhang to
AO144	AAT AAT CAT CCA CTG CAC CT	20	-
JST1	GTA TGT TGT GTG GAA GCT ACC TAC CGA CAT GCC CG	35	pME4564
JST2	ACC GGT CAC TGT ACA TGC TGT GAC CGT TCG TTT TCC	36	*^{p}gpdA*
JST3	AGG TAA TCC TTC TTT CCA TAT TCT GAT GGT TTC	33	*trpC^t*
JST4	CAC AGT ACA CGA GGA TAC AGA TCT TAT AGA ACT GTA C	37	pME4564

Primer name	Primer sequence (5´→ 3´)	Length (bp)	Overhang to
JST5	GTA TGT TGT GTG GAA CGG GTG CGA CAA ATG CTC TC	35	pME4564
JST6	ACC GGT CAC TGT ACA GCC TGC TGT CCG TGG CAC	33	*^{p}gpdA*
JST7	AGG TAA TCC TTC TTT GTC AGC CCG GAG ACG GTG	33	*trpC^t*
JST8	CAC AGT ACA CGA GGA CGC CCA GAA ACC TGA CAA CC	35	pME4564
JST9	AGA TCC CCG GGT ACC TGC TGT GAC CGT TCG TTT TCC	36	*^{p}gpdA*
JST11	CCA TGG AGC ATA CAA ATA GCT	21	-
JST13	TCC CAC TGT AGG ACC AGA G	19	-
JST15	CGT CAG GGT AGC ATC ATT C	19	-
JST16	GAC CTG ATC GGA TGA CAT GC	20	-
JST17	CAC TCT CGA CTG CCG CCT G	19	-
JST21	AGG TAA TCC TTC TTT TTC CTT ATG TTG GGA TTT GAG G	37	*trpC^t*
JST45	TCA GAT CAT CTC GCT TTC GTG T	22	-
JST46	TCA GAC GCC TTC CGT GTT GG	20	-
JST50	ATG ACC TCG GAC CAC CAT TT	20	-
JST53	ATG ACC GGC GAC GAA GTA GC	20	-
JST58	CGG TCA CAA GAG CGT CTG GA	20	-
JST61	ATG TCG CGC AGC AAC GC	17	-
JST62	CTA CCG CAT AAT CTC CTG GTA GA	23	-
JST76b	GTA TGT TGT GTG GAA AGC ACG GAG CAG AGA CCA	33	pPK2
JST77a	GGT TCT GGT ACA CGA CGA GC	20	-
JST90	GGC TAG GCG ACA TTG ACC TG	21	-
JST110	GTA TGT TGT GTG GAA CCG CGA GGG TTG GAG AGG	33	pME4564
JST111	ACC GGT CAC TGT ACA GAC GGG CCT GAT ATT CTT TCG A	37	*^{p}gpdA*
JST112	AGG TAA TCC TTC TTT GTG GCC GTC TTT TCA CAG GC	35	*trpC^t*
JST113	CAC AGT ACA CGA GGA TCT CGT CCG GAC TGA TCC AA	35	pME4564
JST127	CGT ATG TTG TGT GGA AGG ATG GCC AAT GTG GAT TTG AT	38	pME4564
JST128	CAC CGG TCA CTG TAC AGG TAC TGG TGG CTC TTG GGA	36	*^{p}gpdA*
JST129	GAG GTA ATC CTT CTT TTC GGA TTG GAC AGT AGA CAA GTT TG	41	*^{p}gpdA*
JST130	CAC AGT ACA CGA GGA CGC GCA CAG TTA CAC TTC ATA CTC T	40	pME4564
JST137	TCC ACA TTG GCC ATC CTT CCA CAC AAC ATA CGA GCC G	37	*^{p}ODE1*
JST138	AGT GTA ACT GTG CGC GTC CTC GTG TAC TGT GTA AGC	36	*ODE1^t*
JST171	ATG GAG TCT TGG GAG CAC TC	20	-
JST172	TCA GAC ACC AAC CGC AAT	18	-
JST174	TCA GCG AAA GCG CAC TC	17	-
JST175	ATG GCT GCG ACC ACA TC	17	-

Primer name	Primer sequence (5´→ 3´)	Length (bp)	Overhang to
JST176	TCA CTG CTC ATC CGT ACG	18	-
JST177	AAA GAA GGA TTA CCT CTA AAC AAG TGT	27	-
JST178	GGT ACC GAG CTC GAT TTA CTT GTA CAG CTC GTC CA	35	^{p}gpdA
JST179	ACC ACC GCT ACC ACC CTG CTC ATC CGT ACG GC	32	linker C-terminal GFP
JST180	ATT CTT AAT TAA GAT GGA TGG CCA ATG TGG AT	32	pPK2
JST181	GCC CTT GCT CAC CAT GGT ACT GGT GGC TCT TGG	33	N-terminal GFP
JST184	GTA TGT TGT GTG GAA CGA GTG GAG ATG TGG AGT	33	pME4815
JST185	ACC GGT CAC TGT ACA TGG CAT GCG GAG AGA C	31	pME4815
JST186	ATT CTT AAT TAA GAT GAC AAG AGT CAA GCC CAC	33	pME4564
JST187	AGA TCC CCG GGT ACC GAT GGA CGA AGC GAC TC	32	^{p}gpdA
JST188	AGG TAA TCC TTC TTT TTT GAT TTT TAT CAT GAT GAC GGC	39	trpC^t
JST189	AGG ACT CTA GAG GTC CAG CTC CAA ATC AAT TAA C	37	pME4564
JST207	TCA GTG GTT TTC GAT AGA CG	20	-
JST208	ATG ACA ACC AAC TCA TCT GA	20	-
JST210	GTA TGT TGT GTG GAA GCT ACC TAC CGA CAC GCC C	34	pME4564
JST211	GGT CAC TGT ACA GAT GGG ACT CGT ACC ATG TTT C	34	trpC^t
JST212	TGT TGT GTG GAA GAT ACT AAG TAC TGG TTG TGG CTG AC	38	pME4815
JST213	GGT CAC TGT ACA GAT AGG CTT GGA GAT GAC GAG	33	^{p}gpdA
JST216	TGT TGT GTG GAA GAT GAC AAG AGT CAA GCC CAC	33	pME4564
JST217	TCA TTT TTC CAC CTT TCT CA	20	-
JST218	ATG TAC CCA GCA AAC TAC GA	20	-
JST220	TGG AAG ATT AGG ACA TGA	18	-
JST223	ATA GGA CAT TAT CAT CGC	18	-
JST224	GCA GCA AGT TCA CTC GAG	18	-
JST226	ATG CCC GAT CCT TTC GC	17	-
JST228	AGG GTG CGA TGC GTT GTT	18	-
JST229	TTA TGG CTT CGA CCA GTA TGG	21	-
JST230	ATG CTG ACT TCG GCC CCT	18	-
JST231	CTA CAT GTA GTC TTT ATT TTG ATG C	25	-
JST232	ATG TCC TCC AAC ATC CC	17	-
JST233	TCA GAC AAC TTC GCC GTG G	19	-
JST234	ATG TCC CGC CGT CTC CTG	18	-
JST235	CTA CCC GCA GGG GGT GC	17	-
JST236	ATG CAC TTT CAC GAA ATG GCT C	22	-
JST238	ACT TCG CGC AGT ACG ACT	18	-
JST239	AGG TAC TGG TGA AGG CAT	18	-
JST240	TCA GAG AAT GTG AAG ATG	18	-
JST241	CTT CGT CTT CTG TTT TCG	18	-

Primer name	Primer sequence (5´→ 3´)	Length (bp)	Overhang to
JST242	GAG ATC GAC AAC GCT GTC	18	-
JST243	TGT TGT GTG GAA GAT AGC ACG GAG CAG AGA CCA	33	pME4815
JST244	GGT CAC TGT ACA GAT CGA ACC GGT GAT GGA TAC G	34	*PgpdA*
JST245	ATT CTT AAT TAA GAT CTG CTC CTA TTC GGC TCC	33	pPK2
JST246	GGT ACC GAG CTC GAT TCT CGT CCG GAC TGA TCC	33	pPK2
JST266	CTA TCC GCC GCT AGC GTA ATC GGG CAC ATC GTA TGG GTA GCC GCC GCT GAC ACC AAC CGC AAT GC	65	*HA* tag
JST267	CTA TCC GCC GCT AGC GTA ATC GGG CAC ATC GTA TGG GTA GCC GCC GCT GCG AAA GCG CAC TCG T	64	*HA* tag
JST268	CTA TCC GCC GCT AGC GTA	18	-
JST269	TGT TGT GTG GAA GAT GCT GAG GTC ATG GCT GAC	33	pME4564
JST270	CTC CCA AGA CTC CAT TTT GGA CGG CTT TGT GTG	33	*HAC1*
JST271	GCT AGC GGC GGA TAG GGG CTG TGA GAA TCG GGT	33	*HA*
JST272	GGT CAC TGT ACA GAT GGG ACT CGT ACC ATG TTT CA	35	*trpCᵗ*
JST273	GCT AGC GGC GGA TAG TTT GAT TTT TAT CAT GAT GAC GG	38	*HA*
JST288	AGG TGA GAA CCG AGC AC	17	-
JST289	AGT GCA TTC TTG TGA GCC	19	-
JST292	TTA ATT CGA GGA CCC ATT GTA AA	23	-
JST293	CCG ACG TGA CAC AAC GTC	18	-
JS-V5	CGT ATG TTG TGT GGA AAC TAA GTA CTG GTT GTG GCT GAC	39	pPK2
JS-V6	AAG ATC CCC GGG TAC CTT TGG GTG ATG TGC GTG G	34	*PgpdA*
JS-V7	ACA ACC AGT ACT TAG TTT CCA CAC AAC ATA CGA G	34	*PMEK2*
JS-V8	ACG CAC ATC ACC CAA AGG TAC CCG GGG ATC TTT C	34	*PMEK2*
JS-V9	TCC TTC TTT CTA GAA GTT GAA CAG GCC TGT CTG G	34	pME4821
JS-V10	ACA CAG TAC ACG AGG AAG GCT TGG AGA TGA CGA G	34	pME4821
JS-V11	CGT CAT CTC CAA GCC TTC CTC GTG TAC TGT GTA AG	35	*MEK2ᵗ*
JS-V12	AGA CAG GCC TGT TCA ACT TCT AGA AAG AAG GAT TAC CTC	39	*MEK2ᵗ*
JS-V21	GAG GTA ATC CTT CTT TGG TGG CAG TGG CAG TGG	33	pPK2
JS-V22	ACA CGA GGA CTT CTA GCG AAC CGG TGA TGG ATA CGT T	37	pPK2
JS-V23	ATC CAT CAC CGG TTC GCT AGA AGT CCT CGT GTA CTG T	*37*	*VMK1ᵗ*
JS-V24	CAC TGC CAC TGC CAC CAA AGA AGG ATT ACC TCT AAA CAA GT	41	*VMK1ᵗ*
ML1	TTC CAC ACA ACA TAC GAG CC	20	-
ML2	TCC TCG TGT ACT GTG TAA GC	20	-
ML5	TGT ACA GTG ACC GGT GAC TCT T	22	-

Primer name	Primer sequence (5´→ 3´)	Length (bp)	Overhang to
ML6	TCC CGC GGT CGG CAT CTA CTT CAG GGG CAG GGC ATG CT	38	*trpC*[t]
ML8	AAA GAA GGA TTA CCT CTA AAC AA	23	-
ML9	TGT ACA GTG ACC GGT GAC	18	-
pKO2-40B-for	TGT GGA CAA AGG ATT ACG GG	20	-
RO3	GGT ACC CGG GGA TCT TTC G	19	-
RO4	AAA GAA GGA TTA CCT CTA AAC AA	23	-
SAB16	GGT GGT AGC GGT GGT ATG	18	-
SZ9	AAC ACC CAG AAC AAG ATG CGC	21	-
SZ10	GCT TGA CCT GA GAT CCT TG	20	-
SZ11	TGC ATT CTT GGC AAG AGA TGT GTG	24	-
SZ12	AGC TTG TTA TCC TTG TCC TCG GT	23	-
SZ19	ACC TCT GGA GGC AAG GCT T	19	-
SZ20	GCT TGG CCT CTC TCT CT GC	20	-
ZQY11	GCA TGG ACG AGC TGT ACA AGG GTG GTA GCG GTG GT	35	fusion to N-terminal *GFP*

Blue: overhangs for Seamless and FastCloning, purple: overhang for fusion of linker or tag, [p]: promoter, [t]: terminator.

2.2.4.2   Plasmids

For construction of deletion and complementation cassettes, the GeneArt Seamless Cloning and Assembly Kit (Thermo Fisher Scientific) and the FastCloning protocol (Li *et al.*, 2011) were used. Therefore, 1-2 kb flanking sequences up- and downstream of the corresponding gene or region were amplified from genomic *V. longisporum* Vl43 wild type DNA with 15-16 bp homologous overhangs to the desired neighboring fragments. The PCR products were purified with NucleoSpin Gel and PCR Clean-up Kit (Macherey-Nagel) and used for transformation of *E. coli*. All plasmids were verified by Sanger sequencing.

For construction of *Verticillium* strains, the nourseothricin resistance marker (*NAT*[R]) and the hygromycin B resistance marker (*HYG*[R]) were used for selection of transformants. Both resistance markers are flanked by the *A. nidulans* glyceraldehyde-3-phosphate dehydrogenase *gpdA* (AN8041; *A. nidulans* FGSC A4) promoter (Punt *et al.*, 1988; David *et al.*, 2008) and the tryptophan biosynthesis gene *trpC* (AN0648; *A. nidulans* FGSC A4) terminator for constitutive heterologous gene expression and are named *NAT*[R] and *HYG*[R] marker cassettes in the following. The same promoter and terminator were used for ectopic overexpression of *GFP* in *Verticillium* strains.

Plasmids constructed and used in this study are listed in Table 4.

Table 4: Plasmids constructed and used in this study.

Plasmid	Description	Reference
pGreen2	^{p}*gpdA:HYG^R:trpC^t* ; ^{p}*gpdA:GFP:trpC^t*; *KAN^R*, left and right border for ATMT	(Tran *et al.*, 2014)
pJet1.2	Cloning vector with *AMP^R*	Thermo Fisher Scientific
pPK2	Cloning vector with *KAN^R* and *HYG^R*, left and right border for ATMT	(Covert *et al.*, 2001)
pME4564	Cloning vector with *KAN^R* and *HYG^R*, left and right border for ATMT	personal communication Van Tuan Tran, University of Goettingen
pME4815	Cloning vector with *KAN^R* and *NAT^R*, left and right border for ATMT (^{p}*gpdA:NAT^R:trpC^t* in pME4564)	(Balnojan, 2016, MT, University of Goettingen)
pME4816	^{p}VI43-*LSI:^{p}gpdA:NAT^R:trpC^t:LSI^t* in pME4564	This study
pME4817	^{p}VI43-*LSII:^{p}gpdA:NAT^R:trpC^t:LSII^t* in pME4564	This study
pME4818	^{p}VI43-*LS::^{p}gpdA:HYG^R:trpC^t:LS^t* in pPK2	This study
pME4819	^{p}*gpdA:GFP:trpC^t* in pME4815	This study
pME4820	^{p}*HAM5:^{p}gpdA:NAT^R:trpC^t: HAM5^t* in pME4564	This study
pME4821	^{p}*MEK2* in pPK2	This study
pME4822	^{p}*MEK2:^{p}gpdA:HYG^R:trpC^t:MEK2^t* in pPK2	This study
pME4824	*VMK1^t* in pPK2	This study
pME4825	^{p}*VMK1:^{p}gpdA:HYG^R:trpC^t:VMK1^t* in pPK2	This study
pME4826	^{p}*MEK2:MEK2:MEK2^t* in pME4815	This study
pME4827	^{p}*VMK1:VMK1:VMK1^t* in pME4815	This study
pME4828	^{p}*HAM5:HAM5:HAM5^t:^{p}gpdA:HYG^R:trpC^t* in pPK2	This study
pME4829	^{p}VdJR2-*LS:^{p}gpdA:NAT^R:trpC^t: LS^t* in pME4564	This study
pME4830	^{p}*HAC1:^{p}gpdA:HYG^R:trpC^t:HAC1^t* in pPK2	This study
pME4831	^{p}*HAC1:HAC1:HAC1^t* in pME4815	This study
pME4832	*HAC1^u:HA* in pJet1.2	This study
pME4833	*HAC1^i:HA* in pJet1.2	This study
pME4834	^{p}*HAC1:HAC1^i:HAC1^t* in pME4564	This study
pME4835	^{p}*HAC1:HAC1^u:HAC1^t* in pME4564	This study
pME4836	^{p}*ODE1:^{p}gpdA:NAT^R:trpC^t:ODE1^t* in pME4564	This study
pME4837	*ODE1^t* in pPK2	This study
pME4838	^{p}*ODE1:ODE1:GFP:^{p}gpdA:HYG^R:trpC^t:ODE1^t* in pME4837	This study
pME4839	^{p}*ODE1:GFP:ODE1:^{p}gpdA:HYG^R:trpC^t:ODE1^t* in pME4837	This study

AMP^R; ampicillin resistance marker, ATMT: *Agrobacterium tumefaciens*-mediated transformation, *HYG^R*: hygromycin B resistance marker, *KAN^R*: kanamycin resistance marker, *NAT^R*: nourseothricin resistance marker, ^{p}: promoter, ^{t}: terminator, MT: Master thesis.

2.2.4.3   Plasmid and strain construction of *V. longisporum* strains

Plasmid and strain construction of VI43 *LSI* deletion

For construction of the *LSI* (Δ*vl43ass51scaf493:522667-534160*) deletion cassette, the 2005 bp upstream flanking region was amplified with primers JST1/JST2 and a 1023 bp downstream flanking region with primers JST3/JST4 from fungal wild type DNA. The 2194 bp *NAT^R* marker cassette was amplified from pME4815 with primers ML8/ML9. The fragments were ligated to the backbone pME4564 which was PCR amplified using primers ML1/ML2, resulting in plasmid pME4816 used for wild type transformation. Correct replacement of the *LSI* region by the *NAT^R* marker cassette was confirmed by Southern hybridization using the 5´ flanking region amplified with JST1/JST2 as probe and restriction with *Ssp*I (Figure S1). VI43 Δ*LSI* deletion transformants were conserved as VGB201 and VGB233.

Plasmid and strain construction of VI43 *LSII* deletion

For construction of the *LSII* (Δ*vl43ass51scaf493:534161-542607*) deletion cassette, the 1041 bp upstream flanking region was amplified with primers JST5/JST6 and the 2016 bp downstream flanking region with primers JST7/JST8 from fungal wild type DNA. The *NAT^R* marker cassette and the used backbone were amplified as described for the VI43 *LSI* deletion strain and ligated, resulting in plasmid pME4817 used for wild type transformation. Correct replacement of the *LSII* region by the *NAT^R* marker cassette was confirmed by Southern hybridization using the 3´-flanking region amplified with JST7/JST8 as probe and restriction with *Nhe*I (Figure S1). VI43 Δ*LSII* deletion transformants were conserved as VGB193 and VGB214.

Plasmid and strain construction of VI43 *LS* deletion

For construction of the *LS* (Δ*vl43ass51scaf493:522667-542607*) deletion cassette, the 2005 bp upstream flanking region of the *VI43LS20kb* region was amplified with primers JST1/JST2 and the 2016 bp downstream flanking region was amplified with primers JST7/JST8 from fungal wild type DNA. The *HYG^R* marker cassette was amplified from pPK2 with primers RO3/RO4. The fragments were ligated to the plasmid pME4564, which was PCR-amplified using the primers ML1/ML2, resulting in plasmid pME4818 used for VI43 Δ*LSI* transformation. Correct replacement of the previously introduced *NAT^R* marker cassette and the *LSII* region by the *HYG^R* marker cassette was confirmed by Southern hybridization using the 5´- and 3´-flanking region as probes amplified with JST1/JST2 (5´) and JST7/JST8 (3´) and restriction with *Ssp*I (5´) and *Nhe*I (3´; Figure S1). The resulting *LS* deletion transformant was conserved as VGB232.

2.2.4.4 Plasmid and strain construction of *V. dahliae* strains

Plasmid and strain construction of the *V. dahliae LS* deletion

For construction of the *V. dahliae LS* deletion cassette, 1997 bp up- and 2106 bp downstream of the *Vl43LS20kb* homologous region were amplified from *V. dahliae* JR2 genomic DNA using primers JST210/JST2 (5´) and JST7/JST8 (3´). The nourseothricin resistance marker cassette was amplified from pME4815 with primers ML8/ML9 and ligated into pME4564 cut with the restriction enzymes *Eco*RV and *Stu*I. The resulting plasmid pME4829 was used for *V. dahliae* JR2 transformation. Correct replacement of the *Vl43LS20kb* homologous region by the *NAT^R* marker cassette was confirmed by Southern hybridization using the flanking regions amplified with JST210/JST2 (5´) as probes and JST7/JST8 (3´) and restriction with *Mlu*I (5´, not shown) or *Bgl*I (3´; Figure S3). The resulting *V. dahliae* JR2 *LS* deletion transformants were conserved as VGB383 and VGB393.

Plasmid and strain construction of the *HAM5* single and double deletion with *VMK1*

For construction of the *HAM5* (*VDAG_JR2_Chr4g07170a*) deletion cassette, the 1500 bp flanking region 333 bp upstream of the open reading frame (ORF) was amplified with primers JST110/JST111 and the 1000 bp downstream flanking region was amplified with primers JST112/JST113 from wild type fungal DNA. The 2194 bp *NAT^R* marker cassette was amplified with ML8/ML9 from pME4815. The fragments were ligated into the 6728 bp backbone pME4564 amplified with primers ML1/ML2. The resulting plasmid pME4820 was used for wild type and Δ*VMK1* (VGB335) transformation. 5´-and 3´-flanking regions of *HAM5* were amplified using primers JST110/JST111 (5´) and JST112/JST113 (3´), respectively and labeled as probes for Southern hybridization. Restriction enzymes *Xho*I (5´, not shown) and *Sac*I (3´) were used to cut genomic DNA (Figure S5). The resulting *HAM5* single deletion transformants were conserved as VGB279 and VGB280, the *HAM5* and *VMK1* double deletion transformant was conserved as VGB417.

Plasmid and strain construction of the ectopic *HAM5* complementation

For construction of the ectopic *HAM5* complementation cassette, a 7265 bp sequence including 1359 bp 5´-flanking region, 4906 bp *HAM5* ORF, and 1000 bp 3´-flanking region was amplified using JST245/JST246 from fungal genomic DNA. The PCR product was ligated into pPK2 harboring the *HYG^R* marker cassette cut with the restriction enzyme *Eco*RV. The resulting plasmid was named pME4828 and used for Δ*HAM5* transformation. Flanking regions of *HAM5* were amplified using primers JST110/JST111 (5´) and JST112/JST113 (3´) and labeled as probes for Southern hybridization.

Restriction enzymes *Pvu*II (5´, not shown) and *Sac*I (3´) were used to cut genomic DNA (Figure S5). The resulting *HAM5-C* complementation transformant was conserved as VGB415.

Plasmid and strain construction of the *VMK1* deletion

For construction of the *VMK1* (*VDAG_JR2_Chr2g01260a*) deletion cassette, the 898 bp 3´-flanking region was amplified with primers JS-V21/JS-V22 from fungal wild type DNA and ligated to the 10739 bp pPK2 backbone with *HYG^R* marker cassette amplified with JS-V23/JS-V24, resulting in pME4824. The 1472 bp 5´-flanking region was amplified with primers JST77a/JST76b from fungal wild type DNA and cloned into pME4824, amplified with primers ML1/JS-V23, resulting in pME4825 used for wild type transformation. Flanking regions of *VMK1* were amplified using primers JST77a/JST76b (5´) and JS-V21/JS-V22 (3´) and labeled as probes for Southern hybridization. Restriction enzymes *Xho*I (5´, not shown) or *Bgl*I (3´) were used to cut genomic DNA (Figure S6). The resulting *VMK1* deletion transformants were conserved as VGB335 and VGB336.

Plasmid and strain construction of the ectopic *VMK1* complementation

For construction of the ectopic *VMK1* complementation cassette, a 3661 bp sequence including 1473 bp 5´-flanking region, 1260 bp *VMK1* ORF, and 928 bp 3´-flanking region, was amplified from fungal wild type DNA using JST243/JST244. The PCR product was ligated to pME4815 harboring a *NAT^R* marker cassette cut with the restriction enzyme *Eco*RV, resulting in the plasmid pME4827 used for ∆*VMK1* transformation. Flanking regions of *VMK1* were amplified using primers JST77a/JST76b (5´) and JS-V21/JS-V22 (3´) and labeled as probes for Southern hybridization. The restriction enzymes *Vsp*I (5´, not shown) or *Bgl*I (3´) were used to cut genomic DNA (Figure S6). The resulting *VMK1-C* complementation transformant was conserved as VGB413.

Plasmid and strain construction of the *MEK2* single and double deletion with *HAM5*

For construction of the *MEK2* (*VDAG_JR2_Chr1g13070a*) deletion cassette the 1500 bp 5´-flanking region was amplified with primers JS-V5/JS-V6 from fungal wild type DNA and ligated to the 10676 bp pPK2 backbone with *HYG^R* marker cassette amplified with JS-V7/JS-V8, resulting in pME4821.

The 1500 bp 3´-flanking region 385 bp downstream of the ORF was amplified with primers JS-V9/JS-V10 from fungal wild type DNA and ligated to pME4821 amplified with primers JS-V11/JS-V12, resulting in pME4822 used for wild type and ∆*HAM5* (VGB279) transformation. Flanking regions of *MEK2* were amplified using primers JS-V5/JS-V6 (5´) and JS-V9/JS-V10 (3´) and labeled as probes for Southern hybridization. The restriction enzymes *Hind*III (5´, not shown) or *Nru*I (3´) were used to cut genomic DNA (Figure S7).

The resulting *MEK2* single deletion transformants were conserved as VGB337 and VGB338, the *MEK2* and *HAM5* double deletion transformant was conserved as VGB346.

Plasmid and strain construction of the ectopic *MEK2* complementation

For construction of the ectopic *MEK2* complementation cassette, a 5176 bp sequence including 1500 bp 5´-flanking region, 1756 bp *MEK2* ORF, and 1885 bp 3´-flanking region was amplified from fungal wild type DNA using JST212/JST213. The PCR product was ligated to pME4815 harboring a *NAT^R* marker cassette cut with the restriction enzyme *Eco*RV, resulting in the plasmid pME4826 used for Δ*MEK2* transformation. Flanking regions of *MEK2* were amplified using primers JS-V5/JS-V6 (5´) and JS-V9/JS-V10 (3´) and labeled as probes for Southern hybridization. The restriction enzymes *Hind*III (5´, not shown) or *Nru*I (3´; Figure S7) were used to cut genomic DNA. The resulting *MEK2-C* complementation transformant was conserved as VGB389.

Plasmid and strain construction of the *HAC1* deletion

For construction of the *HAC1* (*VDAG_JR2_Chr2g09780a*) deletion cassette, a 1500 bp flanking region 218 bp upstream from the ORF was amplified with JST186/JST187 and a 1445 bp 3´-flanking region was amplified using JST188/JST189 from fungal wild type DNA. The 3942 bp *HYG^R* marker cassette was amplified from pPK2 with primers ML8/RO3. The fragments were ligated to pME4564 cut with restriction enzymes *Eco*RV and *Stu*I, resulting in pME4830 used for wild type transformation. 1500 bp up- and 300 bp downstream flanking regions of *HAC1* were amplified using primers JST186/JST187 (5´) and JST272/JST273 (3´) and labeled as probes for Southern hybridization. Restriction enzyme *Sal*I (5´, not shown; 3´(Figure S8)) was used to cut genomic DNA. The resulting *HAC1* deletion transformants were conserved as VGB371 and VGB372.

Plasmid and strain construction of the ectopic *HAC1* complementation

For construction of the ectopic *HAC1* complementation cassette, a 3636 bp insert containing 1702 bp 5´-flanking, 1634 bp *HAC1* gene, and 300 bp 3´-flanking region was amplified with primers JST216/JST211 and cloned into pME4815 cut with the restriction enzyme *Eco*RV, resulting in plasmid pME4831 used for transformation of the Δ*HAC1* strain. For Southern hybridization (Figure S8) the same restriction enzymes and probes were used as for verification of the *HAC1* deletion strain. The resulting *HAC1-C* complementation transformant was conserved as VGB382.

Plasmid and strain construction of the ectopic *HAC1^u-HA* complementation

For construction of a *HAC1^u-HA* complementation construct the uninduced mRNA splice variant of *HAC1* without stop codon was amplified with primers JST171/JST172 from

complementary DNA (cDNA) isolated from wild type cultures incubated in SXM for four days. The C-terminal *HA*-tag was fused to *HAC1^u* via amplification with a 48 bp *HA* sequence as overhang using JST171/JST267. *HAC1^u-HA* was ligated to the cloning vector pJet1.2, resulting in pME4832.

The 1400 bp 5´-flanking region was amplified with primers JST269/JST270 and a 300 bp 3´-flanking region was amplified with primers JST272/JST273 from fungal wild type DNA. The 1626 bp *HAC1^u-HA* sequence was amplified from pME4832 with JST171/JST268. The fragments were ligated to pME4815 cut with the restriction enzyme *Eco*RV, resulting in pME4834 used for transformation of the ΔHAC1 strain. For Southern hybridization the same probes were used as for verification of the *HAC1* deletion strain. The restriction enzymes *Pvu*II (5´, not shown) and *Sal*I (3´; Figure S8) were used to cut genomic DNA. The resulting *HAC1^u-HA* transformants were conserved as VGB439 and VGB440.

Plasmid and strain construction of the ectopic *HAC1^i-HA* complementation

For construction of a *HAC1^i-HA* complementation construct, the induced splice variant of *HAC1* without stop codon was amplified from cDNA isolated from wild type cultures incubated in SXM for four days with subsequent supplementation with 3 mM dithiothreitol (DTT) for three hours using primers JST171/JST174. The C-terminal *HA*-tag was fused to *HAC1^i* via amplification with a 48 bp *HA* sequence as overhang using JST171/JST266. *HAC1^i-HA* was ligated to the cloning vector pJet1.2, resulting in pME4833 used for transformation of the ΔHAC1 strain. The 1400 bp 5´-flanking region was amplified with primers JST269/JST270 and a 607 bp 3´-flanking region was amplified with primers JST271/JST272 from fungal wild type DNA. The 1299 bp *HAC1^i-HA* sequence was amplified from pME4833 with JST171/JST268. The fragments were ligated to pME4815 cut with the restriction enzyme *Eco*RV, resulting in pME4835 used for transformation of the ΔHAC1 strain. For Southern hybridization the same probes were used as for verification of the *HAC1* deletion strain. The restriction enzymes *Pvu*II (5´, not shown) and *Sal*I (3´; Figure S8) were used to cut genomic DNA. The resulting *HAC1^i-HA* transformants were conserved as VGB437 and VGB438.

Plasmid and strain construction of the ectopic *GFP* overexpression strains JR2 OE-GFP and ΔHAC1 OE-GFP

For construction of the *GFP* overexpression vector with *NAT^R* resistance marker cassette, a 2378 bp fragment containing *GFP* under control of the *gpdA* promoter and *trpC* terminator was amplified from pGreen2 with primers JST184/JST185 and ligated to pME4815 amplified with primers ML1/ML9, resulting in pME4819 used for wild type and ΔHAC1 strain transformation.

The resulting JR2 *OE-GFP* transformant was confirmed by fluorescence microscopy and phenotypic comparison to wild type and conserved as VGB392.

The resulting Δ*HAC1 OE-GFP* transformant was confirmed by fluorescence microscopy, phenotypic comparison to the Δ*HAC1* strain and Southern hybridization. The 300 bp downstream flanking region of *HAC1* was amplified using primers JST272/JST273 and labeled as probe for Southern hybridization. The restriction enzyme *Sal*I (3´; Figure S8) was used to cut genomic DNA. The resulting Δ*HAC1 OE-GFP* transformant was conserved as VGB380.

Plasmid and strain construction of the *ODE1* deletion

For construction of the *ODE1* (*VDAG_JR2_Chr1g29610a*) deletion cassette, the 1000 bp 5´- and 1522 bp 3´-flanking regions were amplified from fungal wild type DNA with primers JST127/JST128 (5´) or JST129/JST130 (3´). The 2194 bp *NAT^R* marker cassette was amplified with ML8/ML9 from pME4815 and ligated to the 6728 bp pME4564 backbone amplified with JST137/JST138, resulting in pME4836 used for wild type transformation. Amplified flanking regions of *ODE1* were labeled as probes for Southern hybridization. The restriction enzymes *Bgl*I (5´, not shown) or *Sca*I (3´, Figure S9) were used to cut genomic DNA. The Δ*ODE1* strains were conserved as VGB331 and VGB332.

Plasmid and strain construction of endogenous *GFP*-tagged *ODE1* complementation

For construction of the *ODE1* complementation cassettes coding for either N- or C-terminal GFP-tagged Ode1, the 1522 bp 3´-flanking region was amplified from fungal wild type DNA with primers JST129/JST130 and ligated to the 10744 bp pPK2 backbone amplified with JST138/JST177, resulting in plasmid pME4837.

For construction of the endogenous *ODE1-GFP* complementation cassette, a 2501 bp PCR product containing the 1000 bp 5´-flanking region and 1501 bp *ODE1* gene without stop codon was amplified from fungal wild type DNA with JST179/JST180. The sequence of 735 bp coding for C-terminal GFP with a 5 aa linker was amplified with primers SAB16/JST178 from pGreen2. Both inserts were ligated to pME4837 cut with the restriction enzyme *Eco*RV, resulting in plasmid pME4838 used for transformation of the Δ*ODE1* strain.

For construction of the endogenous *GFP-ODE1* complementation cassette the 1000 bp 5´-flanking region was amplified with JST180/JST181 and the 1504 bp *ODE1* gene was amplified with JST182/JST183 from fungal wild type DNA. The 732 bp sequence coding for N-terminal GFP and a 5 aa linker was amplified with primers JST98/ZQY11 from

pGreen2. Inserts were ligated to pME4837 cut with the restriction enzyme *Eco*RV, resulting in plasmid pME4839 used for transformation of the Δ*ODE1* strain.

Amplified flanking regions of *ODE1* were labeled as probes for Southern hybridization as described in for the plasmid and strain construction of the *ODE1* deletion. The restriction enzymes *Ava*II (5´, not shown) or *Sca*I (3´, Figure S9) were used to cut genomic DNA.

The expression of the fusion protein was confirmed by fluorescence microscopy and immunoblotting with a GFP-protein binding antibody. The strains were conserved as VGB358 and VGB359 (*ODE1-GFP*) and VGB360 and VGB361 (*GFP-ODE1*).

2.3 Microbiological methods

2.3.1 Transformation of *Escherichia coli*

Chemically competent *E. coli* DH5α cells were transformed by the heat shock method in a modified protocol according to Hanahan *et al.*, 1991. 200 µl competent *E. coli* cells were thawed on ice, mixed with the ligation mixture or plasmid solution, and incubated on ice for 30 min. A heat shock at 42 °C was induced for one minute. Afterwards, the *E. coli* cells were chilled on ice for two minutes. 800 µl SOC medium was added and the cells were incubated for 50 min at 37 °C under constant agitation. Positive transformants were selected on solid LB plates, supplemented with 100 µg/ml ampicillin or 100 µg/ml kanamycin. The plates were incubated at 37 °C overnight and the transformants were tested by colony PCR for plasmid uptake.

2.3.2 Transformation of *Agrobacterium tumefaciens*

A. tumefaciens cells were transformed with plasmid DNA as described in Bui 2017 (Dissertation, University of Goettingen). The heat shock was performed for five minutes at 37 °C.

2.3.3 Transformation of Verticillia

Verticillia were transformed by *A. tumefaciens*-mediated transformation as described in Mullins *et al.*, 2001. *A. tumefaciens* cultures were inoculated in 5 ml liquid LB medium supplemented with 100 µg/ml kanamycin and incubated overnight at 25 °C on a rotary shaker. 20 ml induction medium (IM) [1x MM salts (2.5x stock: 3.625 g/l KH_2PO_4, 5.125 g/l K_2HPO_4, 0.375 g/l NaCl, 1.25 g/l $MgSO_4·7x$ H_2O, 0.165 g/l $CaCl_2·2x$ H_2O, 6.2 mg/l $FeSO_4·7x$ H_2O, 1.25 g/l $(NH_4)_2SO_4$)], 400 ml/l, 10 mM glucose, 0.5% glycerol, 40 mM MES monohydrate (Carl Roth GmbH&Co.KG) supplemented with 200 µM acetosyringone (AS) were inoculated with 0.5 ml to 1 ml of the overnight culture and incubated for four to five hours at 28 °C under constant agitation in a water bath. Equal amounts of *A. tumefaciens* liquid culture and *Verticillium* spore solutions with

1×10^6 spores/ml were mixed and 200 µl/plate of the mixture were distributed on IM solid medium (same as liquid IM except that it contains 5 mM glucose and 1.5% agar, supplementation of sterile MES and AS after autoclaving) covered with a sterile nitrocellulose filter (Ø = 85 mm, Sartorius, Goettingen, Germany). After three days of incubation at 25 °C, filters were transferred to solid PDM supplemented with respective antimycotica hygromycin B (50 µg/ml) and/or nourseothricin (72 µg/ml) and cefotaxime (300 µg/ml). Filters were removed after six to ten days and transformants were separated twice on solid PDM selection plates.

2.3.4 Phenotypic analysis and stress tests

For characterization of the *ex planta* phenotypes, *Verticillium* strains were analyzed by spot inoculation of 50 000 freshly harvested spores on different solid media, including SXM, PDM, Malt extract agar [30% malt extract (Carl Roth GmbH&Co.KG), 5% BD Bacto Peptone (BD Biosciences), 20% agar, pH 7.6], CDM [liquid CDM with 2% agar], CDM with alternative carbon sources [3% cellulose (Carboxymethylcellulose sodium salt, Sigma-Aldrich Chemie GmbH), 3% galactose, or 3% glucose] and incubated at 25 °C for 9-14 days. For induction of oxidative stress, CDM was supplemented with 0.00075% H_2O_2 or 0.004% SDS. CDM supplemented with 0.5 M NaCl or 0.8 M Sorbitol was used for induction of osmotic stress. ER stress induction was achieved by CDM supplementation with 1 µg/ml tunicamycin. CDM supplementation with linoleic acid (LA, 0.125 mg/ml) was used for induction of oxidative stress and for complementation of partial auxotrophy in *ODE1* deletion strains.

2.3.5 Growth quantification

For growth quantification, 50 000 freshly harvested spores were spot inoculated on three 30 ml plates per medium and transformant. Growth was quantified by measurement of two perpendicular diameters per colony at indicated growth conditions. The mean value of three colonies per transformant was considered as one biological replicate (n=1). Significances were calculated using the one-way Anova and Student´s t-test from *Simple Interactive Statistical Analysis* (*SISA)* online tool (http://www.quantitativeskills.com/sisa/tableprocs/meanst.htm).

2.3.6 Microsclerotia observation and quantification of melanization

Microsclerotia formation was visualized by microscopy of colony cross sections with a binocular microscope (Olympus Deutschland GmbH) and microscopy of material scraped off with a scalpel from the colony center using an Axiolab light microscope (Zeiss). Calibration of pictures for magnification was done using the cellSens Dimension version 1.4 software (Olympus GmbH).

For quantification of melanization, 50 000 freshly harvested spores were spot inoculated on three 30 ml CDM with cellulose medium plates per transformant. Pictures from colonies were taken nine days after spot inoculation from the top view after removal of aerial mycelium and the melanized area was measured from eight bit greyscale pictures using ImageJ software (Rasband, 1997). The means of the brightness factor were determined, set relative to wild type, and inverted. The mean value of three colonies per transformant was considered as one biological replicate (n=1). Significances were calculated using the one-way Anova and Student´s t-test from *SISA* online tool.

2.3.7 Conidiospore quantification

For spore quantification, freshly harvested conidia were inoculated in liquid SXM to a concentration of 4 000 conidiospores/ml in triplicates and incubated for five days under constant agitation at 135 rpm in three independent experiments. Spores were harvested through Miracloth (Calbiochem Merck) and diluted in equal volumes of sterile water. Conidiospore concentrations were measured three times per spore solution using the Coulter Z2 Particle Count and Size Analyzer (Beckman Coulter, Krefeld, Germany) and the appropriate Coulter Isoton II Diluent. The mean number of spores from a single transformant per experiment represents n=1. Numbers of spores were normalized to the mean value of three independent experiments determined for wild type. The values determined for two independent transformants from one genotype were summed up in one bar. Error bars indicate the standard deviations. Significances were calculated using the one-way Anova and Student´s t-test from *SISA* online tool.

2.3.8 Localization assay

Localization of Ode1 N- or C-terminally tagged to GFP was examined by fluorescence microscopy. 300 µl liquid PDM was inoculated with ~50 000-100 000 freshly harvested spores per well in an 8 well microscopy chamber (Ibidi) and incubated at 25 °C for 12-20 hours. Hyphal morphology and subcellular localization were observed with a Plan-Neofluar 100x/1.4 oil objective (Zeiss) with 300 ms exposure time for GFP signals and 800 ms exposure time for RFP signals. Vacuoles were visualized by fluorescence microscopy after staining with 0.3 µl FM4-64 Dye (Thermo Fisher Scientific) for one hour in the dark.

2.3.9 Plant infection assays

2.3.9.1 *Brassica napus* infection assay with *V. longisporum*

B. napus plants were used as host for infection assays with *V. longisporum* strains. Per experiment 15 seven-day-old seedlings of oilseed rape were tested by root dipping into a

solution of 1.5×10^6 conidiospores/ml and the mock control plants were treated with sterile demineralized water for 40 min under constant agitation at ~30 rpm. The seedlings were transferred to 70x70x80 mm planting pots (Soparco GmbH) containing a sand:soil (1:1) mixture (Dorsilit, Archut GmbH&Co.KG). The soil was inoculated with either 2.25×10^6 spores or 1.5 ml sterile water for mock plants per pot. The plants were allowed to grow in a climate chamber BrightBoy GroBank (CLF PlantClimatics) at long day conditions with 16 hours of light (fluorescence: 60, GroLEDs: 100, illumination: 95 µmol) at 25 °C and eight hours of darkness at 22 °C. The disease symptoms were scored after 35 days according to the disease rating criteria. The numbers of tested plants, transformants, and independent experiments are indicated.

2.3.9.2 *Solanum lycopersicum* infection assay with *V. dahliae*

S. lycopersicum (moneymaker, B17422) plants were used as host for plant infection assays with *V. dahliae* strains. Per experiment 15 ten-day-old seedlings of tomato were tested by root dipping into a solution of 1×10^7 conidiospores/ml or 3 ml sterile water for the mock control plants for 40 min under constant agitation at ~30 rpm. The seedlings were transferred to 70x70x80 mm planting pots (Soparco) containing a sand:soil (1:1) mixture (Dorsilit, Archut). The soil was inoculated with 3×10^7 *V. dahliae* spores or sterile water for mock plants per pot. The plants were allowed to grow in a climate chamber at long day conditions with 16 hours of light (fluorescence: 60, GroLEDs: 100, illumination: 95 µmol) at 25 °C and eight hours of darkness at 22 °C. The disease symptoms were scored after 21 days according to the disease rating criteria. The numbers of tested plants, transformants and independent experiments are indicated.

2.3.9.3 Disease rating criteria

Disease symptoms induced in *B. napus* and *S. lycopersicum* infection assays with *V. longisporum* and *V. dahliae* were scored according to the following disease rating criteria: The fresh weight excluding the roots, the length of the longest leaf, and the height of the vegetation point per plant were determined and transformed into a score ranging from 1 to 5 relative to the values determined for the uninfected mock plants (rapeseed plants: 100-80% (mock) = 1, 79-60% (mock) = 2, 59-40% (mock) = 3, < 40% (mock) = 4, dead plant = 5; tomato plants: 100-70% (mock) = 1, 69-60% (mock) = 2, 59-40% (mock) = 3, < 40% (mock) = 4, dead plant = 5). Furthermore, a leave symptom index per plant was calculated (leave symptoms score = [(number of healthy leaves x 1) + (number of leaves with weak symptoms x 2) + (number of leaves with strong symptoms x 3) + (number of dead leaves x 4)] / total number of leaves) for rapeseed plants. The disease score per plant was calculated by the mean of the scores for each parameter

[height, length of the longest leaf, weight, leave symptom index (for rapeseed plants only)] ranging from 1 to 5 (1 = healthy, 2 = weak symptoms, 3 = strong symptoms, 4 = very strong symptoms, 5 = dead plant). The number of plants categorized into the disease scores relative to the total number of tested plants from all experiments was visualized in a stack diagram. One bar represents all tested plants from independent experiments inoculated with a single or two independent transformants of the same genotype as indicated.

For tomato plants discoloration of the hypocotyl was examined by observation of cross sections with a binocular microscope (Olympus Deutschland GmbH).

For rapeseed plants inoculated with *V. longisporum* strains, statistical analysis was performed to calculate significant differences regarding the number of dead plants. One-way Anova and Student´s t-test from *SISA* online tool were used for calculation of p-values.

2.3.9.4 Stem assay

To test for fungal outgrowth from plants inoculated with fungal spores or water control, stems were harvested after 21 days for tomato plants or 35 days for rapeseed plants. The stems were surface sterilized by washing with 70% ethanol for eight minutes, followed by 6% sodium hypochlorite solution for eight minutes and subsequent washing with distilled sterile water, twice. The stem ends were removed and slices of the middle part were placed on PDM plates supplemented with chloramphenicol (100 µg/ml). Plates were incubated at 25 °C for seven days and fungal growth was documented.

Fungal outgrowth from *V. dahliae* ΔVMK1, ΔMEK2, ΔHAM5ΔVMK1 and ΔHAM5ΔMEK2 strains was confirmed by control PCR reactions using genomic DNA and primers AO144/JST288 (ΔVMK1, ΔHAM5ΔVMK1) resulting in a 3044 bp PCR product and AO144/JST289 (ΔMEK2, ΔHAM5ΔMEK2) resulting in a 3013 bp PCR product. AO144 targets the *gpdA* promoter in the hygromycin resistance marker cassette, JST288 binds 156 bp upstream of the 1473 bp 5´-flanking region of *VMK1* used for homologous recombination, and JST289 binds 89 bp upstream of the 1500 bp 5´-flanking region of *MEK2* used for homologous recombination.

2.3.9.5 *Arabidopsis thaliana* root colonization assay

Analysis of root colonization capabilities of *Verticillium* strains was performed with *A. thaliana* (Col-0) plants. The root colonization assay was modified from Tran *et al.* 2014. Seeds were surface sterilized for five minutes in a solution containing 70% EtOH and 0.05% Tween80 and dried at 35 °C for 20 min. The sterilized seeds were placed on Murashige and Skoog (MS; Murashige & Skoog, 1962) plates [0.22% MS + vitamin

(Duchefa, Haarlem, Netherlands), 0.05% MES monohydrate (Carl Roth GmbH&Co.KG), 1% sucrose and 1.5% plant agar (Duchefa), pH 5.7], incubated at 4 °C overnight and transferred to the climate chamber for incubation at long day conditions with 16 hours of light (fluorescence: 60, GroLEDs: 100, illumination: 95 µmol) at 25 °C and eight hours of darkness at 22 °C. After 21 days, plants were transferred to 1% water agarose. One day later, roots were inoculated in fresh conidial suspensions (1×10^5 spores/ml) for 35 min and transferred back to 1% water agarose. Two thirds of the plate were covered with aluminum foil to shade the roots. Afterwards, plants were incubated in a plant chamber at long day conditions for the indicated time.

For microscopy, roots were cut and incubated for five minutes in the dark in a staining solution [0.0025% propidium iodide and 0.005% silwet]. The roots were transferred to an object slide with 150 µl H_2O and 50 µl staining solution. Cover slips were fixed with nail polish. Fungal root colonization was examined by fluorescence microscopy. Overview pictures [20x objective (Zeiss)] as well as close up pictures [63x objective (Zeiss)] were taken with 300 ms exposure time for GFP signals and 800 ms exposure time for RFP signals. Volume view pictures shown are maximum intensity projections of a Z-stack of microscope images. Per experiment, fungal strain, and time point root colonization was analyzed for two to three independent plants.

2.4 Nucleic acid methods

2.4.1 Nucleic acid purification

Purification of PCR products and linearized DNA fragments

PCR products used for cloning or as probes for Southern hybridization analysis, as well as fragments cut with restriction enzymes, were separated from side products on an agarose gel by gel electrophoresis, excised from the gel, and purified using the NucleoSpin Gel and PCR Clean-up Kit (Macherey-Nagel) according to the manufacturer´s instructions.

Plasmid purification from *E. coli*

For isolation of a plasmid of interest, *E. coli* strains were inoculated in 5 ml LB medium supplemented with the corresponding antibiotic and incubated at 37 °C on a rotary shaker overnight. Plasmid DNA was purified with the NucleoSpin Plasmid Kit from Macherey-Nagel according to the manufacturer´s protocol.

Genomic DNA purification from *Verticillium*

The extraction method was modified from Kolar *et al.*, 1988. For the isolation of genomic DNA of *Verticillium*, mycelium was harvested from liquid PDM four to seven days post

inoculation by filtration through Miracloth filters (Calbiochem Merck). The mycelium was rinsed with 0.96% NaCl solution, dried, frozen, and ground to fine powder in liquid nitrogen. The powder was mixed with 800 µl of lysis buffer [50 mM tris pH 7.5, 50 mM EDTA pH 8, 3% SDS and 1% ß-mercaptoethanol]. The mixture was incubated at 65 °C for one hour and subsequently mixed with 800 µl phenol. Phases were separated by centrifugation for 20 min at 13000 rpm and 4 °C. The upper phase was transferred into a new tube, mixed with 500 µl chloroform for denaturation of proteins and centrifuged for ten minutes at 13000 rpm and 4 °C. The upper phase was transferred into a new tube, mixed with 400 µl isopropanol and centrifuged for two minutes at 13000 rpm for precipitation of genomic DNA. The precipitated genomic DNA was desalted by washing with 300 µl 70% ethanol and centrifugation for one minute at 13000 rpm. Ethanol was removed and the precipitated genomic DNA was dried with open lid at 65 °C for 20 min. The sediment was resuspended in 50-100 µl deionized H_2O and RNA was cut by RNase A (200 µg/ml) at 65 °C for 30 min. Quality and concentration of genomic DNA were tested by agarose gel electrophoresis.

RNA purification from *Verticillium*

RNA was purified from fungal mycelium harvested at indicated time points from indicated growth conditions using the Direct-zol RNA MiniPrep Kit from Zymo Research according to the manufacturer´s instructions. Mycelium was rinsed with 0.96% NaCl solution, dried, frozen, and ground to fine powder in liquid nitrogen. Approximately 1 ml of the powder was transferred to precooled 15 ml Falcon tubes, mixed with 1 ml TRIzol (Ambion and life technologies, Carlsbad, CA, USA), and frozen in liquid nitrogen.

DNase I was used to cut remaining DNA on columns according to the manufacturer´s protocol. Purified RNA was eluted in prewarmed DNase/RNase free water. Quality and concentration of RNA were defined by determination of the absorption rations at 260 nm/ 280 nm (~1.8) and 260 nm/ 230 nm (~2.0-2.2) for a 1:10 dilution using the Nanodrop ND-1000 spectrophotometer (PeqLab Biotechnology GmbH), and by testing appearance of distinct bands for ribosomal RNAs at ~2.3 kb (28S) and ~1.1 kb (18S) during agarose gel electrophoresis of 1 µl RNA. The extracted RNA was directly used for cDNA synthesis.

2.4.2 Polymerase chain reaction

Polymerase chain reaction (PCR) was used for amplification of DNA fragments for construction of plasmids, Southern probes, confirmation of the presence of genes in fungal genomic DNA, verification of gene annotations on cDNA level, and for colony PCRs (Bergkessel & Guthrie, 2013) to identify *E. coli* transformants harboring a desired plasmid after plasmid transformation. Phusion High-Fidelity DNA Polymerase, Taq DNA Polymerase (both: Thermo Fisher Scientific), and Q5 High Fidelity Polymerase (New

England Biolabs) were used for amplification of DNA. PCR programs were designed according to the manufacturer's instructions. Appropriate annealing temperatures of primer pairs were determined by the use of the online NEB Tm calculator v 1.9.12 (New England Biolabs, Ipswich, MA, USA).

2.4.3 Agarose gel electrophoresis

Agarose gel electrophoresis was used to separate DNA or RNA according to charge and size for analyses of quality and concentration of purified DNA or RNA. Furthermore, it was used to test specificity of PCR products, to separate genomic DNA fragments cut by restriction enzymes in Southern hybridization analyses, and to purify DNA fragments from unspecific products with subsequent gel extraction. Nucleic acid samples were mixed with 6x loading dye [0.25% Bromophenol blue, 0.25% Xylene cyanol FF, 40% sucrose, pH 8.0] and loaded on a 1% agarose gel [1% agarose, 1x TAE buffer (40 mM tris-acetate, 20 mM sodium acetate, 2 mM EDTA, pH 8.3), 0.001 mg/ml ethidium bromide] in 1x TAE buffer. The GeneRuler 1 kb DNA Ladder and GeneRuler 100 bp DNA Ladder (Thermo Fisher Scientific) were used as size standards. Separation was performed with an electric field of 90 V. *In-gel* visualization was achieved by exposure to UV light (λ = 254 nm) using a Gel iX20 Imager and the Intas GDS gel documentation software (Intas Science Imaging Instruments GmbH, Goettingen, Germany).

2.4.4 Abscence confirmation of the *Vl43LS20kb* region in *V. longisporum* Vl32

Seven genes predicted for the *Vl43LS20kb* region were amplified using Phusion High-Fidelity DNA polymerase (Thermo Fisher Scientific) from genomic DNA (2.4.1) of Vl43 and Vl32 with similar concentrations. Primers are listed in Table 3. A part of the histone H2a encoding genes homologous to *V. dahliae* JR2 (*VDAG_JR2_Chr4g01430a*) was amplified with primers SZ19/SZ20 resulting in 854 bp PCR products as positive controls. 1112 bp *LSG-1* (*VDAG_JR2_Chr5g10950a* homolog) was amplified with primers JST229/JST230, 687 bp *LSG-2* (*VDAG_JR2_Chr2g10300a* homolog) with JST231/JST232, 2177 bp *LSG-3* (*VDAG_JR2_Chr2g10290a* homolog) with JST231/JST232, 498 bp *LSG-4* (*VDAG_JR2_Chr2g10280a* homolog) with JST233/JST234, 619 bp *LSG-5* (*VDAG_JR2_Chr2g10270a* homolog) with JST207/JST208, 2448 bp *LSG-6* (*VDAG_JR2_Chr2g10260a* homolog) with JST46/JST50, 527 bp *LSG-7* (*VDAG_JR2_Chr2g10250a* homolog) with JST235/JST236.

2.4.5 Primer walking

Primer walking (Sverdlov & Azhikina, 2005) is a sequencing method used for sequencing of DNA fragments, which extend the sequencing capacities of a single read between

1-1.5 kb obtained from the Sanger sequencing method. The fragment of interest is divided into shorter fragments and sequenced from both ends with specific primers. According to the sequencing result the next sequencing primers are designed in several steps in order to sequence the complete fragment. The method was used to verify the assembly of the *V. longisporum Vl43LS20kb* region. The region was divided into four overlapping fragments, which were amplified using primers JST11/JST218 (5538 bp), JST217/JST208 (5900 bp), JST207/JST50 (5140 bp), and JST21/JST13 (5258 bp). The fragments were ligated to the pJet1.2 cloning vector (Thermo Fisher Scientific) for sequencing with the primers pJet1.2-forward/pJet1.2-reverse sequencing primers (Thermo Fisher Scientific), JST15, JST16, JST17, JST220, JST223, JST224, JST228, JST229, JST231, JST234, pKO2-40B-for, and JST238-242.

2.4.6 Complementary DNA amplification

RNA was extracted and quality of RNA was determined as described in chapter 2.4.1. Reverse transcription of 0.8 µg RNA to cDNA was performed using the Qiagen QuantiTect Reverse Transcription Kit (Hilden, Germany) according to the manufacturer´s protocol. Absence of genomic DNA in cDNA samples was tested using *H2A* as a control gene with the primers SZ19/SZ20.

2.4.7 Quantitative reverse transcriptase PCR

Transcription of *HAC1* was analyzed by quantitative reverse transcriptase (qRT) PCR. RNA was extracted and quality of RNA was determined as described in chapter 2.4.1 from 50 ml liquid SXM cultures inoculated with 1×10^6 spores. Reverse transcription was performed as described in chapter 2.4.6. The cDNA was diluted 1:5. Primers are listed in Table 3 and were designed with annealing temperatures of 60 °C using the Eurofins Genomics Oligo analysis tool. Histone *H2A* (*VDAG_JR2_Chr4g01430a*) and *EIF2B* (*VDAG_JR2_Chr4g00410a*) served as reference genes. Transcription levels were analyzed in triplicates using a CFX Connect Real Time System cycler (Biorad) with Mesa Green qPCR MasterMix Plus for SYBR Assay (Eurogentec) and cycling was 2:20 min at 95 °C followed by 40 cycles of: 95 °C for 20 s, 60 °C for 22 s, and 72 °C for 22 s. Specificity of PCR products was tested with the subsequent melting curve analysis from 65 °C to 95 °C with 5 s per 0.5 °C after 10 s at 95 °C. Primers JST290/JST291 (*HAC1* variants), SZ9/SZ10 (*H2A*), and SZ11/SZ12 (*EIF2B*) were used. Expression levels were quantified relative to the reference genes in *ΔΔCT* method (Livak & Schmittgen, 2001). A gene study of two independent experiments was performed using CFX Manager Software version 3.1 (Biorad).

2.4.8 Verification of intron-exon structures

ORFs and intron-exon-structures of the tested genes were analyzed by PCR amplification of transcripts from cDNA. Amplification of the ORF from genomic DNA served as control. Phusion High-Fidelity DNA polymerase was used according to the manufacturer's instructions.

Due to the size of the 4662 bp spliced *HAM5* transcript, it was amplified from wild type JR2 cDNA prepared from a four-day-old fungal liquid SXM culture in two overlapping fragments with JST53/JST58 (2476 bp) and JST90/JST45 (3227 bp).

The 1068 bp *VMK1* transcript was amplified from cDNA, which was prepared from mycelium obtained from plating of $1x10^6$ conidiospores on solid SXM covered with nitrocellulose membrane and incubation for four days. The primers JST61/JST62 were used.

The 1569 bp *MEK2* transcript was amplified from cDNA (prepared from a four-day-old fungal liquid SXM culture) using primers JST226/JST292.

The 1446 bp *ODE1* transcript was amplified from cDNA (prepared from a six-day-old fungal liquid PDM culture incubated in the dark) using primers JST175/JST176.

The cDNA used for amplification of *HAC1* was isolated from wild type cultures grown in 50 ml SXM ($1x10^7$ spores) and incubated at 25 °C under constant agitation for four days for the un-induced *HAC1* mRNA variant and with subsequent supplementation with 3 mM DTT for three hours for the induced *HAC1* mRNA variant. The 1581 bp un-induced *HAC1* mRNA sequence was amplified with primers JST171/JST172. The 1254 bp induced splice variant of *HAC1* was amplified using primers JST171/JST174.

PCR fragments were analyzed by agarose gel electrophoresis, excised from gel, and purified using the NucleoSpin Gel and PCR Clean-up Kit (Macherey-Nagel) according to the manufacturer´s instructions. Transcripts were fully sequenced. The ORF and splice sites given were confirmed for *HAM5* (*VDAG_JR2_Chr4g07170a*), *VMK1* (*VDAG_JR2_Chr2g01260a*), *MEK2* (*VDAG_JR2_Chr1g13070a*), and *ODE1* (*VDAG_JR2_Chr1g29610a*). The transcript variant given for *HAC1* (*VDAG_JR2_Chr2g09780a*) was confirmed as the uninduced variant *HAC1^u^*. A second splice variant of the *HAC1* mRNA named *HAC1^i^* was identified (sequence given in Figure S10).

2.4.9 Southern hybridization

All *Verticillium* transformants constructed in this study were confirmed by Southern hybridization analysis (Southern, 1975). Genomic DNA was extracted (2.4.1), cut by appropriate restriction enzymes overnight, and separated by agarose gel electrophoresis. The gel was washed under constant agitation in three steps: for ten

minutes in Wash buffer 1 (0.25 M HCl), 25 min in Wash buffer 2 (0.5 M NaOH, 1.5 M NaCl) for denaturation, and 30 min in Wash buffer 3 (0.5 M tris, 1.5 M NaCl, pH 7.4) for neutralization. The genomic DNA fragments were transferred by dry blotting from the gel onto an Amersham Hybond-Nylon membrane (GE Healthcare). The membrane was dried at 70 °C for ten minutes and exposed to UV-light (λ = 254 nm) for three minutes per side of the membrane for cross-linking of the DNA fragments. For labeling with the probe and subsequent detection, the Amersham Gene Images AlkPhos Direct Labeling and Detection System (GE Healthcare) was used according to the manufacturer's instructions.

The probes were hybridized to DNA fragments on the membrane at 60 °C rotating overnight. The membrane was washed twice with prewarmed first washing buffer (2 M urea, 50 mM SDS, 50 mM Na_3PO_4, 150 mM NaCl, 1 mM $MgCl_2$, 2% blocking reagent) for ten minutes at 60 °C rotating, and twice with the second washing buffer (1 M tris base, 1 M NaCl, pH 10) for five minutes at room temperature under constant agitation. Detection of the labeled DNA bands was performed by CDP-Star Detection Reagent (GE Healthcare) application to the membrane, incubation for 5 min, and exposure of an Amersham Hyperfilm ECL (GE Healthcare). The film was developed using an Optimax (Protec GmbH&Co.KG) film processor.

2.5 Protein methods

2.5.1 Protein extraction

For western hybridization, proteins were extracted from mycelium harvested from liquid cultures through Miracloth (Calbiochem Merck) and rinsed with 0.96% NaCl solution. Mycelium was dried, frozen, and ground to fine powder in liquid nitrogen using mortar and pestle. The powder was mixed with B* buffer (300 mM NaCl, 100 mM tris-HCl pH 7.5, 10% glycerol, 2 mM EDTA, 0.02% NP_4O), supplemented with 2 mM DTT and 10 µl/ml Protease inhibitor cocktail mix (Roche; stock solution: one tablet in 500 µl B* buffer). The mixture was centrifuged for 30 min at 13000 rpm at 4 °C. The supernatant was transferred to a new tube and used for further analysis or stored at -20 °C.

2.5.2 Determination of protein concentration by Bradford assay

The concentration of proteins was determined by the Bradford assay (Bradford, 1976). The absorbance of the protein sample mixed with Roti-Quant solution (Carl Roth GmbH&Co.KG) was measured with an Infinite M200 microplate reader operated with Magellan software (Tecan Trading AG). A bovine serum albumin (BSA; Carl Roth GmbH&Co.KG) dilution series was used as standard.

2.5.3 SDS-PAGE

Sodium dodecyl sulfate-polyacrylamide gel electrophoresis (SDS-PAGE; Smith, 1984) was used for separation of protein extracts according to the proteins´ molecular masses. The protein extract (2.5.1) was mixed with sample buffer [250 mM tris-HCl pH 6.8, 15% β-mercaptoethanol, 30% glycerol, 7% SDS, 0.3% Bromophenol blue] and boiled at 95 °C for five minutes. Prestained Protein Ladder (Thermo Fisher Scientific) was used as standard. Indicated amounts of the denaturized protein extracts were loaded on 12% acrylamide gels [Running gel: 3.3 ml H_2O, 2.5 ml tris buffer pH 8.8 (stock: 1.5 M), 100 µl SDS (stock: 10%), 4 ml polyacrylamide (stock: 30%), 100 µl ammonium persulfate (APS; stock: 10%), 10 µl *N,N,N',N'*-tetramethylethane-1,2-diamine (TEMED); stacking gel: 650 µl polyacrylamide (stock: 30%), 1.25 ml gel buffer (3 M tris, pH 8.45, 0.3% SDS), 3 ml H_2O, 15 µl Coomassie Brilliant Blue, 60 µl APS (stock: 10%), 10 µl TEMED], placed in running buffer (25 mM tris-base, 250 mM glycine, 0.1% SDS) and run at 120-200 V in Mini-Protean Tetra Cell (Bio-Rad Laboratories GmbH) for separation of proteins.

2.5.4 Immunoblot hybridization

During immunoblot hybridization, proteins separated by SDS-PAGE (2.5.3) were blotted to a nitrocellulose membrane (Amersham Protran 0.45 µm, GE Healthcare Life Sciences) using a Mini Trans-Blot Cell (Bio-Rad Laboratories) filled with transfer buffer [25 mM tris-base, 192 mM glycerol, 0.02% SDS, 20% methanol]. Wet electroblotting was performed either at 35 V at room temperature overnight or for one hour at 100 V with cool packs. PonceauS (0.2% PonceauS, 3% TCA) staining was used for visualization of transferred proteins as a loading control. The membrane was washed in TBST buffer [tris buffered saline and Tween20: 50 mM tris, 150 mM NaCl, 0.05% Tween20] and blocking in TBST supplemented with 5% milk powder (Sucofin TSI GmbH&Co.KG, Zeven, Germany) for one hour at room temperature was performed to prevent unspecific binding of the antibody. Membranes were incubated in primary antibody α-GFP sc-9996 (1:250; Santa Cruz Biotechnology) or α-HA (1:2000; Sigma-Aldrich Chemie GmbH) in TBST buffer with 5% milk powder at 4 °C overnight. Membranes were washed in TBST buffer for ten minutes at room temperature under constant agitation three times. As secondary antibody α-mouse 115-035-003 (1:2000; Jackson Immuno Research) in TBST buffer with 5% milk powder was applied to the membranes and incubated at room temperature for one to two hours. Membranes were washed in TBST buffer for ten minutes at room temperature under constant agitation three times. Detection of proteins was conducted via horseradish peroxidase (HRP) substrate luminol based chemiluminescence. Two detection solutions (solution 1: 2.5 mM luminol, 400 µM paracoumarat, 100 mM tris-HCl pH 8.5; solution 2: 100 mM tris-HCl pH 8.5, 5.4 mM H_2O_2) were applied to the membrane

and incubated for two minutes at constant agitation in the dark. Signals were detected with the Fusion SL chemiluminescence detector (Peqlab Biotechnology GmbH), operated with the corresponding software Fusion 15.18 (Vilber Lourmat), and Amersham Hyperfilm ECL film (GE Healthcare Life Sciences), which was developed by the use of the Optimax (Protec GmbH&Co.KG) film processor.

2.6 Sequence analyses

The online databases National Center for Biotechnology Information (NCBI; Geer *et al.*, 2010), VertiBase (http://biofung.gobics.de:1555/; coordinated by Prof. Dr. Gerhard H. Braus, University of Goettingen), and Ensembl Fungi (Kersey *et al.*, 2018) were used for BLAST searches. *Verticillium* gene predictions, accession numbers, and sequences were obtained from Ensembl Fungi and VertiBase. Seqbuilder (DNASTAR, Madison, USA) software was used for plasmid and primer design, prediction of restriction sites of enzymes, translation of DNA, and cDNA sequences into amino acid sequences and for calculation of molecular weights of proteins. Appropriate annealing temperatures of primer pairs were determined by the use of the online NEB Tm calculator v 1.9.12 (New England Biolabs, Ipswich, USA) or the Eurofins Genomics Oligo analysis tool for qRT-PCR primers. Sanger sequencing of plasmid DNA or PCR products was performed by the Microsynth Seqlab in Goettingen. Obtained sequences were analyzed using Lasergene (DNA STAR INC., Madison, WI, USA) software. The web server RNAfold (Zuker, 2003) was used for determination of secondary structures in qRT-PCR amplicons and mRNAs. Specificity of qRT-PCR primers was predicted by BLAST searches using Ensembl Fungi.

Prediction of protein domains was obtained using the InterPro website (http://www.ebi.ac.uk/Tools/pfa/iprscan; Jones *et al.*, 2014). The presence of localization signals was analyzed using the online databases cNLS mapper (http://nls-mapper.iab.keio.ac.jp/cgi-bin/NLS_Mapper_form.cgi; Kosugi *et al.*, 2009) and DeepLoc-1.0(Almagro Armenteros *et al.*, 2017; http://www.cbs.dtu.dk/services/DeepLoc/index.php). Multiple alignment of protein sequences was performed with ClustalW (Thompson *et al.*, 1994) or Muscle (Edgar, 2004) algorithms in MEGA6.0 software (Tamura *et al.*, 2013). Protein sequence identity matrices were obtained from multiple sequence alignments using the pairwise sequence identity and similarity calculation (SIAS) tool (http://imed.med.ucm.es/Tools/sias.html). Phylogenetic analysis was performed using Maximum likelihood tree calculations with MEGA6.0 software.

3 RESULTS

3.1 The *V. longisporum Vl43LS20kb* region makes the pathogenic isolate Vl43 more tolerable for the plant and is absent in the asymptomatic isolate Vl32

3.1.1 *V. longisporum* strains Vl43 and Vl32 are able to colonize rapeseed plants with different consequences for plant growth and development

V. longisporum species from different lineages display differences in their pathotypes. Isolates from the lineage A1/D1 are the most pathogenic on rapeseed whereas isolates from the lineage A1/D3 are the least pathogenic, but also colonize rapeseed plants (Novakazi *et al.*, 2015). Two isolates of these lineages, Vl43 (A1/D1) and Vl32 (A1/D3), were isolated from rapeseed fields in the same area in Germany (Zeise & von Tiedemann, 2002). The question about the genomic basis for the establishment of different pathotypes in related species was addressed, focusing on a Lineage Specific region of the pathogenic *V. longisporum* isolate Vl43, which is absent in the genome of the asymptomatic isolate Vl32.

In initial experiments, the colonization behavior of the two *V. longisporum* isolates Vl43 and Vl32 in rapeseed plants was compared by monitoring of induced disease symptoms and subsequent analysis of fungal outgrowth from infected tissue. One-week-old rapeseed plants were inoculated by root dipping into the same numbers of spores obtained from Vl43, Vl32, or into the water control (mock). After 35 days only Vl43 induced visible disease symptoms in the plants, including decreased height and leave length as well as chlorosis and necrosis of the leaves and reduced weight (Figure 7A). About 27% of the plants died from fungal infection with strain Vl43, 30% displayed strong symptoms, 27% weak symptoms and 17% of the tested plants did not show any disease symptoms. Plants infected with strain Vl32 were unaffected and did not show any alterations compared to uninfected mock plants.

Previous studies revealed that symptomatic and asymptomatic *V. longisporum* isolates show only minor lineage-specific phenotypic differences on specific media *ex planta.* No differences in early plant colonization on *A. thaliana* roots were observed regarding their growth on the root surface and formation of hyphopodia as invasion structures (unpublished data of Rebekka Harting from the University of Goettingen and Rabea Schlüter from the University of Greifswald).

Re-isolation experiments from surface sterilized stem sections of rapeseed plants inoculated with either one of the two *V. longisporum* isolates were conducted to test if both strains are able to further colonize the plant and show differences in the colonization

behavior after initial root penetration. After seven days strong fungal outgrowth was visible from Vl43 infected stem sections and to a smaller extend also from plants treated with Vl32 spores (Figure 7B).

Both *V. longisporum* isolates are able to colonize the vascular system of rapeseed plants, but only Vl43 induces plant disease, whereas rapeseed colonization by Vl32 is asymptomatic.
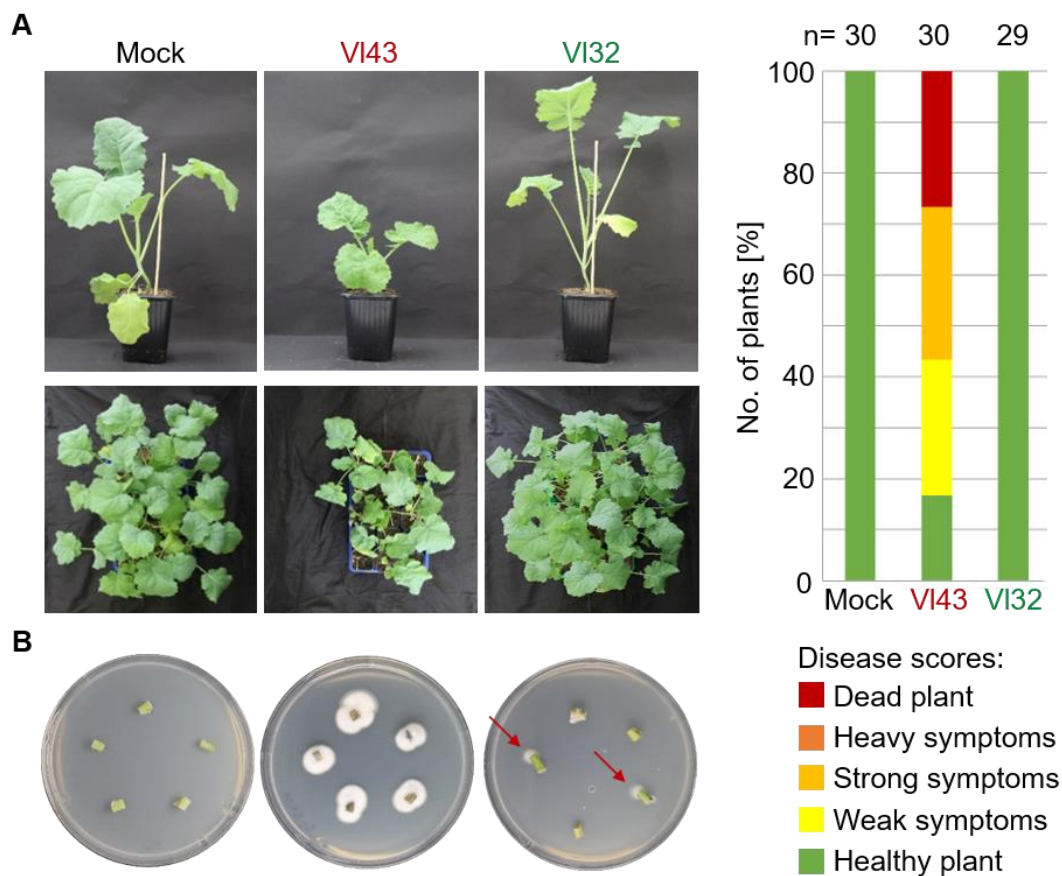

Figure 7: *V. longisporum* strains Vl43 and Vl32 colonize *B. napus* plants either pathogenically or asymptomatically. (**A**) Seven-day-old *B. napus* seedlings were inoculated by root dipping into distilled water as control (mock) or the same number of spores (1.5×10^6 spores/ml) obtained from Vl43 and Vl32. Disease symptoms were scored after 35 days. Single representative *B. napus* plants (top) and overview pictures of 15 plants per strain from a single experiment (bottom) 35 days post inoculation are shown. Parameters fresh weight, height of vegetation point, length of longest leaf, and symptom index of leaves were assessed in two independent experiments and transformed into disease scores per plant relative to control plants. The stack diagram shows the relative number of plants with certain disease scores. n = total number of evaluated plants. *V. longisporum* strain Vl43 induced visible disease symptoms in *B. napus* plants, whereas no disease symptoms can be observed in plants inoculated with Vl32 spores. (**B**) Fungal outgrowth from stem sections of representative plants treated with sterile water (mock), Vl43, or Vl32 spores. Stems were harvested 35 days post inoculation with fungal spores, surface sterilized, cut, and incubated on PDM supplemented with chloramphenicol for seven days at 25 °C. Both fungal strains could be re-isolated from surface sterilized infected stem sections on plate, however, to a smaller extend from plant material inoculated with Vl32 spores (indicated by red arrows).

3.1.2 The pathogenic *V. longisporum* Vl43 genome harbors the *Vl43LS20kb* region, which is absent in the asymptomatic colonizer Vl32

In order to investigate on which genomic basis the different pathotypes of the two *V. longisporum* isolates rely, the genomes of the pathogen and the asymptomatic colonizer were sequenced (BioFung Consortium BMBF). It was found that only very few genes were specific for one of the two *V. longisporum* genomes. Optical mapping of both genomes revealed differences in the chromosome numbers with 16 for Vl32 and 15 for Vl43, correlating with alterations in the chromosome sizes. Genome alignments allowed to explain the differences in the karyotypes between the two *V. longisporum* isolates by massive syntenic rearrangements as previously observed in several species of the genus *Verticillium* (Shi-kunne & Faino, 2017). A correlation between genomic rearrangements and the evolution of LS regions was found in haploid Verticillia (Klosterman *et al.*, 2011; de Jonge *et al.*, 2013; Faino *et al.*, 2016; Chen *et al.*, 2018; Gibriel *et al.*, 2019). Klosterman and coworkers reported on LS regions in the genome of *V. dahliae* VdLs.17 that share no synteny with the genome of *V. alfalfae* VaMs.102, which were suggested to be involved in adaptation to different host niches (Klosterman *et al.*, 2011).

In order to address the question if LS genes are important for the pathotype of the *V. longisporum* isolate Vl43, a bioinformatic screen was used to identify regions present specifically in the genome of the pathogenic *V. longisporum* isolate Vl43, but are absent in the asymptomatic plant colonizer Vl32. Thereby, a region of approximately 20 kb in size was identified, which is absent in the genome of the asymptomatic A1/D3 isolate. This region is named *Vl43LS20kb* in the following. The same region could be identified in the genome of the pathogenic *V. longisporum* A1/D1 isolate Vl145c.

V. longisporum species evolved by hybridization from two parental lineages with a *V. dahliae* strain, or at least a close relative to *V. dahliae,* as one of them (Karapapa *et al.*, 1997; Collins *et al.*, 2003; Clewes *et al.*, 2008; Collado-Romero *et al.*, 2010; Inderbitzin *et al.*, 2011b; Tran *et al.*, 2013). A homologous region to the *Vl43LS20kb* region could be identified in the genome of the *V. dahliae* strain JR2 (Figure 8), but not in the genome of *V. alfalfae* VaMs.102.

Correct genome assembly of the *V. longisporum Vl43LS20kb* region was confirmed by PCR amplification and sequencing by primer walking for the entire region. The absence of this region in the Vl32 genome, proposed by the bioinformatic screen, was confirmed by PCR reactions targeting seven genes, named <u>L</u>ineage <u>S</u>pecific region <u>G</u>ene (*LSG*) *1* to *7,* predicted for the *Vl43LS20kb* region according to the gene annotations for *V. dahliae* JR2 (Ensembl Fungi, de Jonge *et al.*, 2012; Figure 8). PCR products for all seven *LSG*s and the histone encoding gene *H2A* as positive control were obtained using Vl43 genomic DNA as a template, whereas no specific PCR products were obtained from genomic DNA of Vl32 for the seven *LSG*s, but for the positive control (Figure 8A).

All predicted genes of this region were only identified in single copy in the *V. longisporum* Vl43 and Vl145c genomes by BLAST search of the nucleotide sequences. In contrast, the *V. dahliae* JR2 genome harbors two copies for *LSG1* identified by BLAST search of the genomic sequence. One copy located in the *Vl43LS20kb* homologous region between *VDAG_JR2_Chr2g10300a* and *VDAG_JR2_Chr2g10310a* was not annotated. A second copy is located on chromosome five (*VDAG_JR2_Chr5g10950a*).

A

B
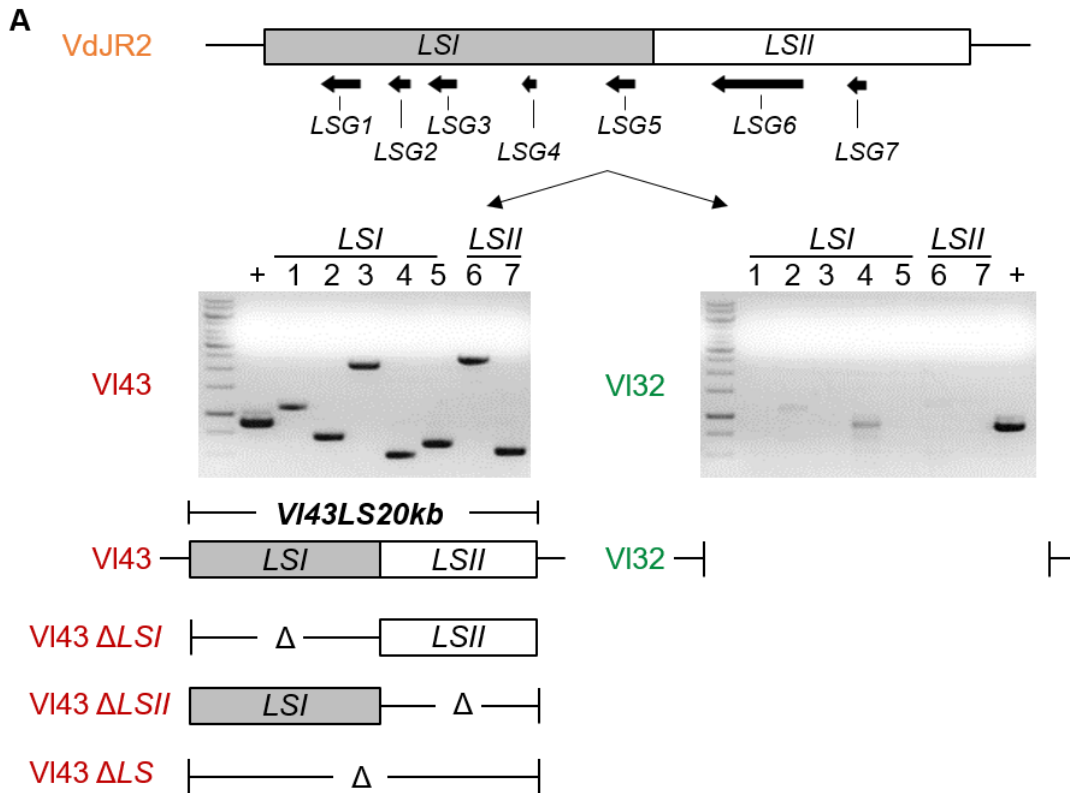
Vl43 genes	Protein size/Mw	Domains	Localization	Vd JR2 homolog/s (*VDAG_JR2_*)	aa sequ. ID
LSG1	173 aa/19 kDa	-	Cytosol	*Chr5g10950a*, 2nd between *Chr2g10300a/ Chr2g10310a*	100% to both VdJR2 copies
LSG2	228 aa/25 kDa	-	Cytosol	*Chr2g10300a*	100%
LSG3	258 aa/29 kDa	bHLH DNA binding	Nucleus	*Chr2g10290a*	99.2%
LSG4	131 aa/15 kDa	-	Nucleus	*Chr2g10280a*	100%
LSG5	163 aa/18 kDa	Zinc finger RING-type, TM-helix	Plasma membrane	*Chr2g10270a*	94.7%
LSG6	666 aa/74 kDa	bZIP	Nucleus	*Chr2g10260a*	99.7%
LSG7	119 aa/13 kDa	-	Nucleus	*Chr2g10250a*	99.2%

Figure 8: The symptomatic *V. longisporum* strain Vl43 harbors a specific *Vl43LS20kb* region in its genome, which is absent in the asymptomatic isolate Vl32. (**A**) Lineage Specific region of *V. longisporum* Vl43. An LS region of approximately 20 kb in size, named *Vl43LS20kb,* is present in the genome of the pathogenic *V. longisporum* isolate Vl43, but absent from the genome of the asymptomatic rapeseed colonizer Vl32. A *Vl43LS20kb* homologous region was identified in the genome of *V. dahliae* JR2. Seven <u>L</u>ineage <u>S</u>pecific region <u>G</u>enes (*LSG1-7*) were predicted for this region in *V. dahliae* (Ensembl Fungi). The presence of the *V. longisporum Vl43LS20kb* region in Vl43 was confirmed by PCR reactions, giving products for *LSG1-7* and the histone H2a encoding gene as a positive control (+). No specific PCR products were obtained from genomic DNA of Vl32 for the genes predicted in the *Vl43LS20kb* region, but for the positive control. The *Vl43LS20kb* region was dissected into two parts *LSI* and *LSII* and Vl43 deletion strains lacking either *LSI*, *LSII*, or the total *Vl43LS20kb* region (Vl43 ΔLSI, ΔLSII, ΔLS) were constructed to analyze the role of this region in virulence of Vl43. (**B**) Characteristics of Vl43 *LSG1-7* deduced proteins. The *Vl43LS20kb* region encodes homologs to *LSG1-7* predicted in *V. dahliae* JR2 (Ensembl Fungi). Protein sequences of the deduced Vl43 proteins Lsg1-7 were proposed according to the Vl43 genomic sequences (VertiBase) and the *V. dahliae* JR2 transcripts (Ensembl Fungi). Protein domains were predicted by InterProScan. A basic helix-loop-helix (bHLH) DNA binding domain was proposed for Lsg3 (184-255 aa, IPR011598) as well as a Zinc finger RING-type domain (65-148 aa, IPR013083) and a transmembrane (TM) helix (15-37 aa, Phobius, TM-helix; 40-163 aa cytosolic; N-terminus non-cytosolic) for Lsg5. A basic-leucine zipper (bZIP) domain was predicted for Lsg6 (137-200 aa, PS50217, IPR004827). Protein localizations were predicted using cNLS mapper and DeepLoc-1.0 tools. The amino acid sequence identities (ID) of the Vl43 and *V. dahliae* JR2 proteins were determined by alignment of the amino acid sequences using NCBI tools and MEGA 6.0 software. Mw: molecular weight.

For six of the seven genes in the *Vl43LS20kb* region, the deduced proteins are rather small with 119-258 amino acids (aa) in length (Figure 8B). Only *LSG6* potentially encodes a larger protein with 666 aa and a molecular weight of 74 kDa. Domains were only predicted for three of the hypothetical proteins. Two of them contain specific transcription factor domains with a basic helix-loop-helix (bHLH) DNA binding domain for Lsg3 and a basic-leucine Zipper (bZIP) domain for Lsg6. For the potential transcription factors Lsg3 and Lsg6, nuclear localization was proposed by the cNLS mapper and DeepLoc-1.0 prediction tools.

Lsg5 contains a Zinc finger RING-type domain and a transmembrane domain. Zinc finger RING-type domains are involved in protein-protein interactions and in mediating ubiquitin transfer to substrates or the Zinc finger RING-type domain protein itself (Joazeiro & Weissman, 2000). DeepLoc-1.0 proposed a localization of Lsg5 to plasma membranes with 54%.

As for Lsg3 and Lsg6, nuclear localization was predicted for Lsg4, whereas Lsg1 and Lsg2 proteins were sorted to the cytosol (Figure 8B). For none of the hypothetical proteins secretion signals were identified.

In summary, bioinformatic analyses identified a *Vl43LS20kb* region in the genome of the pathogenic *V. longisporum* isolate Vl43, which is absent in the asymptomatic strain Vl32. The presence of a homologous region in the haploid *V. dahliae* JR2 corroborates its origin in the parental lineage D1. The *Vl43LS20kb* region encodes six small proteins

without secretion signals and one larger protein, where two of them have the potential to function as transcription factors and one protein is potentially involved in ubiquitination.

3.1.3 The *Vl43LS20kb* region reduces virulence in rapeseed plants

Vl43 deletion strains were constructed to unravel whether the *Vl43LS20kb* region, which is present in the genome of the pathogenic *V. longisporum* isolate but absent in the asymptomatic isolate Vl32, contributes to the differences in pathotypes.

The *Vl43LS20kb* region was dissected into a ~11.5 kb *LSI* region and a ~8.5 kb *LSII* region and Vl43 deletion strains lacking either *LSI*, *LSII*, or the total *LS* region were constructed (Figure 8A). Correct replacement of the regions against the respective marker cassettes was verified by Southern hybridization (Figure S1). The resulting strains Vl43Δ*LSI*, Vl43Δ*LSII*, and Vl43Δ*LS* displayed unaltered *ex planta* phenotypes in comparison to wild type 14 days after spot inoculation under different growth conditions, including simulated xylem medium, minimal medium with different carbon sources (sucrose or galactose), and minimal medium supplemented with different stress inducing agents as Sorbitol, SDS, or H_2O_2 (Figure S2). Small alterations in melanization of the colony centers between independent experiments were not significant.

Infection studies were performed with Vl43 Δ*LSI*, Δ*LSII*, and Δ*LS* strains in comparison to the *V. longisporum* isolates Vl43, Vl32, or water control (mock) to determine the role of the *Vl43LS20kb* genomic region in virulence of Vl43. Rapeseed plants treated with spores obtained from the isolate Vl32 were indistinguishable from uninfected plants, whereas plants inoculated with Vl43 Δ*LSI*, Δ*LSII*, and Δ*LS* spores displayed more severe disease symptoms compared to plants treated with spores from the pathogenic wild type Vl43 after 35 days (Figure 9). Whereas 27% of the plants treated with the Vl43 wild type died from fungal infection, 70% dead plants were scored for Vl43 Δ*LSI*, 83% for Vl43 Δ*LSII*, and 89% for Vl43 Δ*LS* (Figure 9A, B). Significant differences between plants inoculated with spores from Vl43 and the *LSI*, *LSII,* and *LS* deletion strains were determined for the numbers of dead plants (Figure 9C).

Reversely, the region identified upon comparison of a pathogenic and an asymptomatic *V. longisporum* isolate does not promote induction of disease symptoms by the pathogen Vl43, but attenuates pathogenesis in the host-fungus interaction and makes the fungus more tolerable for rapeseed plants.
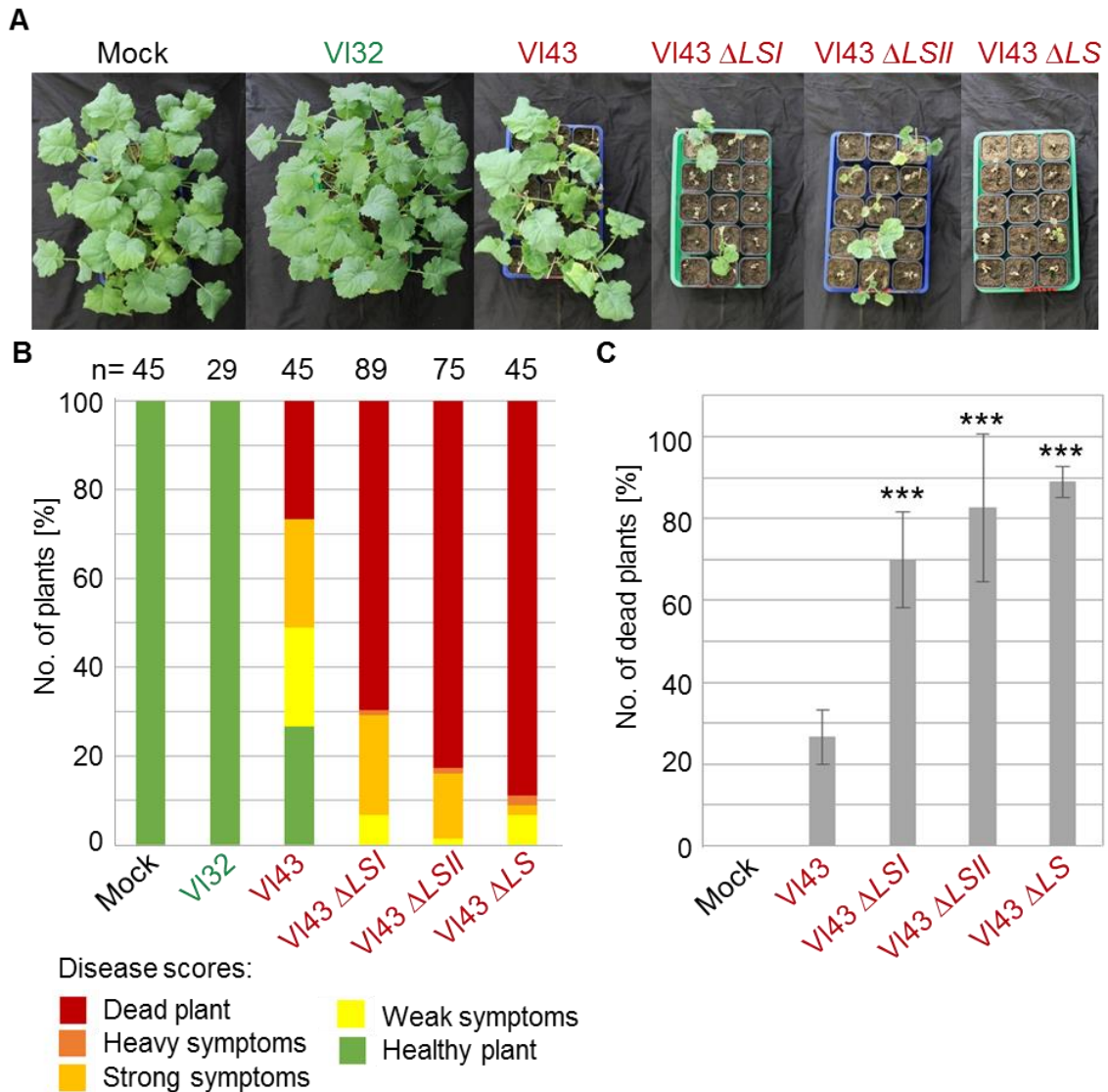
Figure 9: The *Vl43LS20kb* region absent in the asymptomatic *V. longisporum* isolate Vl32 attenuates disease symptom induction of Vl43 in *B. napus*. Seven-day-old *B. napus* seedlings were inoculated by root dipping into water as control (mock) or into the same numbers of spores obtained from Vl32 and Vl43 wild types, Vl43 ΔLSI, ΔLSII, or ΔLS. Disease symptoms were assessed after 35 days. Two independent transformants were tested for Vl43 ΔLSI (VGB201, VGB233) and ΔLSII (VGB193, VGB214), and a single transformant for ΔLS (VGB232) in three independent experiments. For plants treated with spores obtained from Vl32 no disease symptoms were observed. *LSI, LSII* and *LS* deletion strains display increased severity of disease symptoms in comparison to wild type Vl43. (**A**) Overview pictures of *B. napus* plants after 35 days. (**B**) Stack diagram of the relative number of plants with certain disease scores per genotype. Parameters fresh weight, height of vegetation point, length of longest leaf, and symptom index of leaves were assessed and transformed into disease scores per plant relative to control plants. n = total number of evaluated plants. (**C**) The diagram shows the number of dead plants 35 days post inoculation with water control or fungal spores relative to the total number of evaluated plants. Bars represent mean values of three independent experiments with standard deviations. Significant differences compared to wild type Vl43 were calculated with one-way Anova and Student´s t-test: ***p<0.001; n(mock, Vl43, ΔLS)=3; n(Vl43 ΔLSI, ΔLSII)=6.

3.1.4 The homologous *Vl43LS20kb* region in *V. dahliae* is indifferent for virulence towards tomato plants

The *Vl43LS20kb* region identified by comparison of two *V. longisporum* isolates is in the same synteny in the haploid *V. dahliae* strain JR2, suggesting its origin in the haploid parental lineage D1. To address the question if the homologous region in *V. dahliae* has a similar function in attenuation of plant disease symptoms as in *V. longisporum* Vl43, JR2 *LS* deletion strains were constructed (Figure S3) and tested regarding induction of disease symptoms in tomato plants (Figure 10).

Prior to the investigation of the *in planta* phenotype, the *ex planta* phenotypes of *V. dahliae* JR2 ΔLS were tested in comparison to the wild type ten days after spot inoculation on the same media as Vl43 *LS* deletion strains (Figure S4). Like in *V. longisporum* Vl43, the *LS* region is dispensable for vegetative growth of *V. dahliae* JR2 *ex planta* since no significant phenotypic alterations were observed. Only slight reductions in melanization were visible for the JR2 *LS* deletion strain compared to wild type on CDM with galactose as carbon source (Figure S4).
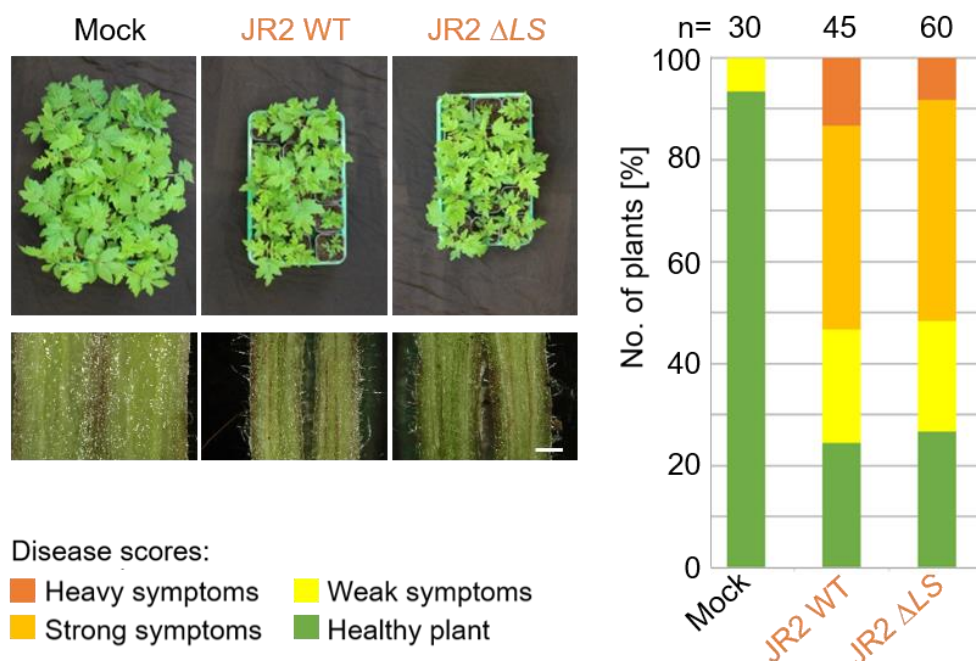
Figure 10: The *Vl43LS20kb* homologous region in *V. dahliae* is indifferent for virulence towards tomato plants. Ten-day-old *S. lycopersicum* seedlings were inoculated by root dipping into water control (mock), the same numbers of spores obtained from the *V. dahliae* wild type JR2, or two independent *LS* deletion transformants (VGB383, VGB393). Overview pictures of control plants and plants inoculated with wild type or JR2 ΔLS and hypocotyl cross sections of representative plants are shown (Scale bar = 1 mm). Disease symptoms fresh weight, height of vegetation point, and length of longest leave were assessed after 21 days in two independent experiments and transformed into a disease score per plant. The stack diagram shows the relative number of plants with a certain disease score. Plants infected with wild type or JR2 ΔLS display similar severity of disease symptoms. n = total number of evaluated plants.

Tomato plant infections were performed to investigate the role of the *V. dahliae* *Vl43LS20kb* homologous region in pathogenicity. *S. lycopersicum* plants were inoculated with spores obtained from two independent ΔLS transformants and the disease symptoms were scored after 21 days. JR2 ΔLS treated tomato plants displayed unaltered severity of disease symptoms and hypocotyl discolorations comparable to wild type infected plants (Figure 10).

Taken together, the *V. longisporum* A1/D1 *Vl43LS20kb* region absent in the asymptomatic *V. longisporum* A1/D3 isolate Vl32 is consistent in *V. dahliae* JR2 and presumably derives from the D1 parental strain. The region encodes several small proteins, two potential transcription factors and one protein potentially involved in protein-protein interactions. In *V. dahliae,* the presence or absence of this region results in similar severity of disease symptoms in tomato plants. In contrast, the same region attenuates disease symptoms induced by the pathogenic *V. longisporum* A1/D1 isolate Vl43 in rapeseed. In conclusion, even pathogenic fungi possess specific genomic regions which make virulence more tolerable for the host plant.

3.2 Vmk1/Mek2 MAPK cascade-mediated microsclerotia formation and pathogenicity in *V. dahliae* are independent from the scaffold protein Ham5

3.2.1 *V. dahliae* Ham5 corresponds to the *N. crassa* scaffold protein HAM-5

The Vmk1 MAPK signaling cascade is homologous to yeast Fus3/Kss1 MAPK pathways and is essential for regulation of virulence in *V. dahliae* (Rauyaree *et al.*, 2005; Sarmiento-Villamil *et al.*, 2018). The MAPK pathway components Vmk1 and the yeast Ste12-like transcription factor Vph1 of *V. dahliae* are essential for regulation of pathogenicity and differ in their impact on microsclerotia formation (Rauyaree *et al.*, 2005; Sarmiento-Villamil *et al.*, 2018). The genomes of the Pezizomycotina, the biggest subdivision of the Ascomycota, harbor a gene encoding a highly conserved protein which was allocated to scaffolding functions in the Fus3/Kss1-like MAPK pathway (Jamet-Vierny *et al.*, 2007; Dettmann *et al.*, 2014; Jonkers *et al.*, 2014, 2016; Frawley *et al.*, 2018). A scaffold protein for this pathway has not yet been described in any filamentous phytopathogen. The role of the *N. crassa* HAM-5 homolog in differentiation and virulence of *V. dahliae* was analyzed combined with the characterization of the MAP2K homolog Mek2 and the MAPK Vmk1 as control.

The *V. dahliae* gene *VDAG_JR2_Chr4g07170a* was identified as a predicted homolog to the *N. crassa* scaffold HAM-5 encoding gene using reciprocal BLAST search of the deduced amino acid sequences against the *V. dahliae* JR2 (Ensembl Fungi) and the

N. crassa OR74A (NCBI database) proteomes. The *HAM5* pre-mRNA of 4906 bp has a predicted intron-exon structure with five exons, which was confirmed by PCR amplification of the spliced transcript from wild type cDNA (Figure 11A).
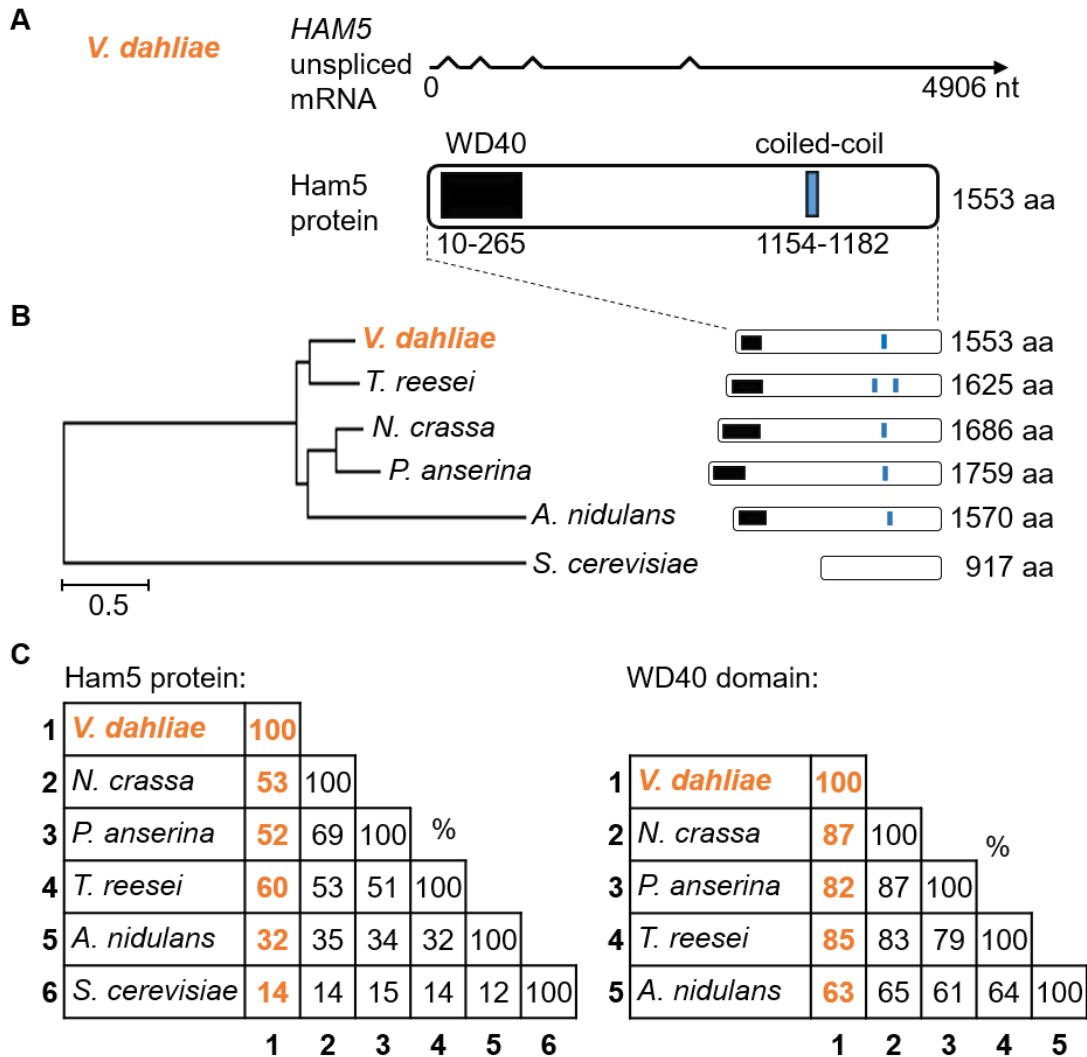

Figure 11: Comparison of *V. dahliae* Ham5 and corresponding proteins in related fungi.
(**A**) The intron-exon structure of *V. dahliae HAM5* predicted by Ensembl Fungi (*VDAG_JR2_Chr4g07170a*) was confirmed by PCR amplification of the spliced transcript from wild type cDNA. The protein consists of 1553 aa and contains predicted WD40 repeats at the N-terminus (black; IPR015943; 10-265 aa) and a coiled-coil domain (blue; 1154-1182 aa). Domains were predicted by InterProScan. (**B**) Phylogenetic tree of the Ham5 protein. Phylogenetic analysis with aa sequences from: *V. dahliae* Ham5 (*VDAG_JR2_Chr4g07170a*), *T. reesei* HAM-5 (AKN58846.1), *N. crassa* HAM-5 (XP_011393509.1*), P. anserina* IDC1 (ABJ96338.2), *A. nidulans* HamE (AN2701), and *S. cerevisiae* Ste5 (NP_010388.1) was performed (ClustalW algorithm). WD40 (IPR015943; black box) and coiled-coil domains (blue bar) were predicted by InterProScan. Scale bar = average number of amino acid substitutions per site. (**C**) Ham5 protein sequence identity matrices of the Ham5 full-length protein homologs and orthologs (left) and their WD40 domains (right) (ClustalW). Amino acid sequence identities are given in %. Pairwise sequence identity and similarity calculation from multiple sequence alignments were performed using SIAS tool.

The deduced Ham5 protein with a length of 1553 aa and a molecular weight of 170 kDa contains N-terminal WD40 repeats and a coiled-coil domain at the C-terminus. The corresponding HAM-5 proteins of related filamentous fungi are similar in length and show conserved protein domains, including C-terminal coiled-coil domains and N-terminal WD40 repeat domains (Figure 11A, B). WD40 repeat domains have been found in several fungal scaffold proteins (Pöggeler & Kück, 2004; Jain, 2019; Hicks *et al.*, 2001). These domains form symmetrical disc-like Beta-propeller structures, shaped by blades assembled around a central channel (Chen *et al.*, 2011) that allow the coordination of multi-protein complexes (Xu & Min, 2011). The WD40 domain was shown to be important for binding of the MAPK MAK-2 to the scaffold HAM-5 in *N. crassa* (Jonkers *et al.*, 2014). A phylogenetic analysis of the *V. dahliae* Ham5 protein, its described homologs in ascomycetes, and the non-homologous yeast scaffold protein Ste5 indicated that *V. dahliae* Ham5 has the highest similarity to *Trichoderma reesei HAM-5* with 60% aa sequence identity, followed by *N. crassa HAM-5* with 53% and *Podospora anserina IDC1* with 52% (Figure 11B, C). *V. dahliae* Ham5 and *A. nidulans* HamE are less closely related, showing only 32% aa sequence identity (Figure 11B, C). The orthologous yeast scaffold protein Ste5 has 14% aa sequence identity with the *V. dahliae* protein, is much smaller, and does not share the domain predictions of the Ham5 homologs (Figure 11B, C).

The proposed WD40 domains of the corresponding Ham5 proteins in related fungi displayed generally higher amino acid sequence similarities than the full-length proteins (Figure 11C). The deduced protein sequence of the putative HAM-5 homolog in *V. dahliae* has 87% identity to *N. crassa* HAM-5. *V. dahliae* Ham5 displays higher amino acid sequence conservation of the entire protein and the WD40 domain to *N. crassa* HAM-5 than *A. nidulans* HamE which shows 35% aa sequence identity to the entire protein and 65% to the WD40 repeat domain of *N. crassa* HAM-5 (Figure 11C).

3.2.2 The *V. dahliae* MAP2K Mek2 and the MAPK Vmk1 show high similarities to *N. crassa* MEK-2 and MAK-2

The *N. crassa* scaffold protein HAM-5 assembles the MAPK cascade components MAK-2 (MAPK), MEK-2 (MAP2K), and NRC-1 (MAP3K) (Dettmann *et al.*, 2014; Jonkers *et al.*, 2014, 2016). The *V. dahliae* homologs to *N. crassa mek-2* and the *V. dahliae* VdLs.17 MAPK encoding gene *VMK1* were identified by reciprocal BLAST search of the deduced amino acid sequences against the *V. dahliae* JR2 (Ensembl Fungi), *N. crassa* OR74A (NCBI database), or the *V. dahliae* VdLs.17 (Ensembl Fungi) proteome.

The potential MAP2K homolog in *V. dahliae* is encoded by the gene *VDAG_JR2_Chr1g13070a*. The *V. dahliae MEK2* pre-mRNA of 1756 bp contains four exons (Figure 12A left).
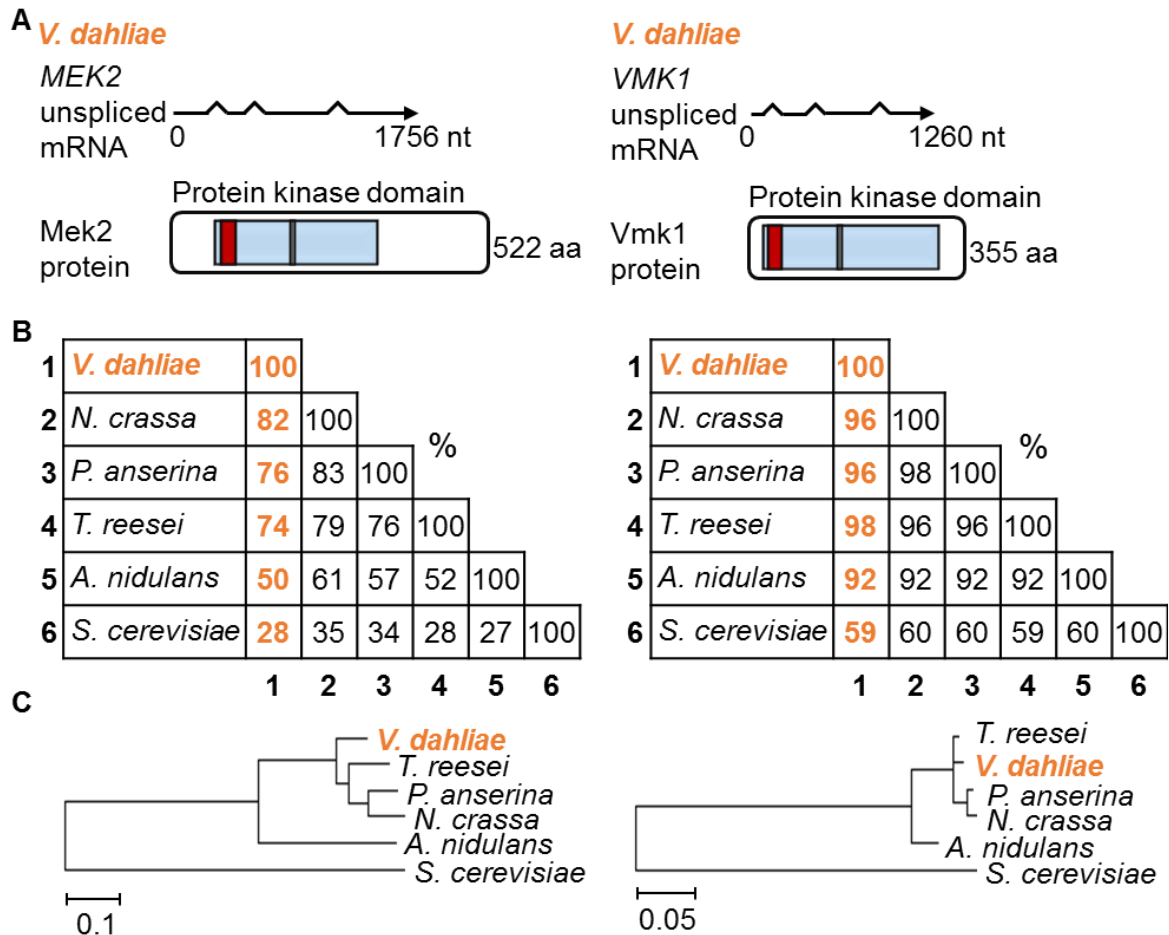

Figure 12: The *V. dahliae* MAP2K Mek2 and MAPK Vmk1 are highly conserved in fungi. (**A**) The unspliced mRNA structure and protein domain predictions of *V. dahliae* Mek2 and Vmk1. Predicted intron-exon structures of the 1756 bp *MEK2* (left) and the 1260 bp *VMK1* (right*)* unspliced mRNAs were confirmed by PCR amplification of spliced transcripts from wild type cDNA. Mek2 consists of 522 aa and contains a protein kinase domain (blue; 67-332 aa; IPR000719), with the serine/threonine-protein kinase active site at 186-198 aa (grey bar; IPR008271) and an ATP binding site (red; 73-96 aa; IPR017441). Vmk1 consists of 355 aa and contains a protein kinase domain (blue; 23-311 aa; IPR000719), with the serine/threonine-protein kinase active site at 143-155 aa (grey bar; IPR008271) and an ATP binding site (red; 29-53 aa; IPR017441). Domains were predicted by InterProScan. (**B**) Protein sequence identity matrices of corresponding Mek2 (left) and Vmk1 (right) proteins from related fungi. Protein sequence identities are given in %. Identifiers of used sequences are given in **C**. ClustalW algorithm, pairwise amino acid sequence identity and similarity calculation were performed using the SIAS online tool. (**C**) Phylogenetic trees of corresponding Mek2 (left) and Vmk1 (right) proteins from related fungi. <u>Left:</u> protein sequences were used from: *V. dahliae* Mek2 (*VDAG_JR2_Chr1g13070a*), *T. reesei* (XP_006963390.1), *P. anserina* (XP_001910826.1), *N. crassa* Mek-2 (XP_011394665.1), *A. nidulans* MkkB (AN3422), *S. cerevisiae* Ste7 (NP_010122.1). <u>Right:</u> protein sequences were used from: *V. dahliae* Vmk1 *(VDAG_JR2_Chr2g01260a)*, *T. reesei* tmk1 (XP_006965066.1), *P. anserina* PaMpk1 (XP_001929742.1), *N. crassa* MAK-2 (AAK25816.1), *A. nidulans* MpkB (AAF12815.2), *S. cerevisiae* Fus3 (NP_009537.1) (ClustalW algorithm). Scale bar = average number of amino acid substitutions per site.

Expression was confirmed by PCR amplification of the spliced transcript from wild type cDNA. The deduced protein Mek2 consists of 522 aa with a molecular weight of 57 kDa and contains a protein kinase domain with a serine/threonine-protein kinase active site and an ATP binding site (Figure 12A left). *V. dahliae* Mek2 possesses high conservation with maximum 82% aa sequence identity to *N. crassa MEK-2* and only 28% to the yeast *S. cerevisiae* MAP2K Ste7 (Figure 12B, C left).

The homologous gene to VdLs.17 *VMK1* (*VDAG_09461*) was identified in *V. dahliae* JR2 (*VDAG_JR2_Chr2g01260a*) with 100% aa sequence identity. The predicted *VMK1* pre-mRNA of 1260 bp contains four exons (Figure 12A, right) and expression was confirmed by PCR amplification of the spliced transcript from wild type cDNA. The deduced protein Vmk1 consists of 355 aa with a molecular weight of 41 kDa. A protein kinase domain with a serine/threonine-protein kinase active site and an ATP binding site was predicted by InterProScan (Figure 12A, right).

The *V. dahliae* MAPK Vmk1 possesses even higher conservation than the MAP2K with 98% aa sequence identity to the corresponding protein in *T. reesei*, followed by 96% to the respective MAP kinase in *N. crassa* and *P. anserina* (Figure 12B, C, right).

Both components of the yeast Fus3-like MAPK pathway, the MAPK Vmk1 and the MAP2K Mek2, are highly conserved in *V. dahliae* JR2, with Mek2 a little less conserved in analyzed species than Vmk1.

3.2.3 Vmk1- and Mek2-mediated regulation of vegetative growth and microsclerotia formation is independent from Ham5

In order to analyze the role of the putative scaffold Ham5 in Vmk1 MAPK pathway-mediated development and virulence of *V. dahliae*, *HAM5*, *MEK2*, and *VMK1* deletion strains as well as *HAM5*/*MEK2* and *HAM5*/*VMK1* double deletion strains were constructed. The genes under control of their native promoters and terminators were ectopically reintegrated into the genomes of the single deletion strains to analyze whether complementation of phenotypes is possible. Prior to functional investigation, correct integration of deletion and complementation constructs was confirmed by Southern hybridization analysis (Figure S5, S6, S7).

Analysis of the *ex planta* phenotype of the *HAM5* deletion strain revealed wild type-like growth. No alterations were observed regarding colony size, melanization, or microsclerotia formation under several tested conditions, including complete media (PDM, Malt extract agar), simulated xylem medium, or minimal medium with different carbon sources (CDM with either sucrose, galactose, glucose, or cellulose). In Figure 13A ΔHAM5 colonies nine days after spot inoculation on SXM and CDM with either sucrose or cellulose as carbon source are shown as examples.
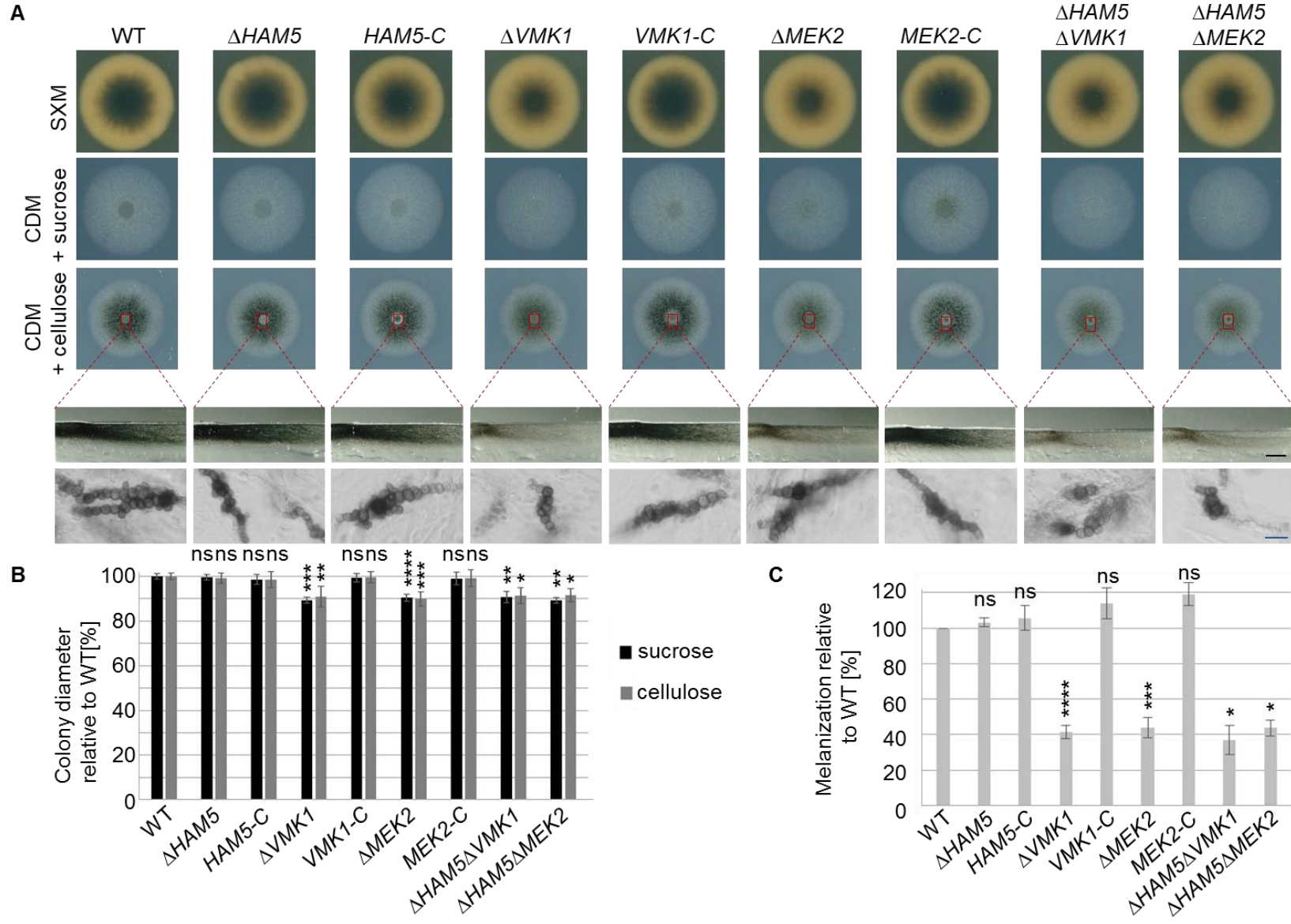
Figure 13: *V. dahliae VMK1-* and *MEK2*-mediated vegetative growth and microsclerotia formation function independent of *HAM5*. The *HAM5* deletion strain was compared to wild type JR2, *VMK1,* and *MEK2* single deletions with respective complementation strains, as well as Δ*HAM5*Δ*VMK1* and Δ*HAM5*Δ*MEK2* double deletions regarding their vegetative growth and microsclerotia formation *ex planta*. 50 000 freshly harvested spores were spot inoculated on SXM or CDM with either sucrose or cellulose as carbon source and incubated at 25 °C for nine days. The e*x planta* phenotypes of two independent transformants per single deletion strain (VGB279, VGB280, VGB335, VGB336, VGB337, VGB338) or one transformant per double deletion (VGB346, VGB417) and complementation strain (VGB389, VGB413, VGB415) were tested. Black scale bar = 1 mm, blue scale bar = 20 µm. (**A**) *Ex planta* phenotypes nine days after spot inoculation. Cross sections of colony centers and microscopy of fungal material scraped from colony centers grown on CDM with cellulose as carbon source (indicated by red boxes and dashed lines) are shown. (**B**) Growth quantification on either CDM with sucrose (black) or cellulose (grey) as carbon source nine days after spot inoculation. Growth of Δ*VMK1,* Δ*MEK2,* Δ*HAM5*Δ*VMK1,* and Δ*HAM5*Δ*MEK2* strains is significantly decreased to about 90% in comparison to wild type. Δ*HAM5* and the complementation strains show wild type-like growth. Growth was quantified by measurement of two perpendicular diameters per colony for three plates per transformant and medium (n=1). Bars represent mean values of three independent experiments with standard deviations relative to wild type. Significant differences to wild type determined with one-way Anova and Student´s t-test are shown with *p<0.05; **p<0.01; ***p<0.001, ****p=0, ns= non-significant. n(Δ*HAM5;* Δ*VMK1;* Δ*MEK2*)=6; n(WT; Δ*HAM5*Δ*VMK1;* Δ*HAM5*Δ*MEK2; HAM5-C*; *VMK1-C*; *MEK2-C*)=3. (**C**) Melanization of colonies grown on CDM with cellulose relative to wild type. Whereas Δ*HAM5* shows wild type-like melanization, Δ*MEK2,* Δ*VMK1,* Δ*HAM5*Δ*MEK2,* and Δ*HAM5*Δ*VMK1* display a significant decrease to 38-46% of the wild type level. Pictures were taken from the top view of the colonies after removal of aerial mycelium. The brightness factor of the colony center was measured for three colonies per transformant (n=1) using the ImageJ software. The means of the brightness factor were determined, set relative to wild type, and inverted to obtain melanization values. Bars represent mean values with standard deviations from two independent experiments. Significant differences to wild type determined with one-way Anova and Student´s t-test are shown with *p<0.05; ***p<0.001, ****p=0, ns= non-significant. n(WT; Δ*HAM5*Δ*VMK1;* Δ*HAM5*Δ*MEK2; HAM5-C*;*VMK1-C*;*MEK2-C*)=2; n(Δ*HAM5*)=3; n(Δ*VMK1;* Δ*MEK2*)=4.

Furthermore, vegetative growth of the Δ*HAM5* strain was tested on minimal medium supplemented with stress inducing agents (0.5 M NaCl, 0.00075% H_2O_2, 0.004% SDS, or 0.8 M Sorbitol) without observation of any phenotypical alterations. Since no self-anastomosis of vegetative hyphae or germination tubes were observed for the *V. dahliae* wild type JR2 under any growth condition, the role of Ham5 in cell fusion was not characterized.

In contrast to the *HAM5* deletion strain, *MEK2* and *VMK1* single and double deletion strains show a ~10% significant decrease in growth on CDM with either sucrose or cellulose as carbon source nine days after spot inoculation which was not observed for the complementation strains *MEK2-C* and *VMK1-C* (Figure 13A, B).

Whereas the *HAM5* deletion strain shows wild type-like melanization, the colony centers formed by strains Δ*MEK2,* Δ*VMK1,* Δ*HAM5*Δ*MEK2,* and Δ*HAM5*Δ*VMK1* on SXM and CDM with sucrose or cellulose as carbon source appear less melanized after nine days (Figure 13A). The differences in melanization become more apparent in cross sections of the colony centers. Microscopy of fungal material from the colony centers for all tested strains showed melanized microsclerotia similar to wild type, however, in qualitatively

reduced frequencies in Δ*MEK2,* Δ*VMK1,* Δ*HAM5*Δ*MEK2,* and Δ*HAM5*Δ*VMK1* (Figure 13A). The melanization of the colony centers of all strains grown on cellulose containing medium was quantified and confirmed the wild type-like melanization in the Δ*HAM5* strain. In contrast, a significant decrease in melanization to less than half was observed for *VMK1* and *MEK2* single or double deletion strains (Figure 13C).

These data corroborate, that MAP2K *MEK2* and MAPK *VMK1* contribute to vegetative growth, microsclerotia formation, and melanization independently from the putative cascade scaffold protein Ham5 in *V. dahliae*.

3.2.4 Mek2- and Vmk1-mediated regulation of virulence is independent from Ham5 in tomato plants

The impact of the putative scaffold protein Ham5 on virulence of *V. dahliae* was investigated in tomato plant infection experiments in comparison to the MAP2K Mek2 and the MAPK Vmk1.

Tomato plants inoculated with spores from Δ*MEK2,* Δ*VMK1*, Δ*HAM5*Δ*MEK2,* or Δ*HAM5*Δ*VMK1* strains displayed plant heights comparable to mock plants after 21 days and no hypocotyl discolorations were observed (Figure 14A). None of the plants inoculated with spores from these strains displayed strong or heavy symptoms. The avirulent *in planta* phenotypes observed for Δ*MEK2* and Δ*VMK1* were complemented in experiments with *VMK1-C and MEK2-C* strains. Plants treated with *VMK1-C* displayed slightly more severe disease symptoms with only 3% healthy plants, whereas *MEK2-C* and wild type treatment resulted in about 20% healthy plants (Figure 14A).

In contrast to *MEK2* and *VMK1* single or double deletion strain treated plants, tomato plants inoculated with Δ*HAM5* displayed disease symptoms indistinguishable from wild type infected plants including severe stunting and discoloration of the vascular system (Figure 14A).

To investigate which of the constructed strains are able to colonize plant tissues, re-isolation from stem sections on agar plates was performed. Fungal outgrowth from stems was observed for all strains, even if to a smaller extend from plants treated with spores from Δ*VMK1,* Δ*MEK2,* Δ*HAM5*Δ*VMK1*, and Δ*HAM5*Δ*MEK2* strains than from plants treated with wild type, Δ*HAM5*, or complementation strains (Figure 14B). For strains causing no symptoms, fungal outgrowth was confirmed by control PCR reactions targeting the transit region of the integrated marker cassettes (Figure 14C). Hence, *MEK2* and *VMK1* single and double deletion strains are able to invade tomato plants, but are impaired in induction of disease symptoms, whereas deletion of *HAM5* allows wild type-like induction of disease symptoms.
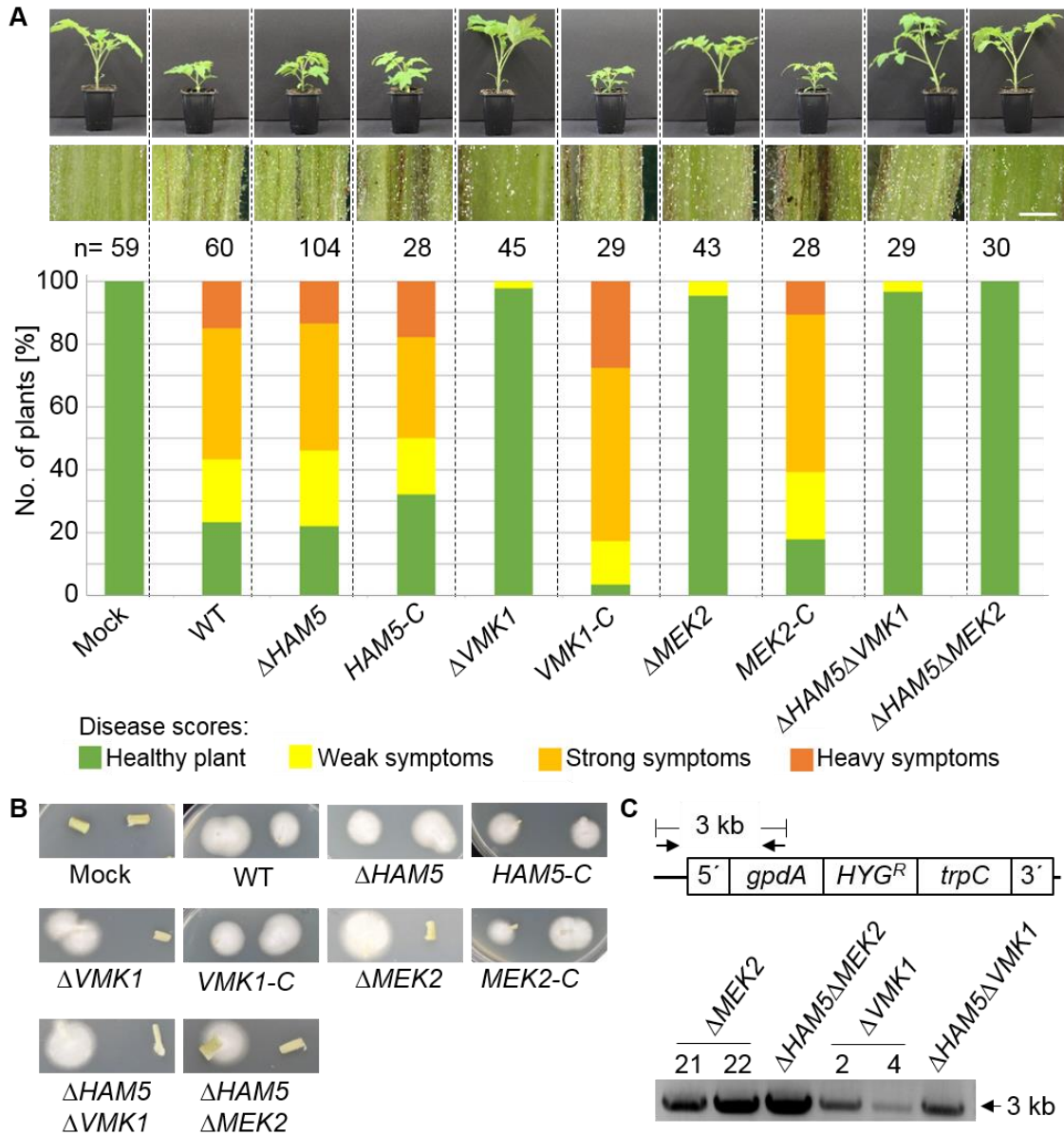
Figure 14: *V. dahliae* Vmk1 pathway-mediated pathogenicity towards *S. lycopersicum* is independent from the scaffold protein. (**A**) Ten-day-old tomato plants were inoculated by root dipping into sterile water as control (mock) or spores obtained from wild type JR2 (WT), *HAM5, VMK1,* and *MEK2* deletions with the respective complementations (*HAM5-C, VMK1-C,* and *MEK2-C*) or double deletion strains. Representative plants and hypocotyl dissections after 21 days are shown. The relative number of plants with certain disease scores are displayed in the stack diagram. Two independent transformants of Δ*HAM5* were tested in three (VGB280) to four (VGB279) independent experiments. Two independent transformants per *VMK1* (transformant numbers 2 and 4 - VGB335, VGB336) and *MEK2* (transformant numbers 21 and 22 - VGB337, VGB338) deletion and a single transformant per double deletion (VGB346, VGB417) and complementation strain (VGB389, VGB413, VGB415) were tested in two independent experiments. n= the total number of evaluated plants; scale bar = 1 mm. (**B**) Stem assay shows fungal outgrowth from stem sections for all tested strains. Stems were surface sterilized, cut, and incubated on PDM supplemented with chloramphenicol for seven days at 25 °C. (**C**) PCR validation of fungal outgrowth from stem assay as *VMK1* and *MEK2* single and double deletion strains. PCR reactions targeting the regions upstream of the 5´-flanking region of *VMK1* or *MEK2* used for homologous recombination and the *gpdA* promoter of the introduced hygromycin resistance marker cassette give products with predicted fragment length about 3 kb for genomic DNA of all tested strains.

These data corroborate that the function of the MAPK cascade components Vmk1 and Mek2 in virulence are independent from the scaffold protein Ham5. This was also observed for the MAPK pathway functions in vegetative growth and microsclerotia formation. Therefore, the cascade either requires a yet unidentified scaffold protein or a direct interplay between the kinases for the tested conditions.

3.3 The unfolded protein response pathway regulator Hac1 controls development and virulence of *V. dahliae*

3.3.1 *HAC1* and *IRE1* genes of the UPR pathway in *V. dahliae*

Efficient biosynthesis and secretion of proteins involved in colonization of the host plant are crucial for the success of plant colonizing fungi and assumed to be regulated by the unfolded protein response pathway (Joubert *et al.*, 2011; Heimel *et al.*, 2013). The UPR pathway senses ER stress correlated with increased protein folding demands via the transmembrane endoribonuclease Ire1 and regulates responsive genes via the bZIP transcription factor Hac1. In the course of this study, the presence of the fundamental components of the UPR pathway in *V. dahliae* was examined by BLAST search of deduced amino acid sequences and the function of the *HAC1* homolog in development and virulence of *V. dahliae* was characterized.

The gene *VDAG_JR2_Chr1g29650a* was identified as *V. dahliae* JR2 *IRE1* homolog by reciprocal BLAST search with the *T. reesei* Ire1 protein sequence of 1243 aa (XP_006962552.1, isolate QM6a). Incorrect annotation of the ORF with a deduced protein length of only 871 aa in *V. dahliae* JR2 is likely. Using the annotation of the homologous gene in VdLs.17 (*VDAG_02974*), the presence of an ORF encoding a 1236 aa protein with proposed Ire1-specific domains, including an ER luminal domain, a protein kinase, and a cytosolic endoribonuclease domain, was identified (Figure 15A). The deduced Ire1 proteins from *V. dahliae* and *T. reesei* display 56% aa sequence identity.

The *V. dahliae* *HAC1* homolog *VDAG_JR2_Chr2g09780a* was identified by reciprocal BLAST search with the deduced amino acid sequence of *A. nidulans* hacA (Q8TFU8.2, isolate FGSC A4) against the *V. dahliae* JR2 (Ensembl Fungi) and *A. nidulans* (NCBI database) proteomes. The gene contains an ORF of 1634 bp. The Ensembl Fungi gene annotation of the potential *HAC1* homolog in *V. dahliae* predicted only one splice variant. The *HAC1* homologs in related filamentous fungi possess two mRNA splice variants, an uninduced *HAC1^u* and an unconventionally spliced *HAC1^i* mRNA which is preferentially spliced in response to ER stress (Heimel, 2015). Therefore, the hypothetically deduced protein of 526 aa with a molecular weight of 58 kDa was named Hac1^u. For Hac1^u an N-terminal basic-leucine zipper domain and an N-terminal nuclear localization signal (NLS)

were predicted (Figure 15B). The deduced Hac1^u proteins from *V. dahliae* and *T. reesei* display 35% aa sequence identity.

Hence, the *V. dahliae* genome harbors *HAC1* and *IRE1* homologs with similar deduced protein sequences and domain predictions to the corresponding proteins in related filamentous fungi.
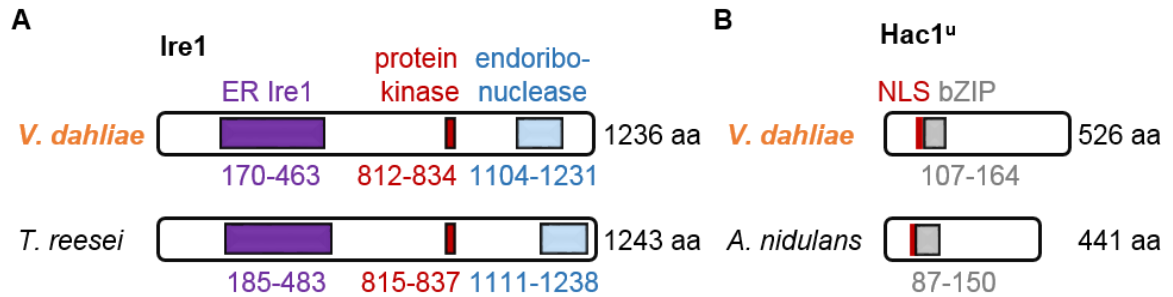

Figure 15: Protein domains of *V. dahliae* Ire1 and Hac1^u in comparison to corresponding proteins of related filamentous fungi. Domains of deduced protein sequences of homologous *IRE1* (*VDAG_02974/ VDAG_JR2_Chr1g29650a* corrected) and *HAC1* (*VDAG_JR2_Chr2g09780a*) genes in *V. dahliae* in comparison to the corresponding proteins in related filamentous fungi predicted by InterProScan and cNLS mapper. (**A**) Domain predictions for *V. dahliae* Ire1 (1236 aa protein; ER luminal Ire1 domain, cd09769, 170-463aa; protein kinase ATP binding site, IPR017441, 812-834 aa; cytosolic C-terminal endoribonuclease domain, PF06479, 1104-1231 aa) and *T. reesei* Ire1 (1243 aa protein; XP_006962552.1, isolate QM6a; cd09769, 170-463 aa; IPR017441, 812-834 aa; PF06479, 1104-1231 aa) are shown. (**B**) Domain predictions for *V. dahliae* Hac1^u (526 aa protein; NLS 94-105 aa; bZIP 107-164 aa, PS50217) and *A. nidulans* HacA^u (441 aa protein; CBF87535.1*;* FGSC A4*;* NLS 55-65 aa; bZIP 87-150aa, PS50217) are shown.

3.3.2 The *HAC1* mRNA is unconventionally spliced in *V. dahliae*

The Ensembl Fungi gene annotation of the potential *HAC1* homolog in *V. dahliae* predicted only one mRNA splice variant with a 53 nt intron, resulting in a spliced 1581 nt mRNA. Since unconventional splicing of the *HAC1* mRNA was described for known homologs preferentially under ER stress inducing conditions, it was tested, whether different mRNA splice variants could be obtained for *V. dahliae HAC1* from liquid cultures in presence or absence of dithiothreitol (DTT). DTT is a reducing agent which prevents the formation of disulfide bonds and thereby induces misfolding of proteins in the ER (Guillemette *et al.*, 2011).The *HAC1* cDNA sequence amplified from un-induced growth was in accordance with the database predicted splice variant, referred to as *HAC1^u* (Figure 16A). Additionally, a second splice variant could be obtained from these growth conditions, which was also amplified from ER stress inducing growth conditions, named *HAC1^i* (Sequence given in S10). The *HAC1^i* mRNA results from splicing of a second intron with 20 nt in size (Figure 16A). Splicing of the 20 nt intron alters the ORF, leading to a shorter variant of 1254 nt.
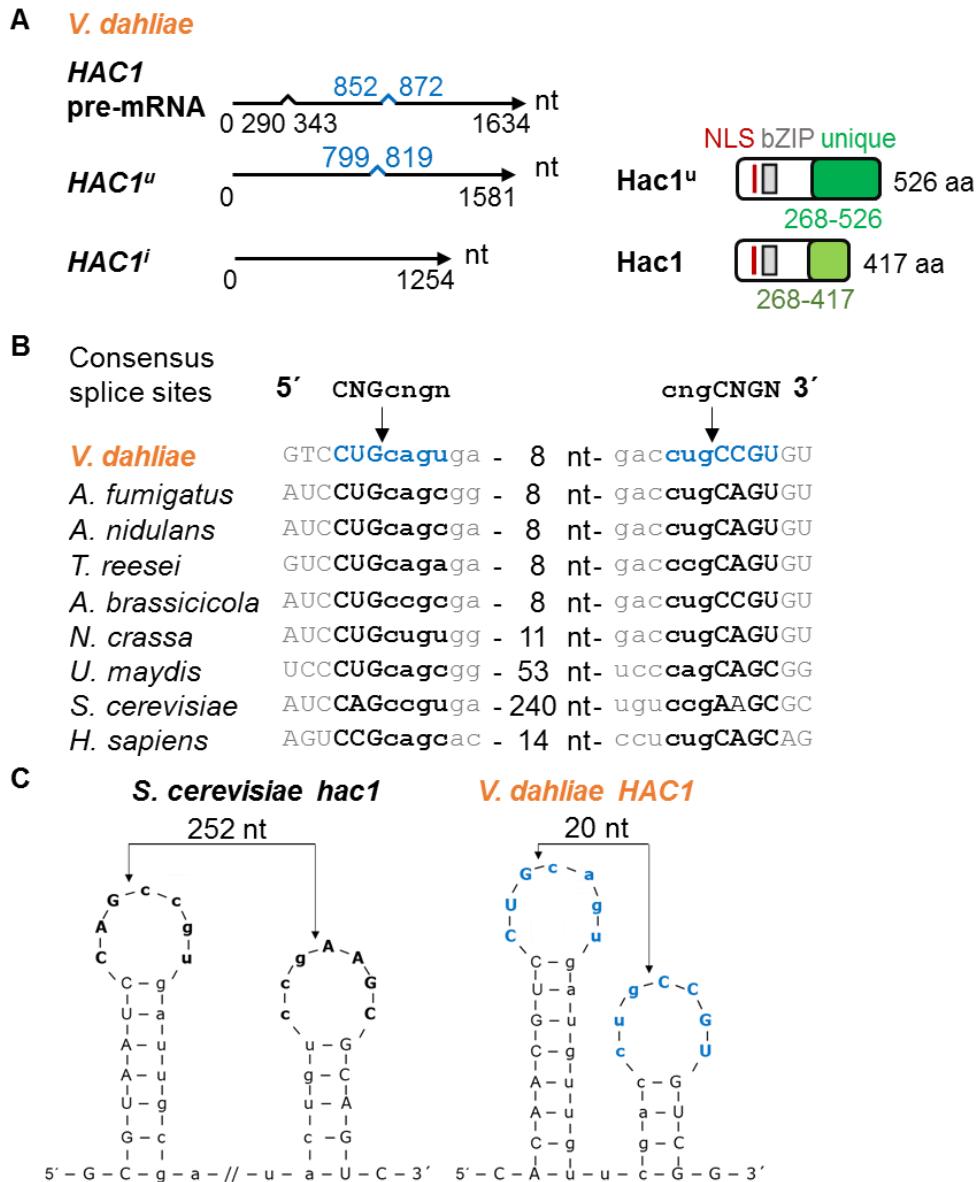
Figure 16: The *V. dahliae HAC1* mRNA is unconventionally spliced. (**A**) mRNA and protein variants of *V. dahliae HAC1*. The 2634 nt *HAC1* pre-mRNA contains a 53 nt conventional (black) and a 20 nt unconventional (blue) intron. *V. dahliae* produces two *HAC1* mRNA variants: splicing of the conventional intron results in *HAC1ᵘ* mRNA (1581 nt) for the potential Hac1ᵘ protein (526 aa), additional unconventional splicing results in a shorter induced *HAC1ⁱ* ORF (1254 nt) encoding the Hac1 protein (417 aa). N-termini (268 aa) of both proteins are identical, containing a basic leucine zipper domain (bZIP, grey, PS50217; 107-164 aa) and a nuclear localization signal (NLS, red, 94-105 aa), whereas Hac1ᵘ and Hac1 possess unique C-termini (dark or light green). (**B**) Alignment of the 5´- and 3´-splice sequences of the unconventionally spliced introns shows high conversation of *V. dahliae HAC1* (*VDAG_JR2_Chr2g09780a*; blue), *A. fumigatus hacA* (XM_743634), *A. nidulans hacA* (AN9397), *T. reesei* QM6a *hac1* (M419DRAFT_128619), *A. brassicicola HacA* (Joubert *et al.*, 2011), *N. crassa hac-1* (NCU01856), *U. maydis cib1 (UMAG_11782)*, *S. cerevisiae* S288C *hac1* (NC_001138.5), *H. sapiens XBP1* (NM_005080.3). The consensus sequence of Ire1 splice sites (Hooks & Griffiths-Jones, 2011) is indicated by CNG'CNGN. Ire1 splice sites are indicated by arrows, intron sequences as lowercase characters, splice sequences as capital letters. Numbers of nucleotides for those not shown are given. (**C**) Twin stem-loop secondary structures of 5´- and 3´-splice sequences of *V. dahliae* and *S. cerevisiae* unconventional *HAC1* introns. Ire1 splice sites are indicated by arrows, intron sequences as lowercase characters, splice sequences as capital letters, discontinuation of intron sequence as //. RNAfold was used for folding prediction (http://rna.tbi.univie.ac.at/cgi-bin/RNAfold.cgi).

In yeast and filamentous ascomycetes, translation of the uninduced mRNA variant into Hac1^u was described to be blocked (Chapman & Walter, 1997; Rüegsegger et al., 2001; Saloheimo et al., 2003; Mulder et al., 2004; Joubert et al., 2011; Heimel, 2015). Differently, translation of the uninduced protein variant, acting as negative regulator of the UPR, was observed in higher eukaryotes (Yoshida et al., 2006, 2009). Hints to protein translation were given in the basidiomycete U. maydis (Heimel et al., 2013). The alternative splice variant HAC1^i encodes a 417 aa Hac1 protein (aa sequence shown in Figure S11) with a molecular weight of 44 kDa. For both hypothetical Hac1 protein variants the N-terminal 268 aa are identical with a nuclear localization signal (NLS) and bZIP domain. The bZIP protein domains are specifically found in transcription factors and are formed by a basic loop responsible for DNA binding and the hydrophobic leucine zipper required for homo- or heterodimerization of two DNA binding proteins (Hurst, 1995). The NLS proposes protein import into the nucleus. Due to the frame shift after unconventional splicing, the C-terminus of the predicted Hac1^u and Hac1 proteins are unique with 258 unique amino acids in Hac1^u versus 149 in Hac1.

The mRNA of HAC1 homologs from several fungal species up to humans was described to be cleaved by the cytosolic endoribonuclease domain of Ire1 by recognition of the conserved consensus splice sequence 5´-CNG'CNGN-3´ which is specific for unconventional splicing (Yoshida et al., 2001; Saloheimo et al., 2003; Mulder et al., 2004; Wimalasena et al., 2008; Richie et al., 2009; Cheon et al., 2011; Hooks & Griffiths-Jones, 2011; Joubert et al., 2011; Heimel et al., 2013; Montenegro-Montero et al., 2015). Alignment of the 5´- and 3´-intron-exon-borders of both introns from V. dahliae HAC1 to the consensus sequence displayed conservation of the 20 nt intron, which was found to be spliced under ER stress induced growth conditions (Figure 16B). The 53 nt intron spliced in both, HAC1^u and HAC1^i, did not match the consensus sequence.

Comparison of the 20 nt intron from V. dahliae HAC1 to homologous sequences in other organisms displays the same intron size in A. brassicicola, A. fumigatus, A. nidulans, and T. reesei. N. crassa (23 nt) and human (26 nt) homologs possess similar intron sizes. The unconventionally spliced intron of the homolog Cib1 in U. maydis shows intermediate length (65 nt), whereas the yeast S. cerevisiae homolog is much longer with a size of 252 nt (Figure 16B).

The mRNA of HAC1 homologs was described to form a twin stem-loop structure in several organisms, which is targeted by the endonuclease domain of Ire1 homologs (Yoshida et al., 2001; Saloheimo et al., 2003; Mulder et al., 2004; Wimalasena et al., 2008; Richie et al., 2009; Cheon et al., 2011; Hooks & Griffiths-Jones, 2011; Joubert et al., 2011; Heimel et al., 2013; Montenegro-Montero et al., 2015). In order to allow predictions about the splice mechanism for V. dahliae HAC1, the secondary structure of

the unconventionally spliced intron was analyzed. Figure 16C shows the twin stem-loop secondary structure of the 20 nt intron from *V. dahliae HAC1* in comparison to the model organism *S. cerevisiae,* calculated by the RNAfold web server with the lowest free energy. The predicted Ire1 cleavage sites are located in the formed seven nucleotides loops.

Similarities between the *V. dahliae* Hac1 protein encoded by the unconventionally spliced mRNA *HAC1[i]* to described UPR regulatory proteins in other fungi and human XBP1 (X-box binding protein) were assessed (Figure 17). The highest similarity was found to *T. reesei* HACI with 55% aa sequence identity. The corresponding *A. nidulans* and *A. fumigatus* proteins display a higher amino acid similarity to the *V. dahliae* protein with 36% than the *S. cerevisiae* homolog with 28%. The similarities to *U. maydis* cib1 and *H. sapiens* XBP1 was below 20% (Figure 17A). The proteins from *V. dahliae* and *T. reesei* cluster in one subclade in the phylogenetic tree (Figure 17B). Considered homologs from ascomycetes form one clade with lower amino acid similarities to the homologs of the basidiomycete *U. maydis* and the *H. sapiens* homolog XBP1.

In summary, *V. dahliae HAC1* shows high similarity to homologs in related fungi. It encodes an unconventionally spliced intron with a proposed twin stem-loop structure, which is presumably recognized by the endoribonuclease Ire1 and displays similarities in the deduced protein sequence and protein domain predictions to UPR regulatory proteins from related fungi.

A

		1	2	3	4	5	6	7
1	*V. dahliae*	100						
2	*U. maydis*	16	100					
3	*S. cerevisiae*	28	18	100				
4	*T. reesei*	55	13	26	100			
5	*A. nidulans*	36	15	26	35	100		
6	*A. fumigatus*	36	13	24	26	35	100	
7	*H. sapiens*	13	15	12	13	16	16	100
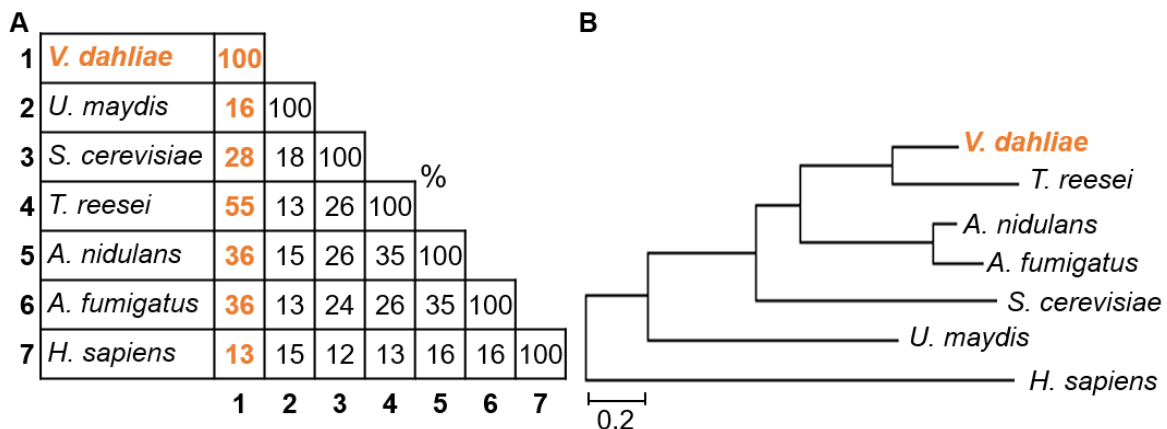
Figure 17: Similarities of Hac1 proteins from different organisms. (**A**) Protein sequence identity matrix of Hac1-like proteins (ClustalW algorithm, sequence identifiers given in **B** were used for the calculation). (**B**) Phylogenetic tree of Hac1-like proteins with *V. dahliae* Hac1 (Figure S11), *U. maydis* cib1[s] (XP_011390112.1; isolate 521), *S. cerevisiae* HAC1[i] (NP_116622.1; isolate *S288C*), *T. reesei* HACI[i] (XP_006964054.1; isolate QM6a), *A. nidulans* HacA[i] (Q8TFU8.2; isolate FGSC A4), *A. fumigatus* HacA[i] (ACJ61678.1; isolate H237), *H. sapiens* XBP1 (NP_001073007.1) sequences. ClustalW algorithm in MEGA6.0 was used with the Maximum likelihood method. The scale bar represents the average number of amino acid substitutions per site.

3.3.3 The unconventionally spliced mRNA variant *HAC1ⁱ* is translated into the Hac1 protein in *V. dahliae*

In order to analyze the role of *HAC1* in the development and virulence of *V. dahliae,* a deletion strain was constructed. The impact of the different splice variants was tested by ectopic reintegration of the *HAC1* gene or either one of the two mRNA splice variants fused to *HA* at the 3´-end under control of the native promoter and terminator. Prior to functional investigation, correct integration of constructs was confirmed by Southern hybridization (Figure S8).

The expression levels of *HAC1* in the complementation strain *HAC1-C* and strains harboring the different splice variants, *HAC1ᵘ-HA* and *HAC1ⁱ-HA*, were tested by quantitative reverse transcriptase PCR reactions in comparison to wild type and Δ*HAC1* (Figure 18A).
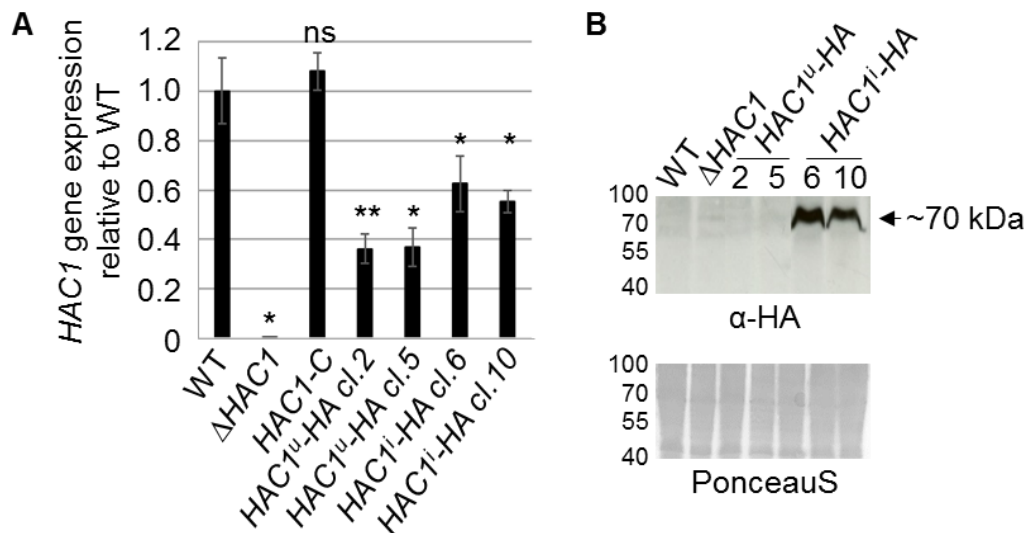
Figure 18: The *V. dahliae* unconventionally spliced mRNA *HAC1ⁱ*, but not the uninduced mRNA *HAC1ᵘ*, is translated into the Hac1 protein. *V. dahliae* wild type JR2 (WT), *HAC1* deletion (Δ*HAC1* - VGB371), complementation (*HAC1-C* - VGB382), as well as two transformants each of strains expressing ectopically integrated *HAC1* mRNA splice variants fused to *HA* at the 3´-end in the Δ*HAC1* strain (*HAC1ᵘ-HA* transformant number 2 and 5 - VGB439, VGB440; *HAC1ⁱ-HA* transformant number 6 and 10 - VGB437, VGB438) were compared. (**A**) Quantification of *HAC1* gene expression by primers targeting both *HAC1* mRNA splice variants. 1×10^6 spores were inoculated in 50 ml SXM and incubated for three days at 25 °C under constant agitation. *HAC1* gene expression is decreased in *HAC1ᵘ-HA* and *HAC1ⁱ-HA*. Mean values of two independent experiments with standard error of the mean normalized to wildtype and reference genes *H2A* and *EIF2B* are shown. Significant differences to wild type calculated with one-way Anova and Student´s t-test are shown with *$p < 0.05$; **$p < 0.01$, ns = non-significant. (**B**) Detection of Hac1 proteins in immunoblots using HA-specific antibody and 80 µg protein extracts isolated from mycelia grown in liquid PDM for four days at 25 °C under constant agitation. PonceauS staining served as a loading control. A strong signal is only visible at ~70 kDa for tagged Hac1 in the constitutively spliced *HAC1ⁱ-HA* strain instead of the predicted 46 kDA, whereas there was no specific band for the predicted Hac1ᵘ-HA protein (59 kDa).

The *HAC1* expression was quantified for cultures grown in liquid simulated xylem medium for three days targeting both, induced and uninduced *HAC1* mRNA variants, with the same primer pair. The *HAC1-C* complementation strain displayed wild type-like *HAC1* expression levels (Figure 18A), whereas expression was reduced to less than 40% in *HAC1^u-HA* and to ~60% in *HAC1^i-HA* (Figure 18A).

Immunoblot analysis was performed to investigate whether both *HAC1* mRNA variants were translated into Hac1^u-HA and Hac1-HA fusion proteins with an HA-antibody (Figure 18B). No bands were observed for *HAC1^u-HA* strains containing the conventionally spliced mRNA variant of *HAC1* (Figure 18B). The predicted band size for the Hac1^u-HA protein of 59 kDa and the Hac1-HA protein of 46 kDa were not detected, but a band with ~70 kDa was obtained for *HAC1^i-HA,* expressing the unconventionally spliced *HAC1* mRNA variant (Figure 18B). These data suggest, that *HAC1^i-HA* is translated into a protein in *V. dahliae*, whereas the translation of *HAC1^u-HA* could not be observed.

3.3.4 *HAC1* is essential for microsclerotia formation of *V. dahliae*

The impact of *V. dahliae HAC1* on growth, microsclerotia formation, and fungal conidiation was investigated by comparison of the *ex planta* phenotypes of the *ΔHAC1*, *HAC1-C*, *HAC1^u-HA* and *HAC1^i-HA* strains.

Vegetative growth of the *HAC1* deletion strain was severely impaired under all tested growth conditions (Figure 19). Colonies formed by the deletion strain ten days after spot inoculation formed less aerial mycelium, appeared less dense, and more transparent in comparison to wild type colonies grown on complete medium (PDM), minimal medium, or minimal medium supplemented with tunicamycin (Figure 19). Melanization of the *ΔHAC1* colony centers was not observed under any tested growth condition. Furthermore, the deletion strain formed smaller colonies compared to wild type for every tested condition. Quantification of vegetative growth showed a significant decrease in the colony diameter about 12% for *ΔHAC1* ten days after spot inoculation on CDM (Figure 19B).

Vegetative growth on minimal medium supplemented with tunicamycin was tested to examine the ability to cope with ER stress. Tunicamycin inhibits the glycosylation of proteins and, thereby, prevents folding in the ER und subsequent protein secretion (Guillemette *et al.*, 2011). The mean colony diameter of *ΔHAC1* grown on CDM supplemented with tunicamycin was 11% smaller than wild type colonies ten days after spot inoculation (Figure 19B). The supplementation of tunicamycin induced no additional decrease in the colony size of *ΔHAC1* relative to wild type and the relative difference was unaltered (Figure 19B).
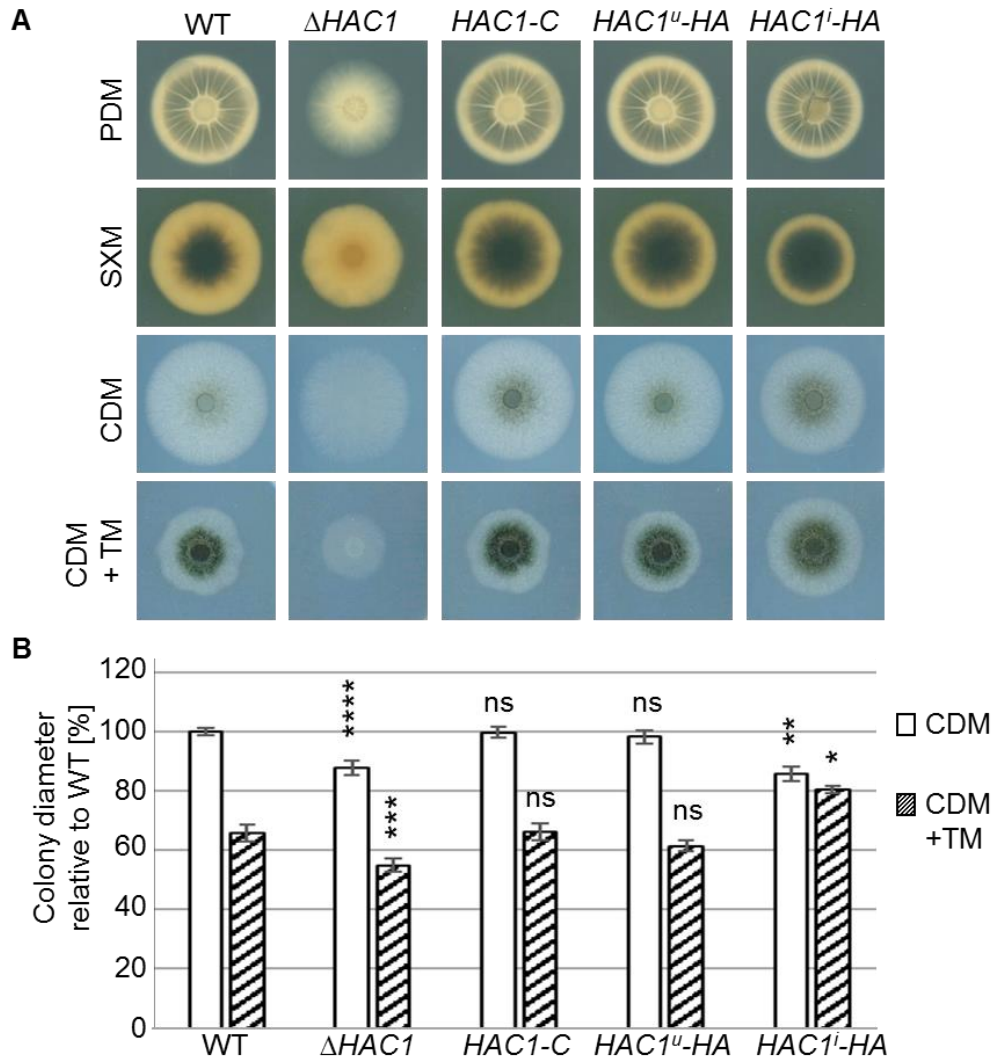
Figure 19: *V. dahliae* **requires the expression of** *HAC1* **for growth with or without tunicamycin-induced ER stress and melanization.** Spot inoculation of 50 000 spores from the wild type JR2 (WT) or Δ*HAC1*, *HAC1-C, HAC1^u-HA*, and *HAC1^i-HA* strains and incubation at 25 °C for ten days. Δ*HAC1* displays reduced vegetative growth compared to wild type. *HAC1-C* and *HAC1^u-HA* strains display wild type-like growth, whereas colony diameters of *HAC1^i-HA* are decreased under non-stress conditions and relatively increased upon supplementation of tunicamycin. (**A**) *Ex planta* phenotypes on PDM, SXM, CDM, and CDM supplemented with 1 µg/ml tunicamycin (TM). Δ*HAC1* forms less aerial mycelium, appears less dense, and more transparent on PDM, CDM, and CDM+TM. Δ*HAC1* displays no melanization in the colony centers. (**B**) Quantification of vegetative growth. Growth was quantified by measurement of two perpendicular colony diameters for three colonies per transformant and medium (n=1). Two independent transformants were tested for Δ*HAC1* (VGB371, VGB372), *HAC1^u-HA* (VGB439, VGB440), and *HAC1^i-HA* (VGB437, VGB438), as well as one *HAC1-C* (VGB382) transformant. Bars represent mean values with standard deviations from three independent experiments for wild type and Δ*HAC1,* and two independent experiment for *HAC1-C, HAC1^u-HA* and *HAC1^i-HA* grown on CDM. Mean values with standard deviations are shown from three independent experiments for wild type, Δ*HAC1,* and *HAC1-C, a*nd two independent experiments for *HAC1^u-HA* and *HAC1^i-HA* grown on CDM+TM. Significant differences to wild type determined with one-way Anova and Student´s t-test are shown with *$p < 0.05$; **$p < 0.01$; ***$p < 0.001$, ****$p = 0$, ns= non-significant.

The *HAC1-C* and *HAC1^u-HA* strains displayed wild type-like growth. Colony diameters of

HAC1^i-HA were decreased on all non-stress inducing media, but increased on CDM

supplemented with tunicamycin (Figure 19). A decrease about 14% in the colony diameter was determined for the *HAC1^i-HA* strain relative to wild type on CDM, whereas supplementation of tunicamycin resulted in a ~15% increase of the colony diameters relative to wild type (Figure 19B). This observations suggests that the presence of the unconventionally spliced *HAC1* mRNA in the *HAC1^i-HA* strain and constitutive activation of the UPR enable a more efficient response to the induced ER stress.

Comparison of the *ex planta* phenotypes of the *HAC1* deletion and the *HAC1-C, HAC1^u-HA,* and *HAC1^i-HA* strains to wild type revealed the absence of melanized colony centers for Δ*HAC1* on all tested media, whereas the *HAC1-C* and *HAC1^i-HA* strains displayed increased melanization. The ability of Δ*HAC1* to develop microsclerotia as resting structures, maybe in an unmelanized form, was further analyzed in comparison to the complementation strains. The differences in melanization are most apparent in the colony centers and in colony cross sections (Figure 20). During microscopy of fungal material from colony centers of Δ*HAC1* no melanized or unmelanized microsclerotia were observed for any medium, as exemplified for CDM in Figure 20.
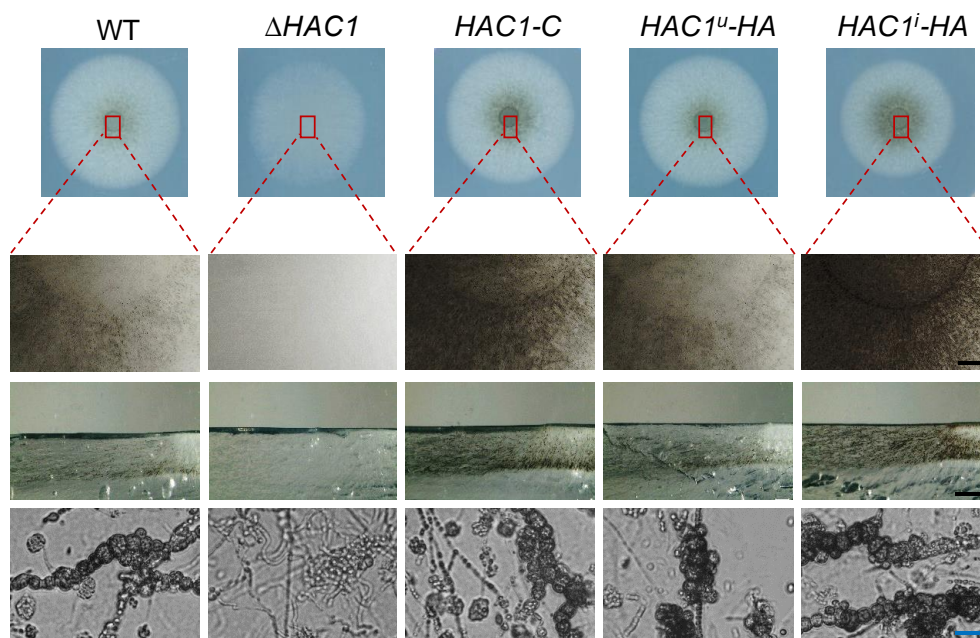
Figure 20: *V. dahliae HAC1* is essential for microsclerotia formation. Microsclerotia formation was examined in Δ*HAC1, HAC1-C, HAC1^u-HA*, and *HAC1^i-HA* strains by spot inoculation of 50 000 spores on CDM and incubation at 25 °C for ten days. Two independent transformants were tested for Δ*HAC1* (VGB371, VGB372), *HAC1^u-HA* (VGB439, VGB440), and *HAC1^i-HA* (VGB437, VGB438) strains and a single transformant for the *HAC1-C* (VGB382) strain. Close up pictures were taken from colony centers (indicated as red boxes) and cross sections were cut to visualize the appearance of microsclerotia as melanized structures in the agar. Fungal material from colony centers was scraped off for microscopy to observe microsclerotia morphology. Neither melanized nor unmelanized microsclerotia were observed for the Δ*HAC1* strain, whereas formation of wild type-like microsclerotia was observed for all other strains. Microsclerotia formation was qualitatively increased in the *HAC1-C* and the *HAC1^i-HA* strains in comparison to wild type. Black scale bar = 1 mm, blue scale bar = 20 µm.

For all complementation strains, wild type-like shaped and melanized microsclerotia could be observed, however, in qualitatively increased occurrence for the *HAC1-C* and *HAC1^i-HA* strains and wild type-like frequencies in the *HAC1^u-HA* strain (Figure 20). The absence of microsclerotia in Δ*HAC1* and the increase in melanization in *HAC1^i-HA* regardless of the decreased *HAC1* expression levels in *HAC1^i-HA* (Figure 18A) corroborate the role of *HAC1* in regulation of microsclerotia formation.

Within the plants vascular system *V. dahliae* forms conidiospores for spreading and systemic colonization of the host. The role of the UPR regulator Hac1 in conidiation was characterized by examination of the ability to form spores in the *HAC1* deletion strain compared to wild type and the *HAC1-C* complementation strain. Therefore, the same number of spores was inoculated in liquid simulated xylem medium and quantified after five days. The *HAC1* deletion strain displayed significantly reduced conidiospore numbers to 15% of the wild type level (Figure 21). Conidia levels of the *HAC1-C* strain were more similar to wild type with 86%.

In summary, *HAC1* is essential for microsclerotia formation and has important impacts on conidiation. Constant activation of the UPR in the *HAC1^i-HA* strain is correlated with increased growth in response to ER stress and increased microsclerotia formation in *V. dahliae*.
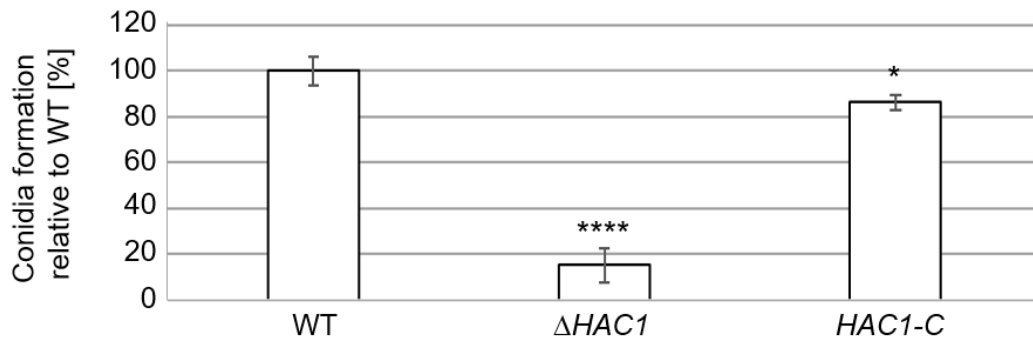
Figure 21: *V. dahliae HAC1* positively regulates conidiospore formation. Quantification of conidiation was performed by inoculation of 4000 spores/ml in liquid SXM and incubation at 25 °C under constant agitation for five days in triplicates. The number of spores was determined for the wild type JR2, two independent transformants of Δ*HAC1* (VGB371, VGB372), and the *HAC1-C* (VGB382) complementation strain in three independent experiments. The numbers of conidia relative to wild type are shown. The values determined for two independent Δ*HAC1* transformants are represented in one bar. Significant differences to wild type determined by one-way Anova and Student´s t-test are shown with ****$p=0$, *$p<0.05$ with n(WT)=3, n(Δ*HAC1*)=6, n(*HAC1-C*)=3. The *HAC1* deletion strain shows reduced conidia formation. Conidia formation of *HAC1-C* was more similar to the wild type-level.

3.3.5 *V. dahliae HAC1* is dispensable for penetration of the *A. thaliana* root cortex

A functional UPR was described to be essential for fungal propagation after penetration of plant cells in *U. maydis.* In both, *U. maydis* and *A. brassicicola,* the UPR regulatory transcription factor is essential for induction of disease symptoms in plants. Different to these two plant pathogenic species, which infect plants via the leaf surface by formation of appressoria, initial colonization of the host plant by *V. dahliae* occurs via the roots by intercellular growth or development of hyphopodia (Reusche *et al.*, 2014; Zhao *et al.*, 2014, 2016). So far, the role of the UPR in initial colonization of the host and virulence was not described for root colonizing plant pathogens. Here, the root colonization behavior of the UPR defective *V. dahliae HAC1* deletion strain was examined (Figure 22).
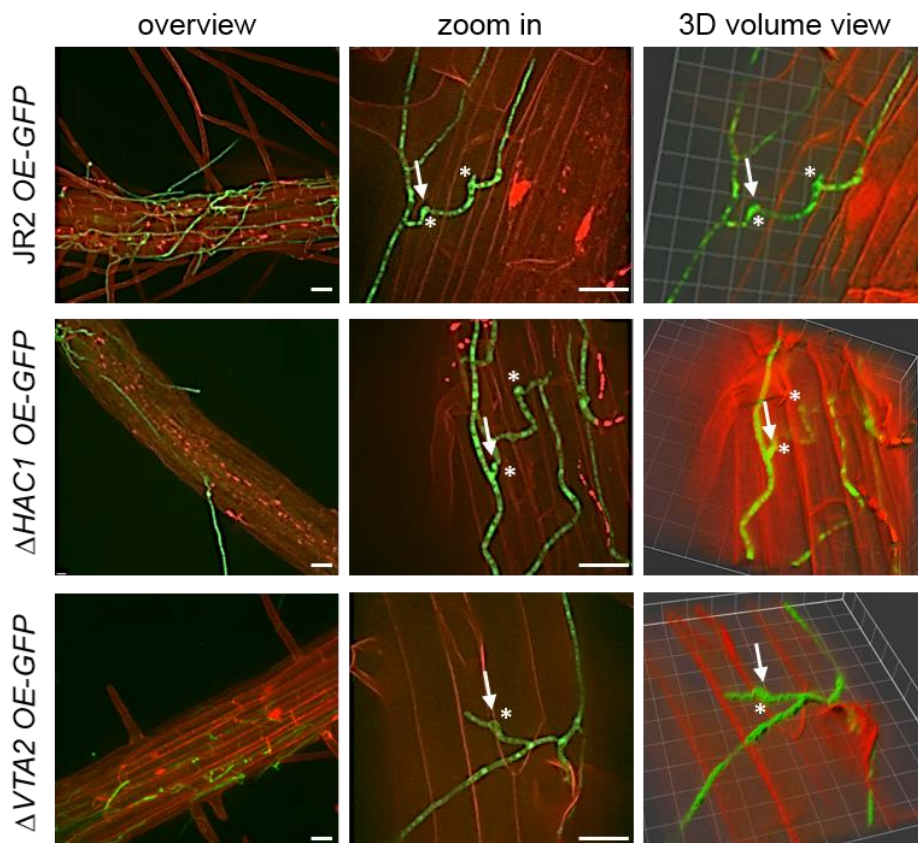
Figure 22: *V. dahliae HAC1* is involved in initial colonization but dispensable for penetration of *A. thaliana* roots. Fluorescence microscopy pictures of three-week-old *A. thaliana* plants seven days post inoculation with the same numbers of spores from wild type JR2, ΔHAC1, and ΔVTA2 constitutively expressing ectopic *GFP*. Overview pictures (left) as well as close up pictures (middle) were taken. 3D volume view pictures (right) calculated as maximum intensity projections of a Z-stack of microscope images are displayed. Four plants inoculated with either *JR2 OE-GFP* (VGB392) or ΔHAC1 OE-GFP (VGB380) strains in two independent experiments and two plants inoculated with spores obtained from ΔVTA2 OE-GFP strain were tested. Root cells were stained with 0.05% propidium iodide/0.01% silwet solution. ΔHAC1 OE-GFP displays reduced propagation on the root surface, but is able to penetrate *A. thaliana* roots and propagate after invasion of the outer layer. Scale bars = 20 µm, white arrows = root penetration sites, asterisks = changes of growth direction.

A *HAC1* deletion strain expressing ectopically integrated *GFP* under control of the *gpdA* promoter was constructed in order to investigate the root colonization behavior in absence of *HAC1*. The Δ*HAC1 OE-GFP* strain was confirmed by fluorescence microscopy and Southern hybridization analysis (Figure S8). Three-week-old *A. thaliana* plants were inoculated with the same number of spores obtained from Δ*HAC1 OE-GFP* as well as from the wild type expressing free *GFP* and the fungal colonization behavior was observed after five to seven days. The *Verticillium* transcription activator of adhesion (*VTA2*) deletion strain served as control. Δ*VTA2* penetrates plant roots like the wild type with less efficient proliferation inside the plant (Tran *et al.*, 2014).

Overall less hyphae of the Δ*HAC1 OE-GFP* strain were observed on the root surface in comparison to wild type and the Δ*VTA2* control strain five to seven days after root dipping (Figure 22). Penetration sites, recognizable by the formation of swollen hyphal tips and change in the growth direction, were observed in absence of *HAC1* similar to wild type and the Δ*VTA2* strain, even if more frequently in the wild type (Figure 22). Furthermore, hyphal growth after invasion of the outer layer was observed for the Δ*HAC1 OE-GFP* strain, as shown in the 3D volume view picture in Figure 22.

Therefore, *V. dahliae HAC1* is involved in initial colonization of the outer root surface, but is neither required for penetration of the *A. thaliana* root nor for invasion of the outer root cortex.

3.3.6 *V. dahliae HAC1* is required for colonization of tomato plants

A. thaliana root colonization assays had shown that *V. dahliae HAC1* is involved in colonization of the root surface, but is dispensable for penetration and initial propagation within the root cortex. To investigate the role of *HAC1* in subsequent steps of plant colonization and induction of disease symptoms, the *HAC1* deletion strain as well as *HAC1-C* and the *HAC1^u-HA* and *HAC1^i-HA* strains were tested in tomato infection experiments (Figure 23).

Δ*HAC1* induced significantly less severe disease symptoms than the wild type 21 days after spore inoculation with about 70% of plants displaying no disease symptoms. None of the Δ*HAC1* treated plants displayed heavy symptoms and no hypocotyl discolorations were observed for any of these plants. The *in planta* phenotype of the Δ*HAC1* strain was partially complemented in *HAC1-C*, *HAC1^u-HA* and *HAC1^i-HA* treated plants. All of these plants displayed discoloration of the hypocotyl comparable to wild type infected plants (Figure 23A). *HAC1-C* treated plants showed only a slight reduction in disease symptoms, whereas inoculation with the *HAC1^u-HA* or *HAC1^i-HA* strains caused similar and even less severe symptoms in tomato plants in comparison to wild type.
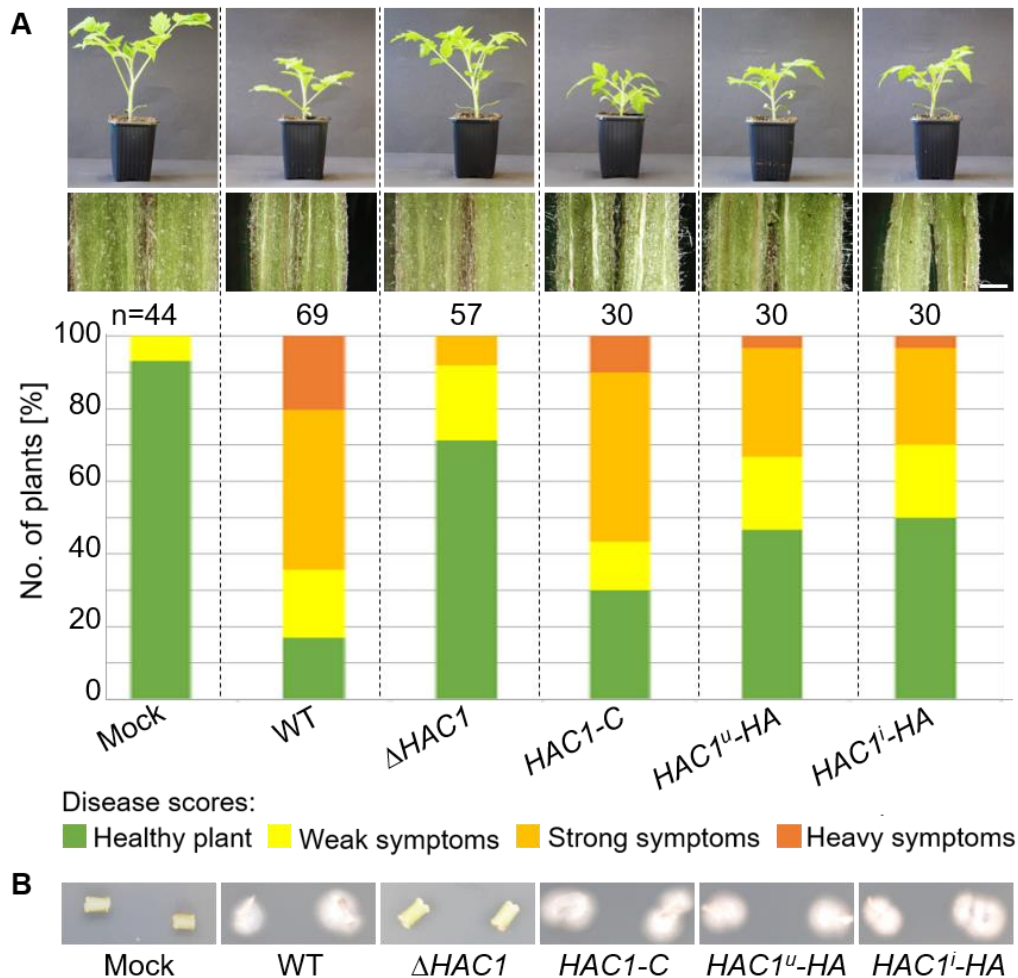
Figure 23: *V. dahliae* HAC1 is required for induction of disease symptoms in *S. lycopersicum*. (**A**) Ten-day-old tomato plants were inoculated by root dipping into water control (mock) or spores obtained from wild type JR2 (WT), *HAC1* deletion, complementation strain (*HAC1-C*), or from strains ectopically expressing either the uninduced (*HAC1^u-HA*) or the induced (*HAC1^i-HA*) mRNA variant under control of the native promoter and terminator. Representative plants and hypocotyl dissections 21 days post inoculation are shown. The relative number of plants with certain disease scores are displayed in the stack diagram. Two independent transformants of *ΔHAC1* (VGB371, VGB372) were tested in three independent experiments. One transformant of *HAC1-C* (VGB382) was tested in two independent experiments. Two independent transformants of *HAC1^u-HA* (VGB439, VGB440) and *HAC1^i-HA* (VGB437, VGB438) were tested in one experiment. Only *ΔHAC1* induced less severe disease symptoms in comparison to wild type. Different to plants treated with all other tested strains, the hypocotyl of *ΔHAC1* inoculated plants appears mock-like (Scale bar = 1 mm). (**B**) Fungal outgrowth from stem sections. Stems were harvested, surface sterilized, cut, and incubated on PDM supplemented with chloramphenicol for seven days at 25 °C. *ΔHAC1* could not be re-isolated from surface sterilized stem sections. Stems from plants infected with all other tested strains displayed fungal outgrowth after seven days.

Fungal outgrowth from treated plants was tested to investigate whether the strains, especially *ΔHAC1,* were able to invade plant tissues. Therefore, stems from tomato plants used for determination of disease scores 21 days after inoculation were surface-sterilized, cut into stem sections, and incubated on PDM agar supplemented with

chloramphenicol for seven days at 25 °C. Fungal outgrowth was observed for all strains except Δ*HAC1* (Figure 23B).

Hence, the absence of *HAC1* caused severely decreased development of disease symptoms in tomato plants and did not allow its re-isolation from infected tissue suggesting that *HAC1* is required to survive within the plants vascular system. Additionally, in an experiment with one repetition with two independent transformants each, a constitutively active UPR in *HAC1^i^-HA* led to the induction of unaltered disease symptoms in tomato plants in comparison to the strain *HAC1^u^-HA* harboring the uninduced mRNA splice variant of *HAC1* with intermediate disease severity. This result suggests that virulence of *V. dahliae* is unaltered in presence of a constitutively active UPR.

3.4 The *V. dahliae* oleate Δ12-fatty acid desaturase Ode1 promotes differentiation with only a minor impact on virulence

3.4.1 *V. dahliae* Ode1 corresponds to the *A. nidulans* oleate Δ12-fatty acid desaturase OdeA

Besides the UPR-monitored secretion of proteins, lipid molecules are involved in host-fungus communication. Linoleic acid and the derived oxylipins from plant and fungus can modulate fungal differentiation and the development of disease symptoms (Calvo *et al.*, 2001; Brodhagen *et al.*, 2008; Brodhun *et al.*, 2009; Reverberi *et al.*, 2010; Scala *et al.*, 2014; Fischer & Keller, 2016; Patkar & Naqvi, 2017). Oleate Δ12-fatty acid desaturases catalyze the oxidation of oleic acid to linoleic acid by introduction of a second double bond at position 12 of the carbon chain (Los & Murata, 1998). The impact of the oleate Δ12-fatty acid desaturase OdeA on fungal differentiation was described in two Aspergilli (Calvo *et al.*, 2001; Chang *et al.*, 2004; Wilson *et al.*, 2004), however, it was not characterized in plant pathogens. The impact of the corresponding desaturase Ode1 in *V. dahliae* on differentiation and virulence was analyzed.

V. dahliae VDAG_JR2_Chr1g29610a was identified as the *A. nidulans odeA* (AAG36933.1) homolog by reciprocal BLAST search of the deduced amino acid sequences against the *V. dahliae* JR2 (Ensembl Fungi) and the *A. nidulans* (NCBI database) proteome with 66% aa sequence identity. The unspliced *V. dahliae ODE1* mRNA of 1504 bp contains two exons. The predicted intron-exon structure was confirmed by PCR amplification of the spliced transcript from wild type cDNA (Figure 24). The deduced Ode1 protein with a length of 481 aa and a predicted molecular weight of 54 kDa contains two fatty acid desaturase (FAD) domains. The cytosolic catalytic center of Δ12-fatty acid desaturases is generally described to be formed by conserved N- and C-terminal histidine clusters described as FAD domains and iron atoms provided from

the membrane-bound donor cytochrome b_5 (Los & Murata, 1998). The *V. dahliae* Ode1 protein was predicted as a transmembrane protein with four putative hydrophobic transmembrane helices, two short non-cytosolic regions, and three hydrophile cytosolic regions, including the N- and C-termini of the protein (Figure 24). The catalytic center of the desaturase was proposed to be directed to the cytosol. Ode1 was suggested to be localized to plastid membranes with 89% and in the ER membrane with 7% probability as the second-best hit by the DeepLoc-1.0 prediction tool. Since fungi do not possess plastids, the localization in the ER is the most likely suggestion from this database. For other fungal Δ12- and Δ15-fatty acid desaturases, localization to the ER was described (Martin *et al.,* 2007; Gostinčar *et al.*, 2009).
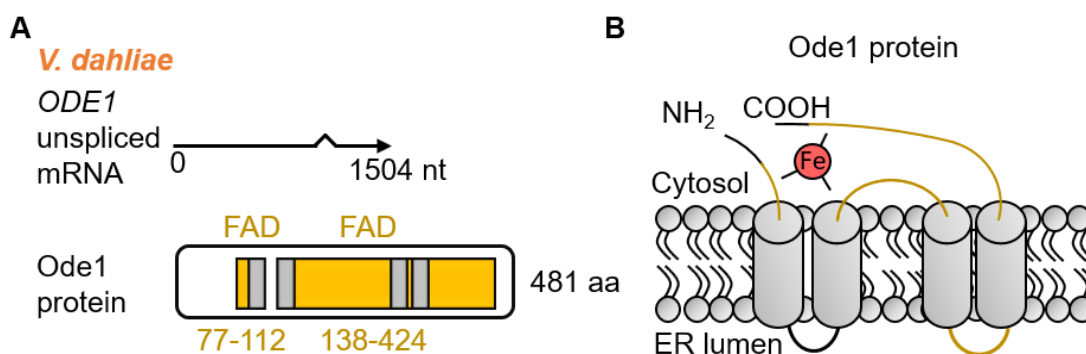
Figure 24: ***V. dahliae ODE1* encodes a membrane-bound oleate Δ12-fatty acid desaturase.** (**A**) The *V. dahliae* oleate Δ12-fatty acid desaturase Ode1 is encoded by the gene *VDAG_JR2_Chr1g29610a.* The intron-exon structure of the 1504 bp ORF predicted by Ensembl Fungi was confirmed by PCR amplification of the spliced transcript from wild type cDNA. The deduced Ode1 protein consists of 481 aa. The protein contains two fatty acid desaturase domains (FAD; yellow; 77-112 aa, IPR021863; 138-424 aa; IPR005804) and four putative transmembrane helices (grey; 105-124 aa, 136-157 aa, 300-319 aa, 331-350 aa; Phobius). Domains were predicted by InterProScan. (**B**) Scheme of the predicted Ode1 protein domain localization based on the InterProScan and DeepLoc-1.0 prediction tools. The N- and C-termini of the protein are directed to the cytosol. An iron atom and the FAD domains form the catalytic center of Ode1. Four transmembrane protein domains were proposed. Yellow = FAD domains, Fe = iron atom (based on Los & Murata, 1998).

3.4.2 *V. dahliae* Ode1 localizes to plasma membranes and cell organelle membranes

In order to analyze the role of Ode1 and Ode1-derived products in development and virulence of *V. dahliae* an *ODE1* deletion strain was constructed. Strains harboring *ODE1* fused to *GFP* either at the 5´- or 3´-end at the endogenous locus under control of the native promoter and terminator were constructed to analyze the protein localization (Figure 25) and used as complementation strains. Prior to functional investigation, correct integration of deletion and GFP-labeled constructs was confirmed by Southern hybridization (Figure S9).
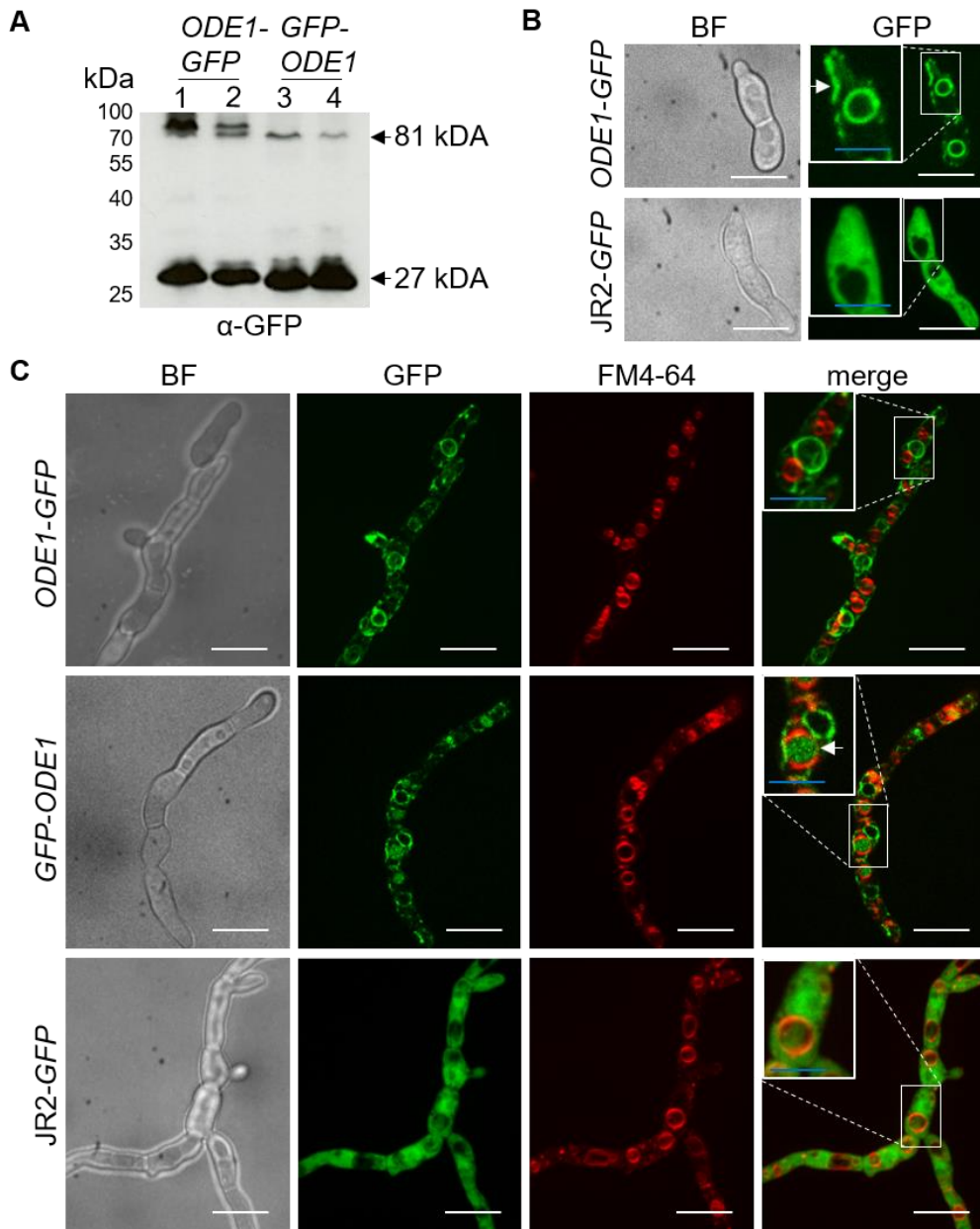
Figure 25: *V. dahliae* **Ode1 is localized to plasma and organelle membranes different to vacuoles.** (**A**) Immunoblot of complementation strains harboring *ODE1-GFP* or *GFP-ODE1* at the endogenous locus under control of the native promoter and terminator. 80 µg protein extracts isolated from *ODE1-GFP* transformant number 1 (VGB358) and 2 (VGB359) or *GFP-ODE1* transformant number 3 (VGB360) and 4 (VGB361) grown in liquid PDM for four days at 25 °C and a GFP-specific antibody were used. Ode1-GFP (81 kDa) and free GFP (27 kDa) were detected, as well as an additional band for *ODE1-GFP* transformants. (**B**) Subcellular localization of Ode1-GFP after 12 hours at 25 °C in liquid PDM. *ODE1-GFP* (VGB358) and wild type JR2 expressing ectopically integrated *GFP* under control of a constitutively active promotor were observed by fluorescence microscopy. Ode1-GFP localized to membranes of round cell organelles and close to hyphal tips of growing hyphae (indicated by white arrow). (**C**) Subcellular localization of Ode1-GFP and GFP-Ode1. Fluorescence microscopy 16 hours post inoculation of fungal spores (VGB358-361) in liquid PDM and incubation at 25 °C in comparison to free GFP in the JR2-*GFP* control strain. Vacuoles were stained in red with FM4-64. Ode1 localized to membranes of round cell organelles different than vacuoles. For *GFP-ODE1*, diffuse GFP signals were observed inside vacuoles as well (indicated by white arrows). Blue scale bars = 20 µm, white scale bars = 10 µm.

The presence of the fusion proteins in fungal cells was verified for two independent transformants per strain in immunoblots (Figure 25A). Ode1 C-terminally fused to GFP displayed two bands, one with the predicted molecular weight of 81 kDa and a second between ~90-100 kDa, whereas only the band at 81 kDa was observed for N-terminally tagged Ode1 (Figure 25A). In both, *GFP-ODE1* and *ODE1-GFP* strains, the band representing free GFP at ~27 kDa was relatively strong in protein extracts isolated from mycelium grown for four days in complete medium (PDM), but more prominent for the strains harboring Ode1 N-terminally fused to GFP (Figure 25A).

For the protein sequence of the *V. dahliae* desaturase Ode1 four transmembrane helices were predicted (Figure 24). The subcellular localization of N- or C-terminal GFP fusion proteins under control of the native promoter was studied in the *ODE1-GFP* and *GFP-ODE1* complementation strains in comparison to the wild type JR2 expressing ectopically integrated *GFP* under control of the constitutively active *gpdA* promotor. The GFP signals were observed by fluorescence microscopy 12 and 16 hours post inoculation of fungal spores in liquid complete medium (Figure 25B, C).

The GFP-signals were localized to membranes of cell organelles and to a minor extend to plasma membranes in fungal hyphae of both, *ODE1-GFP* and *GFP-ODE1* strains (Figure 25B, C). Further, a localization to plasma membranes close to tips of growing hyphae was observed frequently (Figure 25B). Localization of Ode1 in the membranes of vacuoles could be excluded by FM4-64 staining (Figure 25C). Additionally, the presence of a diffuse GFP signal within FM4-64 stained vacuoles was observed in the strain producing Ode1 proteins N-terminally fused to GFP. This observation suggests GFP-Ode1 to be less stable, resulting in the presence of free GFP and fusion protein degradation products in the vacuoles (Figure 25C).

3.4.3 *ODE1* is required for vegetative growth and microsclerotia formation in *V. dahliae*

Oleate Δ12-fatty acid desaturases produce linoleic acid as an important membrane component. Membrane fluidity usually increases correlated with an increasing content of unsaturated fatty acids (Mansilla *et al.*, 2004). Linoleic acid and the derived products are the major precursors for oxylipins with different impacts on fungal differentiation (Champe & El-Zayat, 1989; Brodhun & Feussner, 2011). The role of Ode1 in development of *V. dahliae* was examined testing vegetative growth and formation of microsclerotia as resting structures of the *ODE1* deletion strain under physiological and membrane stress inducing conditions in comparison to wild type and complementation strains.

Vegetative growth of the $\Delta ODE1$ strain was tested by spot inoculation on various media including complete medium, simulated xylem medium, minimal medium with different

carbon sources (sucrose, galactose, glucose, or cellulose), and on media supplemented with stress inducing agents (NaCl, H_2O_2, SDS) to investigate, whether *ODE1* is important for vegetative growth or to deal with membrane stress in *V. dahliae*. Vegetative growth of the Δ*ODE1* strain was decreased in all tested conditions. Examples are shown in Figure 26.
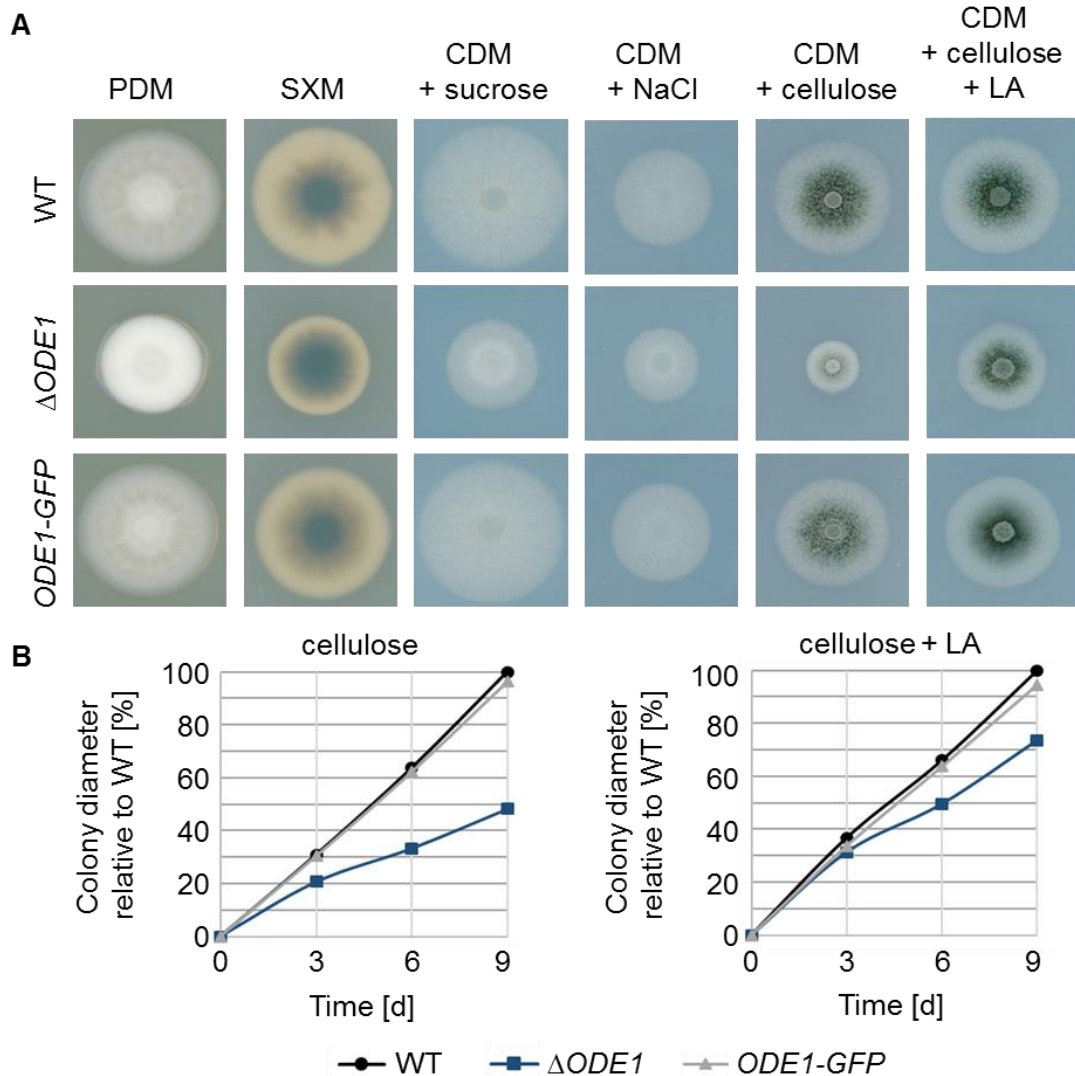
**Figure 26: *V. dahliae ODE1* contributes to vegetative growth.** (**A**) *Ex planta* phenotypes of the *V. dahliae* wild type JR2, Δ*ODE1,* and the *ODE1-GFP* complementation strain nine days after spot inoculation of 50 000 spores on PDM, SXM, CDM supplemented with NaCl (0.5 M), CDM with either sucrose or cellulose as carbon source, and CDM with cellulose supplemented with linoleic acid (LA; 0.125 mg/ml) and incubation at 25 °C. (**B**) Growth quantification of the wild type JR2, Δ*ODE1,* and the *ODE1-GFP* complementation strain three, six, and nine days after spot inoculation of 50 000 spores on CDM with cellulose as carbon source either without (left) or with supplementation of 0.125 mg/ml LA (right). Growth was quantified by measurement of two perpendicular diameters per colony for three independent colonies of the wild type and two independent transformants per genotype (VGB331, VGB332, VGB358, VGB359) in two independent experiments with similar results. Δ*ODE1* displayed ~50% decreased growth in comparison to wild type and the *ODE1-GFP* strain about nine days after spot inoculation on CDM with cellulose. Supplementation of the medium with LA partially complements the growth defect of Δ*ODE1* to ~75% of the wild type level.

Nine days after spot inoculation on complete medium ∆*ODE1* showed a fluffier, whitish phenotype due to the production of more aerial mycelium compared to wild type and complementation strain *ODE1-GFP*. The supplementation of minimal medium with stress inducing agents resulted in decreased growth of all tested strains, but not especially in the ∆*ODE1* strain as shown for sodium chloride in Figure 26A.

The *ODE1* deletion strain displayed the most severe decrease in vegetative growth on minimal medium containing cellulose as carbon source with a ~50% reduction of the colony diameter relative to wild type after nine days (Figure 26A, B). Colony diameters of *ODE1-GFP* were wild type-like (96%). The observed growth defect of ∆*ODE1* could be partially restored by supplementation of the medium with the oleate ∆12-fatty acid desaturase product linoleic acid, resulting in a colony diameter about 75%. Again, *ODE1-GFP* displayed wild type-like colony diameters (95%).

Alterations in melanization were observed for colonies formed by ∆*ODE1*. Colony cross sections of ∆*ODE1* grown on minimal medium with cellulose displayed less melanized structures in the agar after nine days (Figure 27A).

Figure 27: *V. dahliae ODE1 is involved in microsclerotia formation.* Microsclerotia formed by the *V. dahliae* JR2 wild type, *∆ODE1,* and the *ODE1-GFP* complementation strain after spot inoculation of 50 000 spores. Two independent transformants per genotype were tested (VGB331, VGB332, VGB358, VGB359). Black scale bar = 1 mm, blue scale bar = 20 µm, red boxes and dashed lines = cross sections from colony centers. (**A**) Pictures from colonies (top), cross sections (middle) and microscopy of fungal material scraped from colony centers (bottom) after nine days on CDM with cellulose and incubation at 25 °C are shown. (**B**) Colonies (top) and cross sections of colony centers (bottom) after 14 days on CDM with glucose (bottom view) and incubation at 25 °C in the dark are shown.
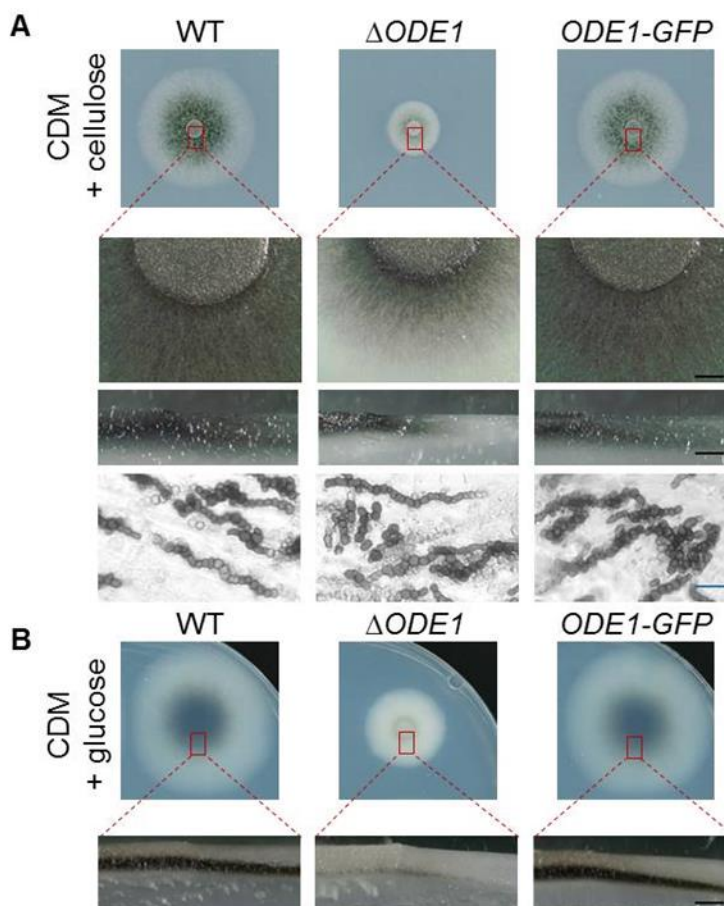
During microscopy of fungal material from colony centers of ∆*ODE1*, wild type-like microsclerotia could be observed. Changing the growth conditions to 14 days incubation in the dark on minimal medium with glucose, a decrease in microsclerotia production in ∆*ODE1* became more apparent (Figure 27B).

Hence, *V. dahliae* Ode1 is essential for wild type-like development of the fungal colony and shows positive impacts on microsclerotia formation. However, Ode1 is dispensable for stress responses under tested conditions. The C-terminal GFP fusion to Ode1 allowed complementation phenotypes close to wild type levels. The observed growth defect of ∆*ODE1* was partially restored in presence of extracellular linoleic acid.

3.4.4 *V. dahliae ODE1* is dispensable for induction of disease symptoms in tomato plants

The *ODE1* deletion strain was less impaired in growth in presence of linoleic acid *ex planta*. Also plants synthesize linoleic acid as an important precursor of defense-related compounds like plant oxylipins and cutin monomers and, therefore, might substitute the defect in fungal linoleic acid biosynthesis (Soliday & Kolattukudy, 1977; Brodhun & Feussner, 2011). During tomato plant infection experiments the impact of the *ODE1* deletion on virulence of *V. dahliae* was investigated.

Tomato plants inoculated with spores obtained from the ∆*ODE1* strain displayed overall similar stunting and hypocotyl discolorations to wild type-infected plants with only slightly reduced numbers of plants with disease symptoms after 21 days. About 70% of the tomato plants inoculated with ∆*ODE1* spores displayed disease symptoms in comparison to 87% of the wild type treated plants (Figure 28).

In summary, the *ODE1* deletion strain displayed generally impaired vegetative growth, correlated with decreased microsclerotia production and allows almost wild type-like induction of disease symptoms. Hardly any decrease in induced disease symptoms was observed in plants inoculated with spores obtained from the *ODE1* deletion strain suggesting a minor or no role of the single gene *ODE1* in virulence of *V. dahliae*. This virulent *in planta* phenotype of a strain with a severe growth defect might result from substitution of the fungal *ODE1* product by linoleic acid provided in plant cells.
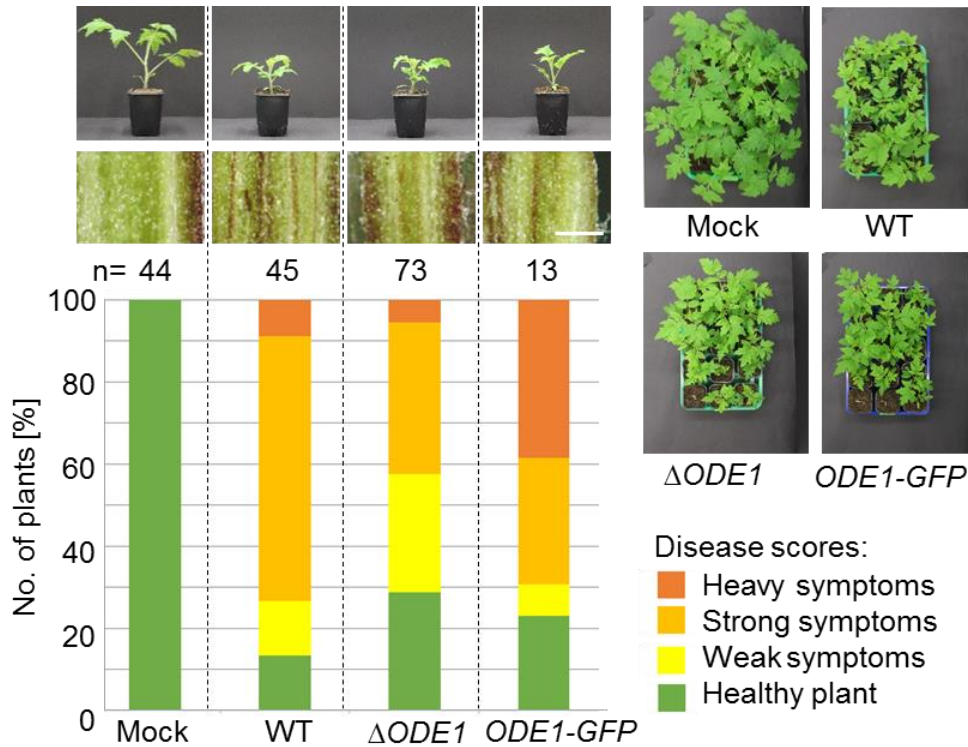
Figure 28: *V. dahliae ODE1* **is not required for induction of severe disease symptoms in** *S. lycopersicum.* Ten-day-old tomato plants were inoculated by root dipping into water control (mock) or spores obtained from wild type JR2 (WT), Δ*ODE1* (VGB331, VGB332), or *ODE1-GFP* complementation (VGB359) strains. Representative plants and overview of 15 plants per genotype from one experiment are shown. Disease symptoms were assessed after 21 days and transferred into disease scores per plant visualized in a stack diagram. Discoloration of hypocotyl dissections is shown. Data are shown from three independent experiments for wild type and Δ*ODE1* (VGB331), two independent experiments for a second Δ*ODE1* transformant (VGB332), and a single experiment for *ODE1-GFP*. Scale bar = 1 mm, n = total number of evaluated plants per genotype.

4 DISCUSSION

The outcome of a host-fungus interaction can be fungal colonization due to plant susceptibility or fungal death combined with plant resistance. Between these two extremes several intermediate outcomes of disease severity can be observed. Several factors affect this relationship between a pathogen and a host, including environmental factors, nutritional conditions, age, and genome variations of both, plant and fungus. Fungal signaling genes were in the focus of this study. The aim was a better understanding of the complex interplay of fungal signaling cascades favoring beneficial or detrimental outcomes in interactions with host plants.

It was shown, that pathogenic *V. longisporum* isolates possess genomic insertions which contribute to attenuation of disease symptoms induced in the interplay with rapeseed plants. These regions can be either species- or host-specific.

Virulence of *V. dahliae* is mediated by MAPK signaling pathways, but the role of scaffold proteins in insulation of these pathways was yet unstudied in plant pathogens. Ham5 is a MAPK scaffold in different ascomycetes. Here it was shown, that MAPK signaling pathways in *V. dahliae* mediate differentiation, stress response, and virulence independent from this scaffold protein.

Plant invasion and suppression of the plant defense responses rely on the secretion of certain tools which can be regulated by the UPR pathway. Therefore, the *V. dahliae* bZIP transcription factor Hac1 and its role in virulence was characterized in this study. The UPR regulator has conserved as well as species-specific impacts on differentiation of *V. dahliae* and is an important factor for virulence.

Virulence can be connected to fungal differentiation. Important regulators of fungal differentiation are lipid metabolites which can act as signaling molecules. Characterization of the fungal oleate Δ12-fatty acid desaturase Ode1, catalyzing the synthesis of linoleic acid, revealed an important contribution to fungal growth with only a minor impact on the induction of disease symptoms.

Figure 29 represents an overview about the findings of this thesis, which will be discussed in detail in the following.
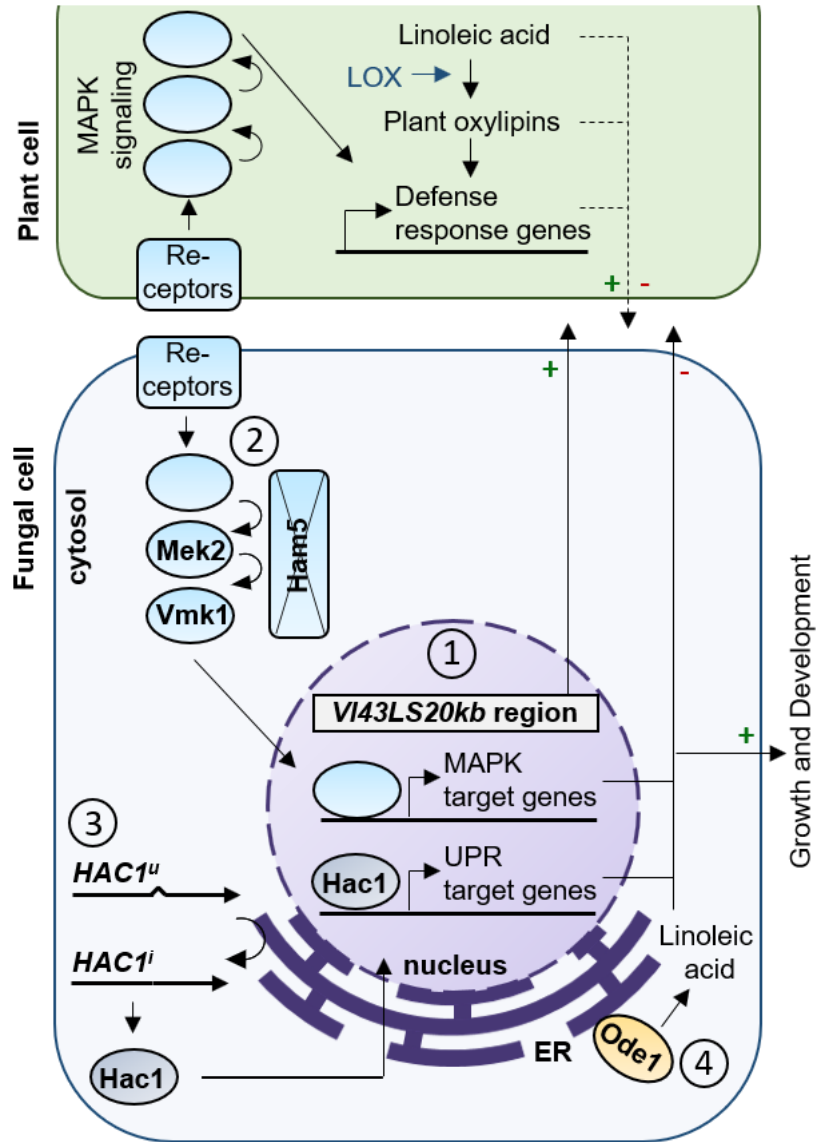
Figure 29: Interactions between haploid *V. dahliae* and amphidiploid *V. longisporum* isolates with their plant hosts studied in this thesis. ① The pathogenic *V. longisporum* isolate Vl43 possesses the genomic region *Vl43LS20kb*, which is absent in the genome of the nonpathogenic isolate Vl32. This region contributes to attenuation of disease symptoms induced in the interplay with rapeseed plants (indicated by arrow with green plus from fungal cell and arrow with dashed line and red minus from plant cell). ② The *V. dahliae* Vmk1 MAPK pathway components Mek2 (MAP2K) and Vmk1 (MAPK) positively control vegetative growth and microsclerotia formation (indicated by arrow with green plus to "Growth and Development") and are required for induction of disease symptoms in plants (indicated by arrow with red minus from fungal cell) independent from the scaffold homolog Ham5 in *V. dahliae*. The MAPK pathway is required for initial penetration and for the susceptibility of the plant (indicated by arrow with dashed lines and green plus from plant cell). ③ Upon interaction with the host, the fungal cell has to cope with an increased demand for secreted proteins, which leads to ER stress. The uninduced mRNA of the UPR regulator Hac1 (*HAC1^u*) is unconventionally spliced (indicated by arrow close to ER membrane) and the *HAC1^i* mRNA is translated into the bZIP transcription factor Hac1, which regulates UPR target genes. *V. dahliae HAC1* is involved in the ER stress response and vegetative growth under non-stress conditions, has a strong impact on conidiation, and is essential for the formation of microsclerotia (indicated by arrow with green plus to "Growth and Development"). *HAC1* is required for the virulence of *V. dahliae* (indicated by arrow with red minus from fungal cell) and potentially regulates expression or secretion of effector proteins, which enables the fungus to circumvent plant defense responses (indicated by arrow with dashed line and green plus from plant cell). ④ The oleate Δ12-fatty acid desaturase Ode1, which catalyzes the synthesis of linoleic acid, supports fungal growth and microsclerotia formation (indicated by arrow with green plus to "Growth and Development"). Ode1 deficiency has only minor effect on development of disease symptoms *in planta*, which might be due to the availability of plant linoleic acid that potentially supports fungal growth and differentiation (indicated by arrow with dashed line and green plus from plant cell).

4.1 The pathogenic *V. longisporum* isolate Vl43 possesses a genomic insertion contributing to disease symptom attenuation in rapeseed plants

4.1.1 *V. longisporum* isolates colonize plants with different pathotypes

V. longisporum is an amphidiploid interspecies hybrid, which evolved from at least three separate hybridization events (Inderbitzin *et al.*, 2011b; Figure 2). All known *V. longisporum* lineages arose by hybridization of the haploid species A1 with one of three *V. dahliae* or *V. dahliae* related strains D1, D2, or D3 (Inderbitzin *et al.*, 2011b). Isolates from the A1/D3 lineage were described overall as the least pathogenic in comparison to the lineages A1/D1 and A1/D2. However, not all isolates of the A1/D3 lineage colonize rapeseed without induction of disease symptoms (Novakazi *et al.*, 2015). In a pathogenicity test involving seven isolates from the lineage A1/D1, four A1/D2, and four A1/D3, a single A1/D3 isolate was the most virulent on rapeseed (Novakazi *et al.*, 2015). In this study, the tested A1/D3 strain Vl32 colonized rapeseed plants without induction of any disease symptoms, whereas the A1/D1 isolate Vl43 induced severe disease symptoms under laboratory conditions (Figure 7). Both isolates were able to enter and propagate within the plants with different outcomes for plant health. Less fungal outgrowth could be observed from stem sections of the asymptomatic strain Vl32, hinting to reduced propagation and reduced fungal biomass within the plant. This might be either due to plant mechanisms reducing fungal growth or a less aggressive colonization behavior of Vl32. Previous experiments comparing Vl43 and Vl32 root colonization did not show differences of the fungal behavior prior to entering the plant on the root surface. Accordingly, propagation of Vl32 within the plant following initial penetration of the roots must be affected. The comparison of the *ex planta* phenotypes of *V. longisporum* isolates from different lineages revealed a difference in the growth behavior of strains from the A1/D1 towards the A1/D3 lineage on malt extract agar. A1/D3 strains Vl32 and Vl19 formed bundles of single hyphae, which were covering the colonies. These bundles were rare in the A1/D1 strains Vl43 and Vl145c. Since Verticillia colonize the vascular system of the host plant and occurrence of disease symptoms is correlated with clogging of vessels hindering the transpiration stream (Yadeta & Thomma, 2013), the formation of arranged hyphal bundles might have a less disturbing influence on the flow of the xylem fluid in Vl32 colonized plants. An impact of directed hyphal growth on the pathotype of plant colonizing fungi was observed in the mutualistic grass colonizing *Epichloë festucae*. Here, hyphae show parallel growth aligned with elongating leaf cells (Christensen *et al.*, 2008). A mutant deficient in the reactive oxygen producing membrane-bound Nox complex (nicotinamide adenine

dinucleotide phosphate oxidase complex), displayed pathogenic development correlated with hyperbranched hyphal growth which was no longer tightly connected to the leave cells (Brown *et al.*, 2016; Tanaka *et al.*, 2006, 2008; Takemoto *et al.*, 2006, 2011). The formation of hyphal bundles in isolates of the *V. longisporum* A1/D3 lineage was observed only on malt extract agar, which is not very similar to the conditions of low nutrient availability given within the vascular system of rapeseed plants. If hyphal bundles are formed within the plant and influence the transpiration stream remains to be elucidated.

4.1.2 The *V. longisporum Vl43LS20kb* region mediates virulence attenuation towards rapeseed plants

Investigation of genomic differences between *V. longisporum* isolates with different pathotypes revealed a high conservation on gene level, but differences in the chromosome numbers and the karyotypes. The additional chromosome observed in the asymptomatic isolate Vl32 was not an accessory chromosome comprising genes that are species-specific, but a result of rearranged genomic regions. Occurrence of frequent synteny breakpoints caused by genomic rearrangements was observed in all Verticillia (Shi-kunne & Faino, 2017). Chromosomal reshuffling in eukaryotes is correlated with alterations in phenotypes and is assumed to confer varying fitness in different niches by gene gains or losses (Coghlan *et al.*, 2005; Tang & Amon, 2013; Dong *et al.*, 2015; Plissonneau *et al.*, 2018). In the haploid species *V. dahliae* a correlation between genomic rearrangements and the evolution of Lineage Specific regions was observed (Klosterman *et al.*, 2011; de Jonge *et al.*, 2013; Chen *et al.*, 2018; Faino *et al.*, 2016; Gibriel *et al.*, 2019)*.* The *V. dahliae* VdLs.17 LS regions 1-4 were proposed to be involved in adaptation of *V. dahliae* to different host niches and in its host range expansion in comparison to *V. alfalfae* (Klosterman *et al.*, 2011). A genomic LS region originating from the parental lineage related to *V. dahliae* is present in the pathogenic isolates Vl43 and Vl145c and absent in the nonpathogenic *V. longisporum* isolate Vl32 (Figure 8). This finding may lead to the assumption that this region contributes to fungal virulence. However, characterization of the *Vl43LS20kb* region unraveled a negative impact on the severity of disease symptoms induced in *V. longisporum* Vl43 colonized rapeseed plants. The significant effect of this region was shown in three different strains deficient in the entire *Vl43LS20kb* region or in either the first or the second part of this region. All of the Vl43 *LS* deletion strains induced more severe disease symptoms in rapeseed plants than the wild type (Figure 9, Figure 30).

The different *LS* deletions did not cause obvious alterations in their *ex planta* phenotypes in comparison to the wild type Vl43 (Figure S2). Increased fungal growth or propagation

with detrimental impact on the host plant cannot be considered as an explanation for the hypervirulent *in planta* phenotype. Instead, negative impacts on pathogenicity might be explained with the hemibiotrophic life style of pathogenic *Verticillium* strains, performing a switch from an initial biotrophic stage to a later necrotrophic stage (Fradin & Thomma, 2006). These stages require differentiated strategies in the crosstalk with the host plant. Fungal tools used to modulate the interaction with the plant can be divided into two groups: those secreted during biotrophic interactions and those, which induce the necrotrophic phase (O'Connell *et al.*, 2012; Lo Presti *et al.*, 2015; Chini *et al.*, 2018; Gibriel *et al.*, 2019). During the biotrophic interaction, the host defense responses are, for example, suppressed by effectors and secondary metabolites. Induction of the necrotrophic stage is correlated with the secretion of lytic enzymes, oxylipins, or fungal effectors which are activating the plant defense responses, induce cell death, and facilitate fungal nutrient uptake (O'Connell *et al.*, 2012; Lo Presti *et al.*, 2015; Chini *et al.*, 2018; Gibriel *et al.*, 2019). Mis-regulation of the tools required for induction of the necrotrophic phase can lead either to a lack of this phase, a premature induction, or rather increased secretion of the respective tools, which might result in hypervirulence. In our case, this means that expression or secretion of tools required to induce the necrotrophic phase might be decreased by certain factors encoded in the *Vl43LS20kb* region in the wild type Vl43. These pathogenicity attenuating factors would make the pathogenic isolate more tolerable for rapeseed plants and would not be required in the asymptomatic colonizer Vl32, due to the absence of the respective targeted tools for induction of the necrotrophic phase.

The *Vl43LS20kb* region, identified in the pathogenic rapeseed colonizer Vl43, encodes six hypothetical small proteins and one larger protein with cytosolic, nuclear, or transmembrane localization, but without secretion signals (Figure 8B). For Lsg1, Lsg2, Lsg4, and Lsg7 no domains were predicted. The absence of a predicted signal peptide makes the secretion of these proteins via the ER/Golgi secretory pathway not very likely. Alternatively, unconventional secretion mechanisms independent from secretion signal sequences exist in fungi (Miura & Ueda, 2018). Unconventional secretion is described, for example, for fungal enzymes with effector properties, such as an isochorismatase in *Phytophthora sojae* and *V. dahliae.* The isochorismatase manipulates defense responses by suppression of salicylic acid accumulation in the host plant (Liu *et al.*, 2014)*.* One should consider that examples for mutants deficient in effectors with hypervirulent phenotypes in fungi are rare and, therefore, the presence of effector encoding genes in the *Vl43LS20kb* region might be less likely. In *U. maydis* 12 effector gene clusters were identified, encoding genes upregulated simultaneously in infected plant tissue (Kämper *et al.*, 2006). Absence of these clusters resulted in decreased

virulence in four cases and in unaffected virulence in seven cases. However, hypervirulence was observed following disruption of the *Um01234-41* effector gene cluster (Kämper *et al.*, 2006). The mechanism explaining this phenotype has not been elucidated yet.

To date, research on LS regions correlated with synteny breakpoints in Verticillia was mainly restricted to identified effectors promoting fungal virulence (de Jonge *et al.*, 2013; Faino *et al.*, 2016; Kombrink *et al.*, 2017; Li, 2019, Dissertation, University Wageningen). Effector gene enrichment in LS regions relative to the core genome was found by comparison of different *V. dahliae* isolates (de Jonge *et al.*, 2013; Gibriel *et al.*, 2019). In contrast, LS and core genomes from different species of the genus displayed the same relative numbers of genes encoding proteins with secretion signals (Klosterman *et al.*, 2011). The number of effector genes relative to the total number of genes encoded in the LS regions of *V. dahliae* strains was rather small (de Jonge *et al.*, 2013; Gibriel *et al.*, 2019). Besides effector protein encoding genes other genes in LS regions might provide potential for niche adaptation.

Lsg3 and Lsg6 encoded by the *Vl43LS20kb* region contain predicted transcription factor domains. Lsg3 is encoded in the *LSI* subregion, whereas Lsg6 is encoded in the *LSII* subregion. Downregulation of virulence-related genes has been observed during transcriptome analysis of related fungal species with different pathotypes. Recently, comparison of the transcriptomes of a *V. dahliae* strain, which causes less severe disease symptoms in cotton in comparison to a more virulent relative, revealed downregulation of pathogenicity-related genes as ,for example, genes involved in hydrophobin and melanin production (Jin *et al.*, 2019). Genome comparison of the same *V. dahliae* strains displayed an enrichment of genes bioinformatically predicted as transcription factors. These transcription factors could downregulate pathogenicity-related genes (Jin *et al.*, 2019). Another example from different *Colletotrichum* species corroborates that differentiated transcriptional regulation during host colonization can decide about the life style of plant colonizing fungi resulting in different pathotypes, which are not necessarily associated with extensive remodeling of the gene repertoire (Hacquard *et al.*, 2016). A limited activation of pathogenicity-related genes *in planta* was observed for the endophytic species *C. tofieldiae* in comparison to the pathogenic relative *C. incanum* (Hacquard *et al.*, 2016). Transcription factors, which are negatively regulating virulence, have been characterized in *A. brassicicola* and *F. oxysporum* (Caracuel *et al.*, 2003; Cho *et al.*, 2012; Brown *et al.*, 2016). In *F. oxysporum* the pH signaling transcription factor PacC negatively regulates genes expressed under low pH conditions and mutants deficient in this repressor display increased virulence in tomato plants (Caracuel *et al.*, 2003). Further, hydrolytic enzymes are transcriptionally repressed

by the *A. brassicicola* transcription factor Amr1 (*Alternaria* melanin regulation 1) known for its role in melanin biosynthesis in other plant pathogenic fungi (Cho *et al.*, 2012). The role of this transcription factor in virulence is unique for *A. brassicicola* and was not observed for homologs as *V. dahliae* VdCmr1 (*V. dahliae Colletotrichum* homologous melanin regulation 1; Cho *et al.*, 2012; Brown *et al.*, 2016; Wang *et al.*, 2018).

For Lsg5 encoded in the *Vl43LS20kb* region, a Zinc finger RING-type domain was predicted (Figure 8B). Zinc finger RING-type domains mediate protein-protein interactions or ubiquitin transfer either to substrates or the Zinc finger RING-type domain protein itself (Joazeiro & Weissman, 2000). The protein possesses an additional transmembrane domain, with a short non-cytosolic and a longer cytosolic region containing the RING domain. The yeast scaffold protein Ste5 of the pheromone response pathway contains a RING-domain required for its interaction with Ste4, a subunit of the G-protein coupled to the transmembrane receptors of the mating pathway (Inouye *et al.*, 1997). Orthologous Ham5 scaffold proteins in ascomycete filamentous fungi do not possess a RING-domain (Figure 11). The regulation of signaling cascades assembled at the membrane following perception of external signals might involve RING-domain transmembrane proteins, such as the protein Lsg5 encoded in the *Vl43LS20kb* region.

Degradation of proteins located in plasma membranes, like receptors, transporters, and channels, by endocytosis is generally triggered by ubiquitination (Piper & Luzio, 2007; Nakamura, 2011). This could be also true for soluble proteins interacting with complexes associated to the membrane. In mammals, Membrane-Associated RING-CH (MARCH) proteins are a well described family of RING-domain proteins, which are located to cell membranes and are important for ubiquitination of cell-surface immune molecules (Goto *et al.*, 2003; Nakamura, 2011; Samji *et al.*, 2014; Zhang *et al.*, 2019). The absence of ubiquitin ligases located to the fungal plasma membrane might result in increased occurrence of certain membrane or membrane-complex-associated proteins. An adaptation of the fungal membrane proteome following interaction with the host plant´s cell wall was described in the plant pathogen *B. cinerea* (Liñeiro *et al.*, 2016). This adaptation might be disturbed in the absence of membrane-bound ubiquitin ligases responsible for degradation of membrane proteins. An increased occurrence of membrane-complex-associated proteins, such as co-receptors or activators of signaling cascades, in absence of a membrane-bound ubiquitin ligase could result in a permanent activation of cascades. This permanent cascade activation might promote virulence, for example by increased secretion of virulence factors.

Defects in signaling cascades important for sensing of the environment, signal transduction, and induction of infection-related morphogenesis result in hypervirulence in

fungi (Brown *et al.*, 2016). In the basidiomycete *U. maydis* the phosphatase Rok1 (regulator of Kpp2) controls dephosphorylation of the partially redundant Fus3/Kss1-like MAP kinases Kpp2 and Kpp6 (kinase PCR-product 2/ 6), which regulate efficient appressorium formation and plant invasion in a negative feedback loop (Di Stasio *et al.*, 2009). *U. maydis rok1*-deficient mutants displayed a hypervirulent phenotype on maize plants correlated with more efficient appressorium formation. As previously mentioned, Nox complex-deficient mutants of *E. festucae* induce disease symptoms *in planta* correlated with hyperbranched hyphal growth with increased fungal biomass (Tanaka *et al.*, 2006; Takemoto *et al.*, 2006; Tanaka *et al.*, 2008; Takemoto *et al.*, 2011; Brown *et al.*, 2016). In the same fungus, the Hog1-like MAPK signaling cascade is involved in downregulation of hydrolytic enzyme secretion and mutants deficient in the MAPK display virulence on their natural symbiotic hosts (Eaton *et al.*, 2010; Brown *et al.*, 2016).

In summary, Lsg3 and Lsg6 have the potential to act as transcription factors with roles in downregulation of mechanisms required for induction of disease symptoms. Lsg5 could regulate signal transduction from the membrane via protein-protein interactions or ubiquitination, targeting components to proteasomal degradation. Further, proteins encoded in the *Vl43LS20kb* region might act as effector proteins, which are unconventionally secreted. The mechanism leading to hypervirulence following deletion of the *Vl43LS20kb* region in Vl43 still remains to be elucidated. This is the first study unraveling an LS region in Verticillia which attenuates virulence in a pathogenic isolate. The absence of this region in the asymptomatic isolate Vl32 shows that not only pathogenicity factors or the loss of genomic regions, but also regions involved in attenuation of pathogenicity, contribute to the differences in the genomes of isolates from different pathotypes.

4.1.3 Host specificity of virulence and putative attenuating factors in Verticillia

In this study, an LS region with functions in attenuation of disease symptoms in the interaction of *V. longisporum* with rapeseed plants was identified. The pathogenesis-reducing mechanism of this region depends either on the fungal species or the host.

The genome of the haploid *V. dahliae* isolate JR2 contains a *Vl43LS20kb* homologous region and *Vl43LS20kb* homologous subregions could be identified rearranged in the genome of the *V. dahliae* strain VdLs.17. In contrast, the *Vl43LS20kb* region is absent from the genome of *V. alfalfae* VaMs.102, which is more closely related to the *V. longisporum* parental lineage A1, and from the *V. longisporum* isolate Vl32 (A1/D3). These findings corroborate the origin of the *Vl43LS20kb* region in the genome of the *V. longisporum* lineage A1/D1 parental species D1.

The *Vl43LS20kb* homologous region encoded in the genome of *V. dahliae* JR2 displays an indifferent role in pathogenicity towards tomato plants (Figure 10, Figure 30). The *V. dahliae* JR2 wild type does not induce disease symptoms in rapeseed plants. Two *V. dahliae* isolates were able to colonize the roots of rapeseed plants, but the isolates remained in the lower parts of the plants without induction of disease symptoms (Zhou *et al*., 2006). Whether the homologous *Vl43LS20kb* region in *V. dahliae* affects the colonization behavior and pathogenicity of this species against rapeseed or other host plants is currently unknown.

The genome of *V. dahliae* JR2 harbors an additional copy of the gene *LSG1* encoded in the *Vl43LS20kb* homologous region, which was not deleted in *V. dahliae* JR2 Δ*LS*. Since all constructed deletion strains in *V. longisporum* Vl43, Δ*LSI*, Δ*LSII*, and Δ*LS*, resulted in induction of more severe disease symptoms in rapeseed plants and the phenotype was even stronger in Δ*LSII* than in Δ*LSI* (Figure 9)*,* the presence of an additional copy of *LSG1* located in the *LSI* subregion does not represent a sufficient explanation for the unaltered pathogenicity of *V. dahliae* JR2 in absence of the homologous *Vl43LS20kb* region.

Even if *V. dahliae* species have a broad host range, the single isolates of the species differ in their host ranges and in virulence towards different host plants (Resende *et al*., 1994; Zeise & von Tiedemann, 2002; Pegg & Brady, 2002; Gibriel *et al*., 2019). For isolates of the same *V. longisporum* lineage, differences in their pathogenicity on different host plants was observed as well (Novakazi *et al*., 2015). Therefore, one can suggest that strains of both species generally display a high degree of specialization and adaptation to a certain host. This specialization might not always be the result of the acquirement of novel genes, but also the differential regulation of existing mechanisms in response to certain environmental factors.

In other plant colonizing fungi, gene losses due to chromosomal rearrangements with significant roles in niche adaptation were described (Sharma *et al*., 2014; Hartmann *et al*., 2017; Plissonneau *et al*., 2018), which might be a possible mechanism in Verticillia as well. Further, asymptomatic or less virulent isolates might contain several pathogenicity-related genes in their genomes, which are inactive due to certain regulatory mechanisms.

Several studies investigating LS regions from subgroups of *V. dahliae* isolates revealed effector genes required for colonization of particular hosts as, for example, the effector NLP-2 (necrosis and ethylene-inducing peptide 1-like protein 2) which is involved in virulence of the strain JR2 on tomato and *A. thaliana*, but dispensable for tobacco infection (Santhanam *et al*, 2013). The *V. dahliae* effector Tom1 is essential for tomato

infection only and the effector Sun1 contributes to virulence specifically in sunflower colonization (Li, 2019, Dissertation, University Wageningen).
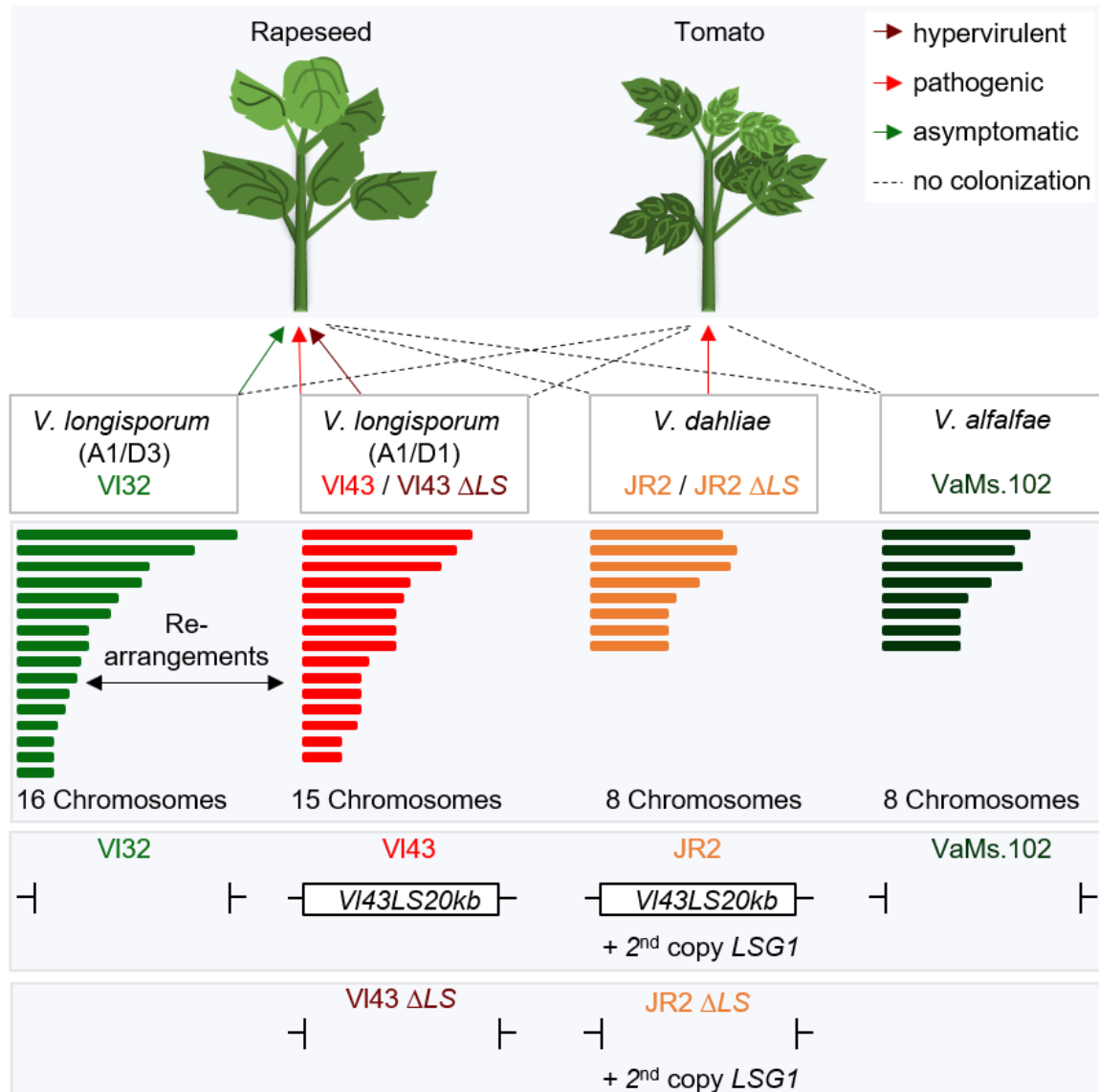
Figure 30: The *Vl43LS20kb* region attenuates pathogenicity of *V. longisporum* Vl43 in rapeseed and the homologous region is indifferent for virulence of *V. dahliae* JR2 in tomato plants. The genomes of *V. longisporum* lineages evolved by hybridization from two haploid parental species, which are *V. dahliae* strains (D2, D3) or close relatives of *V. alfalfae* (A1) and *V. dahliae* (D1). The hybrid genomes differ in their karyotypes due to chromosomal rearrangements and display different chromosome numbers (15 for Vl43; 16 for Vl32). The species *V. dahliae* JR2 and *V. longisporum* Vl43 (A1/D1) harbor the *Vl43LS20kb* region in their genomes, which is absent in *V. longisporum* Vl32 (A1/D3) and *V. alfalfae* VaMs.102. *V. dahliae* JR2 exhibits an additional copy of the gene *LSG1*. Deletion of the *Vl43LS20kb* homologous region in *V. dahliae* JR2 region results in an unaltered virulent phenotype on tomato plants (indicated by the light red arrow for both, the wild type and the *LS* deletion strain), whereas deletion of the *Vl43LS20kb* region in *V. longisporum* Vl43 results in hypervirulence (indicated in dark red), suggesting a species- or host-specific role in attenuation of disease symptoms. *V. longisporum* isolates are unable to colonize tomato as a host (indicated by dashed lines), whereas *V. dahliae* remains in the roots without induction of disease symptoms and is not able to colonize the entire plant (indicated by dashed lines; Zhou *et al.*, 2006). *V. alfalfae* colonizes alfalfa and hops and is not known as a colonizer of tomato or rapeseed plants (indicated by dashed lines; Bhat & Subbarao, 1999).

Further, seven LS genes acquired by horizontal gene transfer from *F. oxysporum*, contributed to the virulence of *V. dahliae* Vd991 in cotton, but were dispensable for virulence on tomato and lettuce (Chen *et al.*, 2018). Integration of these genes into *V. dahliae* strains JR2 or VdLs.17 resulted in increased virulence on cotton, whereas there was no effect on tomato or lettuce hosts (Chen *et al.*, 2018). The underlying mechanisms regulating the observed host-specific induction of disease symptoms is still unknown for all of these examples and remains to be elucidated. One could assume that fungal virulence factors, which are inducing disease symptoms in a certain host, target host-specific mechanisms for regulation of defense responses. The absence of the corresponding target in a different host would make the fungal tool dispensable. Further, recognition of host-specific external signals sent by the plant might be essential for induction of a fungal mechanism that is regulating its virulence.

In summary, the *Vl43LS20kb* region makes *V. longisporum* Vl43 more tolerable for rapeseed plants. Presence of the homologous region in *V. dahliae* JR2 is indifferent for induction of disease symptoms in tomato plants. Different impacts of the genomic region on the host-fungus interaction might be caused either by differential gene regulation in the different organisms, by host dependent gene regulation, or by host-specific targets of virulence factors regulated by the *Vl43LS20kb* region.

4.2 MAPK signaling pathways in *V. dahliae* mediate differentiation, stress response and virulence independent from the scaffold protein Ham5

4.2.1 The Ham5 scaffold function for the Fus3/Kss1-like MAPK cascade is not conserved among filamentous ascomycetes

The perception of environmental signals and subsequent signal transduction are essential to induce adaptation processes in filamentous fungi. For example, sensing of a suitable host has to be forwarded to activate fungal colonization-related mechanisms. The Vmk1 MAPK signaling pathway in *V. dahliae* has a conserved role in fungal pathogenicity (Rauyaree *et al.*, 2005; Sarmiento-Villamil *et al.*, 2018). In homologous pathways of *N. crassa* and *A. nidulans*, a scaffold protein is required for insulation (Dettmann *et al.*, 2014; Jonkers *et al.*, 2014; Frawley *et al.*, 2018) and homologs of this scaffold protein have been bioinformatically predicted in a subdivision of the Ascomycota (Jamet-Vierny *et al.*, 2007). In this study, the impact of the corresponding *V. dahliae* protein Ham5 on Vmk1 MAPK pathway-mediated functions was analyzed.

Vmk1 has a conserved essential role in pathogenicity and MAPK deletion strains displayed reduced conidiation and microsclerotia formation (Rauyaree *et al.*, 2005). A

decrease in vegetative growth on certain media was observed in this study (Figure 13). The MAP2K Mek2 displayed the same impact on the phenotype as Vmk1 regarding microsclerotia formation, vegetative growth, and virulence (Figure 13, Figure 14). In addition to the high conservation of *V. dahliae* Mek2 to characterized homologs (Figure 12), these results provide indirect evidence that the kinase functions in the same MAPK pathway like Vmk1. No hints for additional targets of Mek2 have been observed. V. *dahliae* Vph1 was suggested to act downstream of the cascade as a yeast Ste12-like transcription factor activated upon phosphorylation by Vmk1 (Sarmiento-Villamil *et al.*, 2018). The Vph1-deficient mutant displayed no alterations in its *ex planta* phenotype, but did not induce plant disease symptoms, suggesting that Vph1 is not the only target of the Vmk1 MAPK pathway in *V. dahliae* (Sarmiento-Villamil *et al.*, 2018). This study showed that Vmk1 cascade-mediated functions in growth, microsclerotia formation, and virulence are independent from the presence of Ham5 (Figure 13, Figure 14), corroborating that these functions do not rely on insulation by the potential scaffold protein in *V. dahliae*. In *N. crassa* and *A. nidulans* the Ham5 scaffold protein homologs display similar functions as the Fus3/Kss1-like MAPK (Li *et al.*, 2005; Aldabbous *et al.*, 2010; Frawley *et al.*, 2018). For example, *N. crassa* HAM-5 and MAK-2 are essential for hyphal and germling fusion, have a positive impact on vegetative growth, formation of aerial hyphae, as well as on sexual and asexual development (Li *et al.*, 2005; Aldabbous *et al.*, 2010). Similarly, the homolog IDC1 displays diverse impacts on fungal growth and differentiation in *P. anserina*. IDC1 is involved in the non-self-perception resulting in the reduction of vegetative growth and the induction of melanization in the stationary phase (Jamet-Vierny *et al.*, 2007). In *P. anserine*, IDC1 contributes to sexual and asexual development and aerial hyphae formation (Jamet-Vierny *et al.*, 2007). The observed phenotypes in absence of IDC1 display high similarity to phenotypes observed in absence of components of the cell wall integrity (CWI) MAPK pathway and migration of the respective MAPK to the nucleus is dependent on IDC1 in this fungus. These results led to the positioning of *P. anserina* IDC1 into another signaling cascade than its homologs in *A. nidulans* and *N. crassa* (Jamet-Vierny *et al.*, 2007).

A scaffolding function of *V. dahliae* Ham5 in the CWI MAPK pathway, as suggested in *P. anserina,* is possible, but rather unlikely, since one would expect the observation of an *ex planta* or *in planta* phenotype in absence of a CWI MAPK cascade scaffold protein for the tested conditions. Even if homologs of the CWI MAPK pathway components in *V. dahliae* have not been characterized to date and their functions in fungal growth, differentiation, and virulence are still unknown, homologs of this cascade in related fungi possess effects on the response to cell wall stressors in many cases, and even more conserved, have strong impacts on virulence (Rui & Hahn, 2007; Zhao & Xu, 2007;

Hamel *et al.*, 2012; Segorbe *et al.*, 2017; Jiang *et al.*, 2018a). The cell wall stress response to SDS was unaffected in the absence of Ham5 in *Verticillium* and no impact on virulence was observed in this study. Overlapping functions of the Vmk1 and CWI MAPK pathways regarding their function in microsclerotia production are possible. The *V. dahliae* MAP2K and the MAPK homologs of the CWI pathway could be identified by BLAST searches due to their high conservation and were found to be upregulated in later stages of microsclerotia formation similar to Vmk1 and Mek2 (Xiong *et al.*, 2014). This could be a hint for an impact of the CWI MAPK pathway on microsclerotia production or melanization, which would be expected to be reflected in the deletion phenotype of a scaffold protein as well.

Similar to the CWI MAPK pathway, a scaffold function of Ham5 for the Hog1 MAPK pathway is unlikely. The response to osmotic stress was not affected in absence of Ham5 in *V. dahliae* (NaCl, H_2O_2, Sorbitol). Besides their role in the response to osmotic stressors, the Hog1 MAPK pathway cytosolic osmo-sensor VdSsk1, the MAP2K VdPbs2, and the MAPK VdHog1 display partially overlapping functions with the Vmk1 MAPK pathway with positive impacts on microsclerotia formation or melanization and virulence (Wang *et al.*, 2016; Tian *et al.*, 2016; Zheng *et al.*, 2019; Figure 31).

Shared functions with the cascade components could be shown also for potential receptors of the Vmk1 and Hog1 MAPK pathway. Direct evidence for upstream regulators for the activation of the Vmk1 MAPK pathway has not been given to date, but regulatory impacts of two transmembrane receptors, VdMsb2 and VdSho1, on the Vmk1 MAPK pathway in *V. dahliae* would be possible (Figure 31). Both receptors have been characterized regarding their functions in development and virulence in *V. dahliae* and display positive impacts on conidiation and virulence (Tian *et al.*, 2014; Qi *et al.*, 2016), similar to Vmk1 (Rauyaree *et al.*, 2005). Microsclerotia development and melanization were unaffected in absence of VdSho1 (Qi *et al.*, 2016), whereas microsclerotia production was reduced in a VdMsb2 deletion strain (Tian *et al.*, 2014) similar to Vmk1 and Mek2 deletion strains in this study. Further, the receptors are involved in oxidative stress responses (Tian *et al.*, 2014; Qi *et al.*, 2016). Hints from studies in other fungi are given, which support the assumption that the receptors could have regulatory roles for both, Vmk1 and Hog1 MAPK pathways in *V. dahliae*. In yeast the transmembrane proteins Msb2 and Sho1 are involved in the activation of both, the Kss1 and the Hog1 MAPK pathway (Cullen *et al.*, 2012). Physical interaction of Sho1 with the Fus3/Kss1-like MAPK module could be shown in *F. graminearum* (Gu *et al.*, 2015). In *F. oxysporum*, impacts of the receptors on phosphorylation of the Fus3/Kss1-like MAPK homolog, expression of corresponding target genes, as well as on invasive growth were observed (Perez-Nadales & Di Pietro, 2015). However, Msb2 and Sho1 influence the MAPK-

dependent functions only partially, corroborating the presence of additional regulatory components for this pathway in *F. oxysporum* (Perez-Nadales & Di Pietro, 2015)*.*
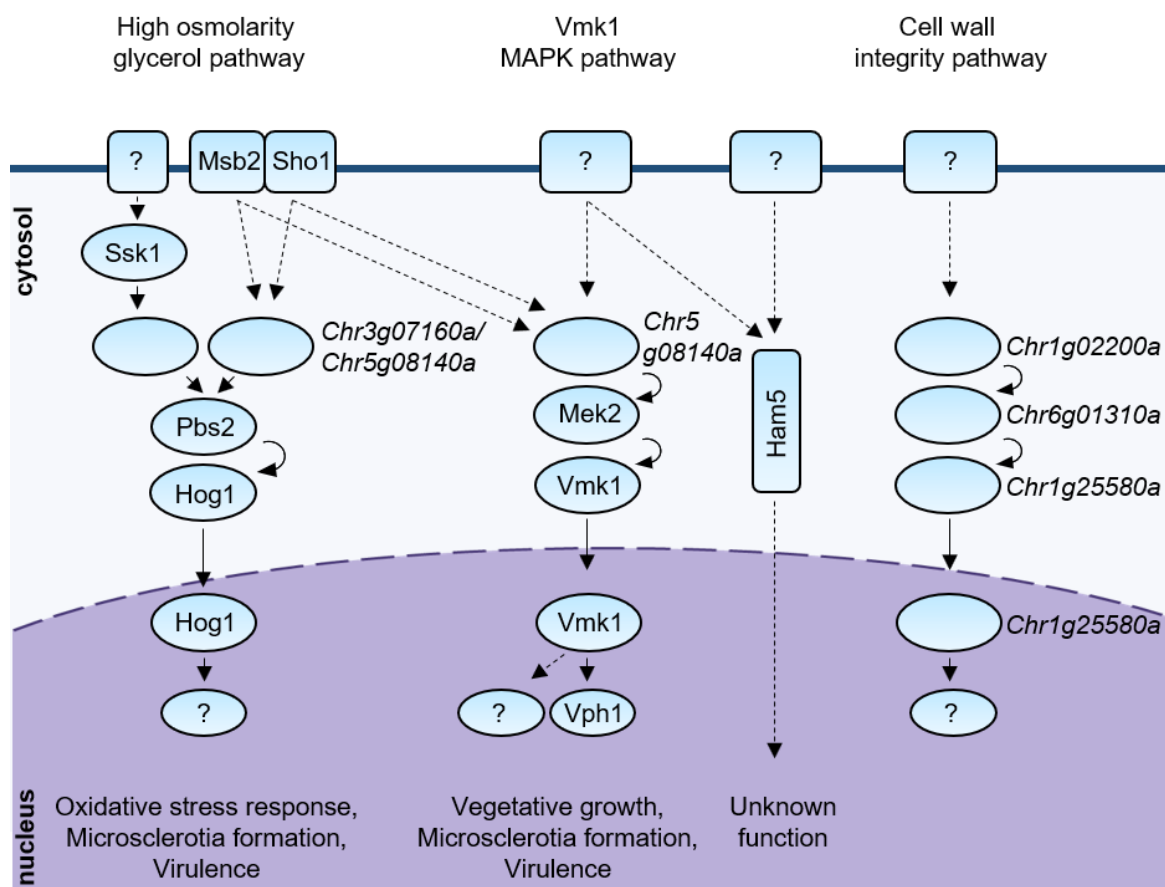
Figure 31: MAPK signaling pathways in *V. dahliae*. In *V. dahliae* components of two MAPK cascades, the Vmk1 and the Hog1 MAPK signaling pathways, were described to date. In this study, the MAP2K Mek2 and the Ham5 homolog of the Vmk1 MAPK cascade were characterized. Ham5 is dispensable for growth, microsclerotia formation, and virulence and therefore cannot be assumed to play a scaffolding role for these functions of the cascade. The functions of Ham5 in *V. dahliae* is unknown. Mek2 displays Vmk1-like positive regulatory roles in vegetative growth, microsclerotia production, and virulence. Indirect evidence was shown for Vph1 to act as a downstream transcription factor homologous to yeast Ste12. Vph1 functions in regulation of virulence but was dispensable for growth and microsclerotia production (Sarmiento-Villamil *et al.*, 2018). Therefore, the presence of other potential targets of Vmk1 can be assumed. The Hog1 MAPK pathway displays similar functions in microsclerotia formation like the Vmk1 MAPK pathway. Both pathways are involved in regulation of virulence, however, the Vmk1 MAPK pathway has a greater impact. Described components are given with their respective names as determined in VdLs.17 (Xiong *et al.*, 2014), but to date unstudied components are indicated with the *V. dahliae* JR2 gene identifiers (gene identifiers abbreviated for a better overview, VDAG_JR2_Chr…). The cell wall integrity MAPK pathway was not yet studied. Dashed lines indicate potential interactions. Question marks indicate, that proteins are unknown.

Structural differences between *V. dahliae* Ham5 to homologs in *N. crassa* and *A. nidulans* could be a reason for the lacking functional conservation. The characterized *HAM5* gene in *V. dahliae* was the only hit during reciprocal BLAST search with known

homologs and the deduced protein possesses a similar domain structure and higher protein sequence identity to *N. crassa* and all other species tested in this study than the *A. nidulans* homolog (Figure 11). However, *V. dahliae* Ham5 contains a shorter WD40 domain with 255 aa in comparison to 335 aa for *N. crassa* (Jonkers *et al.*, 2016) and 311 aa for *A. nidulans* (Frawley *et al.*, 2018). In *N. crassa* the N-terminal WD40 domain of HAM-5 was described to be essential for its function and the interaction with the MAK-2 protein, whereas the C-terminal domain plays a minor role for its function (Jonkers *et al.*, 2014). WD40 repeat domains generally display roles in multi-protein interactions (Xu & Min, 2011) and have been identified in several fungal scaffold proteins (Pöggeler & Kück, 2004; Jain, 2019; Hicks *et al.*, 2001). The N-terminal truncation in *V. dahliae* might have an impact on its function in mediating protein-protein interactions. In conclusion, a scaffolding function of the *V. dahliae* Ham5 homolog for one of the MAPK pathways in *V. dahliae* is rather unlikely, but might be possible in a not yet identified context. Further the Ham5 protein could be required for protein-protein interactions in another cascade (Figure 31). To date the function of the Ham5 protein in *V. dahliae* remains unknown. Even if the tested functions of the Vmk1- and Mek2-mediated MAPK pathway are independent from the Ham5 homolog in *V. dahliae*, it is possible that a non-homologous scaffold protein, different to Ham5, might have insulating function on the cascade.

4.2.2 *V. dahliae* Mek2 and Vmk1 are involved in fungal propagation *in planta*

In the course of this study, it could be shown that the *V. dahliae* MAPK pathway components Mek2 and Vmk1 display crucial roles in induction of disease symptoms in tomato plants (Figure 14A). Hypocotyl discolorations as a hint for the induction of plant defense responses have not been observed following treatment with *MEK2* or *VMK1* deletion strains. These results were similar to findings of two *V. dahliae* Vmk1-deficient isolates from lettuce and tomato with severely reduced virulence and absence of vascular discolorations in tomato, cotton, egg-plant, and watermelon (Rauyaree *et al.*, 2005). During both studies, plant experiments were performed with wounded plant roots, since Verticillia colonize plants preferentially via root wounds (Pegg & Brady, 2002; Su *et al.*, 2018). At this point, the role of Mek2 and Vmk1 in initial plant invasion of the root surface is unknown, but could be tested in root colonization assays. Plant infection experiments with the potential downstream Ste12-like transcription factor Vph1 suggested an essential role of the protein in hyphopodia formation and penetration of the root cortex (Sarmiento-Villamil *et al.*, 2018). Only indirect evidence was given that Vph1 is a target of the Vmk1 MAPK pathway in *V. dahliae* (Sarmiento-Villamil *et al.*, 2018).

This study shows that the Fus3/Kss1-like MAPK pathway components Vmk1 and Mek2 contribute to, but are not essential for fungal propagation inside the plant tissue. Δ*MEK2*, Δ*VMK1*, Δ*HAM5*Δ*MEK2,* or Δ*HAM5*Δ*VMK1* strains were successfully re-isolated from stem sections of infected plants, although to a minor extend compared to wild type or Δ*HAM5* and, therefore, must be able to survive within the plant (Figure 14B, C). Unlike Vmk1 and Mek2 in this study, mutants deficient in Vph1 could not be re-isolated from asymptomatic plants (Sarmiento-Villamil *et al.*, 2018). This might be due to different experimental settings in the respective plant infection experiments, since Vph1 deletion strain-treated plants were not wounded prior to spore inoculation different to Vmk1 and Mek2-treated plants in this study.

In several phytopathogenic fungi, the Fus3/Kss1-like MAPK deletion strains were apathogenic and the MAPK was not only essential for penetration of plant surfaces, but also essential for invasive growth and propagation within wounded plants (Xu & Hamer, 1996; Takano *et al.*, 2000; Zheng *et al.*, 2000; Ruiz-Roldán *et al.*, 2001; Mey *et al.*, 2002). In others, the absence of the MAPK resulted in severely reduced virulence, invasive growth, and propagation, but not in the complete disability of fungal propagation within the host plant as in *V. dahliae* Vmk1- and Mek2-deficient strains in this study (Lev *et al.*, 1999; Di Pietro *et al.*, 2001; Cho *et al.*, 2007). As an example, the *A. brassicicola* Fus3/Kss1-like MAPK Amk1 is essential for penetration of plant surfaces and the *amk1* mutant was avirulent on intact host tissue, whereas it was able to colonize and partially induce disease symptoms on damaged host surfaces (Cho *et al.*, 2007). The supplementation of damaged plant leaf material was sufficient to induce disease symptoms even on intact leaf surfaces, leading to the assumption that biochemical signals from damaged tissue were required to induce infection-related development in the *amk1* mutant (Cho *et al.*, 2007). The inability to penetrate intact host surfaces was correlated with decreased hydrolytic enzyme gene expression levels in absence of Amk1, which was increased on wounded tissue (Cho *et al.*, 2007). A role of the Fus3/Kss1-like MAPK in regulation of cell wall degrading enzymes was observed as well in other phytopathogens as, for example, in *F. oxysporum, Fusarium graminearum,* and *Cochliobolus heterostrophus* (Di Pietro *et al.*, 2001; Lev & Horwitz, 2003; Jenczmionka & Schäfer, 2005; Jiang *et al.*, 2018a)*.* In *C. heterostrophus*, cellulase genes were regulated by the MAPK pathway (Lev & Horwitz, 2003). The *F. oxysporum* MAPK displayed an impact on gene expression of pectate lyases (Di Pietro *et al.*, 2001), whereas the MAPK was dispensable for the production of pectinolytic or amylolytic enzymes in *F. graminearum* and was responsible for lipolytic activities instead (Jenczmionka & Schäfer, 2005).

In this study, the regulation of pectinolytic enzymes was not noticeably altered in absence of Vmk1 and Mek2 and seems to be mainly independent of the respective MAPK pathway in *V. dahliae.* The colony size of Mek2- and Vmk1-deficient strains was unaffected on simulated xylem medium containing pectin as carbon source (Figure 13A). The Vmk1- and Mek2-mediated MAPK pathway probably does not play a major role in the regulation of cellulase genes in *V. dahliae*, since colonies formed on minimal medium with either sucrose or cellulose as carbon source display only slight decreases in vegetative growth in comparison to wild type and the relative difference is the same on both tested media (Figure 13).

In conclusion, it was shown that the *V. dahliae* Fus3/Kss1-like MAPK components Mek2 and Vmk1 contribute to, but are not essential for survival of the fungus within wounded host plants, whereas both proteins are crucial for induction of disease symptoms. It can be assumed that the MAPK pathway has additional functions in virulence, besides substrate degradation, early infection-related morphogenesis, and fungal propagation in the host plant in *V. dahliae*.

4.3 The unfolded protein response regulator Hac1 mediates differentiation and virulence in *V. dahliae*

4.3.1 Unconventional splicing and translation of the bZIP transcription factor Hac1 is conserved in *V. dahliae*

During the different stages of the fungal perception and colonization of a host, signaling cascades coordinate the expression and secretion of tools enabling the interaction. This requires unfolded protein response-mediated adaptation of the protein processing and secretion capacity to changing demands in the ER (Richie *et al.*, 2011; Heimel *et al.*, 2013). In yeast, the ER transmembrane sensor Ire1 processes cytosolic unconventional splicing of the bZIP transcription factor Hac1 encoding mRNA (Shamu & Walter, 1996; Welihinda & Kaufman, 1996; Sidrauski & Walter, 1997; Gonzalez *et al.*, 1999; Okamura *et al.*, 2000; Figure 4). After splicing, the mRNA is translated into a protein that migrates to the nucleus and regulates transcription of UPR target genes (Mori *et al.*, 1996, 1998). The impacts of the homologous transcription factor Hac1 on growth, differentiation, ER stress response, and virulence in *V. dahliae* were characterized in this study.

The Ire1-dependent splicing of the *HAC1* mRNA is conserved in *V. dahliae*, since the *HAC1* mRNA contains an unconventional intron with a high sequence and structural similarity to Ire1 spliced introns in other organisms (Figure 16A; Yoshida *et al.*, 2001; Saloheimo *et al.*, 2003; Mulder *et al.*, 2004; Wimalasena *et al.*, 2008; Richie *et al.*, 2009; Cheon *et al.*, 2011; Hooks & Griffiths-Jones, 2011; Joubert *et al.*, 2011; Heimel *et al.*,

2013; Montenegro-Montero *et al.*, 2015). The intron matches the consensus sequence of the Ire1 targeted splice sequence in *HAC1* homologs (Hooks & Griffiths-Jones, 2011) and formation of the characteristic twin stem-loop structure, required for recognition of the cleavage sites by Ire1, was proposed (Sidrauski & Walter, 1997; Figure 16B, C). The unconventionally spliced mRNA variant of *HAC1* could be amplified from ER stress inducing growth conditions but as well from growth conditions without additional supplementation of ER stressors, suggesting that the *HAC1* mRNA is unconventionally spliced to a certain extend also in absence of those ER stressors.

The Hac1 protein was shown to be translated in the *HAC1^i-HA* strain in immunoblots (Figure 18), which show a shift of the distinct band. A similar band shift has been observed in immunoblot analysis of the homologous Cib1^s protein in *U. maydis*, which was proven to be the correct protein by mass spectrometry (personal communication apl. Prof. Kai Heimel). A possible explanation for the band shift is the formation of SDS stable secondary structures, leading to a slower migration through the gel.

In this study, a role of an uninduced protein variant Hac1^u was not found in *V. dahliae*, similar to other ascomycetes. Translation of the uninduced *HAC1* mRNA into a Hac1^u protein could not be detected in immunoblots, even though the gene was expressed (Figure 17). This could be due to a translational block or a strong instability of the Hac1^u protein. The *HAC1^i-HA* strain, expressing the unconventionally spliced mRNA variant of *HAC1* in absence of the unspliced *HAC1* mRNA variant, was viable and complemented the observed deletion phenotypes regarding microsclerotia formation and induction of disease symptoms *in planta*. This suggests that the presence of *HAC1^u* has no significant role for these functions in *V. dahliae*. Theoretically, both mRNAs, *HAC1^u* and *HAC1^i*, could be translated into proteins with an identical N-terminus but unique C-termini due to the frame shift of the ORF after unconventional splicing (Figure 16A). The bZIP domain and the NLS are located in the identical N-terminus. Therefore, both hypothetical proteins contain the bZIP transcription factor domain important for the formation of dimers, which can be either homo- or heterodimers, and both could be translocated into the nucleus. In higher eukaryotes the *HAC1* homolog *XBP1* is translated into both, the uninduced and the induced protein variants (Yoshida *et al.*, 2006, 2009). Here, the bZIP domain mediates homo- as well as heterodimerization, resulting either in XBP1^u-XBP1^u, XBP1^u-XBP1, or XBP1-XBP1 dimers (Tirosh *et al.*, 2006; Yoshida *et al.*, 2006). Homodimers of the XBP1 protein act as positive UPR regulators by binding to UPR target genes in the nucleus (Yamamoto *et al.*, 2007). Since XBP1^u contains a nuclear export signal, homodimers of this protein reside in the cytosol and heterodimerization prevents nuclear localization of the induced protein variant and thereby acts as negative regulator of the UPR (Tirosh *et al.*, 2006; Yoshida *et al.*, 2006). In the basidiomycete

U. maydis, regulatory roles of the unspliced mRNA of the *HAC1* homolog *cib1*[u] and the protein Cib1[u] were proposed (Heimel *et al.*, 2013). Overexpression of the induced mRNA variant *cib1*[s] results in hyperactivation of the UPR and lethality as long as the unspliced mRNA is not present in the cell. Expression of *cib1*[u] is required for attenuation of the transcriptional UPR regulator in *U. maydis* (Heimel *et al.*, 2013).

The length of the unconventional intron plays an important role in posttranscriptional regulation of the *HAC1* mRNA. The similarity of the short 20 nt unconventional intron in *V. dahliae* to related filamentous ascomycetes (Figure 16B) supports the assumption that the translation of the *HAC1*[u] mRNA might be either blocked or the protein is very unstable due to similar mechanisms. In contrast to *S. cerevisiae*, base-pairing interaction between the unconventional introns and the 5´UTR for inhibition of ribosomal translation cannot be observed in the *HAC1* mRNA of filamentous ascomycetes due to the shortened length (Mulder & Nikolaev, 2009). Truncation of the 5´UTR length was described to result in translation of the *HAC1* mRNA upon ER stress in different Aspergilli, *T. reesei,* and *A. brassisicola* (Saloheimo *et al.*, 2003; Mulder *et al.*, 2004; Joubert *et al.*, 2011). Initially, an impact of upstream open reading frames (uORFs) on translational repression was assumed (Saloheimo *et al.*, 2003; Mulder *et al.*, 2004). Studies in *A. niger* revealed base-pairing of the 5´UTR of the *HAC1* mRNA with an inverted repeat sequence as attenuation mechanism (Mulder & Nikolaev, 2009; Heimel, 2015). Additionally to the translational block of the unspliced *HAC1* mRNA, accelerated degradation of Hac1[u] proteins was observed in yeast (Di Santo *et al.*, 2016). These findings in related fungi might explain the absence of Hac1[u] in *V. dahliae.*

4.3.2 The unfolded protein response regulator Hac1 mediates species-specific differentiation in *V. dahliae*

In this study, it was shown that *V. dahliae HAC1* affects growth and fungal differentiation even in the absence of typical UPR stress inducing agents (Figure 19-21). *V. dahliae HAC1* is essential for the formation of microsclerotia as resting structures and has a positive impact on conidiation. The role of *HAC1* in fungal growth and differentiation in *V. dahliae* is partially conserved to other filamentous fungi, but specific impacts of *HAC1* could be observed as well.

The protein sequence conservation of Hac1 between homologs from *V. dahliae*, yeast, the dimorphic basidiomycete *U. maydis*, ascomycetes, and human is rather low with the highest similarity of 55% between *V. dahliae* and *T. reesei* (Figure 17). The low sequence conservation of Hac1 in the highly conserved pathway might be a result of its function in the crosstalk to developmental programs (Heimel *et al.*, 2013). In several studies, it could be shown that the impact of the Hac1 homologs on fungal growth and

differentiation is highly adapted, since even closely related species show different phenotypes in absence of the UPR regulatory transcription factor (Heimel *et al.*, 2013; Montenegro-Montero *et al.*, 2015).

V. dahliae HAC1 is involved in the response to ER stress. The *HAC1* deletion strain was generally impaired in vegetative growth and did not show a pronounced additional impairment in response to tunicamycin. However, the expression of the induced splice variant of *HAC1* improved the ability to cope with the ER stress situation in *V. dahliae*, although the expression levels of the induced splice variant in *HAC1^i-HA* were more than a third lower than in the wild type (Figure 18-20). Under non-stress conditions, *HAC1^i-HA* displayed reduced growth in comparison to wild type, which might be explained by differential regulation of genes supporting vegetative growth in correlation to a hyperactive UPR. Similar as in *V. dahliae*, genomic integration of the spliced *HAC1* mRNA variant resulted in decreased growth in *Aspergillus niger* correlated with a downregulation of mechanisms for energy generation and cell development, whereas the genes for the protein secretion machinery were upregulated (Carvalho *et al.*, 2012).

In *U. maydis* and *C. neoformans* the UPR has no impact on vegetative growth in absence of ER stress as in yeast (Nikawa *et al.*, 1996; Kaufman, 1999; Cheon *et al.*, 2011; Heimel *et al.*, 2013). In contrast, similar to the observed conidiation defects in *V. dahliae,* the absence of *HAC1* resulted in severe reduction in conidiation in *M. oryzae* (Tang *et al.*, 2015), *A. niger* (Mulder & Nikolaev, 2009), and *A. brassicicola* (Joubert *et al.*, 2011).

Besides the similar impact on conidiation, an important role of Hac1 in vegetative growth in absence of ER stress could be shown for the same fungi as in *V. dahliae* (Mulder & Nikolaev, 2009; Joubert *et al.*, 2011; Tang *et al.*, 2015). The impact of the UPR regulator on fungal growth and conidiation in the absence of ER stress in these species suggests a constitutive activation of the UPR leading to the regulation of certain target genes involved in growth and developmental processes (Heimel, 2015). This is confirmed by the finding that the induced mRNA variant could be amplified from cultures grown under non-stress inducing conditions in *V. dahliae* as mentioned previously. In *A. fumigatus,* a basal UPR activity under non-stress conditions has been observed as well (Feng *et al.*, 2011). Comparison of the transcriptomes of a *HAC1* deletion strain and the wild type, either under non-stress or ER stress conditions, revealed very different gene expression profiles in *A. fumigatus*, corroborating the possibility to adjust the expression of UPR target genes to certain stress levels (Feng *et al.*, 2011).

Different to the ER stress-specific UPR activation or the constitutive activation of the UPR to a certain level, in a few examples, the UPR was activated under specific conditions. The Hac1 homolog is dispensable for unstressed vegetative growth, but

required for growth at higher temperatures and on complex substrates in *A. fumigatus* (Richie *et al.*, 2009). A similar observation was made in *N. crassa,* where the UPR regulator is required especially for growth on crystalline cellulose substrates (Montenegro-Montero *et al.*, 2015). Here, an interplay of the sterol regulatory element binding protein (SREBP) pathway, which regulates the secretion of lignocellulolytic enzymes in filamentous fungi, and the UPR was suggested (Montenegro-Montero *et al.*, 2015; Qin *et al.*, 2017). The secretion of cellulases is suppressed in absence of the UPR regulator in *N. crassa* (Montenegro-Montero *et al.*, 2015; Qin *et al.*, 2017). An impact of the UPR on cellulose degradation and a correlation to secretion of cellulases has been observed as well in *T. reesei* and *A. nidulans* (Collén *et al.*, 2005; Brown *et al.*, 2013; Wang *et al.*, 2014; Qin *et al.*, 2017). A direct role in coupling of the conserved UPR to organism-specific developmental programs was found for the *U. maydis* UPR transcription factor Cib1 (Heimel *et al.*, 2013). The Cib1 protein contains a C-terminal domain specifically required for its interaction with the developmental regulator Clampless 1 (Clp1) of the b mating type-dependent signaling pathway (Heimel *et al.*, 2010, 2013). The heterodimer formation stabilizes Clp1, is important to initiate fungal propagation after penetration, has a role in effector secretion, and is involved in regulation of virulence in the smut fungus (Heimel *et al.*, 2013; Hampel *et al.*, 2016). The b mating type-dependent signaling pathway initiates the morphological switch from yeast to filamentous growth and is specifically found in heterobasidiomycetes (Kothe, 1996). Hac1 proteins in ascomycetes might undergo completely different protein-protein interactions in frame of coupling the UPR to differentiation.

In this study, it could be shown that *HAC1* is essential for the formation of microsclerotia, the melanized resting structures of *V. dahliae* (Figure 19, 20). *HAC1* deletion strains were unable to form microsclerotia under any tested condition and the expression of the induced *HAC1* mRNA variant in *HAC1^i^-HA* resulted in increased microsclerotia formation, regardless of a decreased expression level in comparison to wild type. One suggestion to explain the essential role of *HAC1* in microsclerotia formation is that the UPR is a crucial checkpoint to induce resting structure formation following sensing of unfavorable conditions. Microsclerotia formation can be observed at temperatures below the growth optimum (~20 °C; Soesanto & Termorshuizen, 2001), under nutrient-limited conditions as on complex substrates or in dense cultures, as well as in the presence of several stressors including ER stress inducing agents. The mechanisms activating the formation of microsclerotia in *V. dahliae* are not yet understood, even if several candidates were shown to influence the production. Components of the cAMP signaling pathway, which is stimulated by perception of high-glucose conditions, have negative impacts on the formation of microsclerotia such as the catalytic subunit of the cAMP-

dependent protein kinase A (Tzima *et al.*, 2010, 2012). As previously described in this work, several MAPK signaling components show positive regulatory impacts on microsclerotia formation as for example Vmk1 and Mek2 (Figure 13; Rauyaree *et al.*, 2005; Tian *et al.*, 2014; Qi *et al.*, 2016; Wang *et al.*, 2016; Tian *et al.*, 2016; Zheng *et al.*, 2019). Other candidates are substantial for the melanization as for example Vayg1 (*Verticillium* homolog to *Aspergillus* yellowish green 1), which is required for dihydroxynaphthalene biosynthesis (Fan *et al.*, 2017). Even if all these candidates have impacts on microsclerotia formation or melanization, examples for essential roles comparable to *HAC1* are rare. One example with an essential role in microsclerotia formation is the transcription factor Som1 (sorting mitochondrial 1), which is additionally involved in growth, conidiation, adhesion, and virulence of *V. dahliae* (Bui *et al.*, 2019). Som1 was found to be required for regulation of adhesin encoding genes, such as the transcription activators of adhesion Vta2 and Vta3 which are regulators of flocculin genes involved in adhesion and microsclerotia formation (Tran *et al.*, 2014; Bui *et al.*, 2019). In *S. cerevisiae*, it could be shown that Hac1 is involved in the regulation of flocculin genes and interacts with the general control of amino acid biosynthesis (Herzog *et al.*, 2013) and that ER stressed cells display slightly increased flocculation (Scrimale *et al.*, 2009). Therefore, the absence of microsclerotia in Som1- and Hac1-deficient *V. dahliae* strains hints to a crosstalk of Som1 and the UPR in the regulation of microsclerotia formation.

In conclusion, the UPR regulator *HAC1* is active to a certain extend under non-stress conditions. It is involved in the regulation of growth and sporulation and might be a checkpoint to sense and transduce the necessity of resting structure formation in *V. dahliae* (Figure 32).

4.3.3 *V. dahliae* Hac1 is essential for fungal colonization of the host plant

In this study, it could be shown that the *V. dahliae* UPR regulator *HAC1* is involved in colonization of the root surface, but not required for the penetration and initial invasion of the root cortex (Figure 22). Further, *HAC1* is involved in successful propagation within the host plant (Figure 23). Less fungal growth on the root surface was observed for the *HAC1* deletion strain in comparison to wild type and the *VTA2* deletion strain in root colonization experiments. This can be either caused by impaired growth or by an inability to adhere to the surface. Similar to Hac1, the transcription factor Som1 was found to be required for proliferation on the root surface correlated to its impact on adhesin gene expression (Bui *et al.*, 2019). Therefore, not only the similar impact on microsclerotia formation, but also the potential role of *HAC1* in adhesion could hint into direction of an interplay of the UPR and Som1. However, the impact of *HAC1* on adhesion requires further investigation. Different to *HAC1*, *SOM1* is essential for penetration of the root

surface (Bui *et al.*, 2019). However, target genes of Som1 were found to control different steps of plant root penetration and colonization including the transcription factors Vta2 and Vta3 (Bui *et al.*, 2019).

Similar to *V. dahliae*, the initial penetration of the plant surface was unaffected in the appressorium-forming fungus *A. brassicicola* in absence of the UPR regulator AbHacA (Joubert *et al.*, 2011). In the dimorphic fungus *U. maydis* the Hac1 orthologue is required to induce biotrophic growth within the plant after formation of appressoria and penetration of the plant surface (Heimel *et al.*, 2010; Heimel *et al.*, 2013). In contrast, UPR components are involved in the initial penetration of the plant surface by *M. oryzae* (Yi *et al.*, 2009; Tang *et al.*, 2015; Jiang *et al.*, 2018b).

Since fungal re-isolation from stems was not possible for the *V. dahliae HAC1* deletion strain in this study, one can assume that the fungus is hardly able to propagate in the vascular system and primarily remains in the roots or lower parts of the plant or does not survive after initial colonization of the root cortex. The absence of *HAC1* resulted in severely reduced conidiation in simulated xylem medium (Figure 21), which might disable fungal spreading in the vascular system. Besides the decrease in conidiation, increased sensitivity to plant phytoalexins was observed in the *A. brassicicola* UPR regulator-deficient strain. An altered sensitivity to plant antimicrobial compounds remains to be elucidated in the *V. dahliae HAC1* deletion strain, but could comprise an explanation for the observed *in planta* phenotype. Tomato plants treated with the *HAC1* deletion strain displayed severely decreased disease symptoms, however, in ~30% of the plants rather mild symptoms could be observed (Figure 23A). The induction of these symptoms could be a result from damage caused by the fungus or from the energy costs of successful immune defense responses in the plants. The impairment in adapting to increased protein secretion demands upon host colonization might also be an explanation for the less pathogenic outcome of the interaction of the *HAC1* deletion strain with the host plant as previously suggested in studies with the plant and animal pathogens *A. fumigatus*, *A. brassicicola,* and *U. maydis* (Joubert *et al.*, 2011; Richie *et al.*, 2011; Heimel *et al.*, 2013).

It is possible that the plant is able to activate defense responses and suppress fungal colonization of the *HAC1* deletion strain due to a lack of fungal effector gene expression and secretion, which are required to modulate the plants immune system. Examples for regulation of fungal effector genes by the corresponding UPR transcription factor in the maize colonizer *U. maydis* are given (Hampel *et al.*, 2016). Further, it is possible that *V. dahliae* Hac1 regulates virulence factors independent of ER stress induction, similar to the signal peptide peptidase Ssp1 in *U. maydis* (Pinter *et al.*, 2019). Here, deletion of the

Cib1-regulated gene *ssp1* resulted in an avirulent *in planta* phenotype without impacts of *ssp1* on vegetative growth or ER stress response (Pinter *et al.*, 2019).
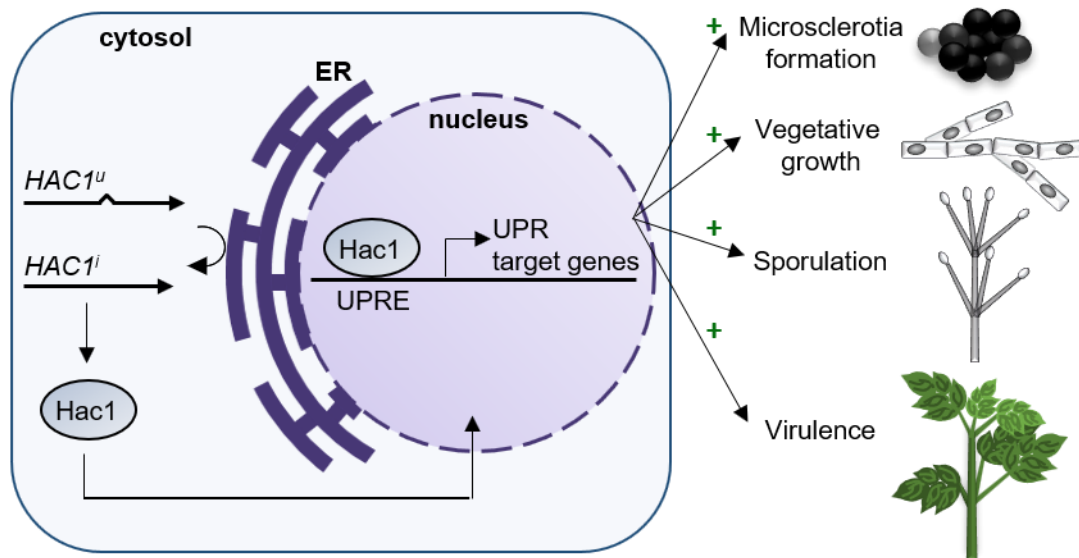
Figure 32: *V. dahliae HAC1* regulates differentiation and virulence. The *HAC1* mRNA occurs in two splice variants in the cell. The *HAC1u* mRNA contains an unconventionally spliced intron, which is presumably targeted by the ER transmembrane endoribonuclease Ire1 (indicated by an arrow located at the ER membrane). Splicing of the unconventional intron results in the mRNA splice variant *HAC1i,* which is translated into the protein Hac1. The transcription factor Hac1 presumably regulates transcription of UPR target genes by binding to UPR elements (UPRE) in their promoters and is essential for the development of microsclerotia as resting structures. Hac1 regulates vegetative growth under non-stress and ER stress conditions. Furthermore, *HAC1* or Hac1-regulated genes are important for sporulation, fungal propagation within host plants, and induction of disease symptoms.

In this study, the impact of the constitutive presence of unconventionally spliced *HAC1i* mRNA on growth, differentiation, and virulence of *V. dahliae* was tested by construction of *HAC1i-HA*. Ectopic integration into the *HAC1* deletion strain resulted in decreased gene expression in comparison to wild type similar to the strain containing an ectopic integration of the *HAC1u* mRNA, *HAC1u-HA* (Figure 18). The decreased expression levels were sufficient to complement the microsclerotia and growth phenotype of the *HAC1* deletion strain in *HAC1u-HA. F*or *HAC1i-HA* even increased microsclerotia formation could be observed. The decreased growth in *HAC1i-HA* is assumed to be caused by a differential gene expression of metabolic genes in response to the perception of ER stress similar to *A. niger* (Carvalho *et al.*, 2012) and not due to an incomplete complementation. However, tomato plants treated with *HAC1u-HA* or *HAC1i-HA* strains displayed a similar induction of disease symptoms with intermediate severity between wild type and *HAC1* deletion strain infected plants, suggesting an impact of the decreased expression levels of *HAC1* on fungal virulence. Since the differences in *HAC1* gene expression to wild type are similar in both strains and both

strains induce similar severities of disease symptoms, an impact of the constitutive presence of unconventionally spliced *HAC1* mRNA on virulence cannot be assumed.

In conclusion, the UPR regulator Hac1 plays a major impact on the fungal ability to colonize host plants, either due to decreased growth and fungal propagation on the root surface as well as decreased conidiation and spreading within the plant, but likely as well due to the inability to evade the plant immune response, since it is not required for penetration, but for propagation inside the host (Figure 32).

4.4 The *V. dahliae* oleate Δ12-fatty acid desaturase Ode1 has important roles in fungal growth and is dispensable for induction of disease symptoms

4.4.1 The *V. dahliae* oleate Δ12-fatty acid desaturase Ode1 contributes to fungal growth and differentiation

Different signaling molecules contribute to the crosstalk between fungi and their host plants and decide about the outcome of the interaction. Besides the secretion of effector proteins, which can be regulated by the UPR (Hampel *et al.*, 2016; Pinter *et al.*, 2019), lipid metabolites can act as signaling molecules (Christensen & Kolomiets, 2011). Since linoleic acid and the derived oxylipins were described to be able to modulate fungal differentiation and the development of disease symptoms (Calvo *et al.*, 2001; Brodhagen *et al.*, 2008; Brodhun *et al.*, 2009; Reverberi *et al.*, 2010; Scala *et al.*, 2014; Fischer & Keller, 2016; Patkar & Naqvi, 2017), the impact of the oleate Δ12-fatty acid desaturase Ode1 on differentiation and virulence of *V. dahliae* was analyzed.

Due to the protein domain structure, the similarity to the corresponding desaturase in *A. nidulans*, and the positive impact of medium supplementation with linoleic acid on growth of the *ODE1* deletion strain (Figure 24, 26), *V. dahliae* Ode1 can be assumed to catalyze the conversion of oleic acid to linoleic acid. In *A. nidulans* and *A. parasiticus*, a depletion of linoleic acid and the derived products as well as an increase in oleic acid following disruption of the homologous *ODE1* gene were observed (Calvo *et al.*, 2001; Chang *et al.*, 2004).

The construction of strains with Ode1 either N- or C-terminally fused to GFP has shown, that the N-terminus of the protein is important for its function. C-terminally GFP tagged Ode1 is more stable than N-terminally GFP tagged Ode1 since diffuse GFP signals in vacuoles were observed for *GFP-ODE1*, which were absent in *ODE1-GFP* (Figure 25C). The vacuolar localization of diffuse GFP suggest an accelerated degradation of the membrane protein by autophagosomes in the vacuoles (Liu *et al.*, 2012). The presence of an additional larger protein version of Ode1, specifically present for *ODE1-GFP* in

immunoblots (Figure 25A), supports possible posttranslational modification of Ode1 as part of the mechanism controlling Ode1 activity.

V. dahliae Ode1 localizes to membranes of cell organelles, presumably ER membranes, and in irregular patterns in the plasma membranes, often close to growing hyphal tips or branch points (Figure 25B, C). The protein sequence predicted that Ode1 is a transmembrane protein, which is a typical feature of desaturases (Uttaro, 2006). A signal peptide sequence predicting ER localization was not identified, however Δ12-desaturases in plants, animals, and lower eukaryotes are generally described to be located either in plastids or in ER membranes (Uttaro, 2006). Even if few fungal Δ12-desaturases have been described, their localization has not yet been shown (Passorn *et al.*, 1999; Sakuradani *et al.*, 1999; Calvo *et al.*, 2001; Watanabe *et al.*, 2004; Chang *et al.*, 2004; Wilson *et al.*, 2004; Wei *et al.*, 2006). The detection of Ode1 at sites of hyphal growth and branch points suggests a directed vesicle transport. The product of the fatty acid desaturase is linoleic acid, which is an important component of fungal plasma membranes with roles in adjusting membrane rigidity (Gostinčar *et al.*, 2009). The presence of the desaturase close to hyphal tips could facilitate growth by serving one of the products required for extension of hyphae. During growth, liquid uptake supports the increase of the cell volume and exocytosis expands the plasma membrane and cell wall (Money, 2016). In related fungi such as Aspergilli and *N. crassa*, growth at hyphal tips or branch points was dependent on a structure close to these locations, named the Spitzenkörper as vesicle supply center, consisting of cytoskeletal elements and vesicles which are distributed to extend the hyphal tips by exocytosis (Harris *et al.*, 2005). In *N. crassa*, chitin and glucan synthases localize to the Spitzenkörper to build up the cell wall (Su *et al.*, 2012). Besides, linoleic acid might not only provide a building block for the membrane. On the other hand, it could increase the membrane fluidity and facilitate exocytosis. In yeast, it has been suggested that increased ergosterol contents in the membrane promote vesicle fusion (Munn *et al.*, 1999).

Even if *V. dahliae* contains more than one gene encoding potential oleate Δ12-fatty acid desaturases in its genome, this study could show that Ode1 provides an important contribution to fungal growth and differentiation (Figure 33). This observations suggests that not all encoded Δ12-fatty acid desaturases might have additive or only partially-redundant functions. Reciprocal BLAST search has unraveled the presence of a second potential homolog to *A. nidulans odeA* with only slightly lower conservation of the deduced amino acid sequence than Ode1, almost the same size (479 aa), and similar domain structure (*VDAG_JR2_Chr2g10170a;* FAD domains: 75-114 aa IPR021863, 142-427 aa IPR005804; four transmembrane helices, Phobius).

Besides, another gene is predicted to encode an OdeA non-homologous Δ12-fatty acid desaturase with 402 aa in length and different domain structure, which was clearly predicted to be localized to the ER membrane using DeepLoc-1.0 and with its N-terminus directed to the ER lumen (*VDAG_JR2_Chr4g12440a;* FAD domain: 85-367 aa IPR005804; N-terminus located in ER 1-53 aa, Phobius; four transmembrane helices, Phobius). Deletion of *ODE1* as a single of these desaturases resulted in a decrease in the colony diameter about 50% in comparison to wild type. This was qualitatively similar on every tested medium including media supplemented with osmotic or cell wall stressors. The only more favorable condition was caused by substitution of linoleic acid (Figure 26).
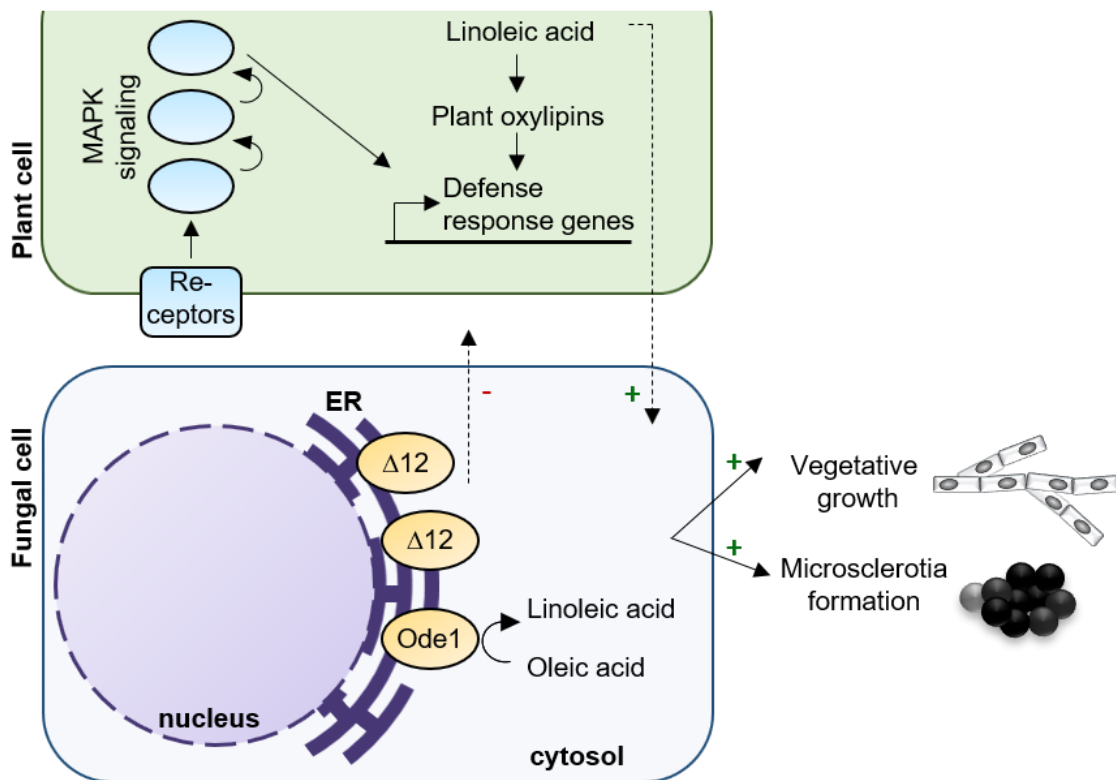
Figure 33: *V. dahliae* Ode1 displays a strong impact on vegetative growth, but is dispensable for induction of disease symptoms. The oleate Δ12-fatty acid desaturase Ode1 catalyzes the conversion of oleic acid into linoleic acid. The *ODE1* defective strain displays impaired vegetative growth and microsclerotia formation, which is partially restored on medium supplemented with linoleic acid. This corroborates a positive impact of Ode1 or Ode1-derived products on growth and microsclerotia formation (indicated by arrows with green plus). The *ODE1* deficiency displays only a minor impact on fungal virulence and the deletion strain is able to induce severe disease symptoms *in planta.* The availability of plant-derived linoleic acid might complement the observed growth defect (indicated by arrow with dashed line and green plus) and promote fungal propagation or enable the biosynthesis of linoleic acid-derived products with unknown impact on the plants defense responses. Additional oleate Δ12-fatty acid desaturases (Δ12) in *V. dahliae* could compensate the defect in *ODE1* and allow modulation of plant defense responses (indicated by arrows with dashed line with red minus).

Similarly, a general decrease in growth was observed for *A. nidulans* and *A. parasiticus* upon deletion of the homologous oleate Δ12-fatty acid desaturases (Calvo *et al.*, 2001; Chang *et al.*, 2004; Wilson *et al.*, 2004). BLAST and domain searches of *A. nidulans* OdeA revealed that the genome of this organism harbors an additional gene encoding a non-homologous protein with predicted Δ12-fatty acid desaturase domain and cytosolic N-terminus (XP_664808.1) similar to the Ode1 non-homologous oleate Δ12-fatty acid desaturase predicted in *V. dahliae*, suggesting that also here other proteins with potentially overlapping functions exist.

With regard to the unaltered phenotype of the *V. dahliae ODE1* deletion strain on stress media, one can conclude that Ode1 and its products are not especially required for the response to stresses even if one could expect that the adaptation of the membrane fluidity might influence stress responses. An increased membrane content of unsaturated fatty acids increased the sensitivity to salt stress in yeast for example (Gostinčar *et al.*, 2009). It is possible that different desaturases are upregulated in response to certain environmental conditions or at certain developmental stages. FAD2, a single of a multitude of desaturases in *A. thaliana,* is activated upon sensing of ER stress and increases the ER stress tolerance by its positive impact on membrane fluidity (Nguyen *et al.*, 2019).

Additionally to the impact on growth, *V. dahliae* Ode1 contributes to microsclerotia formation (Figure 27). Whereas here only a reduced resting structure formation was observed, deletion of the *ODE1* homolog in *A. parasiticus* resulted in a complete loss of sclerotia development (Chang *et al.*, 2004; Wilson *et al.*, 2004). Since the *ODE1* deletion strain displayed no specific stress-dependent phenotype one can assume that the decrease in microsclerotia formation can be seen as a result from the general growth defect and the altered polyunsaturated fatty acid metabolism.

4.4.2 Plant-derived unsaturated fatty acids might replace products synthesized by *V. dahliae* Ode1 during host colonization

V. dahliae Ode1 contributes to fungal growth even if the genome possesses additional genes, which are hypothetically encoding oleate Δ12-fatty acid desaturases. Ode1 is not required for induction of severe disease symptoms in tomato plants as deletion strain infected plants display only a minor decrease in severity of disease symptoms (Figure 28). Therefore, Ode1 is not required for initial colonization and penetration. Inside the plant, the *ODE1* deletion strain might be able to use plant-derived unsaturated fatty acids to compensate for the growth defect. It was shown that the *ODE1* deletion strain was able to use exogenous linoleic acid (Figure 26) and the plant provides linoleic acid which is used as a membrane component, precursor of plant oxylipins, and building blocks for

the cuticula for example (Soliday & Kolattukudy, 1977; Brodhun & Feussner, 2011). Plant linoleic acid and the derived oxylipins are recognized as mimics of the fungal signaling molecules and promote sporulation and mycotoxin production in Aspergilli (Burow *et al.*, 1997; Calvo *et al.*, 1999; Wilson *et al.*, 2004; Brodhagen *et al.*, 2008; Gao & Kolomiets, 2009; Horowitz Brown *et al.*, 2009; Reverberi *et al.*, 2010). In *A. nidulans* and *A. flavus*, perception of exogenous oxylipins via G-protein coupled receptors was confirmed for a few oxylipins (Affeldt *et al.*, 2012, 2014; Fischer & Keller, 2016).

Even if plants might provide substitutes for fungal linoleic acid or its derived compounds, it cannot be excluded that products from other oleate Δ12-fatty acid desaturases contribute to successful host colonization in *V. dahliae*. Endogenous linoleic acid production of the corresponding *A. parasiticus* oleate Δ12-fatty acid desaturase OdeA has positive effects on the colonization of live corn and peanut seeds, even if those provide linoleic acid contents (Wilson *et al.*, 2004). The absence of *odeA* did not alter fungal growth on dead seeds. Therefore, fungal linoleic acid or linoleic acid-derived products were assumed to be required for suppression of defense responses in the seed (Wilson *et al.*, 2004). The expression of plant LOX genes was modulated upon colonization by Aspergilli, resulting in altered jasmonic acid induced plant defense responses (Burow *et al.*, 2000; Tsitsigiannis & Keller, 2007; Horowitz Brown *et al.*, 2009; Gao *et al.*, 2009). Similar results with essential roles of oxylipins from both interaction partners have been found in *F. verticilloides*, where fungal oxylipins produced by LDS1 induce maize LOX3 for suppression of the plant JA-mediated defense responses and promote fungal virulence (Battilani *et al.*, 2018).

In conclusion, *V. dahliae* Ode1 is dispensable for induction of severe disease symptoms even if the respective deletion strain displays a severe growth defect *ex planta*. Therefore, linoleic acid or linoleic acid derived compounds are either dispensable for virulence or the fungus can compensate the loss of Ode1-derived products through the action of other endogenous enzymes or exogenous plant-derived polyunsaturated fatty acids (Figure 33).

References

Affeldt KJ, Brodhagen M & Keller NP (2012) *Aspergillus* oxylipin signaling and quorum sensing pathways depend on G protein-coupled receptors. *Toxins* (Basel). **4:** 695-717.

Affeldt KJ, Carrig J, Amare M & Keller NP (2014) Global survey of canonical *Aspergillus flavus* G protein-coupled receptors. *MBio* **5:** e01501-14.

Aldabbous MS, Roca MG, Stout A, Huang IC, Read ND & Free SJ (2010) The *ham-5, rcm-1* and *rco-1* genes regulate hyphal fusion in *Neurospora crassa. Microbiology* **156:** 2621-2629.

Ali GS & Reddy A (2008) PAMP-triggered immunity: Early events in the activation of Flagellin Sensitive2. *Plant Signal. Behav.* **3:** 423-426.

Almagro Armenteros JJ, Sønderby CK, Sønderby SK, Nielsen H & Winther O (2017) DeepLoc: prediction of protein subcellular localization using deep learning. *Bioinformatics* **33:** 3387-3395.

Andolfi A, Maddau L, Cimmino A, Linaldeddu BT, Basso S, Deidda A, Serra S & Evidente A (2014) Lasiojasmonates A-C, three jasmonic acid esters produced by *Lasiodiplodia* sp., a grapevine pathogen. *Phytochemistry* **103:** 145-153.

Andreou A & Feussner I (2009) Lipoxygenases - Structure and reaction mechanism. *Phytochemistry* **70:** 1504-1510.

Balnojan S (2016) Influence of the Fbx15 protein and adjacent elements on the development and virulence of *Verticillium dahliae. Master thesis at the University of Goettingen.*

Bardwell L, Cook JG, Voora D, Baggott DM, Martinez AR & Thorner J (1998) Repression of yeast Ste12 transcription factor by direct binding of unphosphorylated Kss1 MAPK and its regulation by the Ste7 MEK. *Genes Dev.* **12:** 2887-2898.

Battilani P, Lanubile A, Scala V, Reverberi M, Gregori R, Falavigna C, Dall'asta C, Park Y-S, Bennett J, Borrego EJ & Kolomiets MV (2018) Oxylipins from both pathogen and host antagonize jasmonic acid-mediated defence via the 9-lipoxygenase pathway in *Fusarium verticillioides* infection of maize. *Mol. Plant Pathol.* **19:** 2162-2176.

Bayram Ö, Sarikaya-Bayram Ö, Ahmed YL, Maruyama J, Valerius O, Rizzoli SO, Ficner R, Irniger S & Braus GH (2012) The *Aspergillus nidulans* MAPK module AnSte11-Ste50-Ste7-Fus3 controls development and secondary metabolism. *PLoS Genet.* **8:** e1002816.

Bergkessel M & Guthrie C (2013) Colony PCR. In Laboratory Methods in Enzymology., Lorsch J (ed), San Diego, USA: *Elsevier.* **1:** 299-309.

Berlanger I & Powelson ML (2000) Verticillium wilt. *Plant Heal. Instr. Am. Phytopathol. Soc.* doi:10.1094/PHI-I-2000-0801-01. Updated 2005.

Bertani G (1951) Studies on lysogenesis I. The mode of phage liberation by lysogenic *Escherichia coli. J. Bacteriol.* **62:** 293-300.

Bhat RG & Subbarao KV (1999) Host range specificity in *Verticillium dahliae. Genet. Resist.* **89:** 1218-1225.

Boyce KJ, Chang H, D'Souza CA & Kronstad JW (2005) An *Ustilago maydis* septin is required for filamentous growth in culture and for full symptom development on maize. *Eukaryot. Cell* **4:** 2044-2056.

Bradford MM (1976) A rapid and sensitive method for the quantitation of microgram quantities of protein utilizing the principle of protein-dye binding. *Anal. Biochem.* **72:** 248-254.

Brasier C (2000) The rise of the hybrid fungi. *Nature* **405:** 134-135.

Brodhagen M, Tsitsigiannis DI, Hornung E, Goebel C, Feussner I & Keller NP (2008) Reciprocal oxylipin-mediated cross-talk in the *Aspergillus*-seed pathosystem. *Mol. Microbiol.* **67:** 378-391.

Brodhun F & Feussner I (2011) Oxylipins in fungi. *FEBS J.* **278:** 1047-1063.

Brodhun F, Go C, Hornung E & Feussner I (2009) Identification of PpoA from *Aspergillus nidulans* as a fusion protein of a fatty acid heme dioxygenase/ peroxidase and a cytochrome P450. *J. Biol. Chem.* **284:** 11792-11805.

References

Brown N, de Gouvea P, Krohn N, Savoldi M & Goldman G (2013) Functional characterisation of the non-essential protein kinases and phosphatases regulating *Aspergillus nidulans* hydrolytic enzyme production. *Biotechnol. Biofuels* **6:** 91.

Brown NA, Urban M & Hammond-Kosack KE (2016) The trans-kingdom identification of negative regulators of pathogen hypervirulence. *FEMS Microbiol. Rev.* **40:** 19-40.

Bui (2017) *Verticillium dahliae* transcription factors Som1 and Vta3 control microsclerotia formation and sequential steps of plant root penetration and colonisation to induce disease. *Dissertation at the University of Goettingen.*

Bui T, Harting R, Braus-Stromeyer SA, Tran V, Leonard M, Höfer A, Abelmann A, Bakti F, Valerius O, Schlüter R, Stanley CE, Ambrósio A & Braus GH (2019) *Verticillium dahliae* transcription factors Som1 and Vta3 control microsclerotia formation and sequential steps of plant root penetration and colonisation to induce disease. *New Phytol.* **221:** 2138-2159.

Burow GB, Gardner HW & Keller NP (2000) A peanut seed lipoxygenase responsive to *Aspergillus* colonization. *Plant Mol. Biol.* **42:** 689-701.

Burow GB, Nesbitt TC, Dunlap J & Keller NP (1997) Seed lipoxygenase products modulate *Aspergillus* mycotoxin biosynthesis. *Mol. Plant-Microbe Interact.* **10:** 380-387.

Calvo AM, Gardner HW & Keller NP (2001) Genetic connection between fatty acid metabolism and sporulation in *Aspergillus nidulans. J Biol Chem.* **276:** 25766-25774.

Calvo AM, Hinze LL, Gardner HW & Keller NP (1999) Sporogenic effect of polyunsaturated fatty acids on development of *Aspergillus* spp. *Appl. Environ. Microbiol.* **65:** 3668-3673.

Caracuel Z, Roncero MIG, Espeso EA, González-Verdejo CI, García-Maceira FI & Di Pietro A (2003) The pH signalling transcription factor PacC controls virulence in the plant pathogen *Fusarium oxysporum. Mol. Microbiol.* **48:** 765-779.

Carroll CL, Carter CA, Goodhue RE, Lawell C-YCL & Subbarao KV (2018) A review of control options and externalities for Verticillium wilts. *Phytopathology* **108:** 160-171.

Carvalho ND, Jørgensen TR, Arentshorst M, Nitsche BM, van den Hondel CA, Archer DB & Ram AF (2012) Genome-wide expression analysis upon constitutive activation of the HacA bZIP transcription factor in *Aspergillus niger* reveals a coordinated cellular response to counteract ER stress. *BMC Genomics* **13:** 350.

Castoria R, Fanelli C, Zoina A & Scala F (1995) Analysis of fatty acids in lipids of *Verticillium dahliae* and induction of lubimin accumulation in eggplant. *Plant Pathol.* **44:** 791-795.

Champe SP & El-Zayat AA (1989) Isolation of a sexual sporulation hormone from *Aspergillus nidulans. J. Bacteriol.* **171:** 3982-3988.

Chang P, Wilson RA, Keller NP & Cleveland TE (2004) Deletion of the Δ12-oleic acid desaturase gene of a nonaflatoxigenic *Aspergillus parasiticus* field isolate affects conidiation and sclerotial development. *J. Appl. Microbiol.* **97:** 1178-1184.

Chapman RE & Walter P (1997) Translational attenuation mediated by an mRNA intron. *Curr. Biol.* **7:** 850-859.

Chen C, Harel A, Gorovoits R, Yarden O & Dickman MB (2004) MAPK regulation of sclerotial development in *Sclerotinia sclerotiorum* is linked with pH and cAMP sensing. *Mol. Plant-Microbe Interact*. **17:** 404-413.

Chen CK-M, Chan N-L & Wang AH-J (2011) The many blades of the β-propeller proteins: conserved but versatile. *Trends Biochem. Sci.* **36:** 553-561.

Chen JY, Liu C, Gui YJ, Si KW, Zhang DD, Wang J, Short DPG, Huang JQ, Li NY, Liang Y, Zhang WQ, Yang L, Ma XF, Li TG, Zhou L, Wang BL, Bao YM, Subbarao KV, Zhang GY & Dai XF (2018) Comparative genomics reveals cotton-specific virulence factors in flexible genomic regions in *Verticillium dahliae* and evidence of horizontal gene transfer from *Fusarium. New Phytol.* **217:** 756-770.

Cheon SA, Jung KW, Chen YL, Heitman J, Bahn YS & Kang HA (2011) Unique evolution of the UPR pathway with a novel bZIP transcription factor, Hxl1, for controlling pathogenicity of *Cryptococcus neoformans. PLoS Pathog.* **7:** e1002177.

Chini A, Cimmino A, Masi M, Reveglia P, Nocera P, Solano R & Evidente A (2018) The fungal phytotoxin lasiojasmonate A activates the plant jasmonic acid pathway. *J. Exp. Bot.* **69:** 3095-3102.

Cho Y, Cramer RA, Kim KH, Davis J, Mitchell TK, Figuli P, Pryor BM, Lemasters E & Lawrence CB (2007) The Fus3/Kss1 MAP kinase homolog Amk1 regulates the expression of genes encoding hydrolytic enzymes in *Alternaria brassicicola. Fungal Genet. Biol.* **44:** 543-553.

Cho Y, Srivastava A, Ohm RA, Lawrence CB & Wang K-H (2012) Transcription factor Amr1 induces melanin biosynthesis and suppresses virulence in *Alternaria brassicicola. PLoS Pathog* **8:** e1002974.

Choi KY, Satterberg B, Lyons DM & Elion EA (1994) Ste5 tethers multiple protein kinases in the MAP kinase cascade required for mating in *S. cerevisiae. Cell* **78:** 499-512.

Chou S, Lane S & Liu H (2006) Regulation of mating and filamentation genes by two distinct Ste12 complexes in *Saccharomyces cerevisiae. Mol Cell Biol.* **13:** 4794-4805.

Christensen MJ, Bennett RJ, Ansari HA, Koga H, Johnson RD, Bryan GT, Simpson WR, Koolaard JP, Nickless EM & Voisey CR (2008) *Epichloë* endophytes grow by intercalary hyphal extension in elongating grass leaves. *Fungal Genet. Biol.* **45:** 84-93.

Christensen SA & Kolomiets MV (2011) The lipid language of plant–fungal interactions. *Fungal Genet. Biol.* **48:** 4-14

Clewes E, Edwards SG & Barbara DJ (2008) Direct molecular evidence supports long-spored microsclerotial isolates of *Verticillium* from crucifers being interspecific hybrids. *Plant Pathol.* **57:** 1047-1057.

Coghlan A, Eichler EE, Oliver SG, Paterson AH & Stein L (2005) Chromosome evolution in eukaryotes: a multi-kingdom perspective. *Trends Genet.* **21:** 673-682.

Cole SJ, Yoon AJ, Faull KF & Diener AC (2014) Host perception of jasmonates promotes infection by *Fusarium oxysporum* formae speciales that produce isoleucine- and leucine-conjugated jasmonates. *Mol. Plant Pathol.* **15:** 589-600.

Coleman JJ, Rounsley SD, Rodriguez-Carres M, Kuo A, Wasmann CC, Grimwood J, Schmutz J, Taga M, White GJ, Zhou S, Schwartz DC, Freitag M, Ma L, Danchin EGJ, Henrissat B, Coutinho PM, Nelson DR, Straney D, Napoli CA, Barker BM, *et al.* (2009) The genome of *Nectria haematococca*: contribution of supernumerary chromosomes to gene expansion. *PLoS Genet.* **5:** e1000618.

Collado-Romero M, Jiménez-Díaz RM & Mercado-Blanco J (2010) DNA sequence analysis of conserved genes reveals hybridization events that increase genetic diversity in *Verticillium dahliae. Fungal Biol.* **114:** 209-218.

Collén A, Saloheimo M, Bailey M, Penttilä M & Pakula TM (2005) Protein production and induction of the unfolded protein response in *Trichoderma reesei* strain Rut-C30 and its transformant expressing endoglucanase I with a hydrophobic tag. *Biotechnol. Bioeng.* **89:** 335-344.

Collins A, Okoli CAN, Morton A, Parry D, Edwards SG & Barbara DJ (2003) Isolates of *Verticillium dahliae* pathogenic to crucifers are of at least three distinct molecular types. *Phytopathology* **93:** 364-376.

Conn PM (2011) The unfolded protein response and cellular stress. In *Methods in Enzymology.* Conn MP (ed). Los Angeles, CA, USA: *Elsevier* **489:** 384.

Covert SF, Kapoor P, Lee M, Briley A & Nairn CJ (2001) *Agrobacterium tumefaciens*-mediated transformation of *Fusarium circinatum. Mycol. Res.* **105:** 259-264.

Cox JS, Shamu CE & Walter P (1993) Transcriptional induction of genes encoding endoplasmic reticulum resident proteins requires a transmembrane protein kinase. *Cell* **73:** 1197-206.

Cullen PJ, Sprague Jr. GF (2012) The regulation of filamentous growth in yeast. *Genetics* **190:** 23-49.

Dagenais TRT, Chung D, Giles SS, Hull CM, Andes D & Keller NP (2008) Defects in conidiophore development and conidium-macrophage interactions in a dioxygenase mutant of *Aspergillus fumigatus. Infect. Immun.* **76:** 3214-3220.

References

Dall'Asta C, Falavigna C, Galaverna G & Battilani P (2012) Role of maize hybrids and their chemical composition in *Fusarium* infection and fumonisin production. *J. Agric. Food Chem.* **60:** 3800-3808.

Dall'Asta C, Giorni P, Cirlini M, Reverberi M, Gregori R, Ludovici M, Camera E, Fanelli C, Battilani P & Scala V (2015) Maize lipids play a pivotal role in the fumonisin accumulation. *World Mycotoxin J.* **8:** 87-97.

David H, Ozçelik IS, Hofmann G & Nielsen J (2008) Analysis of *Aspergillus nidulans* metabolism at the genome-scale. *BMC Genomics* **9:** 163.

Debuchy R & Turgeon BG (2006) Mating-type structure, evolution, and function in Euascomycetes. In *The Mycota (A comprehensive treatise on fungi as experimental systems for basic and applied research).* Kües U. FR (ed). Berlin, Heidelberg: *Springer* **1:** 293-323.

de Jonge R, Bolton MD, Kombrink A, Van Den Berg GCM, Yadeta KA & Thomma BPHJ (2013) Extensive chromosomal reshuffling drives evolution of virulence in an asexual pathogen. *Genome Res.* 23: 1271-1282.

de Jonge R, Peter van Esse H, Maruthachalam K, Bolton MD, Santhanam P, Saber MK, Zhang Z, Usami T, Lievens B, Subbarao KV & Thomma BPHJ (2012) Tomato immune receptor Ve1 recognizes effector of multiple fungal pathogens uncovered by genome and RNA sequencing. *Proc. Natl. Acad. Sci.* **109:** 5110-5115.

Depotter JRL, Deketelaere S, Inderbitzin P, von Tiedemann A, Höfte M, Subbarao KV, Wood TA & Thomma BPHJ (2016a) *Verticillium longisporum*, the invisible threat to oilseed rape and other brassicaceous plant hosts. *Mol. Plant Pathol.* **17:** 1004-1016.

Depotter JRL, Seidl MF, van den Berg GCM, Thomma BPHJ & Wood TA (2017) A distinct and genetically diverse lineage of the hybrid fungal pathogen *Verticillium longisporum* population causes stem striping in British oilseed rape. *Environ. Microbiol.* **19:** 3997-4009.

Depotter JRL, Seidl MF, Wood TA & Thomma BPHJ (2016b) Interspecific hybridization impacts host range and pathogenicity of filamentous microbes. *Curr. Opin. Microbiol.* **32:** 7-13.

Depotter JRL, Thomma BPHJ & Wood TA (2019) Measuring the impact of *Verticillium longisporum* on oilseed rape (*Brassica napus*) yield in field trials in the United Kingdom. *Eur. J. Plant Pathol.* **153:** 321-326.

Dettmann A, Heilig Y, Valerius O, Ludwig S & Seiler S (2014) Fungal communication requires the MAK-2 pathway elements STE-20 and RAS-2, the NRC-1 adapter STE-50 and the MAP kinase scaffold HAM-5. *PLoS Genet.* **10:** e1004762.

Di Santo R, Aboulhouda S & Weinberg DE (2016) The fail-safe mechanism of post-transcriptional silencing of unspliced *HAC1* mRNA. *Elife* **5:** e20069.

Di Stasio M, Brefort T, Mendoza-Mendoza A, Münch K & Kahmann R (2009) The dual specificity phosphatase Rok1 negatively regulates mating and pathogenicity in *Ustilago maydis. Mol. Microbiol.* **73:** 73-88.

Djonovic S, Vargas WA, Kolomiets MV, Horndeski M, Wiest A & Kenerley CM (2007) A proteinaceous elicitor Sm1 from the beneficial fungus *Trichoderma virens* is required for induced systemic resistance in maize. *Plant Physiol.* **145:** 875-889.

Dong S, Raffaele S & Kamoun S (2015) The two-speed genomes of filamentous pathogens: waltz with plants. *Curr. Opin. Genet. Dev.* **35:** 57-65.

Eaton CJ, Cox MP, Ambrose B, Becker M, Hesse U, Schardl CL & Scott B (2010) Disruption of signaling in a fungal-grass symbiosis leads to pathogenesis. *Plant Physiol.* **153:** 1780-1794.

Edgar RC (2004) MUSCLE: multiple sequence alignment with high accuracy and high throughput. *Nucleic Acids Res.* **32:** 1792-1797.

Ellenberger T, Fass D, Arnaud M & Harrison SC (1994) Crystal structure of transcription factor E47: E-box recognition by a basic region helix-loop-helix dimer. *Genes Dev.* **8:** 970-980.

Enebak SA, Haase DL, Pinto JR & Riley LE (2012) Soil fumigation: the critical use exemption, quarantine pre-shipment rules, re-registration decision, and their effect on the 2012 growing season. *Natl. Proc. For. Conserv. Nurs. Assoc.* **68:** 26-30.

References

Evans JL, Moclock MA & Gealt MA (1986) The fatty acid composition of the conidia and mycelia of the fungus *Aspergillus nidulans. Can. J. Microbiol.* **32:** 179-181.

Eynck C, Koopmann B, Grunewaldt-Stoecker G, Karlovsky P & von Tiedemann A (2007) Differential interactions of *Verticillium longisporum* and *V. dahliae* with *Brassica napus* detected with molecular and histological techniques. *Eur. J. Plant Pathol.* **118:** 259-274.

Eynck C, Koopmann B & von Tiedemann A (2009) Identification of *Brassica* accessions with enhanced resistance to *Verticillium longisporum* under controlled and field conditions. *J. Plant Dis. Prot.* **116:** 63-72.

Faino L, Seidl MF, Shi-Kunne X, Pauper M, Van Den Berg GCM, Wittenberg AHJ & Thomma BPHJ (2016) Transposons passively and actively contribute to evolution of the two-speed genome of a fungal pathogen. *Genome Res.* **26:** 1091-1100.

Fan R, Klosterman SJ, Wang C, Subbarao K V, Xu X, Shang W & Hu X (2017) Vayg1 is required for microsclerotium formation and melanin production in *Verticillium dahliae. Fungal Genet. Biol.* **98:** 1-11.

Feng X, Krishnan K, Richie DL, Aimanianda V, Hartl L, Grahl N, Powers-Fletcher M V., Zhang M, Fuller KK, Nierman WC, Lu LJ, Latgé J-P, Woollett L, Newman SL, Cramer RA, Rhodes JC & Askew DS (2011) HacA-independent functions of the ER stress sensor IreA synergize with the canonical UPR to influence virulence traits in *Aspergillus fumigatus. PLoS Pathog.* **7:** e1002330.

Feys B (1994) Arabidopsis mutants selected for resistance to the phytotoxin coronatine are male sterile, insensitive to methyl jasmonate, and resistant to a bacterial pathogen. *Plant Cell online* **6:** 751-759.

Fischer GJ & Keller NP (2016) Production of cross-kingdom oxylipins by pathogenic fungi: An update on their role in development and pathogenicity. *J. Microbiol.* **54:** 254-264.

Fitzell R, Evans G & Fahy P (1980) Studies on the colonization of plant roots by *Verticillium dahliae* Klebahn with use of immunofluorescent staining. *Aust. J. Bot.* **28:** 357-368.

Fleissner A, Leeder AC, Roca MG, Read ND & Glass NL (2009) Oscillatory recruitment of signaling proteins to cell tips promotes coordinated behavior during cell fusion. *Proc. Natl. Acad. Sci. U. S. A.* **106:** 19387-19392.

Floerl S, Druebert C, Majcherczyk A, Karlovsky P, Kües U & Polle A (2008) Defence reactions in the apoplastic proteome of oilseed rape (*Brassica napus* var. *napus*) attenuate *Verticillium longisporum* growth but not disease symptoms. *BMC Plant Biol.* **8:** 129.

Fogelqvist J, Tzelepis G, Bejai S, Ilbäck J, Schwelm A & Dixelius C (2018) Analysis of the hybrid genomes of two field isolates of the soil-borne fungal species *Verticillium longisporum. BMC Genomics* **19:** 14.

Fradin EF & Thomma BPHJ (2006) Physiology and molecular aspects of Verticillium wilt diseases caused by *V. dahliae* and *V. albo-atrum. Mol. Plant Pathol.* **7:** 71-86.

Fradin EF, Zhang Z, Juarez Ayala JC, Castroverde CD, Nazar RN, Robb J, Liu CM & Thomma BPHJ (2009) Genetic dissection of Verticillium wilt resistance mediated by tomato Ve1. *Plant Physiol.* **150:** 320-332.

Frawley D, Karahoda B, Sarikaya-Bayram Ö & Bayram Ö (2018) The HamE scaffold positively regulates MpkB phosphorylation to promote development and secondary metabolism in *Aspergillus nidulans. Sci. Rep.* **8:** 16588.

Fu C, Iyer P, Herkal A, Abdullah J, Stout A & Free SJ (2011) Identification and characterization of genes required for cell-to-cell fusion in *Neurospora crassa. Eukaryot. Cell* **10:** 1100-1109.

Gao X, Brodhagen M, Isakeit T, Brown SH, Göbel C, Betran J, Feussner I, Keller NP & Kolomiets MV (2009) Inactivation of the lipoxygenase *ZmLOX3* increases susceptibility of maize to *Aspergillus* spp. *Mol. Plant-Microbe Interact.* **22:** 222-231.

Gao X & Kolomiets MV (2009) Host-derived lipids and oxylipins are crucial signals in modulating mycotoxin production by fungi. *Toxin Rev.* **28:** 79-88.

Gao X, Shim W-B, Göbel C, Kunze S, Feussner I, Meeley R, Balint-Kurti P & Kolomiets MV (2007) Disruption of a maize 9-Lipoxygenase results in increased resistance to fungal

pathogens and reduced levels of contamination with mycotoxin fumonisin. *Mol. Plant-Microbe Interact.* **20:** 922-933.

Geer LY, Marchler-Bauer A, Geer RC, Han L, He J, He S, Liu C, Shi W & Bryant SH (2010) The NCBI BioSystems database. *Nucleic Acids Res.* **38:** S492-S496.

Gibriel HAY, Li J, Zhu L, Seidl MF & Thomma BPHJ (2019) *Verticillium dahliae* strains that infect the same host plant display highly divergent effector catalogs. *bioRxiv* (ahead of print) doi:10.1101/528729.

Gonzalez TN, Sidrauski C, Dörfler S & Walter P (1999) Mechanism of non-spliceosomal mRNA splicing in the unfolded protein response pathway. *EMBO J.* **18:** 3119-3132.

Good M, Tang G, Singleton J, Reményi A & Lim WA (2009) The Ste5 scaffold directs mating signaling by catalytically unlocking the Fus3 MAP kinase for activation. *Cell* **136:** 1085-1097.

Goodrich-Tanrikulu M, Howe K, Stafford A & Nelson MA (1998) Changes in fatty acid composition of *Neurospora crassa* accompany sexual development and ascospore germination. *Microbiology* **144:** 1713-1720.

Gostinčar C, Turk M & Gunde-Cimerman N (2009) Environmental impacts on fatty acid composition of fungal membranes. In *Fungi from different environments*, Misra JK & Deshmukh SK (eds). Enfield, NH, USA: *Science Publishers* **1:** 278-325.

Goto E, Ishido S, Sato Y, Ohgimoto S, Ohgimoto K, Nagano-Fujii M & Hotta H (2003) c-MIR, a human E3 ubiquitin ligase, is a functional homolog of herpesvirus proteins MIR1 and MIR2 and has similar activity. *J. Biol. Chem.* **278:** 14657-14668.

Griffiths DA (1970) The fine structure of developing microsclerotia of *Verticillium dahliae* Kleb. *Arch. fuer Mikrobiol.* **74:** 207-212.

Gu Q, Chen Y, Liu Y, Zhang C & Ma Z (2015) The transmembrane protein FgSho1 regulates fungal development and pathogenicity via the MAPK module Ste50-Ste11-Ste7 in *Fusarium graminearum. New Phytol.* **206:** 315-328.

Guillemette T, Calmes B, Simoneau P & Index FH (2014) Impact of the UPR on the virulence of the plant fungal pathogen *A. brassicicola. Virulence* **5:** 357-364.

Guillemette T, Ram AF, Carvalho ND, Joubert A, Simoneau P & Archer DB (2011) Methods for investigating the UPR in filamentous fungi. *Methods Enzymol.* **490:** 1-29.

Hacquard S, Kracher B, Hiruma K, Münch PC, Garrido-Oter R, Thon MR, Weimann A, Damm U, Dallery J-F, Hainaut M, Henrissat B, Lespinet O, Sacristán S, Ver Loren van Themaat E, Kemen E, McHardy AC, Schulze-Lefert P & O'Connell RJ (2016) Survival trade-offs in plant roots during colonization by closely related beneficial and pathogenic fungi. *Nat. Commun.* **7:** 1-12.

Hamel L-P, Nicole M-C, Duplessis S & Ellis BE (2012) Mitogen-activated protein kinase signaling in plant-interacting fungi: distinct messages from conserved messengers. *Plant Cell* **24:** 1327-1351.

Hampel M, Jakobi M, Schmitz L, Meyer U, Finkernagel F, Doehlemann G & Heimel K (2016) Unfolded protein response (UPR) regulator Cib1 controls expression of genes encoding secreted virulence factors in *Ustilago maydis. PLoS One* **11**: e0153861.

Hanahan D, Jessee J & Bloom FR (1991) Plasmid transformation of *Escherichia coli* and other bacteria. *Methods Enzymol.* **204:** 63-113.

Harris SD, Read ND, Roberson RW, Shaw B, Seiler S, Plamann M & Momany M (2005) Polarisome meets Spitzenkörper: microscopy, genetics, and genomics converge. *Eukaryot. Cell* **4:** 225-229.

Hartmann FE, Sánchez-Vallet A, McDonald BA & Croll D (2017) A fungal wheat pathogen evolved host specialization by extensive chromosomal rearrangements. *ISME J.* **11:** 1189-1204.

Hastie AC (1973) Hybridization of *Verticillium albo-atrum* and *Verticillium dahliae. Trans. Br. Mycol. Soc.* **60:** 511-523.

Hastie AC (1989) The analysis of *Verticillium* strain relationship. In *Vascular wilt diseases of plants.* Tjamos EC & Beckman CH (eds). Berlin, Heidelberg: *Springer.* **28:** 315-323.

References

Heale JB & Karapapa VK (1999) The Verticillium threat to Canada's major oilseed crop: canola. *Can. J. Plant Pathol.* **21:** 1-7.

Heimel K (2015) Unfolded protein response in filamentous fungi - implications in biotechnology. *Appl. Microbiol. Biotechnol.* **99:** 121-132.

Heimel K, Freitag J, Hampel M & Ast J (2013) Crosstalk between the unfolded protein response and pathways that regulate pathogenic development in *Ustilago maydis. Plant Cell* **25:** 4262-4277.

Heimel K, Scherer M, Schuler D & Kämper J (2010) The *Ustilago maydis* Clp1 protein orchestrates pheromone and b-dependent signaling pathways to coordinate the cell cycle and pathogenic development. *Plant Cell* **22:** 2908-2922.

Heitman J & Kronstad JW, Taylor JW, Casselton LA (eds) (2007) Sex in Fungi. WA, USA: *American Society of Microbiology* **1:** 1-542.

Herskowitz I (1995) MAP kinase pathways in yeast: for mating and more. *Cell* **80:** 187-197.

Herzog B, Popova B, Jakobshagen A, Shahpasandzadeh H & Braus GH (2013) Mutual cross talk between the regulators Hac1 of the unfolded protein response and Gcn4 of the general amino acid control of *Saccharomyces cerevisiae. Eukaryot. Cell* **12:** 1142-1154.

Hetz C (2012) The unfolded protein response: controlling cell fate decisions under ER stress and beyond. *Nat. Rev. Mol. Cell Biol.* **13:** 89-102.

Hicks J, Lockington RA, Strauss J, Dieringer D, Kubicek CP, Kelly J & Keller N (2001) RcoA has pleiotropic effects on *Aspergillus nidulans cellular* development. *Mol. Microbiol.* **39:** 1482-1493.

Hollensteiner J, Wemheuer F, Harting R & Kolarzyk AM (2017) *Bacillus thuringiensis* and *Bacillus weihenstephanensis* inhibit the growth of phytopathogenic *Verticillium* species. *Front. Microbiol.* **7:** 1-19.

Hooks KB & Griffiths-Jones S (2011) Conserved RNA structures in the non-canonical Hac1/Xbp1 intron. *RNA Biol.* **8:** 552-556.

Horowitz Brown S, Scott JB, Bhaheetharan J, Sharpee WC, Milde L, Wilson RA & Keller NP (2009) Oxygenase coordination is required for morphological transition and the host-fungus interaction of *Aspergillus flavus. Mol. Plant-Microbe Interact.* **22:** 882-894.

Horowitz Brown S, Zarnowski R, Sharpee WC & Keller NP (2008) Morphological transitions governed by density dependence and lipoxygenase activity in *Aspergillus flavus. Appl. Environ. Microbiol.* **74:** 5674-5685.

Hurst HC (1995) Transcription factors 1: bZIP proteins. *Protein Profile* **2:** 101-168.

Husain A, Ahmad A & Agrawal PK (1993) (-)-Jasmonic acid, a phytotoxic substance from *Botryodiplodia theobromae*: characterization by NMR spectroscopic methods. *J. Nat. Prod.* **56:** 2008-2011.

Inderbitzin P, Bostock RM, Davis RM, Usami T, Platt HW & Subbarao KV (2011a) Phylogenetics and taxonomy of the fungal vascular wilt pathogen *Verticillium*, with the descriptions of five new species. *PLoS One* **6:** e28341.

Inderbitzin P, Davis RM, Bostock RM & Subbarao KV (2011b) The ascomycete *Verticillium longisporum* is a hybrid and a plant pathogen with an expanded host range. *PLoS One* **6:** e18260.

Inderbitzin P & Subbarao KV (2014) *Verticillium* systematics and evolution: how confusion impedes Verticillium wilt management and how to resolve it. *Phytopathology* **104:** 564-574.

Ingram R (1968) *Verticillium dahliae* var. *longisporum*, a stable diploid. *Trans. Br. Mycol. Soc.* **51:** 339-341.

Inouye C, Dhillon N & Thorner J (1997) Ste5 RING-H2 domain: role in Ste4-promoted oligomerization for yeast pheromone signaling. *Science* **278:** 103-106.

Jabnoun-Khiareddine H, Daami-Remadi M, Hibar K, Robb J & El Mahjoub M (2006) effect of temperature on Verticillium wilts of tomato in Tunisia. *Plant Pathol. J.* **5:** 1-6.

References

Jain BP (2019) Genome wide analysis of WD40 proteins in *Saccharomyces cerevisiae* and their orthologs in *Candida albicans*. *Protein J.* **38:** 58-75.

Jamet-Vierny C, Debuchy R, Prigent M & Silar P (2007) *IDC1*, a Pezizomycotina-specific gene that belongs to the PaMpk1 MAP kinase transduction cascade of the filamentous fungus *Podospora anserina. Fungal Genet. Biol.* **44:** 1219-1230.

Jenczmionka NJ & Schäfer W (2005) The Gpmk1 MAP kinase of *Fusarium graminearum* regulates the induction of specific secreted enzymes. *Curr. Genet.* **47:** 29-36.

Jiang C, Zhang X, Liu H & Xu J-R (2018a) Mitogen-activated protein kinase signaling in plant pathogenic fungi. *PLoS Pathog.* **14:** e1006875.

Jiang H, Lin L, Tang W, Chen X, Zheng Q, Huang J, Yang T, Su L, Dong Y, Wang B & Wang Z (2018b) Putative interaction proteins of the ubiquitin ligase Hrd1 in *Magnaporthe oryzae. Evol. Bioinform. Online* **14:** 1176934318810990.

Jin L, Chen D, Liao S, Zhang Y, Yu F, Wan P, Yu D, Wu Q & Zhang Y (2019) Transcriptome analysis reveals downregulation of virulence-associated genes expression in a low virulence *Verticillium dahliae* strain. *Arch. Microbiol.* (ahead of print) doi:10.1007/s00203-019-01663-7.

Joazeiro CA & Weissman AM (2000) RING finger proteins: mediators of ubiquitin ligase activity. *Cell* **102:** 549-552.

Jones P, Binns D, Chang HY, Fraser M, Li W, McAnulla C, McWilliam H, Maslen J, Mitchell A, Nuka G, Pesseat S, Quinn AF, Sangrador-Vegas A, Scheremetjew M, Yong S-Y, Lopez R & Hunter S (2014) InterProScan 5: genome-scale protein function classification. *Bioinformatics* **30:** 1236-1240.

Jonikas MC, Collins SR, Denic V, Oh E, Quan EM, Schmid V, Weibezahn J, Schwappach B, Walter P, Weissman JS & Schuldiner M (2009) Comprehensive characterization of genes required for protein folding in the endoplasmic reticulum. *Science* **323:** 1693-1697.

Jonkers W, Fischer MS, Do HP, Starr TL & Glass NL (2016) Chemotropism and cell fusion in *Neurospora crassa* relies on the formation of distinct protein complexes by HAM-5 and a novel protein HAM-14. *Genetics* **203:** 334-391.

Jonkers W, Leeder AC, Ansong C, Wang Y, Yang F, Starr TL, Camp DG, Smith RD & Glass NL (2014) HAM-5 functions as a MAP kinase scaffold during cell fusion in *Neurospora crassa. PLoS Genet.* **10:** e1004783.

Joubert A, Simoneau P, Campion C, Poupard P, François JM, Georgeault S, Sellier E & Guillemette T (2011) Impact of the unfolded protein response on the pathogenicity of the necrotrophic fungus *Alternaria brassicicola. Mol. Microbiol.* **79:** 1305-1324.

Kämper J, Kahmann R, Bölker M, Ma L-J, Brefort T, Saville BJ, Banuett F, Kronstad JW, Gold SE, Müller O, Perlin MH, Wösten HAB, de Vries R, Ruiz-Herrera J, Reynaga-Peña CG, Snetselaar K, McCann M, Pérez-Martín J, Feldbrügge M, Basse CW, *et al*. (2006) Insights from the genome of the biotrophic fungal plant pathogen *Ustilago maydis. Nature* **444:** 97-101.

Karapapa VK, Bainbridge BW & Heale JB (1997) Morphological and molecular characterization of *Verticillium longisporum* comb. nov., pathogenic to oilseed rape. *Mycol. Res.* **101:** 1281-1294.

Kaufman RJ (1999) Stress signaling from the lumen of the endoplasmic reticulum: coordination of gene transcriptional and translational controls. *Genes Dev.* **13:** 1211-1233.

Kersey PJ, Allen JE, Allot A, Barba M, Boddu S, Bolt BJ, Carvalho-Silva D, Christensen M, Davis P, Grabmueller C, Kumar N, Liu Z, Maurel T, Moore B, McDowall MD, Maheswari U, Naamati G, Newman V, Ong CK, Paulini M, *et al*. (2018) Ensembl Genomes 2018: an integrated omics infrastructure for non-vertebrate species. *Nucleic Acids Res.* **46:** D802-D808.

Klosterman SJ, Atallah ZK, Vallad GE & Subbarao KV (2009) Diversity, pathogenicity, and management of *Verticillium* species. *Annu. Rev. Phytopathol.* **47:** 39-62.

Klosterman SJ, Subbarao KV, Kang S, Veronese P, Gold SE, Thomma BPHJ, Chen Z, Henrissat B, Lee YH, Park J, Garcia-Pedrajas MD, Barbara DJ, Anchieta A, de Jonge R, Santhanam P, Maruthachalam K, Atallah Z, Amyotte SG, Paz Z, Inderbitzin P, *et al*. (2011) Comparative

genomics yields insights into niche adaptation of plant vascular wilt pathogens. *PLoS Pathog.* **7:** e1002137.

Kohno K (2010) Stress-sensing mechanisms in the unfolded protein response: similarities and differences between yeast and mammals. *J. Biochem.* **147:** 27-33.

Kohno K, Normington K, Sambrook J, Gething MJ & Mori K (1993) The promoter region of the yeast *KAR2* (*BiP*) gene contains a regulatory domain that responds to the presence of unfolded proteins in the endoplasmic reticulum. *Mol. Cell. Biol.* **13:** 877-890.

Koike ST, Subbarao KV, Davis RM, Gordon TR & Hubbard J (1994) Verticillium wilt of cauliflower in California. *Plant Dis.* **78:** 1116-1121.

Kolar M, Punt PJ, van den Hondel CAMJJ & Schwab H (1988) Transformation of *Penicillium chrysogenum* using dominant selection markers and expression of an *Escherichia coli lacZ* fusion gene. *Gene* **62:** 127-134.

Kombrink A, Rovenich H, Shi-Kunne X, Rojas-Padilla E, van den Berg GCM, Domazakis E, de Jonge R, Valkenburg DJ, Sánchez-Vallet A, Seidl MF & Thomma BPHJ (2017) *Verticillium dahliae* LysM effectors differentially contribute to virulence on plant hosts. *Mol. Plant Pathol.* **18:** 596-608.

Kosugi S, Hasebe M, Tomita M & Yanagawa H (2009) Systematic identification of cell cycle-dependent yeast nucleocytoplasmic shuttling proteins by prediction of composite motifs. *Proc. Natl. Acad. Sci.* **106:** 10171-10176.

Kothe E (1996) Tetrapolar fungal mating types: sexes by the thousands. *FEMS Microbiol. Rev.* **18:** 65-87.

Kozutsumi Y, Segal M, Normington K, Gething M-J & Sambrook J (1988) The presence of malfolded proteins in the endoplasmic reticulum signals the induction of glucose-regulated proteins. *Nature* **332:** 462-464.

Kranz JE, Satterberg B & Elion EA (1994) The MAP kinase Fus3 associates with and phosphorylates the upstream signaling component Ste5. *Genes Dev.* **8:** 313-327.

Krishnan K & Askew DS (2014) The fungal UPR: a regulatory hub for virulence traits in the mold pathogen *Aspergillus fumigatus. Virulence* **5:** 334-340.

Lazo GR, Stein PA & Ludwig RA (1991) A DNA transformation-competent Arabidopsis genomic library in *Agrobacterium. Biotechnology* **9:** 963-967.

Lev S & Horwitz BA (2003) A mitogen-activated protein kinase pathway modulates the expression of two cellulase genes in *Cochliobolus heterostrophus* during plant infection. *Society* **15:** 835-844.

Lev S, Sharon A, Hadar R, Ma H & Horwitz BA (1999) A mitogen-activated protein kinase of the corn leaf pathogen *Cochliobolus heterostrophus* is involved in conidiation, appressorium formation, and pathogenicity: diverse roles for mitogen-activated protein kinase homologs in foliar pathogens. *Proc. Natl. Acad. Sci. U.S.A.* **96:** 13542-13547.

Li C, Wen A, Shen B, Lu J, Huang Y & Chang Y (2011) FastCloning: a highly simplified, purification-free, sequence- and ligation-independent PCR cloning method. *BMC Biotechnol* **11:** 92.

Li D, Bobrowicz P, Wilkinson HH & Ebbole DJ (2005) A mitogen-activated protein kinase pathway essential for mating and contributing to vegetative growth in *Neurospora crassa. Genetics* **170:** 1091-1104.

Li G, Zhou X & Xu J-R (2012) Genetic control of infection-related development in *Magnaporthe oryzae. Curr. Opin. Microbiol.* **15:** 678-684.

Li J (2019) Identification of host-specific effectors mediating pathogenicity of the vascular wilt pathogen *Verticillium dahliae. Dissertation at the Wageningen University.*

Liñeiro E, Chiva C, Cantoral JM, Sabidó E & Fernández-Acero FJ (2016) Modifications of fungal membrane proteins profile under pathogenicity induction: a proteomic analysis of *Botrytis cinerea* membranome. *Proteomics* **16:** 2363-2376.

Liu T, Song T, Zhang X, Yuan H, Su L, Li W, Xu J & Liu S (2014) Unconventionally secreted effectors of two filamentous pathogens target plant salicylate biosynthesis. *Nat. Commun.* **5:** 4686.

Liu XH, Gao HM, Xu F, Lu JP, Devenish RJ & Lin FC (2012) Autophagy vitalizes the pathogenicity of pathogenic fungi. *Autophagy* **8:** 1415-1425.

Livak KJ & Schmittgen TD (2001) Analysis of relative gene expression data using real-time quantitative PCR and the $2^{-\Delta\Delta C_T}$ Method. *Methods* **25:** 402-408.

López-Ráez JA, Verhage A, Fernández I, García JM, Azcón-Aguilar C, Flors V & Pozo MJ (2010) Hormonal and transcriptional profiles highlight common and differential host responses to arbuscular mycorrhizal fungi and the regulation of the oxylipin pathway. *J. Exp. Bot.* **61:** 2589-2601.

Lo Presti L, Lanver D, Schweizer G, Tanaka S, Liang L, Tollot M, Zuccaro A, Reissmann S & Kahmann R (2015) Fungal effectors and plant susceptibility. *Annu. Rev. Plant Biol.* **66:** 513-545.

Los DA & Murata N (1998) Structure and expression of fatty acid desaturases. *Biochim. Biophys. Acta.* **1394:** 3-15.

Luo X, Xie C & Dong J (2014) Interactions between *Verticillium dahliae* and its host: vegetative growth, pathogenicity, plant immunity. *Appl. Microbiol. Biotechnol.* **98:** 6921-6932.

Ma L-J, van der Does HC, Borkovich KA, Coleman JJ, Daboussi M-J, Di Pietro A, Dufresne M, Freitag M, Grabherr F, Henrissat B, Houterman PM, Kang S, Shim W-B, Woloshuk C, Xie X, Xu J-R, Antoniw J, Baker SE, Bluhm BH, Breakspear A, *et al.* (2010) Comparative genomics reveals mobile pathogenicity chromosomes in *Fusarium. Nature* **464:** 367-373.

Madhani HD & Fink GR (1998) The riddle of MAP kinase signaling specificity. *Trends Genet.* **14:** 151-155.

Malavazi I, Goldmanm GH & Brown NA (2014) The importance of connections between the cell wall integrity pathway and the unfolded protein response in filamentous fungi. *Brief. Funct. Genomics* **13:** 456-470.

Malcolm GM, Kuldau GA, Gugino BK & del Mar Jiménez-Gasco M (2013) Hidden host plant associations of soilborne fungal pathogens: an ecological perspective. *Phytopathology* **103:** 538-544.

Mansilla MC, Cybulski LE, Albanesi D & de Mendoza D (2004) Control of membrane lipid fluidity by molecular thermosensors. *J. Bacteriol.* **186:** 6681-6688.

Marcus S, Polverino A, Barr M & Wigler M (1994) Complexes between STE5 and components of the pheromone-responsive mitogen-activated protein kinase module. *Proc. Natl. Acad. Sci. U.S.A.* **91:** 7762-7766.

Martin CE, Oh C-S & Jiang Y (2007) Regulation of long chain unsaturated fatty acid synthesis in yeast. *Biochim. Biophys. Acta.* **1771:** 271-285.

Mazur P, El-zayat AE, Champe SP (1991) Structure and synthesis of sporogenic psi factors from *Aspergillus nidulans. J. Chem. Soc. Chem. Commun.* **20:** 1486-1487.

Mehrabi R, Bahkali AH, Abd-Elsalam KA, Moslem M, Ben M'Barek S, Gohari AM, Jashni MK, Stergiopoulos I, Kema GHJ & de Wit PJ (2011) Horizontal gene and chromosome transfer in plant pathogenic fungi affecting host range. *FEMS Microbiol. Rev.* **35:** 542-554.

Menardo F, Praz CR, Wyder S, Ben-David R, Bourras S, Matsumae H, McNally KE, Parlange F, Riba A, Roffler S, Schaefer LK, Shimizu KK, Valenti L, Zbinden H, Wicker T & Keller B (2016) Hybridization of powdery mildew strains gives rise to pathogens on novel agricultural crop species. *Nat. Genet.* **48:** 201-205.

Metzenberg RL & Glass NL (1990) Mating type and mating strategies in *Neurospora. BioEssays* **12:** 53-59.

Mey G, Oeser B, Lebrun MH & Tudzynski P (2002) The biotrophic, non-appressorium-forming grass pathogen *Claviceps purpurea* needs a Fus3/Pmk1 homologous mitogen-activated protein kinase for colonization of rye ovarian tissue. *Mol. Plant. Microbe. Interact.* **15:** 303-312.

Miersch O, Bohlmann H & Wasternack C (1999) Jasmonates and related compounds from *Fusarium oxysporum. Phytochemistry* **50:** 517-523.

Milgroom MG, del Mar Jiménez-Gasco M, Olivares García C, Drott MT & Jiménez-Díaz RM (2014) Recombination between clonal lineages of the asexual fungus *Verticillium dahliae* detected by genotyping by sequencing. *PLoS One* **9:** e106740.

Miura N & Ueda M (2018) Evaluation of unconventional protein secretion by *Saccharomyces cerevisiae* and other fungi. *Cells* **7:** E128.

Miyazaki T, Nakayama H, Nagayoshi Y, Kakeya H & Kohno S (2013) Dissection of Ire1 functions reveals stress response mechanisms uniquely evolved in *Candida glabrata. PLoS Pathog*. **9:** e1003160.

Money NP (2016) Fungal Cell Biology and Development. In *The Fungi*. Watkinson SC Boddy L & Money NP (eds). New York, NY, USA: *Academic Press* **3:** 37-66.

Montenegro-Montero A, Goity A & Larrondo LF (2015) The bZIP transcription factor HAC-1 is involved in the unfolded protein response and is necessary for growth on cellulose in *Neurospora crassa. PLoS One* **10:** e0131415.

Mori K, Kawahara T, Yoshida H, Yanagi H & Yura T (1996) Signalling from endoplasmic reticulum to nucleus: transcription factor with a basic-leucine zipper motif is required for the unfolded protein-response pathway. *Genes to Cells* **1:** 803-817.

Mori K, Ma W, Gething MJ & Sambrook J (1993) A transmembrane protein with a cdc2+/CDC28-related kinase activity is required for signaling from the ER to the nucleus. *Cell* **74:** 743-756.

Mori K, Ogawa N, Kawahara T, Yanagi H & Yura T (1998) Palindrome with spacer of one nucleotide is characteristic of the cis-acting unfolded protein response element in *Saccharomyces cerevisiae. J. Biol. Chem*. **273:** 9912-9920.

Mösch HU, Kübler E, Krappmann S, Fink GR & Braus GH (1999) Crosstalk between the Ras2p-controlled mitogen-activated protein kinase and cAMP pathways during invasive growth of *Saccharomyces cerevisiae*. *Mol. Biol. Cell* **10:** 1325-1335.

Mulder HJ & Nikolaev I (2009) HacA-dependent transcriptional switch releases *hacA* mRNA from a translational block upon endoplasmic reticulum stress. *Eukaryot. Cell* **8:** 665-675.

Mulder HJ, Saloheimo M, Penttilä M & Madrid SM (2004) The transcription factor HACA mediates the unfolded protein response in *Aspergillus niger*, and up-regulates its own transcription. *Mol. Genet. Genomics* **271:** 130-140.

Mullins ED, Chen X, Romaine P, Raina R, Geiser DM & Kang S (2001) *Agrobacterium*-mediated transformation of *Fusarium oxysporum*: an efficient tool for insertional mutagenesis and gene transfer. **91:** 173-180.

Munn AL, Heese-Peck A, Stevenson BJ, Pichler H & Riezman H (1999) Specific sterols required for the internalization step of endocytosis in yeast. *Mol. Biol. Cell* **10:** 3943-3957.

Murashige T & Skoog F (1962) A revised medium for rapid growth and bioassays with tobacco tissue cultures. *Plant Physiol*. **15:** 473-497.

Nakamura N (2011) The role of the transmembrane RING finger proteins in cellular and organelle function. *Membranes* **1:** 354-393.

Nguyen VC, Nakamura Y & Kanehara K (2019) Membrane lipid polyunsaturation mediated by fatty acid desaturase 2 (FAD 2) is involved in endoplasmic reticulum stress tolerance in *Arabidopsis thaliana. Plant J.* (ahead of print) doi:10.1111/tpj.14338.

Nikawa J, Akiyoshi M, Hirata S & Fukuda T (1996) *Saccharomyces cerevisiae IRE2/HAC1* is involved in *IRE1*-mediated *KAR2* expression. *Nucleic Acids Res.* **24:** 4222-4226.

Novakazi F, Inderbitzin P, Sandoya G, Hayes RJ, von Tiedemann A & Subbarao KV (2015) The three lineages of the diploid hybrid *Verticillium longisporum* differ in virulence and pathogenicity. *Phytopathology* **105:** 662-673.

O'Connell RJ, Thon MR, Hacquard S, Amyotte SG, Kleemann J, Torres MF, Damm U, Buiate EA, Epstein L, Alkan N, Altmüller J, Alvarado-Balderrama L, Bauser CA, Becker C, Birren BW, Chen Z, Choi J, Crouch JA, Duvick JP, Farman MA, *et al.* (2012) Lifestyle transitions in plant

pathogenic *Colletotrichum* fungi deciphered by genome and transcriptome analyses. *Nat. Genet.* **44:** 1060-1065.

Oberhofer M & Leuchtmann A (2012) Genetic diversity in epichloid endophytes of *Hordelymus europaeus* suggests repeated host jumps and interspecific hybridizations. *Mol. Ecol.* **21:** 2713-2726.

Okamura K, Kimata Y, Higashio H, Tsuru A & Kohno K (2000) Dissociation of Kar2p/BiP from an ER sensory molecule, Ire1p, triggers the unfolded protein response in yeast. *Biochem. Biophys. Res. Commun.* **279:** 445-450.

Ortoneda M, Guarro J, Madrid MP, Caracuel Z, Roncero MIG, Mayayo E & Di Pietro A (2004) *Fusarium oxysporum* as a multihost model for the genetic dissection of fungal virulence in plants and mammals. *Infect. Immun.* **72:** 1760-1766.

Park G, Xue C, Zhao X, Kim Y, Orbach M & Xu J-R (2006) Multiple upstream signals converge on the adaptor protein Mst50 in *Magnaporthe grisea. Plant Cell online* **18:** 2822-2835.

Park G, Xue C, Zheng L, Lam S & Xu J-R (2002) *MST12* regulates infectious growth but not appressorium formation in the rice blast fungus *Magnaporthe grisea. Mol. Plant-Microbe Interact.* **15:** 183-192.

Passorn S, Laoteng K, Rachadawong S, Tanticharoen M & Cheevadhanarak S (1999) Heterologous expression of *Mucor rouxii* Δ^{12}-desaturase gene in *Saccharomyces cerevisiae. Biochem. Biophys. Res. Commun.* **263:** 47-51.

Patkar RN, Benke PI, Qu Z, Chen YYC, Yang F, Swarup S & Naqvi NI (2015) A fungal monooxygenase-derived jasmonate attenuates host innate immunity. *Nat. Chem. Biol.* **11:** 733-740.

Patkar RN & Naqvi NI (2017) Fungal manipulation of hormone-regulated plant defense. *PLoS Pathog.* **13:** e1006334.

Patterson JC, Klimenko ES & Thorner J (2010) Single-cell analysis reveals that insulation maintains signaling specificity between two yeast MAPK pathways with common components. *Sci. Signal.* **3:** ra75.

Pegg GF (1984) The impact of Verticillium diseases in agriculture. *Phytopathol. Mediterr.* **23:** 176-192.

Pegg GF & Brady BL (2002) Verticillium wilts. Pegg GF & Brady BL (eds) Wallingford, UK: *CABI Publishing* **1:** 1-552.

Perez-Nadales E & Di Pietro A (2015) The transmembrane protein Sho1 cooperates with the mucin Msb2 to regulate invasive growth and plant infection in *Fusarium oxysporum. Mol. Plant Pathol.* **16:** 593-603.

Di Pietro A, García-Maceira FI, Méglecz E & Roncero MIG (2001) A MAP kinase of the vascular wilt fungus *Fusarium oxysporum* is essential for root penetration and pathogenesis. *Mol. Microbiol.* **39:** 1140-1152.

Pinter N, Hach CA, Hampel M, Rekhter D, Zienkiewicz K, Feussner I, Poehlein A, Daniel R, Finkernagel F & Heimel K (2019) Signal peptide peptidase activity connects the unfolded protein response to plant defense suppression by *Ustilago maydis. PLoS Pathog.* **15:** e1007734.

Piper RC & Luzio JP (2007) Ubiquitin-dependent sorting of integral membrane proteins for degradation in lysosomes. *Curr. Opin. Cell Biol.* **19:** 459-465.

Plett JM, Daguerre Y, Wittulsky S, Vayssieres A, Deveau A, Melton SJ, Kohler A, Morrell-Falvey JL, Brun A, Veneault-Fourrey C & Martin F (2014) Effector MiSSP7 of the mutualistic fungus *Laccaria bicolor* stabilizes the *Populus* JAZ6 protein and represses jasmonic acid (JA) responsive genes. *Proc. Natl. Acad. Sci.* **111:** 8299-8304.

Plissonneau C, Hartmann FE & Croll D (2018) Pangenome analyses of the wheat pathogen *Zymoseptoria tritici* reveal the structural basis of a highly plastic eukaryotic genome. *BMC Biol.* **16:** 5.

Pöggeler S & Kück U (2004) A WD40 repeat protein regulates fungal cell differentiation and can be replaced functionally by the mammalian homologue striatin. *Eukaryot. Cell* **3:** 232-240.

Printen JA & Sprague GF (1994) Protein-protein interactions in the yeast pheromone response pathway: Ste5p interacts with all members of the MAP kinase cascade. *Genetics* **138:** 609-619.

Pryciak PM & Huntress FA (1998) Membrane recruitment of the kinase cascade scaffold protein Ste5 by the Gbetagamma complex underlies activation of the yeast pheromone response pathway. *Genes Dev.* **12**: 2684-2697.

Punt PJ, Dingemanse MA, Jacobs-Meijsing BJM, Pouwels PH & van den Hondel CAMJJ (1988) Isolation and characterization of the glyceraldehyde-3-phosphate dehydrogenase gene of *Aspergillus nidulans. Gene* **69:** 49-57.

Qi X, Zhou S, Shang X & Wang X (2016) VdSho1 regulates growth, oxidant adaptation and virulence in *Verticillium dahliae. J. Phytopathol.* **164:** 1064-1074.

Qin L, Wu VW & Glass NL (2017) Deciphering the regulatory network between the SREBP pathway and protein secretion in *Neurospora crassa. MBio* **8:** e00233-17.

Raffaele S & Kamoun S (2012) Genome evolution in filamentous plant pathogens: why bigger can be better. *Nat. Rev. Microbiol.* **10:** 417-430.

Ralhan A, Schöttle S, Thurow C, Iven T, Feussner I, Polle A & Gatz C (2012) The vascular pathogen *Verticillium longisporum* requires a jasmonic acid-independent COI1 function in roots to elicit disease symptoms in Arabidopsis shoots. *Plant Physiol.* **159:** 1192-1203.

Rambo GW & Bean GA (1974) Sterols and fatty acids of aflatoxin and non-aflatoxin producing isolates of *Aspergillus. Phytochemistry* **13:** 195-198.

Rana A, Sahgal M & Johri BN (2017) *Fusarium oxysporum*: genomics, diversity and plant-host interaction. In *Developments in fungal biology and applied mycology.* Satyanarayana T, Deshmukh SK & Johri BN (eds). Berlin, Heidelberg: *Springer* **1:**159-199.

Rasband W (1997) Rasband. ImageJ, *U. S. Natl. Institutes Heal. Bethesda, Maryland, USA.* Available at: http://imagej.nih.gov/ij.

Rauyaree P, Ospina-Giraldo MD, Kang S, Bhat RG, Subbarao KV, Grant SJ & Dobinson KF (2005) Mutations in *VMK1*, a mitogen-activated protein kinase gene, affect microsclerotia formation and pathogenicity in *Verticillium dahliae. Curr. Genet.* **48:** 109-116.

Resende ML V., Flood J & Cooper RM (1994) Host specialization of *Verticillium dahliae,* with emphasis on isolates from cocoa (*Theobroma cacao*). *Plant Pathol.* **43:** 104-111.

Reusche M, Truskina J, Thole K, Nagel L, Rindfleisch S, Tran VT, Braus-Stromeyer SA, Braus GH, Teichmann T & Lipka V (2014) Infections with the vascular pathogens *Verticillium longisporum* and *Verticillium dahliae* induce distinct disease symptoms and differentially affect drought stress tolerance of *Arabidopsis thaliana. Environ. Exp. Bot.* **108:** 23-37.

Reverberi M, Punelli F, Scarpari M, Camera E, Zjalic S, Ricelli A, Fanelli C & Fabbri AA (2010) Lipoperoxidation affects ochratoxin A biosynthesis in *Aspergillus ochraceus* and its interaction with wheat seeds. *Appl. Microbiol. Biotechnol.* **85:** 1935-1946.

Richie DL, Feng X, Hartl L, Aimanianda V, Krishnan K, Powers-Fletcher M V, Watson DS, Galande AK, White SM, Willett T, Latgé J-P, Rhodes JC & Askew DS (2011) The virulence of the opportunistic fungal pathogen *Aspergillus fumigatus* requires cooperation between the endoplasmic reticulum-associated degradation pathway (ERAD) and the unfolded protein response (UPR). *Virulence* **2:** 12-21.

Richie DL, Hartl L, Aimanianda V, Winters MS, Fuller KK, Miley MD, White S, McCarthy JW, Latgé J-P, Feldmesser M, Rhodes JC & Askew DS (2009) A role for the unfolded protein response (UPR) in virulence and antifungal susceptibility in *Aspergillus fumigatus. PLoS Pathog.* **5:** e1000258.

Riemann M, Haga K, Shimizu T, Okada K, Ando S, Mochizuki S, Nishizawa Y, Yamanouchi U, Nick P, Yano M, Minami E, Takano M, Yamane H & Lino M (2013) Identification of rice *Allene Oxide Cyclase* mutants and the function of jasmonate for defence against *Magnaporthe oryzae. Plant J.* **74:** 226-238.

Rispail N & Di Pietro A (2009) *Fusarium oxysporum* Ste12 controls invasive growth and virulence downstream of the Fmk1 MAPK cascade. *Mol. Plant-Microbe Interact.* **22:** 830-839.

References

Rispail N, Soanes DM, Ant C, Czajkowski R, Grünler A, Huguet R, Perez-Nadales E, Poli A, Sartorel E, Valiante V, Yang M, Beffa R, Brakhage AA, Gow NAR, Kahmann R, Lebrun M-H, Lenasi H, Perez-Martin J, Talbot NJ, Wendland J, *et al.* (2009) Comparative genomics of MAP kinase and calcium–calcineurin signalling components in plant and human pathogenic fungi. *Fungal Genet. Biol.* **46:** 287-298.

Ron D & Walter P (2007) Signal integration in the endoplasmic reticulum unfolded protein response. *Nat. Rev. Mol. Cell Biol.* **8:** 519-529.

Rouxel T, Grandaubert J, Hane JK, Hoede C, van de Wouw AP, Couloux A, Dominguez V, Anthouard V, Bally P, Bourras S, Cozijnsen AJ, Ciuffetti LM, Degrave A, Dilmaghani A, Duret L, Fudal I, Goodwin SB, Gout L, Glaser N, Linglin J, *et al.* (2011) Effector diversification within compartments of the *Leptosphaeria maculans* genome affected by repeat-induced point mutations. *Nat. Commun.* **2:** 202.

Rüegsegger U, Leber JH & Walter P (2001) Block of *HAC1* mRNA translation by long-range base pairing is released by cytoplasmic splicing upon induction of the unfolded protein response. *Cell* **107:** 103-114.

Rui O & Hahn M (2007) The Slt2-type MAP kinase Bmp3 of *Botrytis cinerea* is required for normal saprotrophic growth, conidiation, plant surface sensing and host tissue colonization. *Mol. Plant Pathol.* **8:** 173-184.

Ruiz-Roldán MC, Maier FJ & Schäfer W (2001) *PTK1*, a mitogen-activated-protein kinase gene, is required for conidiation, appressorium formation, and pathogenicity of *Pyrenophora teres* on barley. *Mol. Plant-Microbe Interact.* **14:** 116-125.

Sabbagh Jr. W, Flatauer LJ, Bardwell AJ & Bardwell L (2001) Specificity of MAP kinase signaling in yeast differentiation involves transient versus sustained MAPK activation. *Mol. Cell* **8:** 683-691.

Sakuradani E, Kobayashi M, Ashikari T & Shimizu S (1999) Identification of Δ12-fatty acid desaturase from arachidonic acid-producing *Mortierella* fungus by heterologous expression in the yeast *Saccharomyces cerevisiae* and the fungus *Aspergillus oryzae*. *Eur. J. Biochem.* **261:** 812-820.

Saloheimo M, Valkonen M & Penttilä M (2003) Activation mechanisms of the HACI-mediated unfolded protein response in filamentous fungi. *Mol. Microbiol.* **47:** 1149-1161.

Samji T, Hong S & Means RE (2014) The membrane associated RING-CH proteins: a family of E3 ligases with diverse roles through the cell. *Int. Sch. Res. Not.* **2014:** 637295.

Sanders IR (2011) Mycorrhizal symbioses: how to be seen as a good fungus. *Curr. Biol.* **21:** R550-552.

Santhanam P, Esse HP Van, Albert I, Faino L, Nürnberger T & Thomma BPHJ (2013) Evidence for functional diversification within a fungal NEP1-like protein family. *Mol. Plant Pathol.* **26:** 278-286.

Sarmiento-Villamil JL, Prieto P, Klosterman SJ & Garcia-Pedrajas, Maria D (2018) Characterization of two homeodomain transcription factors with critical but distinct roles in virulence in the vascular pathogen *Verticillium dahliae. Mol. Plant Pathol.* **19:** 986-1004.

Scala V, Giorni P, Cirlini M, Ludovici M, Visentin I, Cardinale F, Fabbri AA, Fanelli C, Reverberi M, Battilani P, Galaverna G & Dall'Asta C (2014) LDS1-produced oxylipins are negative regulators of growth, conidiation and fumonisin synthesis in the fungal maize pathogen *Fusarium verticillioides. Front. Microbiol.* **5:** 669.

Schaeffer HJ & Weber MJ (1999) Mitogen-activated protein kinases: specific messages from ubiquitous messengers. *Mol. Cell. Biol.* **19:** 2435-2444.

Scholz SS, Schmidt-Heck W, Guthke R, Furch ACU, Reichelt M, Gershenzon J & Oelmüller R (2018) *Verticillium dahliae*-Arabidopsis interaction causes changes in gene expression profiles and jasmonate levels on different time scales. *Front. Microbiol.* **9:** 217.

Schröder M, Chang JS & Kaufman RJ (2000) The unfolded protein response represses nitrogen-starvation induced developmental differentiation in yeast. *Genes Dev.* **14:** 2962-2975.

Schwarz DS & Blower MD (2016) The endoplasmic reticulum: structure, function and response to cellular signaling. *Cell. Mol. Life Sci.* **73:** 79-94.

References

Scrimale T, Didone L, de Mesy Bentley KL & Krysan DJ (2009) The unfolded protein response is induced by the cell wall integrity mitogen-activated protein kinase signaling cascade and is required for cell wall integrity in *Saccharomyces cerevisiae*. *Mol. Biol. Cell* **20:** 164-175.

Segorbe D, Di Pietro A, Pérez-Nadales E & Turrà D (2017) Three *Fusarium oxysporum* mitogen-activated protein kinases (MAPKs) have distinct and complementary roles in stress adaptation and cross-kingdom pathogenicity. *Mol. Plant Pathol.* **18:** 912-924.

Seidl MF & Thomma BPHJ (2014) Sex or no sex: evolutionary adaptation occurs regardless. *BioEssays* **36:** 335-345.

Selin C, de Kievit TR, Belmonte MF & Fernando WGD (2016) Elucidating the role of effectors in plant-fungal interactions: progress and challenges. *Front. Microbiol.* **7:** 600.

Shamu CE & Walter P (1996) Oligomerization and phosphorylation of the Ire1p kinase during intracellular signaling from the endoplasmic reticulum to the nucleus. *EMBO J.* **15:** 3028-3039.

Sharma R, Mishra B, Runge F & Thines M (2014) Gene loss rather than gene gain is associated with a host jump from monocots to dicots in the smut fungus *Melanopsichium pennsylvanicum. Genome Biol. Evol.* **6:** 2034-2049.

Shi-kunne X & Faino L (2018) Evolution within the fungal genus Verticillium is characterized by chromosomal rearrangement and gene loss. *Environ. Microbiol.* **20:** 1362-1373.

Short DPG, Gurung S, Hu X, Inderbitzin P & Subbarao KV (2014) Maintenance of sex-related genes and the Co-occurrence of both mating types in *Verticillium dahliae. PLoS One* **9:** e112145.

Sidrauski C, Cox JS & Walter P (1996) tRNA ligase is required for regulated mRNA splicing in the unfolded protein response. *Cell* **87:** 405-413.

Sidrauski C & Walter P (1997) The transmembrane kinase Ire1p is a site-specific endonuclease that initiates mRNA splicing in the unfolded protein response. *Cell* **90:** 1031-1039.

Siebold M & von Tiedemann A (2013) Effects of experimental warming on fungal disease progress in oilseed rape. *Glob. Chang. Biol.* **19:** 1736-1747.

Smith BJ (1984) SDS polyacrylamide gel electrophoresis of proteins. In *Methods in Molecular Biology*. Walker JM (ed). Clifton, NJ, USA: *Humana Press* **1:** 41-55.

Smith G (1949) The effect of adding trace elements to Czapek-Dox medium. *Transactions of the British Mycological Society.* **32**: 280-283.

Soesanto L & Termorshuizen AJ (2001) Effect of temperature on the formation of microsclerotia of *Verticillium dahliae. J. Phytopathol.* **149:** 685-691.

Soliday CL & Kolattukudy PE (1977) Biosynthesis of Cutin. *Plant Physiol.* **59:** 1116-1121.

Song Y, Liu L, Wang Y, Valkenburg D-J, Zhang X, Zhu L & Thomma BPHJ (2018) Transfer of tomato immune receptor Ve1 confers Ave1-dependent Verticillium resistance in tobacco and cotton. *Plant Biotechnol. J.* **16:** 638-648.

Southern EM (1975) Detection of specific sequences among DNA fragments separated by gel electrophoresis. *J. Mol. Biol.* **98:** 503-517.

Stergiopoulos I & de Wit PJ (2009) Fungal effector proteins. *Annu. Rev. Phytopathol.* **47:** 233-263.

Stukenbrock EH, Christiansen FB, Hansen TT, Dutheil JY & Schierup MH (2012) Fusion of two divergent fungal individuals led to the recent emergence of a unique widespread pathogen species. *Proc. Natl. Acad. Sci. U.S.A.* **109:** 10954-10959.

Su X, Lu G, Rehman L, Li X, Sun L, Guo H & Cheng H (2018) *mCherry*-labeled *Verticillium dahliae* could be utilized to investigate its pathogenicity process in *Nicotiana benthamiana. Genes* **9:** 508.

Su X, Schmitz G, Zhang M, Mackie RI & Cann IKO (2012) Heterologous gene expression in filamentous fungi. In *Advances in Applied Microbiology*. Gadd GM & Sariaslani S (eds). Urbana, IL, USA: *Academic Press Inc* **81:** 1-61.

References

Subbarao KV, Kabir Z, Martin FN & Koike ST (2007) Management of soilborne diseases in strawberry using vegetable rotations. *Plant Dis.* **91:** 964-972.

Sverdlov E & Azhikina T (2005) Primer Walking. *Encycl. Life Sci.* doi:10.1038/npg.els.0005382.

Takano Y, Kikuchi T, Kubo Y, Hamer JE, Mise K & Furusawa I (2000) The *Colletotrichum lagenarium* MAP kinase gene *CMK1* regulates diverse aspects of fungal pathogenesis. *Mol. Plant-Microbe Interact.* **13:** 374-383.

Takemoto D, Kamakura S, Saikia S, Becker Y, Wrenn R, Tanaka A, Sumimoto H & Scott B (2011) Polarity proteins Bem1 and Cdc24 are components of the filamentous fungal NADPH oxidase complex. *Proc. Natl. Acad. Sci.* **108:** 2861-2866.

Takemoto D, Tanaka A & Scott B (2006) A p67Phox-like regulator is recruited to control hyphal branching in a fungal-grass mutualistic symbiosis. *The Plant Cell Online* **18:** 2807-2821.

Tamura K, Stecher G, Peterson D, Filipski A & Kumar S (2013) MEGA6: Molecular Evolutionary Genetics Analysis version 6.0. *Mol. Biol. Evol.* **30:** 2725-2729.

Tanaka A, Christensen MJ, Takemoto D, Park P & Scott B (2006) Reactive oxygen species play a role in regulating a fungus-perennial ryegrass mutualistic interaction. *Plant Cell* **18:** 1052-1066.

Tanaka A, Takemoto D, Hyon G-S, Park P & Scott B (2008) NoxA activation by the small GTPase RacA is required to maintain a mutualistic symbiotic association between *Epichloë festucae* and perennial ryegrass. *Mol. Microbiol.* **68:** 1165-1178.

Tang W, Ru Y, Hong L, Zhu Q, Zuo R, Guo X, Wang J, Zhang H, Zheng X, Wang P & Zhang Z (2015) System-wide characterization of bZIP transcription factor proteins involved in infection-related morphogenesis of *Magnaporthe oryzae. Environ. Microbiol.* **17:** 1377-1396.

Tang Y-C & Amon A (2013) Gene copy-number alterations: a cost-benefit analysis. *Cell* **152:** 394-405.

Thaler JS, Owen B & Higgins VJ (2004) The role of the jasmonate response in plant susceptibility to diverse pathogens with a range of lifestyles. *Plant Physiol.* **135:** 530-538.

Thatcher LF, Manners JM & Kazan K (2009) *Fusarium oxysporum* hijacks COI1-mediated jasmonate signaling to promote disease development in Arabidopsis. *Plant J.* **58:** 927-939.

Thines B, Katsir L, Melotto M, Niu Y, Mandaokar A, Liu G, Nomura K, He SY, Howe GA & Browse J (2007) JAZ repressor proteins are targets of the SCF[COI1] complex during jasmonate signalling. *Nature* **448:** 661-665.

Thompson JD, Higgins DG & Gibson TJ (1994) ClustalW: improving the sensitivity of progressive multiple sequence alignment through sequence weighting, position-specific gap penalties and weight matrix choice. *Nucleic Acids Res.* **22:** 4673-4680.

Tian L, Wang Y, Yu J, Xiong D, Zhao H & Tian C (2016) The Mitogen-activated protein kinase kinase VdPbs2 of *Verticillium dahliae* regulates microsclerotia formation, stress response, and plant infection. *Front. Microbiol.* **7:** 1532.

Tian L, Xu J, Zhou L & Guo W (2014) VdMsb regulates virulence and microsclerotia production in the fungal plant pathogen *Verticillium dahliae. Gene* **550:** 238-244.

Timpner C, Braus-Stromeyer SA, Tran VT & Braus GH (2013) The Cpc1 regulator of the cross-pathway control of amino acid biosynthesis is required for pathogenicity of the vascular pathogen *Verticillium longisporum. Mol. Plant-Microbe Interact.* **26:** 1312-1324.

Tran VT, Braus-Stromeyer SA, Kusch H, Reusche M, Kaever A, Kühn A, Valerius O, Landesfeind M, Aßhauer K, Tech M, Hoff K, Pena-Centeno T, Stanke M, Lipka V & Braus GH (2014) Verticillium transcription activator of adhesion Vta2 suppresses microsclerotia formation and is required for systemic infection of plant roots. *New Phytol.* **202:** 565-581.

Tran VT, Braus-Stromeyer SA, Timpner C & Braus GH (2013) Molecular diagnosis to discriminate pathogen and apathogen species of the hybrid *Verticillium longisporum* on the oilseed crop *Brassica napus. Appl. Microbiol. Biotechnol.* **97:** 4467-4483.

Travers KJ, Patil CK, Wodicka L, Lockhart DJ, Weissman JS & Walter P (2000) Functional and genomic analyses reveal an essential coordination between the unfolded protein response and ER-associated degradation. *Cell* **101:** 249-258.

References

Tsitsigiannis DI, Bok J-W, Andes D, Nielsen KF, Frisvad JC & Keller NP (2005a) *Aspergillus* cyclooxygenase-like enzymes are associated with prostaglandin production and virulence. *Infect. Immun.* **73:** 4548-4559.

Tsitsigiannis DI & Keller NP (2006) Oxylipins act as determinants of natural product biosynthesis and seed colonization in *Aspergillus nidulans. Mol. Microbiol.* **59:** 882-892.

Tsitsigiannis DI & Keller NP (2007) Oxylipins as developmental and host-fungal communication signals. *Trends Microbiol.* **15:** 109-118.

Tsitsigiannis DI, Kowieski TM, Zarnowski R & Keller NP (2004a) Endogenous lipogenic regulators of spore balance in *Aspergillus nidulans. Eukaryot. Cell* **3:** 1398-1411.

Tsitsigiannis DI, Kowieski TM, Zarnowski R & Keller NP (2005b) Three putative oxylipin biosynthetic genes integrate sexual and asexual development in *Aspergillus nidulans. Microbiology* **151:** 1809-1821.

Tsitsigiannis DI, Zarnowski R & Keller NP (2004b) The lipid body protein, PpoA, coordinates sexual and asexual sporulation in *Aspergillus nidulans. J. Biol. Chem.* **279:** 11344-11353.

Turgeon BG & Yoder OC (2000) Proposed nomenclature for mating type genes of filamentous ascomycetes. *Fungal Genet. Biol.* **31:** 1-5.

Turrà D, Segorbe D & Di Pietro A (2014) Protein kinases in plant-pathogenic fungi: conserved regulators of infection. *Annu. Rev. Phytopathol.* **52:** 267-288.

Tzima A, Paplomatas EJ, Rauyaree P & Kang S (2010) Roles of the catalytic subunit of cAMP-dependent protein kinase A in virulence and development of the soilborne plant pathogen *Verticillium dahliae. Fungal Genet. Biol.* **47:** 406-415.

Tzima AK, Paplomatas EJ, Tsitsigiannis DI & Kang S (2012) The G protein b subunit controls virulence and multiple growth- and development-related traits in *Verticillium dahliae. Fungal Genet. Biol.* **49:** 271-283.

Uttaro AD (2006) Biosynthesis of polyunsaturated fatty acids in lower eukaryotes. *IUBMB Life* **58:** 563-571.

Van Drogen F, Stucke VM, Jorritsma G & Peter M (2001) MAP kinase dynamics in response to pheromones in budding yeast. *Nat. Cell Biol.* **3:** 1051-1059.

Vallad GE & Subbarao KV (2008) Colonization of resistant and susceptible lettuce cultivars by a green fluorescent protein-tagged isolate of *Verticillium dahliae. Phytopathology* **98:** 871-885.

Velásquez AC, Castroverde CDM & He SY (2018) Plant-Pathogen warfare under changing climate conditions. *Curr. Biol.* **28:** R619-R634.

Wang G, Zhang D & Chen S (2014) Effect of earlier unfolded protein response and efficient protein disposal system on cellulase production in Rut C30. *World J. Microbiol. Biotechnol.* **30:** 2587-2595.

Wang Y, Hu X, Fang Y, Anchieta A, Goldman PH, Hernandez G & Klosterman SJ (2018) Transcription factor VdCmr1 is required for pigment production, protection from UV irradiation, and regulates expression of melanin biosynthetic genes in *Verticillium dahliae. Microbiology* **164:** 685-696.

Wang Y, Tian L, Xiong D, Klosterman SJ, Xiao S & Tian C (2016) The mitogen-activated protein kinase gene, VdHog1, regulates osmotic stress response, microsclerotia formation and virulence in *Verticillium dahliae. Fungal Genet. Biol.* **88:** 13-23.

Watanabe K, Oura T, Sakai H & Kajiwara S (2004) Yeast Δ12 fatty acid desaturase: gene cloning, expression, and function. *Biosci. Biotechnol. Biochem.* **68***:* 721-727.

Wei DS, Li MC, Zhang XX, Zhou H & Xing LJ (2006) A novel Δ^{12}-fatty acid desaturase gene from methylotrophic yeast *Pichia pastoris* GS115. *Acta Biochim. Pol.* **53:** 753-759.

Welihinda AA & Kaufman RJ (1996) The unfolded protein response pathway in *Saccharomyces cerevisiae.* Oligomerization and trans-phosphorylation of Ire1p (Ern1p) are required for kinase activation. *J. Biol. Chem.* **271:** 18181-18187.

Widmann C, Gibson S, Jarpe MB & Johnson GL (1999) Mitogen-activated protein kinase: conservation of a three-kinase module from yeast to human. *Physiol. Rev.* **79:** 143-180.

Wilhelm S (1955) Longevity of the Verticillium wilt fungus in the laboratory and field. *Phytopath* **45:** 180-181.

Williams GC (1975) Sex and evolution. In *Monographs in Population Biology.* Princeton, NJ, USA: *Princeton University Press* **8:** 170-193.

Wilson RA, Calvo AM, Chang P-K & Keller NP (2004) Characterization of the *Aspergillus parasiticus* Δ^{12}-desaturase gene: a role for lipid metabolism in the *Aspergillus*-seed interaction. *Microbiology* **150:** 2881-2888.

Wimalasena TT, Enjalbert B, Guillemette T, Plumridge A, Budge S, Yin Z, Brown AJP & Archer DB (2008) Impact of the unfolded protein response upon genome-wide expression patterns, and the role of Hac1 in the polarized growth, of *Candida albicans. Fungal Genet. Biol.* **45:** 1235-1247.

Woodcock DM, Crowther PJ, Doherty J, Jefferson S, DeCruz E, Noyer-Weidner M, Smith SS, Michael MZ & Graham MW (1989) Quantitative evaluation of *Escherichia coli* host strains for tolerance to cytosine methylation in plasmid and phage recombinants. *Nucleic Acids Res.* **17:** 3469-3478.

Wu C, Leberer E, Thomas DY & Whiteway M (1999) Functional characterization of the interaction of Ste50p with Ste11p MAPKKK in *Saccharomyces cerevisiae. Mol. Biol. Cell* **10:** 2425-1440.

Xiong D, Wang Y, Ma J, Klosterman SJ, Xiao S & Tian C (2014) Deep mRNA sequencing reveals stage-specific transcriptome alterations during microsclerotia development in the smoke tree vascular wilt pathogen, *Verticillium dahliae. BMC Genomics* **15:** 1-19.

Xu C & Min J (2011) Structure and function of WD40 domain proteins. *Protein Cell* **2:** 202-214.

Xu G, Jansen G, Thomas DY, Hollenberg CP & Ramezani Rad M (1996) Ste50p sustains mating pheromone-induced signal transduction in the yeast *Saccharomyces cerevisiae. Mol. Microbiol.* **20:** 773-783.

Xu J-R (2000) MAP kinases in fungal pathogens. *Fungal Genet. Biol.* **31:** 137-152.

Xu JR & Hamer JE (1996) MAP kinase and cAMP signaling regulate infection structure formation and pathogenic growth in the rice blast fungus *Magnaporthe grisea. Genes Dev.* **10:** 2696-2706.

Yadeta KA & Thomma BPHJ (2013) The xylem as battleground for plant hosts and vascular wilt pathogens. Front. *Plant Sci.* **4:** 97.

Yi M, Chi M-H, Khang CH, Park S-Y, Kang S, Valent B & Lee Y-H (2009) The ER chaperone LHS1 is involved in asexual development and rice infection by the blast fungus *Magnaporthe oryzae. Plant Cell online* **21:** 681-695.

Yoshida H, Matsui T, Yamamoto A, Okada T & Mori K (2001) XBP1 mRNA is induced by ATF6 and spliced by IRE1 in response to ER stress to produce a highly active transcription factor. *Cell* **107:** 881-891.

Yoshida H, Oku M, Suzuki M & Mori K (2006) pXBP1[U] encoded in XBP1 pre-mRNA negatively regulates unfolded protein response activator pXBP1[S] in mammalian ER stress response. *J. Cell Biol.* **172:** 565-575.

Yoshida H, Uemura A & Mori K (2009) pXBP1[U], a negative regulator of the unfolded protein response activator pXBP1[S], targets ATF6 but not ATF4 in proteasome-mediated degradation. *Cell Struct. Funct.* **34:** 1-10.

Zeise K & von Tiedemann A (2002) Host specialization among vegetative compatibility groups of *Verticillium dahliae* in relation to *Verticillium longisporum. J. Phytopathol.* **150:** 112-119.

Zhang Y, Tada T, Ozono S, Yao W, Tanaka M, Yamaoka S, Kishigami S, Fujita H & Tokunaga K (2019) Membrane-associated RING-CH (March) 1 and 2 are March family members that inhibit HIV-1 infection. *J. Biol. Chem.* **294:** 3397-3405.

Zhao P, Zhao Y-L, Jin Y, Zhang T & Guo H-S (2014) Colonization process of *Arabidopsis thaliana* roots by a green fluorescent protein-tagged isolate of *Verticillium dahliae. Protein Cell* **5:** 94-98.

Zhao X, Kim Y, Park G & Xu J-R (2005) A mitogen-activated protein kinase cascade regulating infection-related morphogenesis in *Magnaporthe grisea. Plant* Cell **17:** 1317-1329.

References

Zhao X, Mehrabi R & Xu JR (2007) Mitogen-activated protein kinase pathways and fungal pathogenesis. *Eukaryot. Cell* **6:** 1701-1714.

Zhao X & Xu J-R (2007) A highly conserved MAPK-docking site in Mst7 is essential for Pmk1 activation in *Magnaporthe grisea. Mol. Microbiol.* **63:** 881-894.

Zhao Y, Zhou T & Guo H (2016) Hyphopodium-specific VdNoxB/VdPls1- dependent ROS-Ca^{2+} signaling is required for plant infection by *Verticillium dahliae. PLoS Pathog.* **12:** e1005793.

Zheng J, Tang C, Deng C & Wang Y (2019) Involvement of a response regulator VdSsk1 in stress response, melanin biosynthesis and full virulence in *Verticillium dahliae. Front. Microbiol.* **10:** 1-10.

Zheng L, Campbell M, Murphy J, Lam S & Xu J-R (2000) The BMP1 Gene Is Essential for Pathogenicity in the Gray Mold Fungus *Botrytis cinerea. Mol. Plant-Microbe Interact.* **13:** 724-732.

Zhou L, Hu Q, Johansson A & Dixelius C (2006) *Verticillium longisporum* and *V. dahliae*: infection and disease in *Brassica napus. Plant Pathol.* **55:** 137-144.

Zuker M (2003) Mfold web server for nucleic acid folding and hybridization prediction. *Nucleic Acids Res.* **31:** 3406-3415.

Supplementary Figures
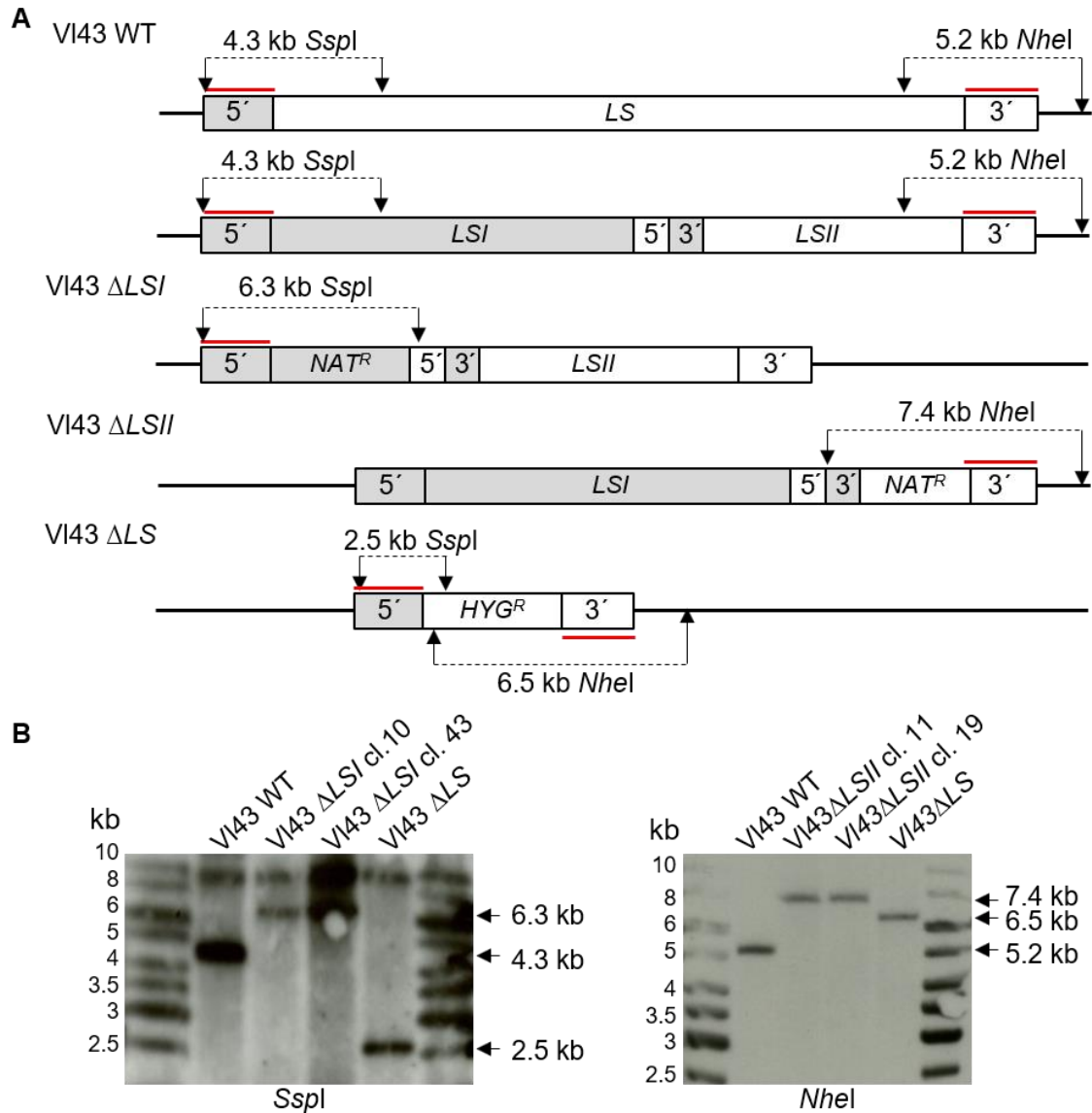
Figure S1: Southern hybridization of *V. longisporum* Vl43 *LSI*, *LSII*, and *LS* deletion strains. (**A**) Vl43 Δ*LSI*, Δ*LSII*, and Δ*LS* strains were constructed by replacement of genomic regions against nourseothricin or hygromycin resistance marker cassettes under control of a *gpdA* promoter and a *trpC* terminator (*NAT^R* or *HYG^R*) by homologous recombination of the up- and downstream flanking regions. The *Vl43LS20kb* region was dissected into a 11.5 bp *LSI* region and a 8.5 bp *LSII* region. The *LSI* deletion strain was used as parental strain of the *LS* deletion strain. Restriction sites of *Ssp*I and *Nhe*I used for Southern hybridization analysis are indicated by arrows. Expected fragment lengths labeled with the 5´- or 3´-flanking regions as probes (indicated in red) are given. (**B**) Confirmation of Vl43 *LSI*, *LSII*, and *LS* deletion strains by Southern hybridization. **Left**: 2.0 kb 5´-flanking region was used as a probe and genomic DNA was cut using the restriction enzyme *Ssp*I. The predicted bands of 4.3 kb for Vl43 wild type, 6.3 kb for *LSI* deletion transformants number 10 (VGB201) and 43 (VGB233), and 2.5 kb for the *LS* deletion strain (VGB232), and an additional unspecific band at ~ 8 kb present in all genotypes were obtained. **Right**: the 2.0 kb 3´-flanking region was used as probe and genomic DNA was cut using the restriction enzyme *Nhe*I. The predicted bands of 5.2 kb for Vl43 wild type, 7.4 kb for *LSII* deletion transformants 11 (VGB193) and 19 (VGB214), and 6.5 kb for the *LS* deletion strain (VGB232) were obtained.
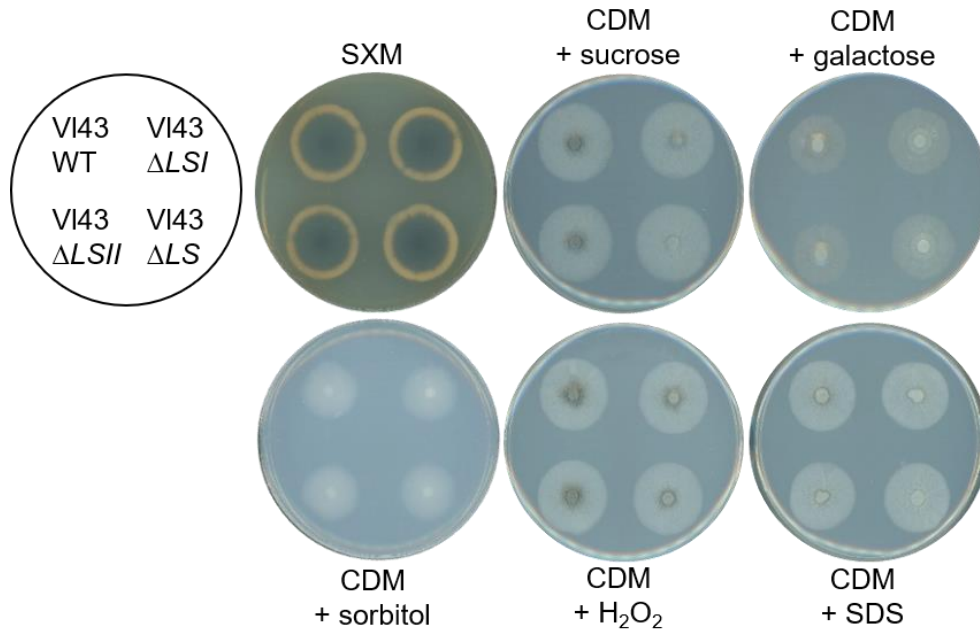
Figure S2: ***V. longisporum Vl43LS20kb* region is dispensable for vegetative growth on standard and stress inducing media *ex planta*.** *Ex planta* phenotypes of Vl43 *LSI, LSII*, and *LS* deletion strains compared to wild type Vl43 14 days after spot inoculation of 50 000 spores on SXM, CDM with either sucrose or galactose as carbon source, or CDM supplemented with either 0.8 M sorbitol, 0.00075% H_2O_2, or 0.004% SDS incubated at 25 °C. Two independent transformants were tested for Vl43 Δ*LSI* (VGB201, VGB233) and Vl43 Δ*LSII* (VGB193, VGB214), and a single transformant for Vl43 Δ*LS* (VGB232).

A

JR2 WT

5.1 kb *Bgl*I

| 5´ | *Vl43LS20kb* region | 3´ |

JR2 Δ*LS*

2.9 kb *Bgl*I

| 5´ | *NAT*^R | 3´ |

B
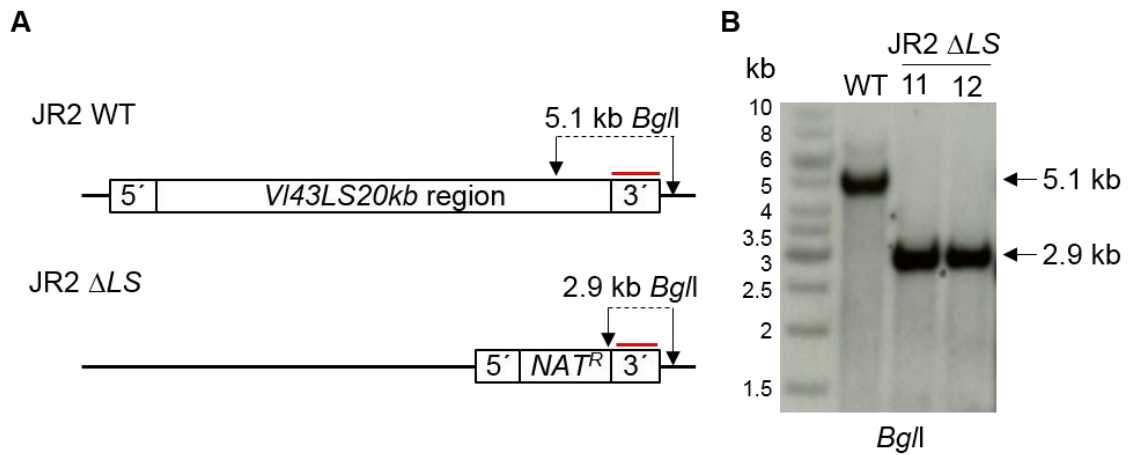
Figure S3: Southern hybridization of *V. dahliae LS* deletion transformants. (**A**) Scheme of restriction sites used for Southern hybridization. *V. dahliae* JR2 lacking the *Vl43LS20kb* homologous region was constructed by replacement of the genomic region against a nourseothricin resistance marker cassettes under control of a *gpdA* promoter and a *trpC* terminator (*NAT*^R) by homologous recombination of the up- and downstream flanking regions. Restriction sites of *Bgl*I are indicated by arrows and the expected fragment lengths labeled with the 3´-flanking region as a probe (indicated in red) are given. (**B**) Confirmation of two independent transformants of the *V. dahliae* JR2 *LS* deletion strain (VGB383, VGB393) by Southern hybridization using restriction enzyme *Bgl*I and 2.1 kb 3´-flanking region as a probe. Genomic DNA of the wild type was used as a control. The predicted bands of 5.1 kb for the wild type and 2.9 kb for the deletion were obtained.
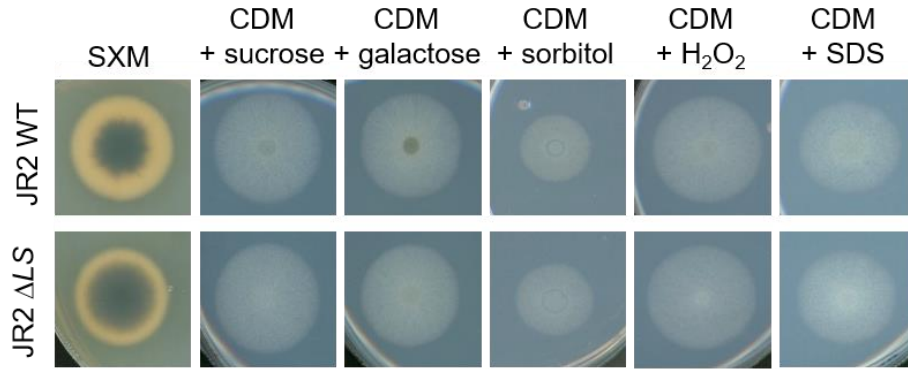
Figure S4: The *V. dahliae* JR2 *LS* deletion strain displays no significant alterations in its *ex planta* phenotype. *Ex planta* phenotypes of the *V. dahliae* JR2 *LS* deletion strain ten days after spot inoculation of 50 000 spores on SXM, CDM with either sucrose or galactose as carbon source, or CDM supplemented with 0.8 M sorbitol, 0.00075 % H_2O_2, or 0.004 % SDS incubated at 25 °C. Two independent transformants were tested (VGB383, VGB393).
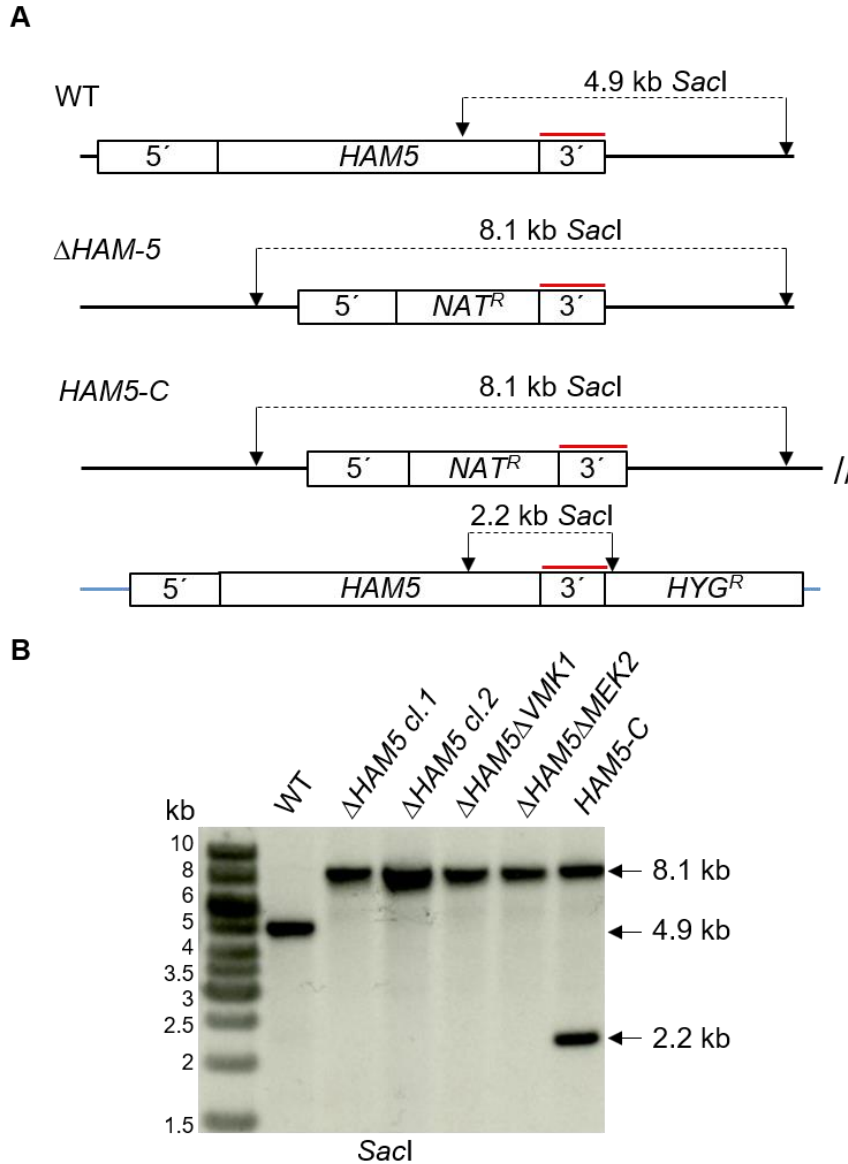
Figure S5: Southern hybridization of *V. dahliae HAM5* single and *VMK1/MEK2* double deletions and complementation strains. (**A**) Scheme of restriction sites used for Southern hybridization. *HYG^R*: the hygromycin resistance cassette under control of the *gpdA* promoter and a *trpC* terminator; *NAT^R*: the nourseothricin resistance cassette under control of the *gpdA* promoter and a *trpC* terminator; restriction sites of *SacI* are indicated by arrows and the expected fragment lengths labeled with the 3´-flanking region as a probe (indicated in red) are given. Ectopic integration sites of complementation strains are indicated by // at the end of the endogenous locus and by a blue line for the ectopic locus. (**B**) Southern hybridization for confirmation of strains: *ΔHAM5* transformant number 1 (VGB279) and 2 (VGB280), *ΔHAM5ΔVMK1* (VGB417)*, ΔHAM5ΔMEK2* (VGB346), *HAM5-C* (VGB415). Genomic DNA from wild type JR2 was used as a control. The 3´-flanking regions of *HAM5* was used as a probe and genomic DNA was cut using the restriction enzyme *SacI*. The predicted bands of 4.9 kb for wild type, 8.1 kb for the deletion, and 2.2 kb and 8.1 kb for the complementation were observed.
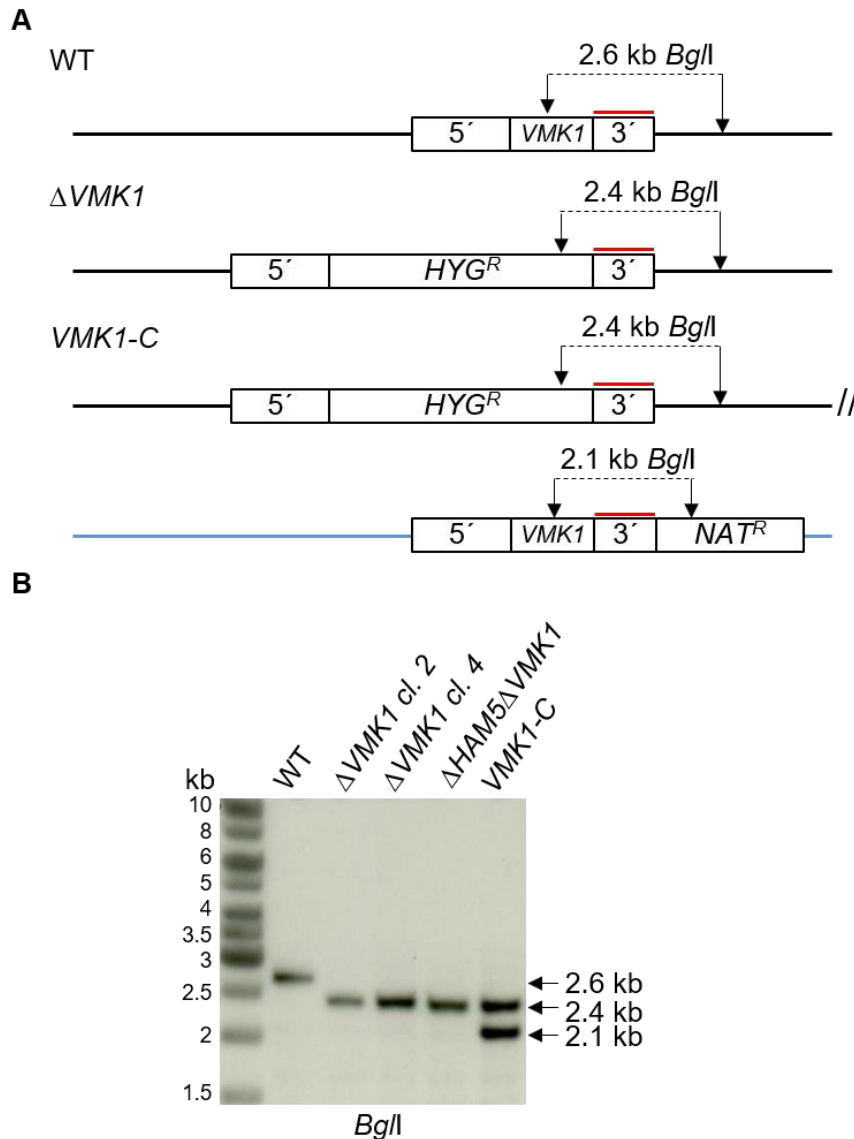
Figure S6: Southern hybridization of *V. dahliae VMK1* single and *HAM5/VMK1* double deletions and complementation strains. (**A**) Scheme of restriction sites used for Southern hybridization. *HYG^R*: the hygromycin resistance cassette under control of the *gpdA* promoter and a *trpC* terminator; *NAT^R*: the nourseothricin resistance cassette under control of the *gpdA* promoter and a *trpC* terminator; restriction sites of *Bgl*I are indicated by arrows and the expected fragment lengths labeled with the 3´-flanking region as a probe (indicated in red) are given. Ectopic integration sites of complementation strains are indicated by // at the end of the endogenous locus and by a blue line for the ectopic locus. (**B**) Southern hybridization for confirmation of strains: Δ*VMK1* transformant number 2 (VGB335) and 4 (VGB336), Δ*HAM5ΔVMK1* (VGB417)*, VMK1-C* (VGB413). Genomic DNA was used from wild type JR2 as a control. The 3´-flanking region of *VMK1* was used as a probe and genomic DNA was cut using the restriction enzyme *Bgl*I. The predicted bands of 2.6 kb for wild type, 2.4 kb for the deletion, and 2.1 kb and 2.4 kb for the complementation were observed.
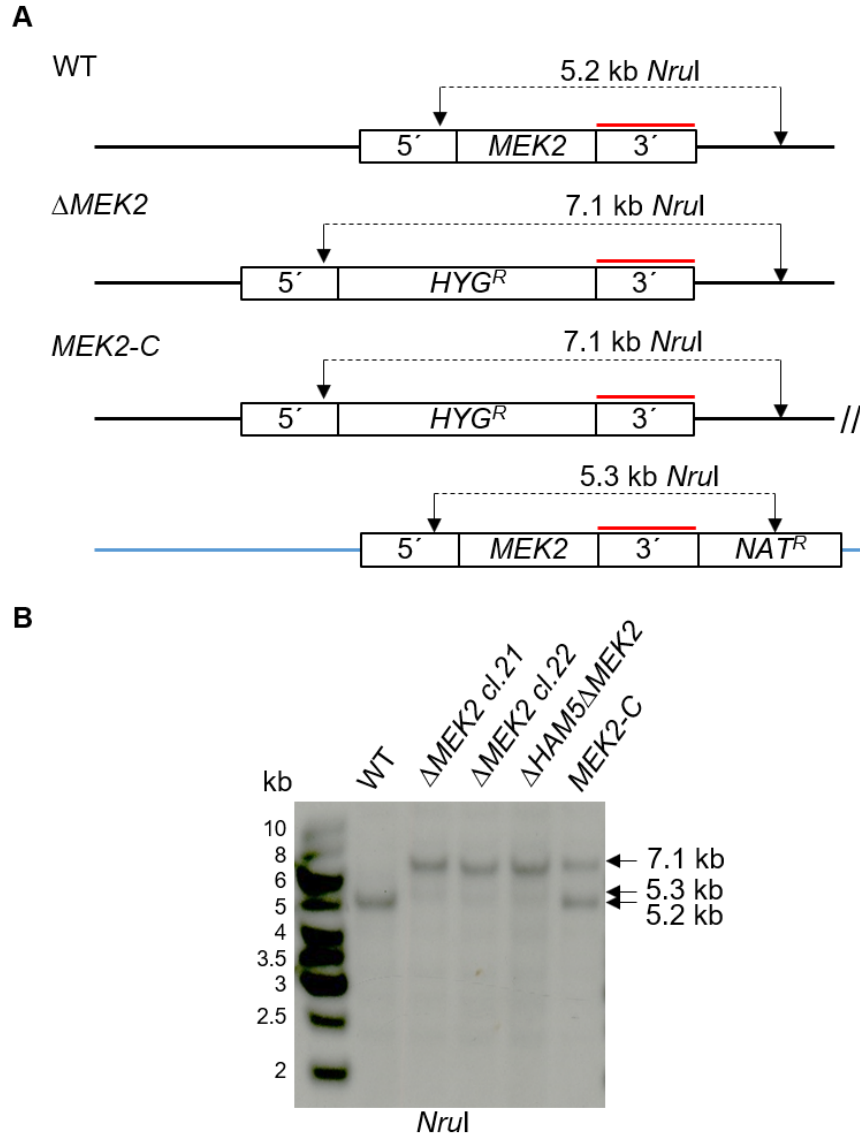
Figure S7: Southern hybridization of *V. dahliae MEK2* single and *HAM5/MEK2* double deletions and complementation strains. (**A**) Scheme of restriction sites used for Southern hybridization. *HYG^R*: the hygromycin resistance cassette under control of the *gpdA* promoter and a *trpC* terminator; *NAT^R*: the nourseothricin resistance cassette under control of the *gpdA* promoter and a *trpC* terminator; restriction sites of *Nru*I are indicated by arrows and the expected fragment length labeled with the 3´-flanking region as a probe (indicated in red) are given. Ectopic integration sites of complementation strains are indicated by // at the end of the endogenous locus and by a blue line for the ectopic locus. (**B**) Southern hybridization for confirmation of strains: Δ*MEK2* transformant number 21 (VGB337) and 22 (VGB338), Δ*HAM5*Δ*MEK2* (VGB346), and *MEK2-C* (VGB389). Genomic DNA was used from wild type JR2 as a control. The 3´-flanking region of *MEK2* was used as a probe and genomic DNA was cut using the restriction enzyme *Nru*I. The predicted bands of 5.2 kb for WT, 7.1 kb for the deletion, and 5.3 kb and 7.1 kb for the complementation were observed.
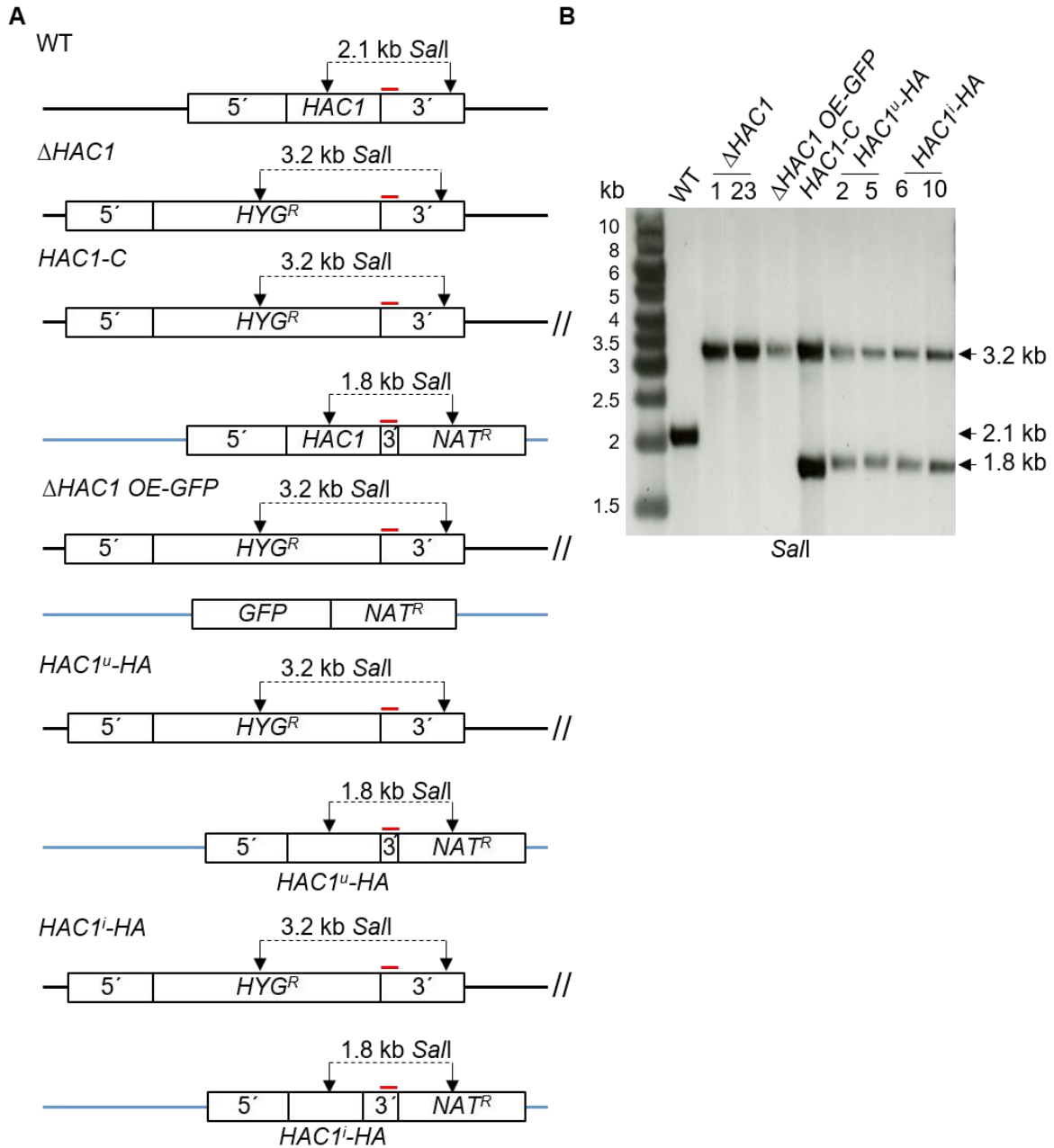
Figure S8: Southern hybridization of *V. dahliae HAC1* deletion, *HAC1* deletion with ectopic *GFP* overexpression, *HAC1* complementation, as well as *HAC1*^*u*-HA and *HAC1*^*i*-HA strains. (**A**) Scheme of restriction sites used for Southern hybridization. *HYG*^*R*: the hygromycin resistance cassette under control of the *gpdA* promoter and a *trpC* terminator; *NAT*^*R*: the nourseothricin resistance cassette under control of the *gpdA* promoter and a *trpC* terminator; restriction sites of *Sal*I are indicated by arrows. Expected fragment lengths labeled with the 3´-flanking region as a probe (indicated in red) are given. Ectopic integration sites of complementation strains are indicated by // at the end of the endogenous locus and by a blue line for the ectopic locus. (**B**) Southern hybridization for confirmation of strains: Δ*HAC1* transformant number 1 (VGB371) and 23 (VGB372), Δ*HAC1 OE-GFP* (VGB380), *HAC1-C* complementation (VGB382), *HAC1*^*u*-HA transformant number 2 (VGB439) and 5 (VGB440), and *HAC1*^*i*-HA transformant number 6 (VGB437) and 10 (VGB438). The 3´-flanking region of *HAC1* was used as a probe. Genomic DNA was cut using the restriction enzyme *Sal*I. The predicted bands of 2.1 kb for wild type, 3.2 kb for Δ*HAC1* and Δ*HAC1 OE-GFP,* and 3.2 kb and 1.8 kb for the *HAC1-C, HAC1*^*u*-HA, and *HAC1*^*i*-HA strains were obtained.
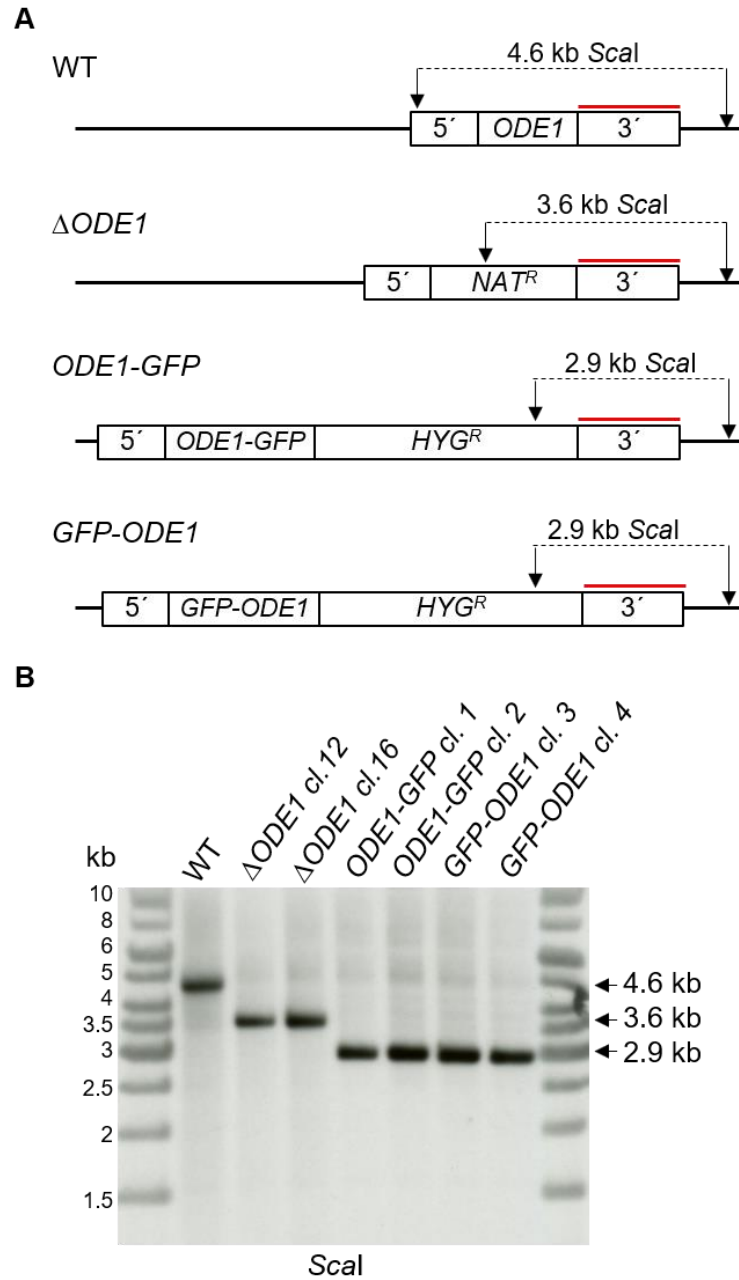
Figure S9: Southern hybridization of *V. dahliae ODE1* deletion and complementation strains. (**A**) Scheme of restriction sites used for Southern hybridization. *HYG^R^:* the hygromycin resistance cassette under control of the *gpdA* promoter and a *trpC* terminator; *NAT^R^:* the nourseothricin resistance cassette under control of the *gpdA* promoter and a *trpC* terminator; restriction sites of *Sca*I are indicated by arrows and the expected fragment lengths labeled with the 3´-flanking region as a probe (indicated in red) are given. (**B**) Southern hybridization for confirmation of strains: Δ*ODE1* transformant number 12 (VGB331) and 16 (VGB332), *ODE1-GFP* transformant number 1 (VGB358) and 2 (VGB359), and *GFP-ODE1* transformant number 3 (VGB360) and 4 (VGB361). The 3´-flanking region of *ODE1* was used as a probe. Genomic DNA was cut using the restriction enzyme *Sca*I. The predicted bands of 4.6 kb for wild type, 3.6 kb for the deletion, and 2.9 kb for the endogenous complementation strains were observed.

```
   1    ATG GAG TCT TGG GAG CAC TCC ACC ACA CCA      30
  31    ATG ATC AAG TTC GAG GAC TCG CCA GCC GAG      60
  61    TCT TTC GTC TCG ACA CCA GGC GAC ATG TAC      90
  91    CCG TCA CTC TTC CCA GAG TCC GCC TCC CCC     120
 121    AAC ACC CTC GAT CCT TCC AAC ATG ATG AGC     150
 151    CCT TCC TCA CCC CAA GAC CTC ACC ATT GCC     180
 181    GAC ACG GAT ATG CCT CTC TCC GAG GCT TCC     210
 211    GCC GGC GAC AAG AAG GGG TCC AAG AAG CGC     240
 241    AAG TCC TGG GGT CAG GTC CTT CCC GAG CCC     270
 271    AAG ACC AAC TTG CCG CCC AGG AAA CGA GCC     300
 301    AAG ACT GAG GAT GAG AAG GAG CAG CGT CGT     330
 331    GTG GAA CGC GTT CTG CGC AAC CGC CGT GCT     360
 361    GCC CAG TCT TCG AGG GAG CGC AAG AGG CTC     390
 391    GAG GTT GAG GCC CTC GAG ATG AAG AAC AAG     420
 421    GAG CTC GAG ACT GCC CTG AAC CAC GCA CAA     450
 451    CAG GCG AAC GCT AGG TTG ATG GAG GAG CTT     480
 481    ACC AAG TTC CGC CGT GGT TCC GGT GCC GTC     510
 511    GCC CGT TCT TCT TCC CCC TTT GAC TCC TTC     540
 541    CAC AAC AGC AAC TCG GTC ACC CTC TCC CCC     570
 571    GAG CTG TTC GGC TCT CAA GAC GGC CGC CGG     600
 601    CCA TCA GTG GCC GAC TCC GAG TCG ACA CTC     630
 631    GTC GAC GGT TTG ATG GCG GCC TCC AAG TCC     660
 661    GCC GCG ACC GTC AAC CCC GCC TCC CTC TCG     690
 691    CCC GCC CTC ACC CCC GTC CCC GAG ACG GAT     720
 721    GAG ACC AGC GCC CAA CAA GAA GCT GCC GTG     750
 751    GCC GCC CCT TCC CCT GTC GCC CTT TCC TCC     780
 781    GAC GTG ACA CAA CGT CCT GCC GTG TCG GTC     810
 811    GGA GGA AAT GCC TCA GTC GTG GGT GGC CTC     840
 841    GCA GAC TTC CCT GCA CCC AAC ATG GAC TTT     870
 871    GTA CCT TCA GCT TCA GAT GCT CAT GAT CAC     900
 901    TTC CTC GGC GGT CAT TTC AGC GTG TCA GAG     930
 931    GCC TTT GAT GCA GAT CGC TAT GTC CTT GAG     960
 961    AGC GGG CTT CTC TCT TCC CCC AAC TCA GTC     990
 991    GAT TAT GAC AAC GAT ATT ATG GCT GGT GAC    1020
1021    TCG TCC GCG TTC GCA TCC GCG TTC AAC TTC    1050
1051    GAC ATG GAC GAG TTC CTC AAC GAT GAG GCC    1080
1081    AGC GCA GCC GCC ACT GAC GCG TCA GCA GCG    1110
1111    GAG AAC AGC GCA GCG GAC CCG GAC TAC GGC    1140
1141    CGC CGT GCC CTT AAC CCT GAG ACT CAA GTC    1170
1171    TCT TCA GAA AAT CCT AAC CTG CAG CCC CAA    1200
1201    TCT GGC GCG TCC ACT TAT GGA TGC GAC GAT    1230
1231    GGA GGC ATT GCG GTT GGT GTC TGA           1254
```

Figure S10:   The cDNA sequence of *V. dahliae* JR2 *HAC1^i^*. The *V. dahliae* JR2 *HAC1^i^* sequence with 1254 nucleotides was obtained by cDNA synthesis from mycelium of wild type cultures grown in 50 ml SXM (1x10^7 spores) for four days under constant agitation at 25 °C and subsequent supplementation with 3 mM DTT for three hours. *HAC1^i^* was amplified using primers JST171/JST174 and was fully sequenced.

```
  1    MESWEHSTTP    MIKFEDSPAE    SFVSTPGDMY    PSLFPESASP    40
 41    NTLDPSNMMS    PSSPQDLTIA    DTDMPLSEAS    AGDKKGSKKR    80
 81    KSWGQVLPEP    KTNLPPRKRA    KTEDEKEQRR    VERVLRNRRA    120
121    AQSSRERKRL    EVEALEMKNK    ELETALNHAQ    QANARLMEEL    160
161    TKFRRGSGAV    ARSSSPFDSF    HNSNSVTLSP    ELFGSQDGRR    200
201    PSVADSESTL    VDGLMAASKS    AATVNPASLS    PALTPVPETD    240
241    ETSAQQEAAV    AAPSPVALSS    DVTQRPAVSV    GGNASVVGGL    280
281    ADFPAPNMDF    VPSASDAHDH    FLGGHFSVSE    AFDADRYVLE    320
321    SGLLSSPNSV    DYDNDIMAGD    SSAFASAFNF    DMDEFLNDEA    360
361    SAAATDASAA    ENSAADPDYG    RRALNPETQV    SSENPNLQPQ    400
401    SGASTYGCDD    GGIAVGV
```

Figure S11:   The amino acid sequence of *V. dahliae* JR2 Hac1. The deduced protein sequence from *HAC1[i]* with 417 aa in length. Red: NLS predicted by cNLS Mapper (94-105 aa); Blue: N-terminal basic-leucine zipper domain (bZIP, PS50217; 107-164 aa).

155

List of Figures

List of Tables

List of Supplementary Figures

Abbreviations

5´	upstream flanking region
3´	downstream flanking region
12-OH-JA	12-hydroxy jasmonic acid
α	antibody
°C	degree Celsius
Δ	deletion
λ	wavelength
µg	microgram
µl	microliter
µm	micrometer
µmol	micromol
aa	amino acid(s)
AMP^R	ampicillin resistance marker cassette
Amr	*Alternaria* melanin regulation
APS	ammonium persulfate
AS	acetosyringone
ATF	activating transcription factor
ATMT	*Agrobacterium tumefaciens*-mediated transformation
bHLH	basic helix-loop-helix
BLAST	basic local alignment search tool
bp	base pair(s)
bZIP	basic leucine zipper
CDM	Czapek-Dox medium
cDNA	complementary deoxyribonucleic acid
Cib	Clp1 interacting bZIP1
cl.	clone/ transformant
cm	centimeter(s)
COI	coronatine insensitive
C-terminus	carboxy terminus
CWDE(s)	cell wall degrading enzyme(s)
CWI	cell wall integrity
DIC	differential interference contrast
DNA	deoxyribonucleic acid
DTT	dithiothreitol
ECL	enhanced chemiluminescence
EDTA	2,2´,2´´,2´´´-(Ethane-1,2-diyldinitrilo) tetra-acetic acid
ER	endoplasmic reticulum
ERAD	endoplasmic reticulum associated protein degradation
et al.	*et alii* (and others)
EtOH	ethanol
FAD	fatty acid desaturase
FLO	flocculation
FM4-64	*N*-(3-Triethylammoniumpropyl)-4-(6-(4-(Diethylamino) Phenyl) Hexatrienyl) Pyridinium Dibromide
Fus	cell fusion
g	gram
GFP	green fluorescent protein
GmbH	Gesellschaft mit beschränkter Haftung
^PgpdA	*A. nidulans* glyceraldehyde-3-phosphate dehydrogenase promoter
G-protein	guanine nucleotide-binding protein

Abbreviations

H_2O_2	hydrogen peroxide
HA	hemagglutinin
Hac	homologous to Atf/Creb (activating transcription factor/ cAMP response element-binding protein)
HAC1-C	*HAC1* complementation
HAC1^i	induced messenger RNA variant of *HAC1*
HAC1^i-HA	induced messenger RNA variant of *HAC1* with 5´ hemagglutinin sequence
HAC1^u	uninduced messenger RNA variant of *HAC1*
HAC1^u-HA	uninduced messenger RNA variant of *HAC1* with 5´ hemagglutinin sequence
Ham	hyphal anastomosis mutant
HAM5-C	*HAM5* complementation
Hog	high osmolarity glycerol
HRP	horseradish peroxidase
Hxl	*HAC1* and XBP1-like gene
Ire	inositol requiring
IRTG	international research training group
JA	jasmonic acid
JA-Ile	jasmonoyl isoleucine
JAZ	jasmonate ZIM-domain
KAN^R	kanamycin resistance marker cassette
kb	kilobase(s)
kDA	kilo Dalton
KGaA	Kommanditgesellschaft auf Aktien
Kpp	kinase PCR-product
Kss	kinase suppressor of Sst2 (super sensitive 2) mutations
l	liter
LA	linoleic acid
LasA	JA ester lasiojasmonate A
LB	lysogeny broth
LDS(s)	linoleate diol synthase(s)
LOX(s)	lipoxygenase(s)
LS	lineage specific
LSG(s)	*lineage specific region gene(s)*
M	molar
MAK	mitogen activated kinase
MAPK	mitogen activated protein kinase(s)
MEK	MAPK/ERK kinase
MEK2-C	*MEK2* complementation
MES	2-(N-Morpholino)-ethane sulphonic acid monohydrate
Mb	mega base pair(s)
mg	milli gram(s)
min	minute(s)
ml	milliliter(s)
mm	millimeter(s)
mM	millimolar
mRNA	messenger RNA
ms	millisecond(s)
Msb	multicopy suppression of a budding defect
Mw	molecular weight
n	number of elements
NAT^R	nourseothricin resistance marker cassette

NLP	necrosis and ethylene-inducing peptide 1-like protein
NLS	nuclear localization signal
nm	nanometer(s)
Nox	nicotinamide adenine dinucleotide phosphate oxidase
nt	nucleotide(s)
N-terminus	amino terminus
OD	optical density
Ode	oleate desaturase
OE	overexpression
ORF	open reading frame
PAMP(s)	pathogen-associated molecular pattern(s)
PCR	polymerase chain reaction
PDM	potato dextrose medium
PERK	protein kinase RNA-like endoplasmic reticulum kinase
PIM	protease inhibitor mix
PRoTECT	Plant Responses To Eliminate Critical Threats
Psi	precious sexual inducer
Ppo	precious sexual inducer factor-producing oxygenase
p-value	probability value
qRT-PCR	quantitative reverse transcriptase PCR
RB	right border
RIDD	regulated Ire1-dependent decay
RING	really interesting new gene
rpm	revolutions per minute
RNA	ribonucleic acid
Rok	regulator of Kpp2 (kinase PCR-product 2)
RT	room temperature
^{s}	spliced
s	second(s)
SDS	sodium dodecyl sulfate
Sho	synthetic high osmolarity-sensitive
SIAS	sequence identity and similarity
SISA	*Simple Interactive Statistical Analysis*
Slt	suppressor of lytic phenotype
Smk	sporulation-specific mitogen-activated protein kinase
SOB	super optimal broth
SOC	super optimal broth supplemented with glucose
Som	sorting mitochondrial
SREBP	sterol regulatory element binding protein
Ste	sterile
Sun	sunflower
SXM	simulated xylem medium
TE	trace elements
Tec	transposon enhancement control
TEMED	*N,N,N',N'*-tetramethylethane-1,2-diamine
TM-helix	transmembrane helix
Tom	tomato
tris	2-Amino-2-hydroxymethyl-propane-1,3-diol
Trl	tRNA ligase
trpC^{t}	*A. nidulans* tryptophane biosynthesis gene terminator
uORF(s)	upstream open reading frames
UPR	unfolded protein response
UPRE	unfolded protein response element

UTR	untranslated region
UV	ultra-violet
V	volt
Va	*Verticillium alfalfae*
Vayg	*Verticillium* homolog to *Aspergillus* yellowish green
Vd	*Verticillium dahliae*
VdCmr	*V. dahliae* homolog to *Colletotrichum* melanin regulation
Ve/Vel	velvet
VGB	*Verticillium* strain collection Gerhard H. Braus
Vl43LS20kb	*Verticillium longisporum* 43 approximately 20 kb lineage specific
Vl	*Verticillium longisporum*
Vmk	Verticillium mitogen activated protein kinase
VMK1-C	*VMK1* complementation
WD40	tryptophan-aspartic acid dipeptide ending structural motif of circa 40 amino acids
WT	wild type
XBP	X-box binding protein